

FUNDAMENTALS AND APPLICATIONS OF ATMOSPHERIC PRESSURE
CHEMICAL IONIZATION QUADRUPOLE ION TRAP MASS SPECTROMETRY
FOR THE ANALYSIS OF EXPLOSIVES

By

RICHARD FRED REICH, JR.

A THESIS PRESENTED TO THE GRADUATE SCHOOL
OF THE UNIVERSITY OF FLORIDA IN PARTIAL FULFILLMENT
OF THE REQUIREMENTS FOR THE DEGREE OF
MASTER OF SCIENCE

UNIVERSITY OF FLORIDA

2001

20010405 018

REPORT DOCUMENTATION PAGE			Form Approved OMB No. 0704-0188	
Public reporting burden for this collection of information is estimated to average 1 hour per response, including the time for reviewing instructions, searching existing data sources, gathering and maintaining the data needed, and completing and reviewing the collection of information. Send comments regarding this burden estimate or any other aspect of this collection of information, including suggestions for reducing this burden, to Washington Headquarters Services, Directorate for Information Operations and Reports, 1215 Jefferson Davis Highway, Suite 1204, Arlington, VA 22202-4302, and to the Office of Management and Budget, Paperwork Reduction Project (0704-0188), Washington, DC 20503.				
1. AGENCY USE ONLY (Leave blank)	2. REPORT DATE 22.Mar.01	3. REPORT TYPE AND DATES COVERED THESIS		
4. TITLE AND SUBTITLE FUNDAMENTALS AND APPLICATIONS OF ATMOSPHERIC PRESSURE CHEMICAL IONIZATION QUADRUPOLE ION TRAP MASS SPECTROMETRY FOR THE ANALYSIS OF EXPLOSIVES		5. FUNDING NUMBERS		
6. AUTHOR(S) CAPT REICH RICHARD F JR				
7. PERFORMING ORGANIZATION NAME(S) AND ADDRESS(ES) UNIVERSITY OF FLORIDA		8. PERFORMING ORGANIZATION REPORT NUMBER CI01-67		
9. SPONSORING/MONITORING AGENCY NAME(S) AND ADDRESS(ES) THE DEPARTMENT OF THE AIR FORCE AFIT/CIA, BLDG 125 2950 P STREET WPAFB OH 45433		10. SPONSORING/MONITORING AGENCY REPORT NUMBER		
11. SUPPLEMENTARY NOTES				
12a. DISTRIBUTION AVAILABILITY STATEMENT Unlimited distribution In Accordance With AFI 35-205/AFIT Sup 1		12b. DISTRIBUTION CODE		
13. ABSTRACT (Maximum 200 words)				
14. SUBJECT TERMS		15. NUMBER OF PAGES 206		
		16. PRICE CODE		
17. SECURITY CLASSIFICATION OF REPORT	18. SECURITY CLASSIFICATION OF THIS PAGE	19. SECURITY CLASSIFICATION OF ABSTRACT	20. LIMITATION OF ABSTRACT	

To my wife Erica, who displayed strength,
support and sacrifice throughout
difficult times, and to whom I wish to
express my love and gratitude.

ACKNOWLEDGMENTS

First I would like to thank my research director, Dr. Richard Yost, for what he has taught me about mass spectrometry and for guiding me through my master's work. I would also like to thank the other members of my committee, Dr. Robert Kennedy and Dr. Joseph Delfino. I thoroughly enjoyed their classes on separations chemistry and water analysis, and I would highly recommend these classes to anyone. I would like to acknowledge the Yost research group for all their help and support. Specifically I would like to thank Kevin McHale, who is a wizard at electrospray and sacrificed several hours of his time to unselfishly assist me in my times of desperation.

Special thanks go to Dr. Jehuda Yinon and Dr. Fred Volk, who provided the explosive samples that made this research possible. I would also like to thank my former team leader and best friend, Mr. Stephen Aubert, who also provided me with samples, but more importantly, encouraged me to go back to school.

Last, thanks go to my wife and my parents. I am very grateful for their patience with my effort and support when I needed them.

TABLE OF CONTENTS

	<u>page</u>
ACKNOWLEDGMENTS	iii
ABSTRACT.....	vi
CHAPTERS	
1 INTRODUCTION	1
Electrospray Ionization	4
Atmospheric Pressure Chemical Ionization	7
Instrumentation	10
API Stack	12
Ion Optics.....	14
Mass Analyzer	16
Sample Compounds	28
Thesis Summary.....	36
2 PRINCIPLES OF ESI-MS, APCI-MS, AND MS/MS OF EXPLOSIVES	39
Experimental	40
Instrumentation	40
Samples	42
Results and Discussion	43
Nitroaromatic Compounds.....	43
Nitrate Esters.....	75
Nitramines.....	83
Nitro Aliphatic Compound	95
Conclusion	95
3 ADDUCT ION FORMATION OF EXPLOSIVES	106
Experimental	107
Instrumentation	107
Samples	108
Results and Discussion	109
Effects of Additives on ESI-MS and APCI-MS	109
MS/MS of Adduct Ions	117
Conclusion	123

4 LC/APCI-MS METHOD DEVELOPMENT FOR THE ANALYSIS OF EXPLOSIVES.....	127
Experimental	128
Instrumentation	128
Samples	129
Results and Discussion	130
Chlorinated Solvent Study	130
APCI Tune Method Development	136
Improved Explosive Detection with Chloroform	144
LC/APCI-MS and LC/APCI-MS/MS of Explosives	152
Conclusion	169
5 APPLICATION OF LC/APCI-MS METHOD FOR ANALYSIS OF REAL SAMPLES.....	175
Experimental	176
Instrumentation	176
Samples	176
Results and Discussion	178
Calibration Curve.....	178
Water Sample.....	183
Soil Samples.....	183
Soot Samples.....	187
SEMTEX.....	192
Conclusion	195
6 CONCLUSIONS AND FUTURE WORK	197
Conclusions.....	197
Future Work	200
LIST OF REFERENCES.....	201
BIOGRAPHICAL SKETCH	205

Abstract of Thesis Presented to the Graduate School
of the University of Florida in Partial Fulfillment of the
Requirements for the Degree of Master of Science

FUNDAMENTALS AND APPLICATIONS OF ATMOSPHERIC PRESSURE
CHEMICAL IONIZATION QUADRUPOLE ION TRAP MASS SPECTROMETRY
FOR THE ANALYSIS OF EXPLOSIVES

By

Richard Fred Reich, Jr.

May 2001

Chairman: Richard A. Yost
Major Department: Chemistry

The goal of this research was to develop a liquid chromatography (LC)/atmospheric pressure chemical ionization (APCI)-mass spectrometry (MS) and tandem mass spectrometry (MS/MS) method for the analysis of explosives. APCI and electrospray ionization (ESI) are soft ionization techniques which produce characteristic ions of explosives at atmospheric pressure. Most explosives are susceptible to impurities in the solvent and form adduct ions instead of molecular-type ions. Additives allow specific adduct ions to be preferentially formed, which increases the sensitivity for explosives and improves spectral consistency. However, these adduct ions are formed by weak van der Waals forces that can be easily dissociated by the energy imparted during

vaporization. APCI may prove more efficient than ESI in producing adduct ions of explosives, because these adduct ions are formed in the gas phase after vaporization unlike ESI, which forms them in solution.

In this study, the ESI-MS, APCI-MS, and MS/MS of thirty-two different explosives are investigated to determine characteristic ions for analysis. The impact of different additives on the adduct ion formation of explosives is studied, along with the adduct ion's ability to form structurally informative daughter ions during MS/MS. The use of chlorinated solvents with APCI-MS is shown to greatly improve the sensitivity for explosives; this sensitivity is dependent on the concentration and electron attachment rate constant of the solvent. The fundamentals of different APCI parameters are studied and optimized for the detection of explosives.

LC/APCI-MS and LC/APCI-MS/MS methods developed using 0.1% chloroform are capable of isocratically separating eight different explosives under five minutes with the identification of major parent ions and daughter ions of each explosive. The method is sensitive for each explosive down to 5 ppb (parts-per-billion) with a linear dynamic range that reaches up to 1000 ppb. The method is effective at detecting and quantitating trace amounts of explosives in complex matrices including contaminated water and soil, as well as detonation soot.

CHAPTER 1 INTRODUCTION

The ability to detect and quantitate trace amounts of explosives is of great importance for both forensic and environmental applications. Explosive analysis is becoming an increasingly demanding area of forensic science with ongoing terrorist activity [Fainberg, 1992], such as the destruction of Pan Am flight 103 over Scotland in 1988, followed by the truck bombings at the World Trade Center in New York City in 1993 and the Murrah Federal Building in Oklahoma City in 1995, as well as an incident at the Centennial Olympic Park (Atlanta, Georgia) in 1996. Forensic scientists may be required to definitively identify trace levels of explosives from post-blast debris resulting from a bombing, as well as determine the molecular composition of the explosive formulation. This may prove difficult since the explosive residues are often trapped in complex matrices (e.g., wood, metal, glass, debris) from which they may require extraction, and which may easily contaminate the analytical system. Extraction of explosive residue from complex matrices is also a common problem for environmental scientists, who are required to detect the level of explosive contamination in groundwater and soil resulting from munitions manufacturing plants [Crockett et al., 1996].

A wide variety of analytical techniques has been developed for the analysis of explosives [Yinon, 1999] with chromatographic and mass spectrometric methods being the most widely used. Mass spectrometry (MS) offers unique advantages of high molecular specificity and detection sensitivity. The major drawback of MS is its limitation in handling mixtures of compounds. Tandem mass spectrometry (MS/MS) can

alleviate this problem only to a certain extent. Complex mixtures such as soil samples and post-explosion residues contain many interfering substances from the matrix, which may require chromatographic separation to separate explosive analytes from unwanted accompanying substances.

Many different chromatographic methods have been used for the analysis of explosives including thin-layer chromatography (TLC) [Yinon and Zitrin, 1981], gas chromatography (GC) [Yinon and Zitrin, 1981], high-performance liquid chromatography (HPLC, or LC) [Yinon and Zitrin, 1981], solid-phase microextraction (SPME)/HPLC [Wu et al., 1999], supercritical fluid chromatography (SFC) [Douse, 1988], ion chromatography (IC) [Reutter et al., 1983], and capillary electrophoresis (CE) [Oehrle, 1996]. Of these separation techniques, only GC and LC have been interfaced with MS for the analysis of explosives.

The use of GC/MS for the analysis of explosives has the advantage of the powerful separation capability of GC with the high reliability and sensitivity of MS; however, it is limited to those explosives which can be eluted from the GC column [Yinon and Zitrin, 1993]. Several explosives, especially some nitrate esters and nitramines, are thermally labile and have been shown to decompose under GC conditions, while others are too involatile to be analyzed by GC. High temperature GC is generally difficult to employ since most explosives will not survive the thermal conditions required for their vaporization and separation. This is a dilemma especially for explosives with very low vapor pressures such as pentaerythritol tetranitrate (PETN) and 1,3,5-trinitro-1,3,5-triazacyclohexane (RDX), which decompose at elevated temperatures [Kolla, 1994]. Some of these difficulties can be reduced by using cold on-column capillary

injection techniques [Yinon 1996] and short columns [Tamiri and Zitrin, 1986]. Various gas-phase ionization techniques have been used to analyze explosives by GC/MS and by solids probe mass spectrometry. These techniques include electron ionization (EI), chemical ionization (CI), and electron-capture negative ionization (ECNCI); unfortunately, these gas-phase ionization techniques require that the analyte molecule be vaporized before being ionized, which often result in fragmentation of fragile explosive ions [Fetterolf, 1995].

LC/MS is important for the determination of explosive constituents that cannot be vaporized and/or are thermally labile. LC is typically less sensitive than GC, because of the broad peak shape and lower peak heights. Also, the resolution between substances of similar polarity such as isomers is lower than in GC. However, LC has special advantages in the analysis of very dirty samples, because the columns and the eluents are more stable to contamination from accompanying substances in extracts of debris or soil [Kolla, 1994]. Another benefit of using LC/MS is that it employs atmospheric pressure ionization (API) techniques that are generally softer (less fragmentation) than EI, CI, or ECNCI. Gentle ionization allows for the production of molecular (M^+ and M^-) or $[M+H]^+$ and $[M-H]^-$ ions from explosive compounds, which provides information about the nominal molecular weight of the intact molecule. Four different types of ionization techniques have been used for the LC/MS analysis of explosives: direct liquid introduction (DLI) [Yinon, 1983], thermospray (TS) [Voyksner and Yinon, 1986], electrospray ionization (ESI) [Straub and Voyksner, 1993], and atmospheric pressure chemical ionization (APCI) [Schilling, 1996]. The focus of the research in this thesis pertains to ESI and APCI of explosives; therefore, DLI and TS will not be discussed

further. A detailed description of DLI and TS ionization techniques and their application in explosive analysis can be found elsewhere [Yinon, 1993].

Electrospray Ionization

ESI is a liquid-phase ionization technique that allows the transfer of ions from solution to the gas phase. This is a strongly endothermic and endoergic process, because in solution the ion is strongly interacting with a number of solvent molecules, which form a solvation “sphere” around the ion [Cole, 1997]. The act of freeing an ion from the solvent can lead to fragmentation, because the energy required for desolvation is often larger than the energy required to break individual bonds within the ion. Nevertheless, ESI is the softest ionization technique available, where softness can be defined as the degree to which fragmentation of the ions is avoided. Ion desolvation in ESI is achieved gradually by thermal energy at relatively low temperatures; thus little or no fragmentation of sample ions occur.

The ESI process begins as a solution of the analyte is passed through a metal capillary that is held at high potential (3 – 5 kV), (Figure 1-1). Because the electrospray capillary tip (needle) has a very thin wall (0.1 mm), the electric field at the capillary tip is very high (10^6 V/m). The effect of the high electric field as the solution emerges is to generate a mist of highly charged droplets [Gaskell, 1997]. Nebulization of the solution emerging from the capillary may be facilitated by a sheath flow of nebulizer gas (typically nitrogen). The necessity for the sheath gas is dependent on the flow rate employed, the physical properties of the solvent (surface tension, boiling point, and Van der Waal’s constant) and the sign of the potential applied to the capillary tip (since a high

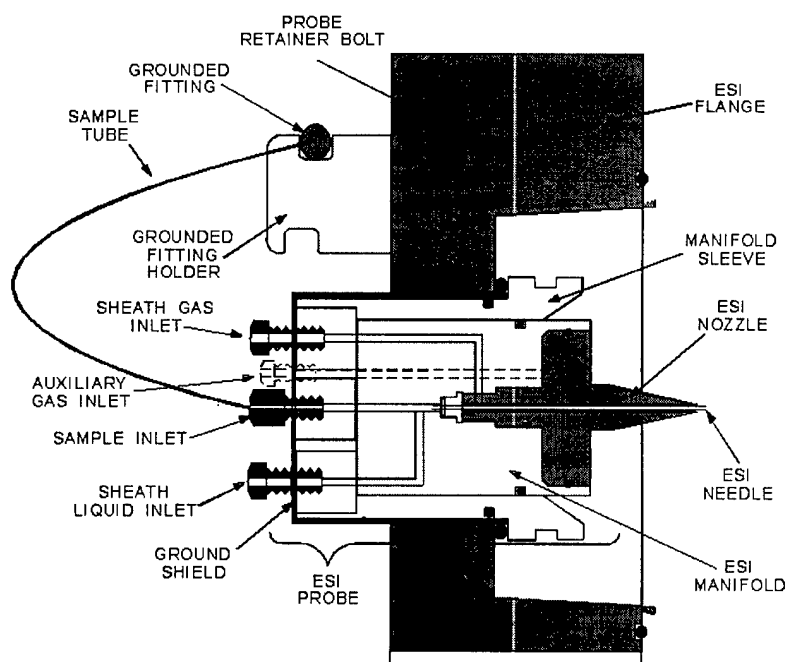
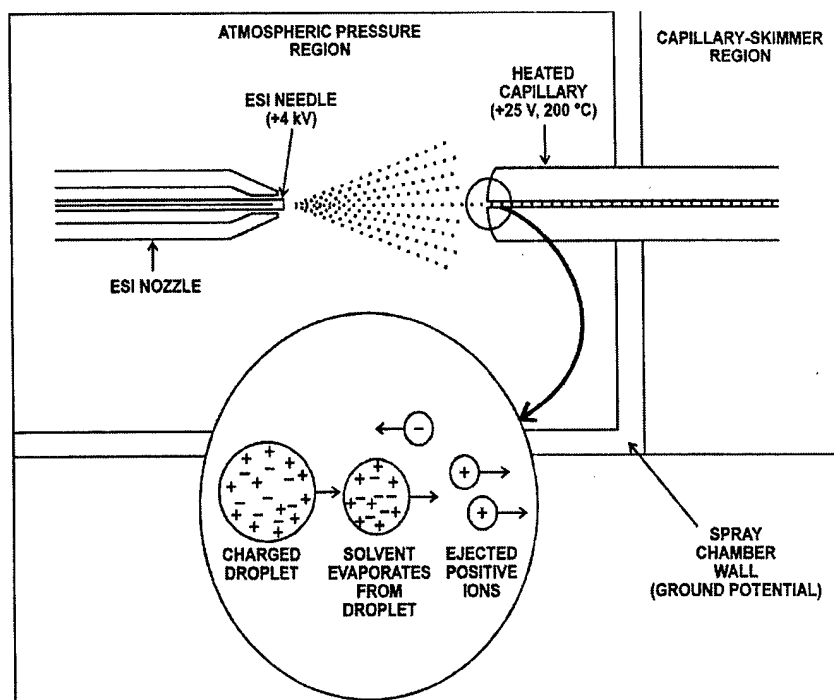


Figure 1-1. ESI process in the positive ion polarity mode (above); Cross sectional view of the ESI probe assembly on the LCQ (below). Reproduced from LCQ Xcalibur software online manual.

negative potential, in particular, may lead to a corona discharge unless suppressed by use of an appropriate sheath gas) [Gaskell, 1997].

ESI can be operated to produce both positive and negative ions depending on the polarity of the potential applied to the capillary tip. Assuming a negative potential, negative ions in solution will accumulate at the surface, which is thus drawn out in a downfield direction to establish a “Taylor cone”. At a high enough imposed field, the cone is drawn to a filament which produces negatively charged droplets via a “budding” process when the surface tension is exceeded by the applied electrostatic force. The charged droplets produced move down an electric field between the capillary tip and a counter-electrode (heated capillary), which is located 1-3 cm from the ESI needle, resulting in a current that can be measured. Ions become desolvated as they move towards the counter-electrode. An auxiliary (aux) gas, typically nitrogen, can also be applied to assist in droplet evaporation.

Two mechanisms have been proposed for the desolvation process: the charge residue model (CRM) originally proposed by Malcolm Dole et al. [1968] and the ion evaporation model (IEM) originated by Iribarne and Thomson [1976]. The CRM holds that a sequence of Rayleigh instabilities (sometimes called “Coulomb explosions” in which the charge density eventually becomes large enough to overcome the surface tension of the droplet and cause it to divide) with intervening periods of solvent evaporation ultimately produces droplets each of which contains only one solute molecule. That molecule becomes a free gas-phase ion by retaining some of the droplet’s charge as the last of the solvent evaporates. The IEM assumes the same sequence of

evaporation and Rayleigh instabilities but argues that before a droplet reaches the ultimate stage contemplated by Dole, the field on its surface becomes strong enough to overcome solvation forces and lift a solute ion from the droplet surface into the ambient gas [Kearle and Peschke, 1999].

Atmospheric Pressure Chemical Ionization

APCI is also a soft ionization technique, but it differs from ESI in that it is a gas-phase ionization technique. APCI is similar to CI in the type of ionizing reactions that occur except that it is accomplished in an ionization chamber at atmospheric pressure instead of a pressure of 1 Torr. In the APCI source, ionization is initiated either by low-energy electrons from a radioactive beta source or by a corona discharge [Bruins, 1991]. It is not possible to use a heated filament to produce electrons as the primary source of ionization as in CI, because APCI operates at atmospheric pressure and the filament would rapidly burn out. The APCI process begins as a solution of the analyte is passed through a heated nebulizer interface that uses pneumatic nebulization to convert the liquid flow into droplets, which are then swept by means of a sheath gas (nitrogen) through a quartz tube heater (vaporizer) to vaporize the solvent and analyte [Chapman, 1993] (Figure 1-2). The mixture of vaporized solvent and analyte molecules flows towards the ion formation region where a corona discharge (source of ionization used in thesis research) initiates chemical ionization at atmospheric pressure using nitrogen and/or the vaporized solvent as the reagent gas. The high ionization efficiency of APCI is due to the short mean free path at 760 Torr and thus the increased number of collisions between the sample molecules and reagent ions.

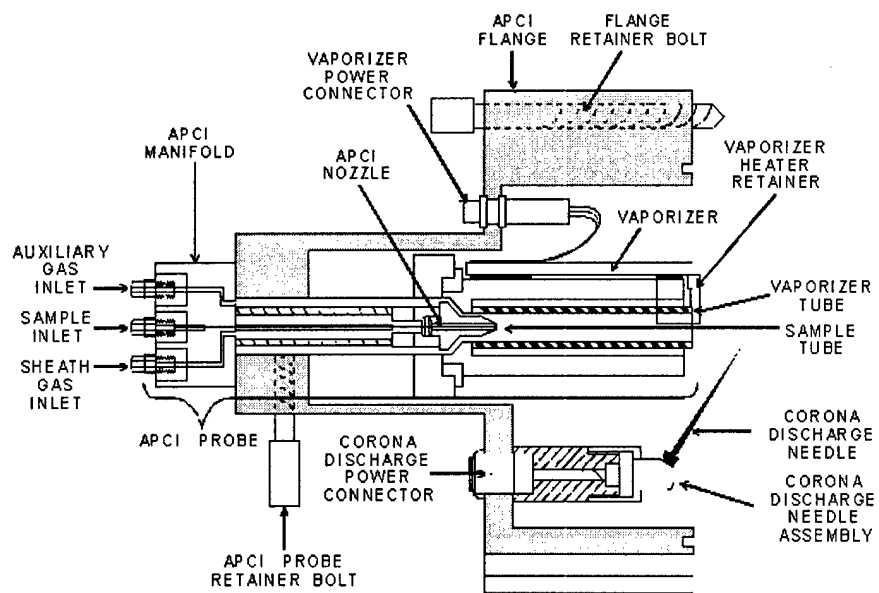
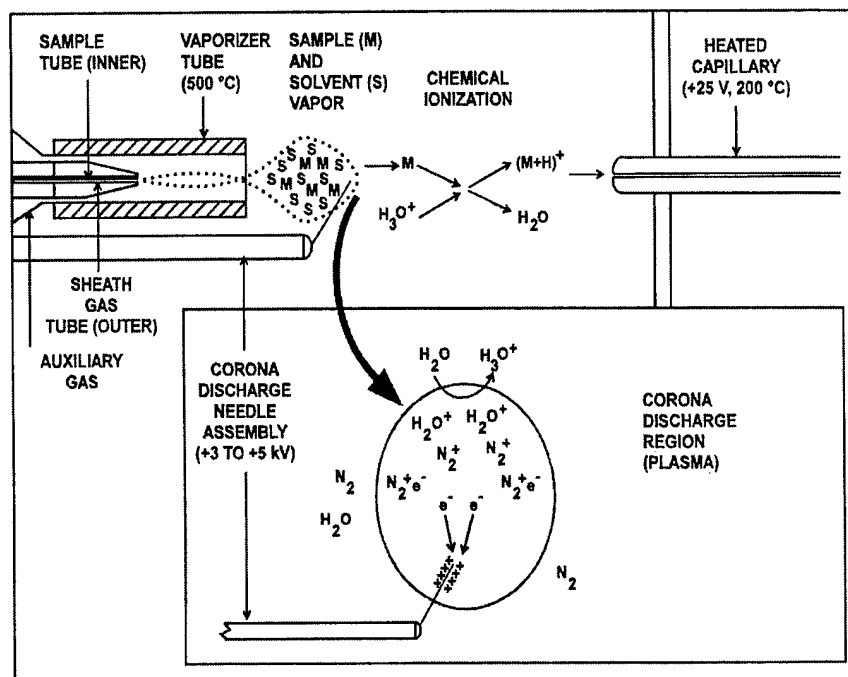


Figure 1-2. APCI process in the positive ion polarity mode (above); Cross sectional view of the APCI probe assembly on the LCQ (below). Reproduced from LCQ Xcalibur software online manual.

APCI relies on ion-molecule reactions that generally involve reagent ions derived from the solvent. These ion-molecule reactions include proton transfer, charge exchange, electrophilic (positive ions) or nucleophilic (negative ions) addition, and anion abstraction (positive ions) or nucleophilic displacement (negative ions). Most reagent ions are capable of participating in more than one of the listed reactions. Proton transfer occurs with positive ions when a reagent ion (XH^+) protonates a sample molecule (M), as shown in equation 1-1. For negative ions, proton transfer takes place when a reagent ion (X^-) accepts a proton from an analyte molecule (MH), shown in equation 1-2. The tendency for these reactions to occur may be assessed from knowledge of proton affinity values.



With analyte molecules that do not contain acidic or basic sites, a major alternative to proton transfer is ionization to produce molecular ions by charge exchange (electron transfer). Charge exchange with positive ions takes place between a reactant ion (X^+) generated from a molecule having a high ionization potential, and a sample molecule (M) having a lower ionization potential. Conversely, charge exchange occurs in the negative mode when the reactant ion (commonly O_2^-) has a lower ionization potential than the sample molecule. Charge exchange reactions with positive and negative ions are shown in equations 1-3 and 1-4, respectively:



With positive ions, the major reaction of sample molecules (M) of higher proton affinity than reagent ions (X^+) is proton transfer; however, if the sample molecules have a lower proton affinity, they can still undergo electrophilic addition to produce a stable addition complex (adduct ion), as shown in equation 1-5. Conversely with negative ions, stable addition complexes may be formed by nucleophilic attack (nucleophilic addition) (equation 1-6) with reagent anions of low proton affinity, such as Cl^- and O_2^- , which cannot usually react by proton transfer.



Another set of ion-molecule reactions available for the production of positive and negative sample ions is anion abstraction (equation 1-7) and nucleophilic displacement (equation 1-8), respectively. These reactions occur when reagent ions react with sample molecules to form neutrals, resulting in fragment ions from the sample.



Instrumentation

All experiments reported in this thesis were performed on the Finnigan LCQ (San Jose, CA), a commercial, bench-top quadrupole ion trap mass spectrometer (QITMS) (Figure 1-3). The LCQ employs external ionization and may be equipped with either of two API modes: ESI or APCI. The main advantage of an external ionization source over in situ ionization used with the ion trap derives from the separation of neutral analyte from the mass analysis region. An external ion source greatly reduces the likelihood for ion-molecule reactions and memory effects within the ion trap [Bier et al., 1993]. The

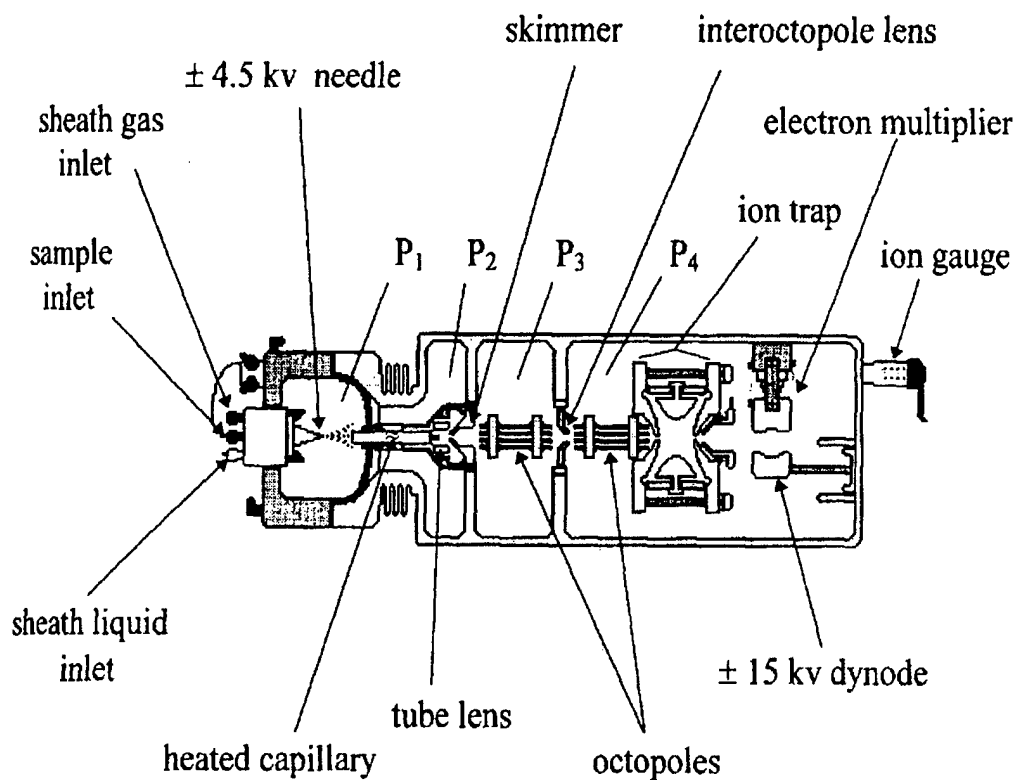


Figure 1-3. Cross sectional view of Finnigan LCQ. $P_1 \approx 760$ Torr, $P_2 \approx 1$ Torr, $P_3 \approx 1 \times 10^{-3}$ Torr, $P_4 \approx 2.5 \times 10^{-5}$ Torr, and $P_{\text{trap}} \approx 1-2 \times 10^{-3}$ Torr. Reproduced from Cole, 1997.

quadrupole ion trap is a good candidate for coupling with ion sources operating at high pressures like ESI and APCI, because ion traps can operate at higher pressures than any other type of analyzer.

API Stack

In the LCQ, fully or partially desolvated ions formed by ESI or APCI are sampled by the API stack (Figure 1-4). The API stack consists of the components of the API source that are held under vacuum (1 Torr) and are shared by both ESI and APCI, which include the heated capillary, tube lens, and skimmer. The heated capillary assists in desolvating ions that are produced by the ESI or APCI probe. The heated capillary is an elongated, cylindrical tube made of metal that has a hole bored through the center of its long axis. A heater embedded in the capillary surrounds the hole and heats the capillary to temperatures up to 300 °C. Ions are drawn into the heated capillary from the atmospheric pressure region and transported to the capillary-skimmer region of the vacuum manifold by a decreasing pressure gradient. A potential of typically +/-25 V (positive for positive ions and negative for negative ions) assists in repelling ions from the heated capillary to the skimmer.

Ions from the heated capillary enter the tube lens (tube gate). The tube lens has a potential applied to it, which is mass-dependent and acts to focus the ions towards the opening of the skimmer. The potential is positive for positive ions and negative for negative ions. The tube lens also serves as a gate to stop the injection of ions into the mass analyzer. A potential of -200 V is used to deflect positive ions away from the opening in the skimmer, and a potential of +200 V is used to deflect negative ions away from the opening in the skimmer. Ions from the tube lens pass through the skimmer and move toward the first octopole.

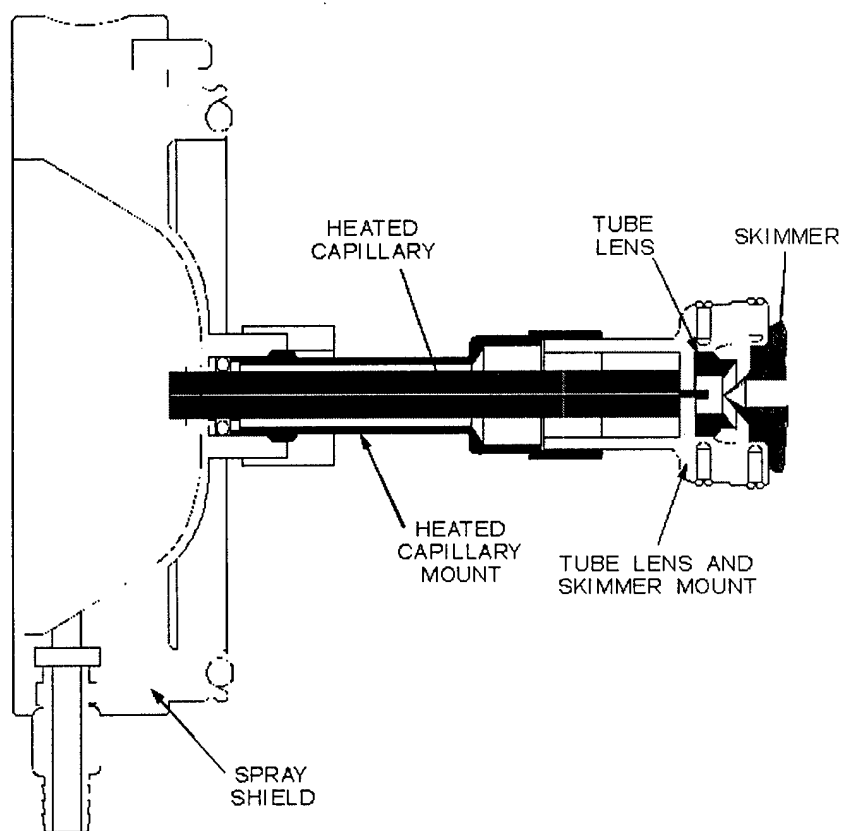


Figure 1-4. Cross sectional view of the API stack on the LCQ.
Reproduced from LCQ Xcalibur software online manual.

The skimmer acts as a vacuum baffle between the higher pressure capillary-skimmer region (at 1 Torr) and the lower pressure first octopole region (at 10^{-3} Torr) of the vacuum manifold. The skimmer is at ground potential. The bore of the heated capillary is offset with respect to the opening in the skimmer to reduce the number of neutral molecules and large charged particles that pass through the skimmer and create detector noise.

Ion Optics

Ions enter the ion optics after passing through the skimmer (Figure 1-5). The ion optics transmit ions from the API source to the mass analyzer. The ion optics consist of two octopoles and an interoctopole lens. Each octopole is an octagonal array of cylindrical rods that acts as an ion transmission device. An RF voltage (2.45 MHz, 400 V_{p-p}) and DC offset voltage (typically -10 to $+10$ V) are applied to the rods to give rise to an electric field that guides the ions along the axis of the octopole. During ion transmission, the offset voltage is negative for positive ions and positive for negative ions. The octopole RF voltage is turned off during mass analysis to help prevent ions from entering the mass analyzer during the analytical scan.

The two octopoles are separated by the interoctopole lens, which assists in the focusing and gating of ions. The interoctopole lens also serves as a baffle between the first octopole region (at 10^{-3} Torr) and the analyzer region (2×10^{-5} Torr) of the vacuum manifold. During ion transmission, a potential between -10 and $+10$ V is typically applied to the interoctopole lens. The potential is negative for positive ions and positive for negative ions. During gating, the potential is $+300$ V for positive ions and -300 V for

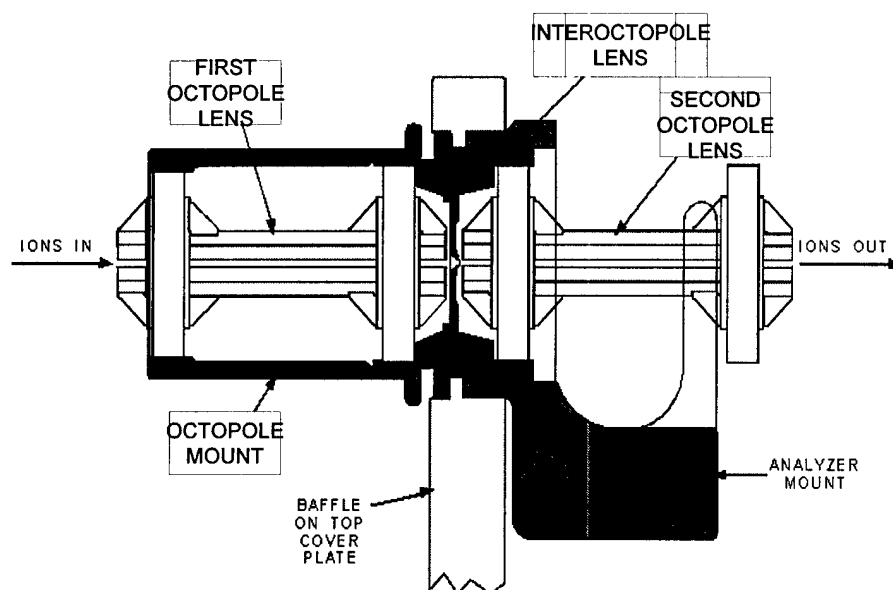


Figure 1-5. Cross sectional view of ion optics on the LCQ.
Adapted from LCQ Xcalibur software online manual.

negative ions to help prevent ions from entering the mass analyzer during the analytical scan.

Mass Analyzer

The ion optics direct ions into the quadrupole ion trap mass analyzer where mass analysis occurs (Figure 1-6). The quadrupole ion trap (QIT) confines ions in a small volume between a ring electrode and two endcap electrodes by appropriately oscillating radio-frequency (RF) electric fields [Watson, 1997]. Hyperbolic endcap electrodes are arranged on opposite sides of a ring electrode also having a hyperbolic inner surface, and are separated by two silicon nitride spacer rings that position the stainless steel electrodes at the proper distance apart and also serve as electrical insulators. The entrance endcap electrode is the electrode that is closest to the ion optics, and the exit endcap electrode is the electrode that is closest to the ion detection system. Both endcap electrodes have a small hole in their centers to permit the passage of ions into and out of the mass analyzer cavity. A DC offset voltage (-10 V for positive ions; +10 V for negative ions) is applied to the mass analyzer electrodes to draw in ions from the ion optics. An RF voltage of constant frequency (760 kHz) and variable amplitude (0 to 8500 V_{0-p}) is then applied to the ring electrode, which produces a three-dimensional quadrupolar field within the mass analyzer. The time-varying field drives ionic motion in both the axial and radial directions. Ionic motion must be stable in both directions for an ion to remain trapped.

Ions stored inside the trap follow trajectories described by the second-order Mathieu differential equation [Mathieu, 1868]. Solutions to the differential equation are in terms of two reduced parameters, a_z and q_z , which can be used to determine whether an ion will have a stable or unstable trajectory in the trap under the defined conditions of the

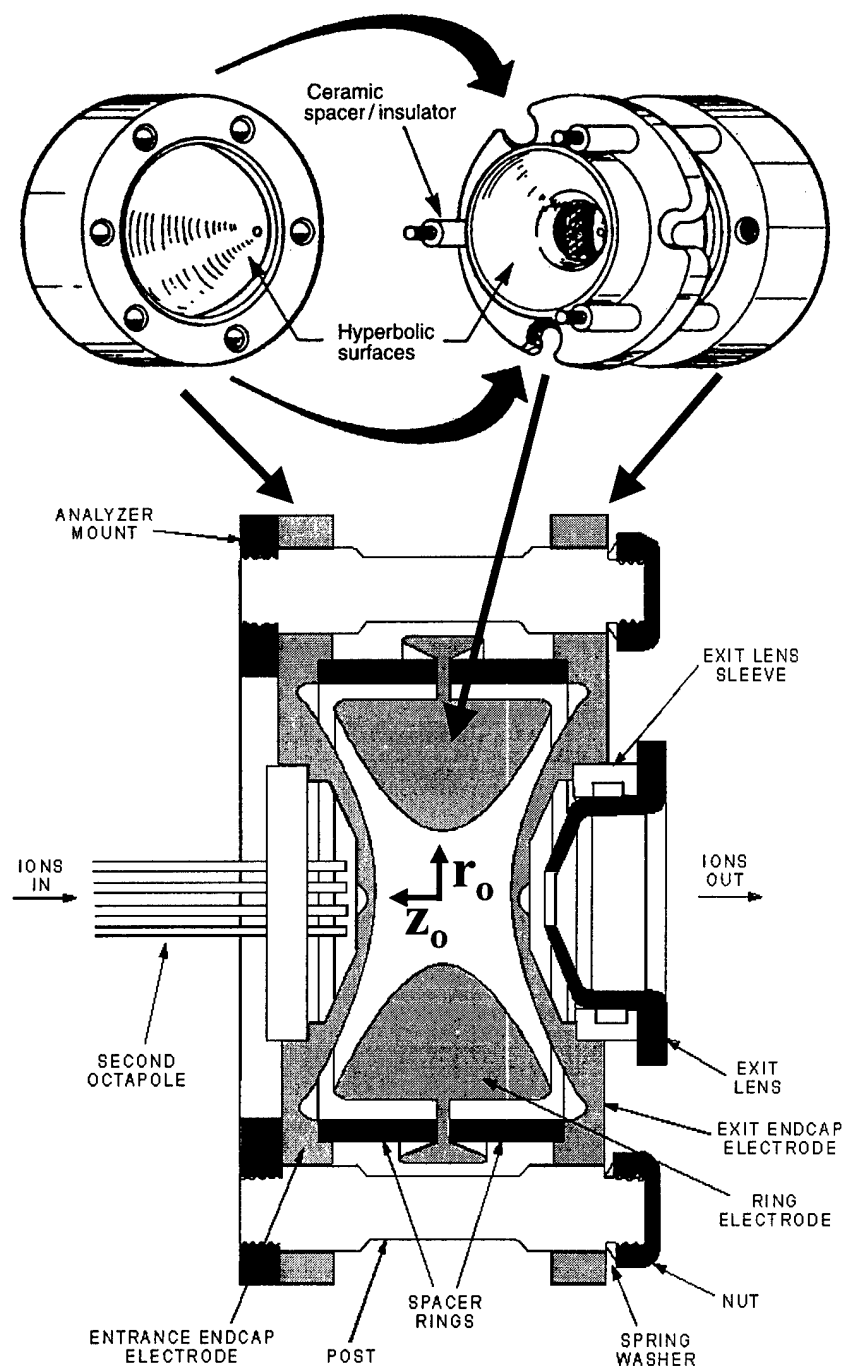


Figure 1-6. Three-dimensional view of ring and endcap electrodes of ion trap (above). Adapted from Louris, J., et al., *Anal. Chem.* **1987**, 59, 1677. Cross sectional view of the quadrupole ion trap on the LCQ (below). Adapted from LCQ Xcalibur software online manual.

electric field. The values of a_z and q_z depend on the dimensions of the trap and the potentials applied according to equations 1-9 and 1-10:

$$a_z = -2a_r = \frac{-16eU}{m(r_o^2 + 2z_o^2)\Omega^2} \quad (1-9)$$

$$q_z = -2q_r = \frac{-8eV}{m(r_o^2 + 2z_o^2)\Omega^2} \quad (1-10)$$

The subscripts z and r represent axial and radial motion between and perpendicular to the endcaps, respectively; U is the DC amplitude applied to the ring electrode (if any), V is the RF potential applied to the ring electrode, e is the charge on an ion, m is the mass of an ion, r_o is the inner radius of the ring electrode, z_o is the axial distance from the center of the device to the nearest point on one of the endcap electrodes, and Ω is the angular drive frequency. The angular drive frequency is equal to $2\pi f_{RF}$ where f_{RF} is the frequency of the main RF voltage in Hertz.

From the known solutions to the Mathieu equation one can generate a stability diagram (Figure 1-7) that shows the common region in (a_z, q_z) space for which the radial and axial components of the ion trajectory are stable simultaneously such that the ion can be confined in the trap. The parameters β_z and β_r at any given coordinate of a and q relate to the secular frequency ω of the ion in the z and r directions, respectively (equation 1-11).

$$\omega_u = 0.5 \beta_u \Omega \quad (1-11)$$

As the value of β approaches zero, the ion's secular frequency approaches zero, and the ion is not contained. When the value of β equals one, the ion's secular frequency equals half the frequency of the RF field, and the magnitude of its oscillation increases so that the ion escapes the trap or collides with one of the endcap surfaces. When β has a value

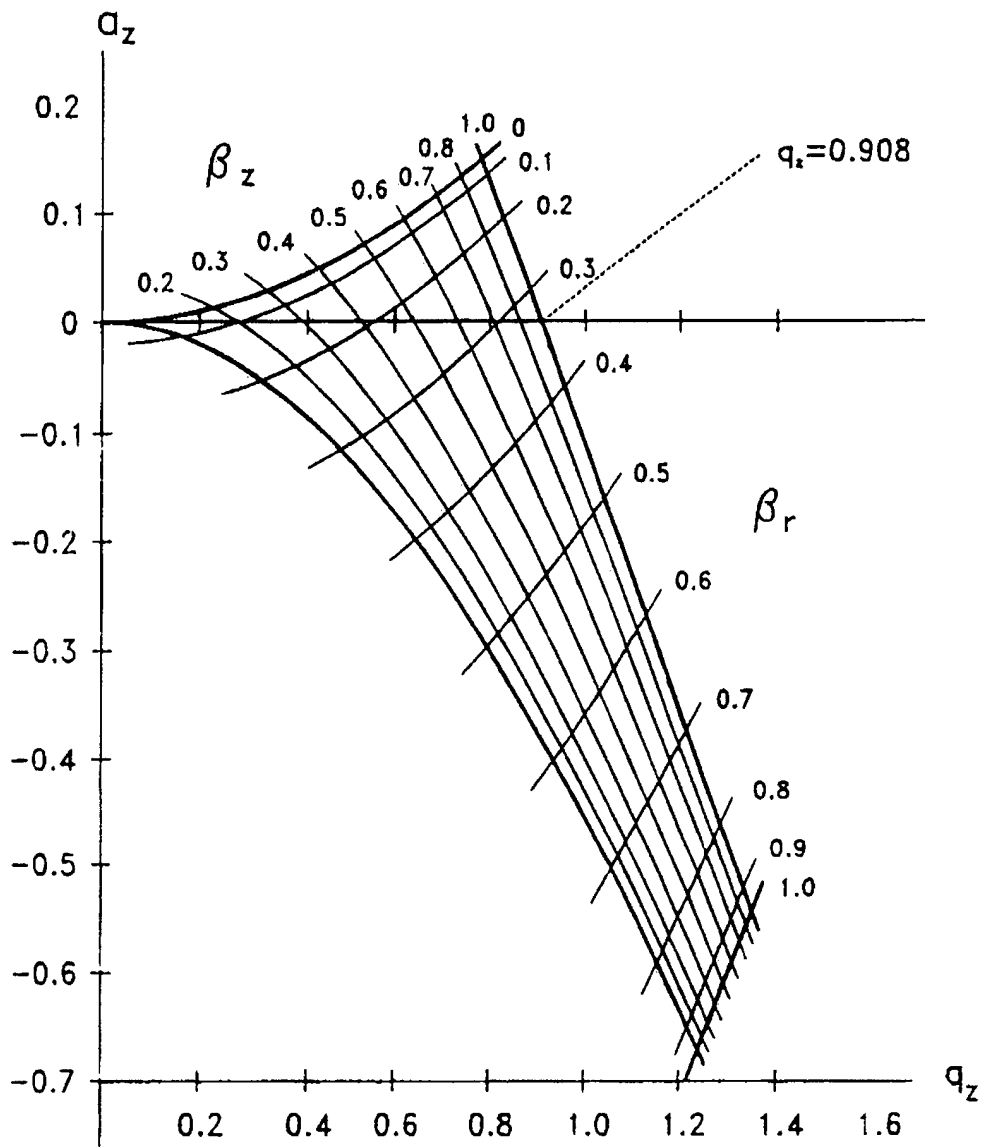


Figure 1-7. Mathieu stability diagram for the ion trap. The lines labeled β_r and β_z describe the oscillatory characteristics of ion motion. Reproduced from March and Todd, 1995.

between zero and unity, the ion can be trapped by the oscillating fields and will oscillate in a periodic mode at its secular frequency in z and r .

The ion trap has a storage capacity of approximately 10^6 ions [McLuckey et al, 1994]; however, the ion trap can trap or hold only a certain number of ions before repulsive forces (space charge) cause distortions in the applied trapping field, causing a degradation in resolution, a reduction in peak height, and a shift in mass assignments [Cleven et al, 1994]. At severe space-charge conditions, the mass peaks are further broadened and reduced in peak height to the point where they disappear into the baseline. Beyond the extreme limit of space charge, the ion density becomes so large that additional ions injected into the quadrupole field may not be trapped at all, or previously trapped ions may be displaced [Cole, 1997]. In order to control the number of ions that accumulate in the trap a method was developed by Finnigan MAT [Stafford et al., 1987] called automatic gain control (AGC). The AGC quantitatively assesses the ion generation rate by use of a prescan, and then inversely applies a period of ionization (ion injection time) during each operational cycle of the ion trap to ensure that the number of ions in the trap never reaches an adverse level of space-charge. The AGC prescan and analytical scan combined make one microscan, as shown in the scan function on Figure 1-8.

During the ion injection time, ions transmitted from the ion optics are directed into the ion trap where they accumulate before they are scanned out and detected. The ions enter the trap with a range of kinetic energies. Unless the ions enter the trap at the correct phase angle of the RF drive potential, they will not have the correct combination of velocity and displacement to remain in stable orbits and be trapped [Kishore and

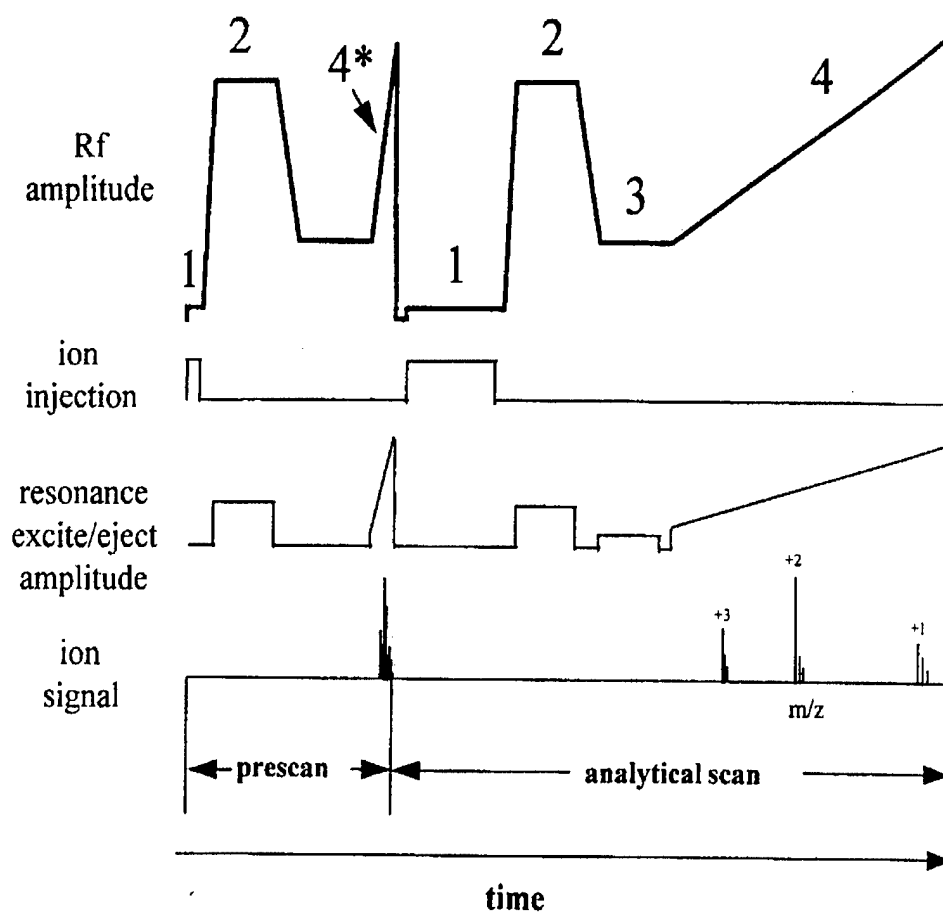


Figure 1-8. A simplified scan function for the quadrupole ion trap showing the prescan and the analytical scan which makes up one microscan. The four steps of the QIT operation: ion injection (1), isolation (2), excitation (3), and mass analysis (4) are shown in the scan function. The prescan mass analysis step (4*) is rapid, because only an ion-current measurement is required. Reproduced from Cole, 1997.

Ghosh, 1979]. Even if they meet these conditions, they still enter the trap with too much kinetic energy to be trapped forever. To remove some of this kinetic energy, a helium damping gas is introduced into the trap through a nipple on the exit endcap electrode. The flow of gas (1 mL/min) into and out of the trap is matched so that the partial pressure of helium in the mass analyzer cavity is maintained at approximately 1 mTorr. The ions are kinetically cooled to the center of the trap (over a period of a few milliseconds) through collisions with the low-molecular-weight helium atoms. As a result, mass resolution is improved, because the ions are ejected from the ion trap in dense ion packets, and sensitivity is increased, because they are also focused tightly along the z-axis so that they are transmitted to the detector efficiently.

After ions have been successfully stored in the QIT, a number of different mass analyses can be performed. These include single-stage full scan (MS), two-stage full scan (MS/MS), multi-stage full scan (MSⁿ, n = number of stages from 3 to 10), selected ion monitoring (SIM), selected reaction monitoring (SRM), and consecutive reaction monitoring (CRM). With MS, the ions formed in the ion source are stored in the mass analyzer, and then are sequentially scanned out of the mass analyzer to produce a full mass spectrum.

MS/MS includes two stages of mass analysis. In the first stage, the ions formed in the ion source are stored in the mass analyzer. Ions of one mass-to-charge ratio (m/z), the parent ions, are then selected and all other ions are ejected from the mass analyzer. This selection occurs with the use of a sum-of-sines tailored waveform (TWF) consisting of many discrete frequencies, which is applied to the endcaps in dipolar fashion to isolate a narrow m/z window (isolation window). The TWF applies a resonance ejection RF

voltage at all frequencies corresponding to the secular frequency of the unwanted m/z ions, which results in them being resonantly ejected from the trap. Resonant ejection of an ion occurs when an auxiliary RF field is applied that matches its secular frequency in the z -direction. The ion absorbs kinetic energy to the point that its magnitude of oscillation increases so that it escapes the trap or collides with one of the endcap surfaces. The TWF leaves a “frequency notch” around the frequencies corresponding to the m/z of the parent ion.

The parent ions are then excited with a resonance excitation RF voltage, which is applied across the endcap electrodes. The resonance excitation RF voltage has lower amplitude than the resonance ejection RF voltage, and thus is not strong enough to eject an ion from the mass analyzer. However, ion motion in the axial direction is enhanced and the ion gains kinetic energy. After many collisions with the helium damping gas present in the mass analyzer, the ion gains enough internal energy to cause it to dissociate into product ions. This process is called collision-induced dissociation (CID). The amount of energy imparted in the CID process significantly influences the type of fragmentation induced; it can be increased by either increasing the resonant excitation amplitude or the time of resonant excitation [March and Todd, 1995]. Within compound classes, the amount of energy required to fragment an ion is generally proportional to the m/z of the ion. Ions of higher m/z generally require a greater resonant excitation amplitude or a longer period of time [Bier et al., 1995]. The CID process can be used to obtain structurally characteristic fragmentation patterns that can be used to identify selected analytes in complex mixtures. In the second stage of mass analysis, the product

ions are stored in the mass analyzer. They are then sequentially scanned out of the mass analyzer to produce a full product ion mass spectrum.

MSⁿ on the LCQ can have two to ten stages of mass analysis. The first two stages are similar to MS/MS except that the product ions are not scanned out. Instead, product ions of one m/z are selected and all other ions are resonantly ejected from the mass analyzer. The selected product ions now become the new parent ions for the next stage of mass analysis. With each stage of analysis, the selected parent ions undergo CID to produce product ions. In the n th stage of mass analysis, the final product ions are stored in the mass analyzer, and are then sequentially scanned out to produce a full final product ion mass spectrum.

SIM (selected ion monitoring) is a single-stage technique in which a particular ion or set of ions is monitored. Ions of one or more m/z are selected from the stored ions and all other ions are ejected from the mass analyzer. The selected ions are then sequentially scanned out of the mass analyzer to produce a SIM mass spectrum. SIM experiments are useful in detecting small quantities of a target compound in a complex mixture when the mass spectrum of the target compound is known. Thus, SIM is useful in trace analysis, because it can provide lower detection limits than full scan MS. This is possible since all ions except for the selected ions are ejected from the trap, which can significantly improve the signal-to-noise ratio (S/N). Also, since only a few ions are monitored, more time can be spent accumulating these ions into the trap. One disadvantage of SIM is reduced specificity. In SIM, only specific ions are monitored. Therefore, any compound that produces those ions appears to be the target compound. Thus, a false positive result may be obtained. To reduce the possibility of false positives, a two-stage mass analysis

technique called SRM (selected reaction monitoring) can be used in which the production of one or more targeted product ions from a specified parent ion are monitored. The specificity obtained in SRM can be much greater than that obtained in SIM, because pairs of ions are being monitored (one product ion for each parent ion). A false positive result is less likely, because the interfering compound must form an ion of the same m/z as the target compound which then fragments to form a product ion of the same m/z as the selected product ion from the target compound.

CRM is the multi-stage analog of SIM and SRM, in which a multi-step reaction path (from 3 to 10 steps) is monitored. The specificity can increase as the number of consecutive reactions monitored increases. However, the sensitivity decreases as the number of consecutive reactions monitored increases. This is especially true if there are many fragmentation pathways available to the ion being monitored.

All of the mass analyses discussed require that ions be sequentially scanned out of the ion trap. Scanning mass analysis with the LCQ uses the mass selective instability mode [Stafford et al., 1982], in which ions are scanned out of the trap along the $a_z = 0$ line in the Mathieu stability diagram (Figure 1-9). This is accomplished by having no DC potential difference between the ring electrode and the endcap electrodes. The RF drive frequency ($f_{RF} = \Omega/2\pi = 760$ kHz) and initial amplitude (storage voltage) are chosen so that all ions with a m/z value greater than a threshold value ($q_z < 0.908$ and $\beta_z < 1.0$ on mass-selective instability operating line, Figure 1-9) are stored. The minimum m/z is usually chosen to be greater than the m/z associated with air, water, and solvent ions. During ion scan out, the ring electrode RF voltage is ramped at a constant rate corresponding to approximately 5,500 Da/s (Da = dalton). As the ring electrode RF

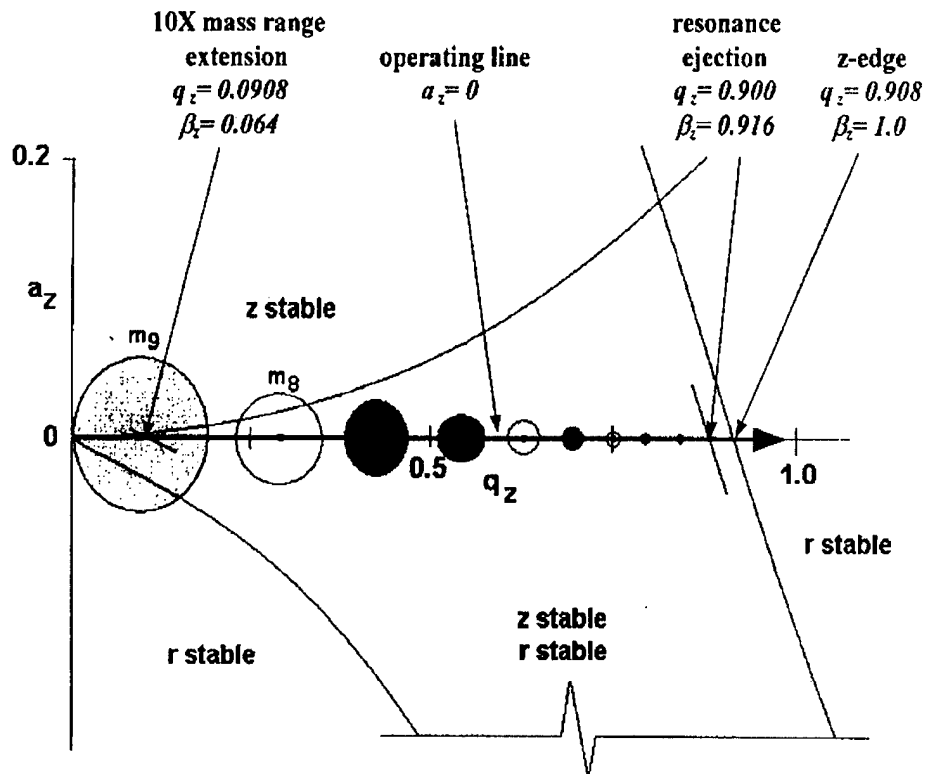


Figure 1-9. A portion of the QIT stability diagram showing the mass-selective instability operating line at $a_z = 0$. The circles represent ion q_z values on the operating line for various ions with different m/z (e.g., where $m_9^+ > m_8^+$). The mass selective instability scan is supplemented with resonance ejection at $q_z = 0.900$ for a normal scan or at $q_z = 0.0908$ to extend the mass range by a factor of 10. Reproduced from Cole, 1997.

voltage increases, ions of increasing m/z become successively unstable in the axial direction as they cross the $\beta_z = 1.0$ edge of the stability diagram (q_z of 0.908) and are ejected from the mass analyzer.

One of the inherent features of the ion trap during the mass selective instability scan is that while the ions of lower m/z are being scanned out of the ion trap to the detector, the higher m/z ions are still in the trap, and the space-charge that they contribute causes a broadening of the peaks formed as the lower m/z ions are being ejected [March and Todd, 1995]. This deleterious effect on peak shape can be reduced dramatically through a technique called axial modulation (or resonant ejection). This is performed on the LCQ by applying a supplementary oscillating field between the endcap electrodes at a frequency of just less than half of the RF drive potential (348 kHz, $\beta_z = 0.916$) and amplitude at a resonant ejection q_z of 0.900. As ions are scanned along the $a_z = 0$ line by ramping the RF voltage on the ring electrode, ions of increasing m/z consecutively come into resonance with the resonance ejection amplitude at $q_z = 0.900$. As the ions come in resonance with the supplementary RF field, the ions gain kinetic energy and are quickly ejected in a tight packet from the ion trap in the z direction. The RF voltage at which an ion is ejected from the mass analyzer is defined as its resonance ejection RF voltage. This use of axial modulation greatly improves mass resolution, and enables the trapping of a larger number of ions in the ion trap without sacrificing resolution and peak shape, since resonant ejection is more tolerant of space-charge effects.

Ions retain a narrow spatial distribution in the r -dimension and exit through a hole in the center of the endcaps. Essentially 100% of the ions can be ejected from the ion trap, but because they do so in approximately equal numbers from each endcap and only

ions ejected from one endcap are detected, ion transmission is reduced by a factor of two. Ions that exit through the exit endcap electrode are focused by the conversion dynode accelerating potential through the exit lens (at ground potential) towards the ion detection system (Figure 1-10). The ion detection system includes a 15-kV conversion dynode and a channel electron multiplier located at the rear of the vacuum manifold behind the mass analyzer. The ion detection system is oriented off-axis to the mass analyzer to prevent neutrals from striking the conversion dynode or electron multiplier. As a result, the noise is reduced.

Sample Compounds

Thirty-two different nitro (NO₂) explosives were investigated to determine their amenability to ESI and APCI, and subsequently to develop analytical methods for their trace detection. They can be divided according to the atom to which the NO₂ group is attached. Nitro compounds contain a C-NO₂ group and can be subdivided into nitroaromatic and nitroaliphatic compounds, nitrate esters contain a C-O-NO₂ group, and nitramines a C-N-NO₂ group. Several explosives were selected to be investigated from each group in order to understand the influence of chemical structure on ionization.

The nitroaromatic compounds investigated, as shown in Figure 1-11, include 2,4,6-trinitrotoluene (TNT), MW = 227; tetryl, MW = 287; 2,4,6-trinitro-*m*-cresol (TNC), MW = 243; and 2,4,6-trinitroaniline (TNA), MW = 228. The following explosives, which are also nitroaromatic, are manufacturing by-products of TNT: *o*-nitrotoluene (2-NT), MW = 137; *m*-nitrotoluene (3-NT), MW = 137; *p*-nitrotoluene (4-NT), MW = 137; 2,3-dinitrotoluene (2,3-DNT), MW = 182; 2,4-dinitrotoluene (2,4-DNT),

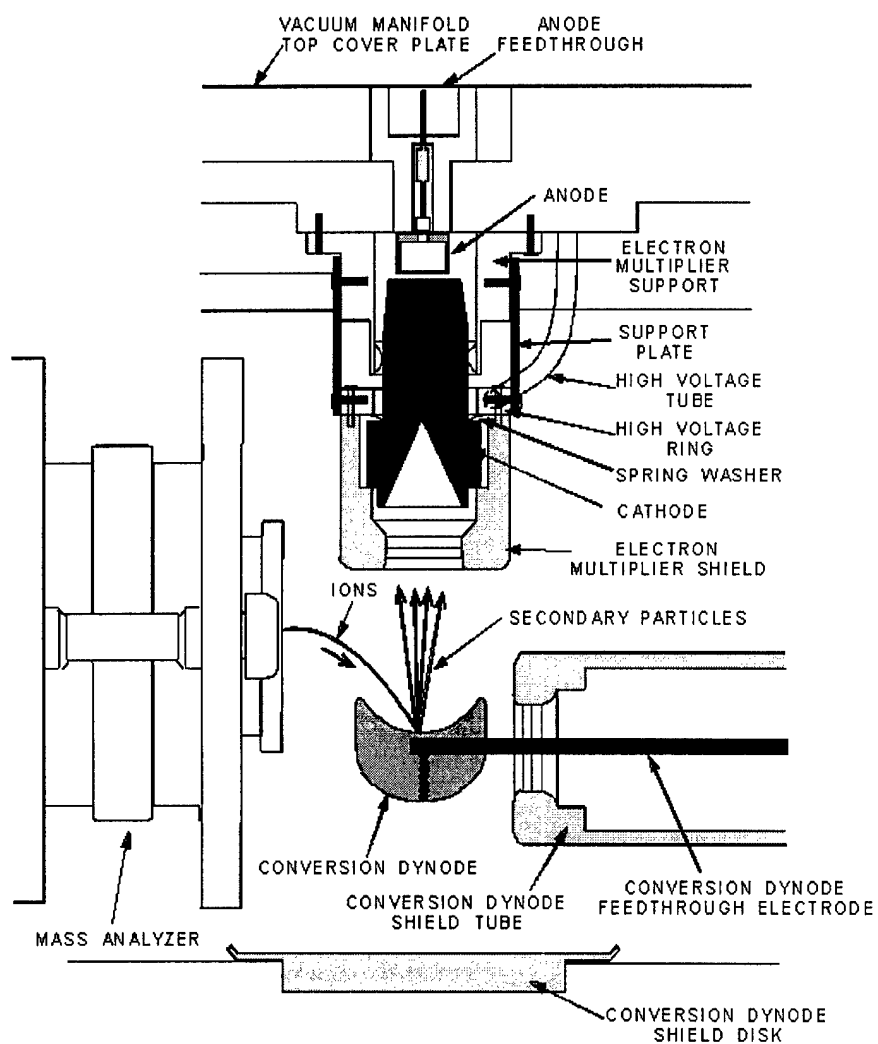


Figure 1-10. Cross sectional view of the ion detection system on the LCQ, showing the electron multiplier and the conversion dynode. Reproduced from LCQ Xcalibur software online manual.

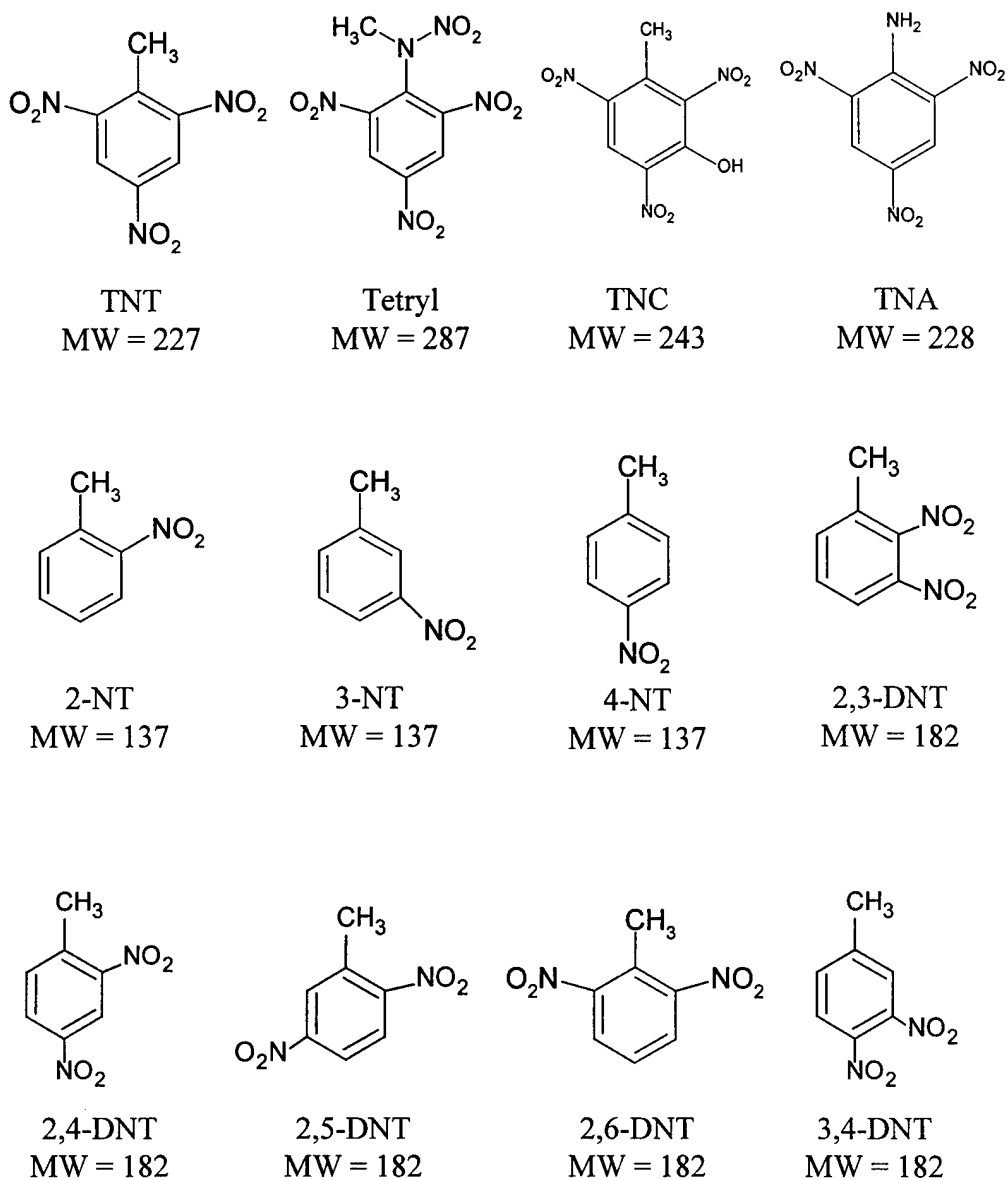


Figure 1-11. Chemical structures and molecular weights for nitroaromatic compounds.

MW = 182; 2,5-dinitrotoluene (2,5-DNT), MW = 182; 2,6-dinitrotoluene (2,6-DNT), MW = 182; and 3,4-dinitrotoluene (3,4-DNT). The TNT manufacturing process is shown in Figure 1-12 along with the typical percent yields of each by-product.

The following nitroaromatic explosives, shown in Figure 1-13, are the main degradation products of TNT formed via biotransformation and found in contaminated soil: 2-amino-4,6-dinitrotoluene (2-A-4,6-DNT), MW = 197; 4-amino-2,6-dinitrotoluene (4-A-2,6-DNT), MW = 197; 2,4-diamino-6-nitrotoluene (2,4-DA-6-NT), MW = 167; and 2,6-diamino-4-nitrotoluene (2,6-DA-4-NT), MW = 167. The biotransformation scheme of TNT is shown in Figure 1-14. Figure 1-13 shows the structure of three nitroaromatic compounds that are formed through photodecomposition of TNT from sunlight and are readily detected in pink water (explosive contaminated water). These compounds include 1,3,5-trinitrobenzene (TNB), MW = 213; 1,3-dinitrobenzene (DNB), MW = 168; and nitrobenzene (NB), MW = 123. The remaining two nitroaromatic compounds are microbial degradation products of 2,4-DNT, the most abundant by-product from the TNT manufacturing process. These compounds are 2-amino-4-nitrotoluene (2-A-4-NT), MW = 153; and 4-amino-2-nitrotoluene (4-A-2-NT), MW = 153.

The nitrate esters investigated, as shown in Figure 1-15, include pentaerythritol tetranitrate (PETN), MW = 316; 1,2,4-butanetriol trinitrate (BTTN), MW = 241; 1,1,1-trimethylolethane trinitrate (TMETN), MW = 255; diethyleneglycoldinitrate (DEGDN), MW = 196; and triethyleneglycoldinitrate (TEGDN), MW = 240.

The nitramines investigated, as shown in Figure 1-16, include nitroguanidine (NQ), MW = 104; 1,3,5-trinitro-1,3,5-triazacyclohexane (RDX), MW = 222; 1,3,5,7-tetranitro-1,3,5,7-tetrazacyclooctane (HMX), MW = 296; 2,4,6,8,10,12-hexanitro-

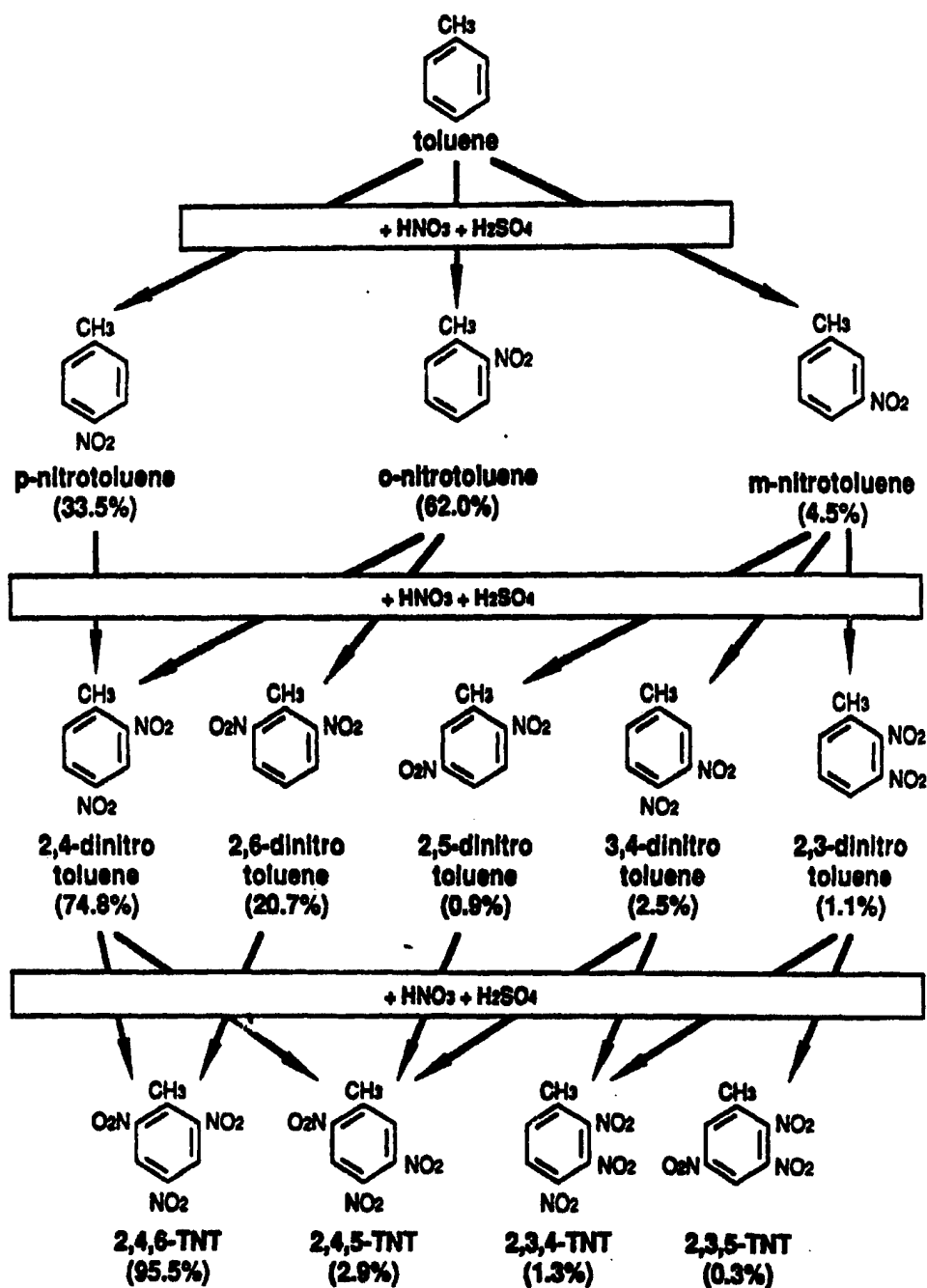


Figure 1-12. TNT process chemistry: three-stage nitration of toluene with nitric and sulfuric acids. Adapted from technical manual for military explosives TM-9-1300-214. Undated.

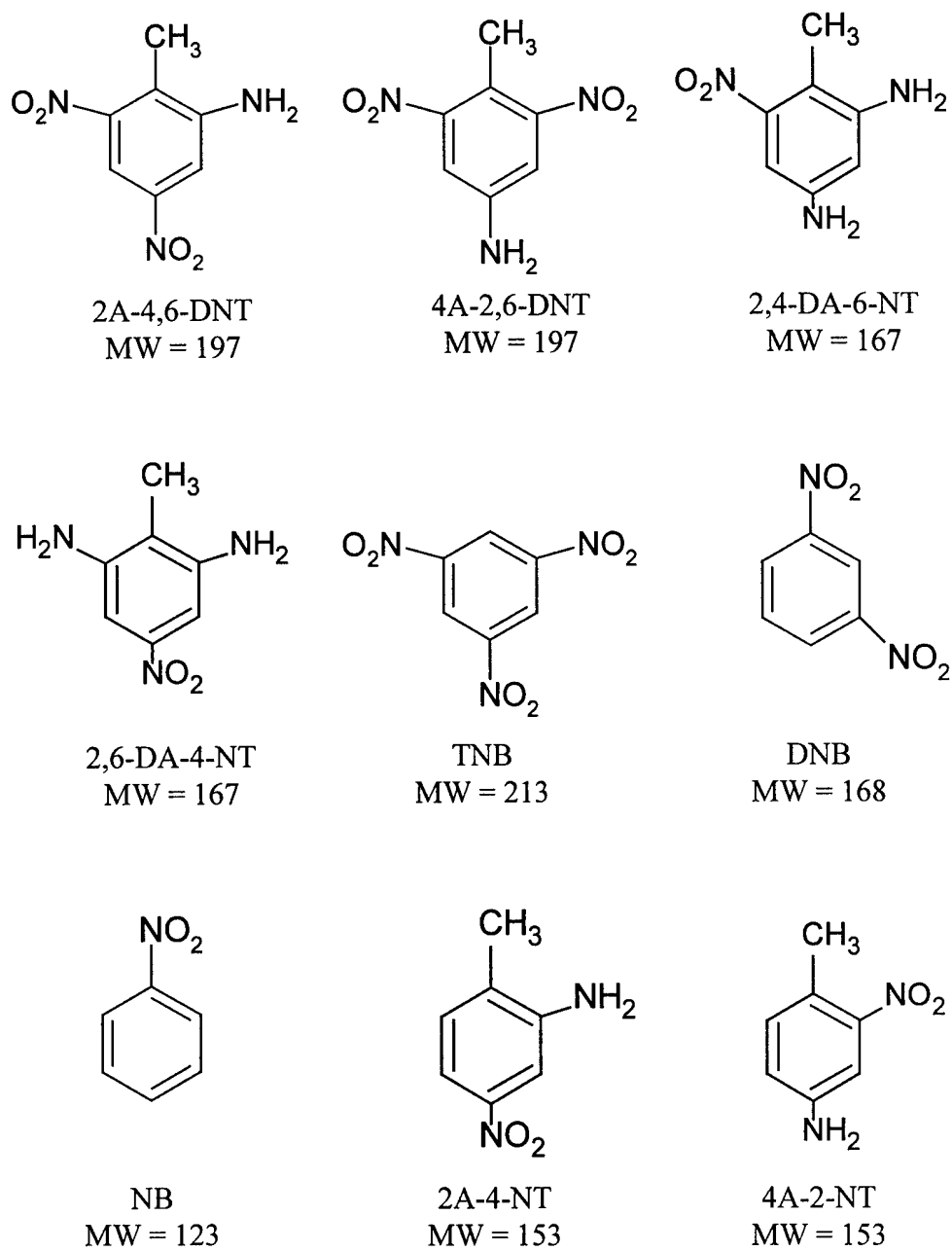


Figure 1-13. Chemical structures and molecular weights for nitroaromatic compounds.

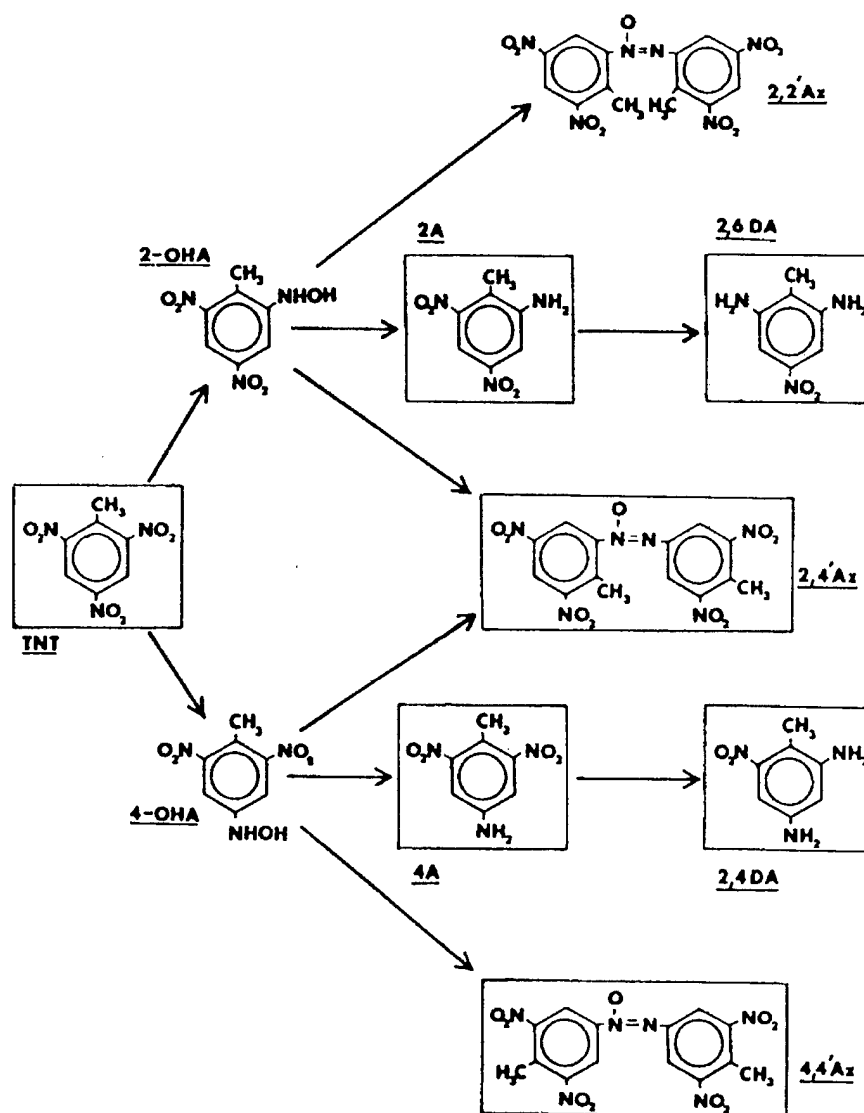


Figure 1-14. Biotransformation scheme of TNT in compost. Compounds boxed were identified in solvent extracts. Adapted from Kaplan, D.L. and Kaplan, A.M., *Appl. Environ. Microbiol.*, **1982**, 44, 757.

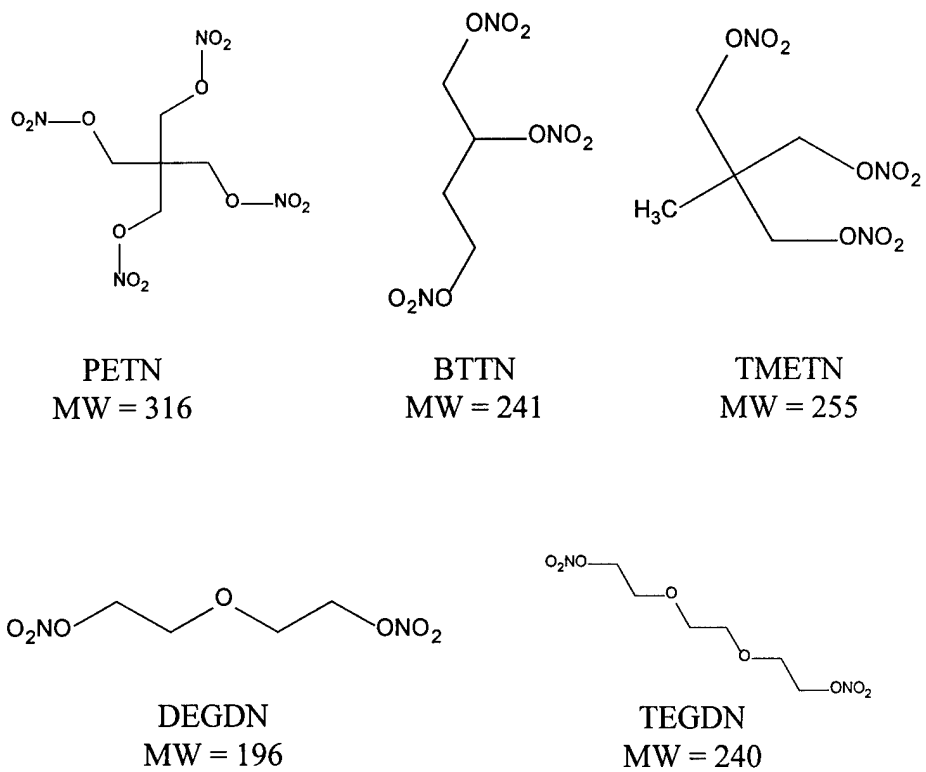


Figure 1-15. Chemical structures and molecular weights for nitrate esters.

2,4,6,8,10,12-hexazaisowurtzitane (CL-20), MW = 438; and 1,3,3-trinitroazetidine (TNAZ), MW = 192. Only one nitroaliphatic compound, 5-nitro-2,4-dihydro-3*H*-1,2,4-triazol-3-one (NTO), MW = 130 (Figure 1-16) was investigated.

2-A-4,6-DNT and 4-A-2,6-DNT samples were provided by Dr. Fred Volk of the Fraunhofer Institute of Chemical Technology, Germany. BTTN, TMETN, DEGDN, TEGDN, NQ, CL-20, TNAZ, and NTO samples were provided by the High Explosive Research and Development (HERD) Facility at Eglin AFB, Florida. All of the remaining explosive samples were provided by Dr. Jehuda Yinon of the Weizmann Institute of Science, and obtained from the Analytical Laboratory of the Israeli Police Headquarters. All samples were acquired in a dry crystalline form from one of our two collaborators, and were stored in a dessicator and refrigerated at 4°C to prevent decomposition. All stock solutions were prepared by dissolving the samples in acetone to a concentration of approximately 1000 to 2000 ppm (1-2 mg/mL). The stock solutions were also refrigerated at 4°C.

Thesis Overview

This thesis is organized into six chapters. Chapter 1 is the introduction to the research and gives the background information on the instrumentation and test compounds that were used. Chapter 2 covers the optimization of ESI and APCI parameters, characteristic ions formed by explosives in ESI and APCI, and their MS/MS spectra. The adduct ion formation of explosives in ESI and APCI is discussed in Chapter 3. Chapter 4 covers the development of LC/APCI-MS and LC/APCI-MS/MS methods based on chloride adducts of explosives. Chapter 5 discusses the trace detection of

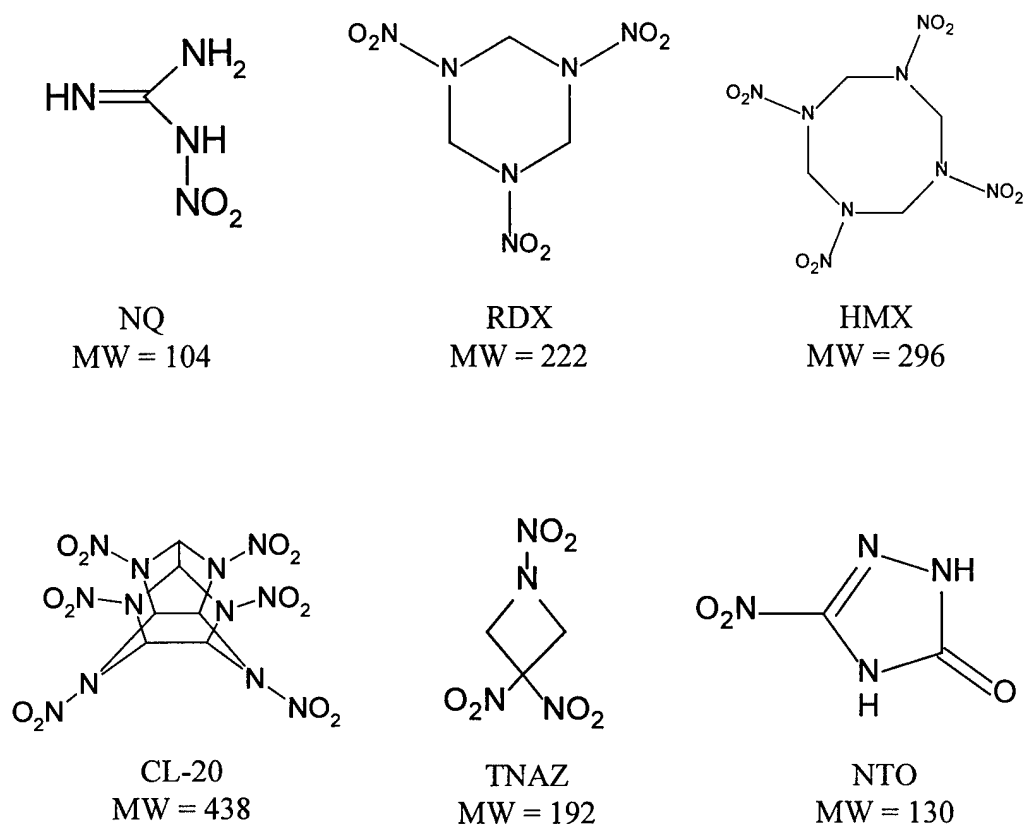


Figure 1-16. Chemical structures and molecular weights for nitramines and NTO (nitroaliphatic compound).

explosives in environmental and forensic samples by application of the LC/APCI-MS and LC/APCI-MS/MS methods described in Chapter 4. Chapter 6 summarizes the major conclusions presented in this work and gives suggestions for future work in this area.

CHAPTER 2

PRINCIPLES OF ESI-MS, APCI-MS, AND MS/MS OF EXPLOSIVES

A method using ESI-MS or APCI-MS for the trace detection of explosives in forensic and environmental applications would have great importance. Explosives are thermally labile compounds, whose mass spectra formed from hard ionization techniques (e.g. EI, CI and ECNCI) are typically complicated with various fragment ions and little or no information about the intact molecule itself. This often makes the trace detection of explosives in complex matrices (e.g. soil, soot, and waste water) difficult, because the mass spectra are already overridden with background ions from the matrix. ESI and APCI are soft ionization techniques that have already been shown in the literature [Straub and Voyksner, 1993; Casetta and Garofolo, 1994; Schilling, 1996; Yinon et al., 1997; McAvoy et al., 1999; McClellan et al., 1999; Cassada et al., 1999; and Schreiber et al., 2000] to produce less fragmentation of explosives and provide molecular or molecular type ions (e.g., protonated or deprotonated species or adduct ions) of suitable intensity for their trace detection.

The LCQ can operate in either of two ion polarity modes, positive or negative. Both positively and negatively charged ions are formed in the API source of the MS detector. The LCQ can control whether positive ions or negative ions are transmitted to the mass analyzer for mass analysis by changing the polarity of the potentials applied to the API source and ion optics. In ESI, preformed ions in solution are transformed into ions in the gas phase. The ion polarity of choice is determined by the polarity of the preformed ions in solution; acidic molecules form negative ions in solution and basic

molecules form positive ions. However, most explosives are not easily protonated or deprotonated in solution. Negative ESI-MS has been shown to be the best choice of polarity for the ionization of explosives, because the bulky electron-withdrawing nitro groups in the neutral explosives facilitate the formation of anions in solution [Straub and Voyksner, 1993]. APCI-MS of explosives has also shown enhanced sensitivity in the negative mode due to the charge-stabilizing electronegative nitro groups, and because of the propensity for some compounds to undergo electron capture [Schilling, 1996]. An added benefit of using negative ionization for ESI and APCI is that less chemical noise is typically generated from other sample components than positive ionization, therefore resulting in improved selectivity. The ESI-MS and APCI-MS of a variety of nitro explosives were studied, including nitroaromatic compounds, nitramines, nitrate esters, and one nitroaliphatic compound, on a commercial QITMS, the Finnigan LCQ. Results from ESI-MS, APCI-MS and tandem mass spectrometry (MS/MS) are presented.

Experimental

Instrumentation

All experiments were performed on the Finnigan LCQ (San Jose, CA), a commercial, bench-top QITMS instrument with the ability to perform both ESI and APCI. For ESI experiments, samples were infused into the mass spectrometer at a flow rate of 5 $\mu\text{L}/\text{min}$ using the LCQ syringe pump and analyzed in the negative ion mode of the LCQ. Some compounds were more amenable to positive ionization due to the presence of basic functional groups (e.g. R-NH_2), and these compounds were analyzed in the positive ion mode of the LCQ. Each ESI spectrum presented is the average of 50 analytical scans, each consisting of 3 microscans. The maximum injection time was set

to 50 ms. For data acquisition in the negative ion mode, the AGC target values for full scan and MS/MS scans were lowered by a factor of two (2×10^7 for full scan and 2×10^6 for MSⁿ), compared to the values for positive ions, because the detector gain for positive ions is about 2 times higher than that for negative ions [Schwartz et al., 1998].

For APCI experiments, samples were introduced into the mass spectrometer via flow injection analysis (also called loop injection analysis). Sample solutions were loaded into a 100 μ L sample loop, and then flushed into the APCI source at 1 mL/min with the solvent from an LC, producing a flow injection peak of about 6 s in width. The LCQ syringe pump was not used, because higher flow rates are required for APCI (0.5 to 2.0 mL/min) compared to ESI (1 to 10 μ L/min). Operating at flow rates lower than 0.4 mL/min is often insufficient to maintain a stable corona discharge for APCI [Cole, 1997]. The maximum allowable flow rate on the LCQ syringe pump is 100 μ L/min. The large sample loop volume was used to increase the width of the flow injection peak. The negative ion mode was used for all explosives. Some explosives were not efficiently ionized in the negative mode, and proved to be more amenable to positive ionization. In these cases, the positive ion mode was used. The number of analytical scans averaged for each APCI spectrum presented was dependent on the width of the flow injection peak, and each analytical scan consisted of 3 microscans. The same maximum injection times and AGC target values were used as in the ESI experiments.

The LCQ software was used to tune various operating parameters for the API source and ion optics. During sample introduction, these parameters were changed to optimize the ion intensity of the molecular or similar ion of the sample ($[M-H]^-$ or $[M]^-$ for negative; $[M+H]^+$ or $[M]^+$ for positive). It is difficult to optimize tune parameters during flow injection analysis due to the transient sample signal; therefore ion optics

settings determined in ESI were applied to APCI, and only API parameters were optimized individually.

MS/MS spectra of the explosives were acquired in ESI rather than APCI mode due to the ease of ion interrogation during continuous infusion compared to flow injection analysis. This is possible because the characteristics of MS/MS data are typically not dependent on the processes by which the ions are formed. Molecular or molecular-type ions were isolated with the narrowest isolation window which did not reduce the ion signal. Explosives form fragile ions that require larger isolation widths than stable ions in order to be isolated without fragmentation [McClellan et al., 1999]. This is because fragile ions are more sensitive to the isolation waveform applied during isolation and can fragment if the isolation window is too narrow.

Ions formed from explosives also typically require lower collision energies to achieve efficient CID. In order to fragment a selected parent ion efficiently, an appropriate resonance excitation amplitude must be applied to resonantly excite the ion for CID. If too low a resonant excitation amplitude is applied, the ion will not fragment efficiently; or, whereas if the resonant ejection amplitude is too great, the ion will be ejected from the trap. The resonant excitation amplitude on the LCQ is applied as a percentage of an activation amplitude. The input activation percentage is then mass-normalized to generate the appropriate resonant excitation to be applied to the endcaps [Schwartz et al., 1999]. For the MS/MS experiments, the maximum activation amplitude was increased to the point where the parent ion intensity was reduced to 5-10%.

Samples

The sample solutions for the ESI experiments were prepared by diluting the acetone stock solutions to a concentration of 20 ppm with 50% HPLC-grade isopropanol

(IPA): 50% HPLC-grade water (H_2O) (v/v). IPA was used with electrospray, because it has been shown to assist in solution nebulization, desolvation, and transfer of ions in solution to the gas phase [Straub and Voyksner, 1993]. H_2O was necessary to support the formation of ions in solution, but was limited to 50% due to its relatively high surface tension and solvation energy, which makes ion desorption difficult. For negative ESI, 0.1% ammonium hydroxide (NH_4OH) was added to promote deprotonation of solvent or sample molecules, whereas 0.1% acetic acid (HAc) was added to promote protonation during positive ESI.

The sample solutions for the APCI experiments were prepared by diluting the acetone stock solutions to a concentration of 20 ppm with 35% HPLC-grade H_2O : 65% HPLC-grade methanol (MeOH) (v/v). APCI is less sensitive to solvent conditions than ESI, and in general, most solvents are compatible with APCI. However when analyzing explosives, it is useful to use solvents that are easily vaporized, so that lower vaporizer temperatures can be used to prevent thermal degradation of the thermally labile explosives.

Results and Discussion

Nitroaromatic Compounds

The ESI-MS spectrum of 2,4,6-trinitrotoluene (TNT) (Figure 2-1A) shows the production of the $[\text{M}-\text{H}]^-$ ion at m/z 226. The ESI of TNT has been reported to produce $[\text{M}-\text{H}]^-$ and $[\text{M}]^-$ ions, whose ratios are dependent upon the pH of the solution [McClellan, 2000]. Since the ESI of TNT was performed with 0.1% NH_4OH , the majority of TNT was ionized as the $[\text{M}-\text{H}]^-$ ion. In contrast, the APCI-MS spectrum of TNT (Figure 2-1B) shows the predominant formation of the $[\text{M}]^-$ ion at m/z 227 when no

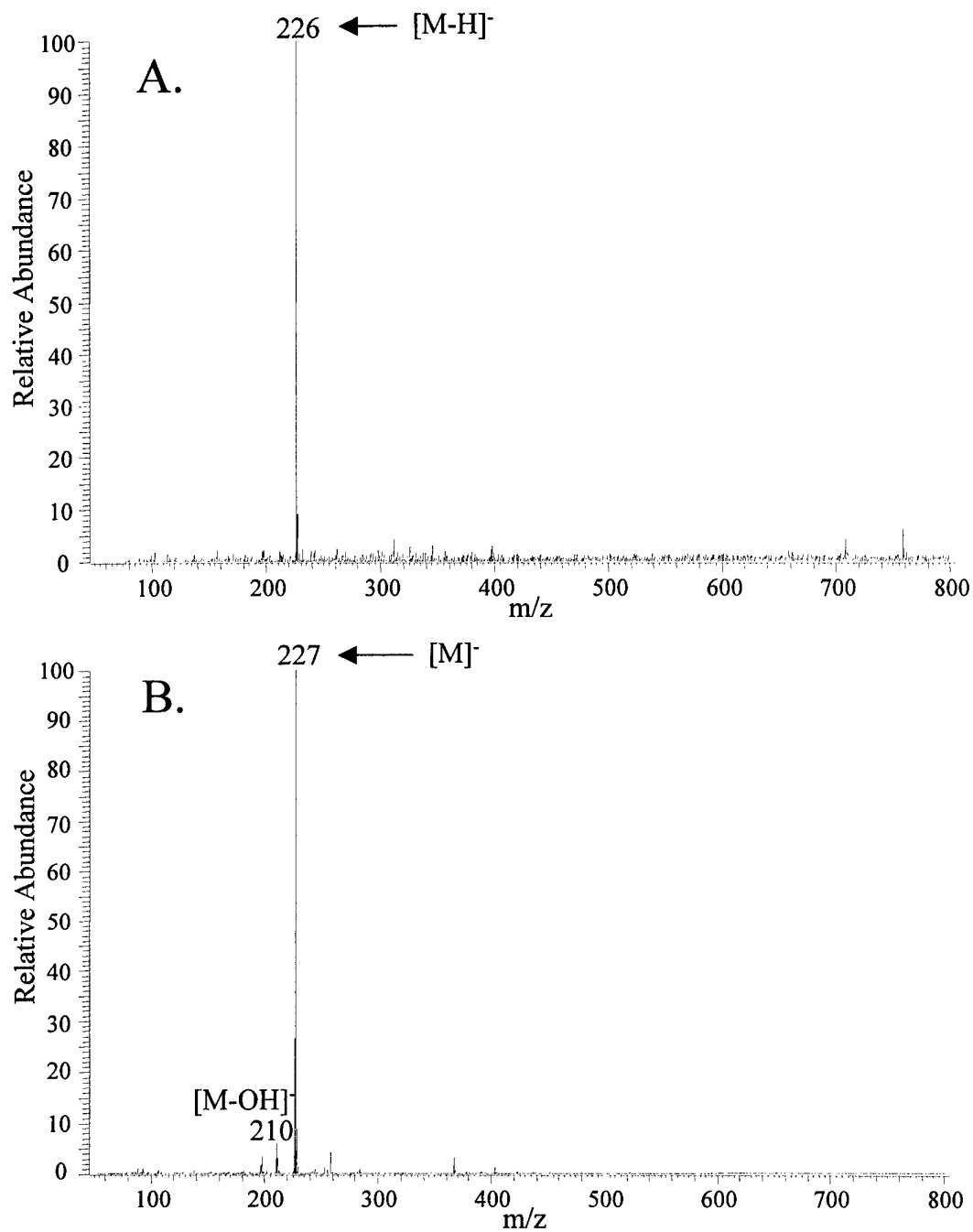
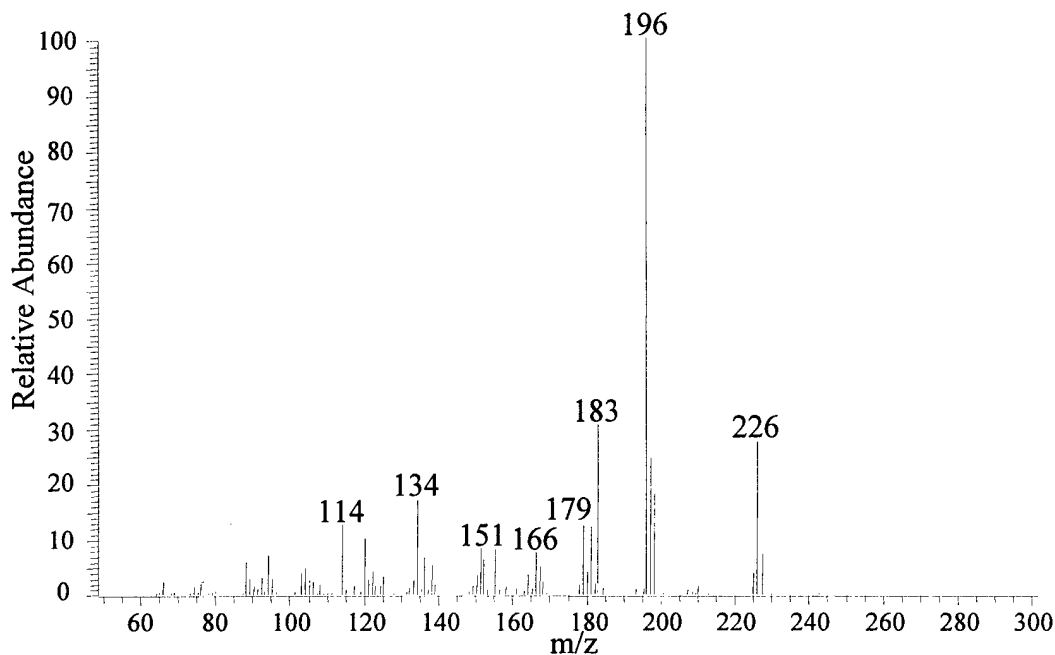


Figure 2-1. Mass spectra of TNT (MW = 227): A. Negative ESI, B. Negative APCI.

NH₄OH is added. The APCI-MS spectrum also shows a very low intensity fragment ion, [M-OH]⁻, at m/z 210. The MS/MS spectrum of the [M-H]⁻ ion of TNT (Figure 2-2) shows the production of characteristic daughter ions that are consistent with those observed in the CID of the [M]⁻ ion produced via NCI [Yinon and Zitrin, 1993].

The ESI-MS spectrum of tetryl (Figure 2-3A) does not include any molecular-type ions, but it does contain an assortment of fragment ions, adduct ions, and dimer ions. The spectrum of tetryl is further complicated by the presence of its hydrolysis product, *N*-methylnitrobenzamide, which also forms fragment ions and adduct ions. Tetryl undergoes hydrolysis to form *N*-methylnitrobenzamide in the ion source of the mass spectrometer, and its abundance is dependent on the amount of residual water and the pressure in the source [Yinon et al, 1993]. This is apparent in the APCI-MS spectrum of tetryl (Figure 2-3B), which shows a greater abundance of the [M-H]⁻ ion (m/z 241) of *N*-methylnitrobenzamide. There is more water present in the APCI source compared to the ESI source due to the higher flow rate (1 mL/min compared to 5 μL/min) of the solution, which also results in a higher pressure. Fragment ions, adduct ions, and dimer ions are also present in the APCI-MS spectrum of tetryl. The MS/MS spectrum of the [M+Cl]⁻ ion (m/z 322) of tetryl is shown in Figure 2-4, daughter ions at m/z 257, 246, and 199, corresponding to the neutral losses of 65 amu (Cl + NO), 76 amu (NO₂ + NO), and 123 amu (2NO₂ + NO + H), respectively.

The ESI-MS spectrum of 2,4,6-trinitro-*m*-cresol (TNC) (Figure 2-5A) shows the production of one molecular-type ion, [M-H]⁻, at m/z 242. The APCI-MS spectrum of TNC (Figure 2-5B) also shows the presence of [M-H]⁻ even without the addition of 0.1% NH₄OH, because a proton is easily abstracted from the OH group on the aromatic ring of the molecule. The APCI of TNC also produces fragment ions and sodiated dimer clusters



Daughter Ions of $[M-H]^-$ Ion (m/z 226) of TNT

Daughter Ions (m/z)	Neutral Loss (amu)	Neutral(s) Lost
196	30	NO
183	43	NO + CH
179	47	NO + OH
166	60	2NO
151	75	2NO + CH ₃
134	92	2NO ₂
114	112	--

Figure 2-2. Daughter ion mass spectrum of $[M-H]^-$ ion (m/z 226) produced by ESI of TNT. Spectrum acquired at a resonant excitation q_z of 0.25, isolation window of 3 amu, and collision energy of 30%.

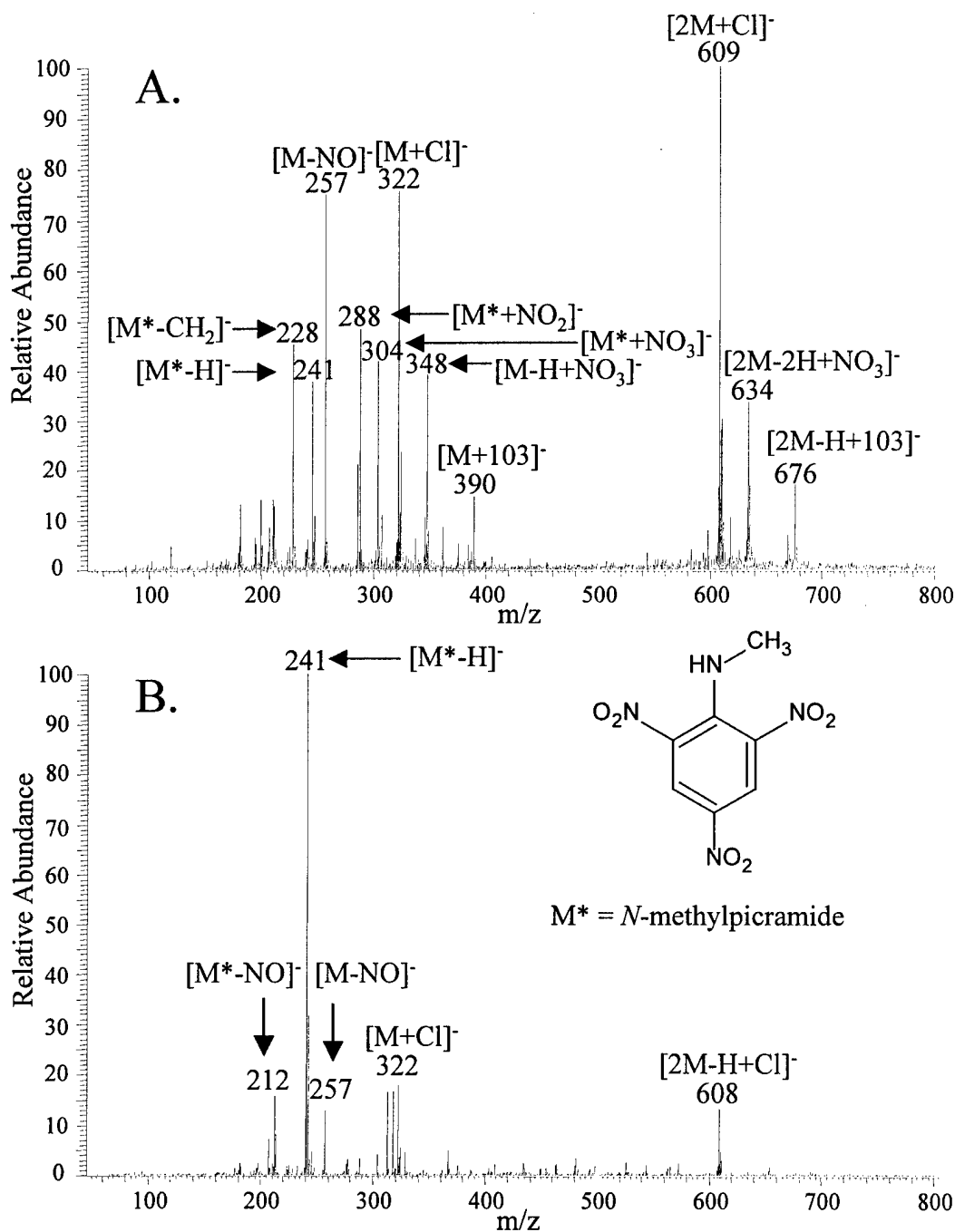
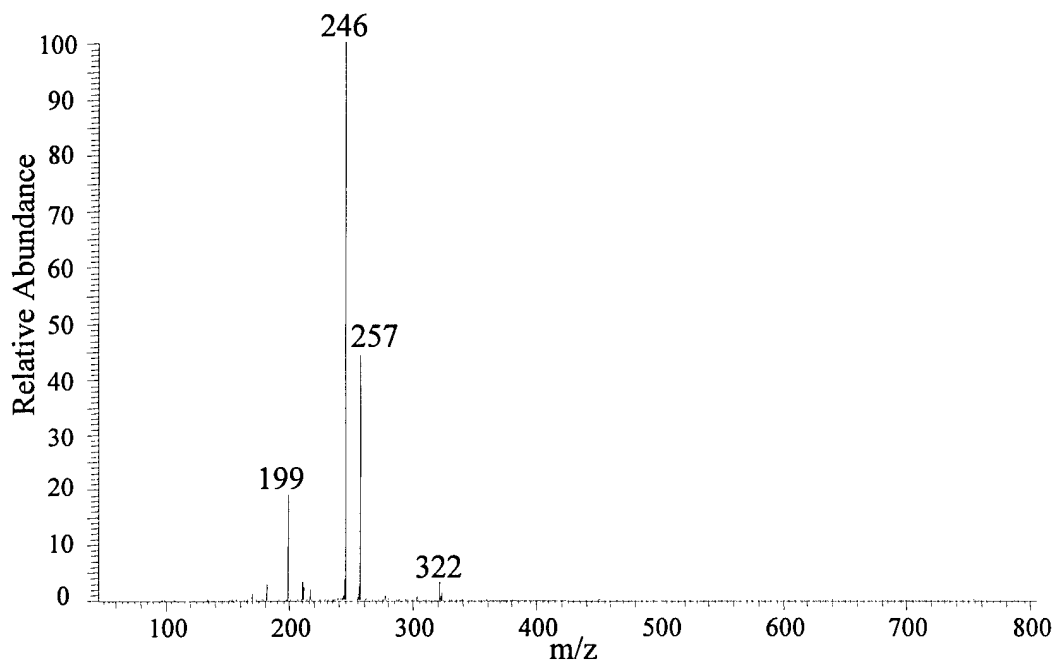


Figure 2-3. Mass spectra of tetryl (MW = 287): A. Negative ESI, B. Negative APCI. The inset shows the structure of *N*-methylpicramide, the hydrolysis product of tetryl.



Daughter Ions of $[M+Cl]^-$ Ion (m/z 322) of Tetryl

Daughter Ions (m/z)	Neutral Loss (amu)	Neutral(s) Lost
257	65	Cl + NO
246	76	NO ₂ + NO
199	123	2NO ₂ + NO + H

Figure 2-4. Daughter ion mass spectrum of $[M+Cl]^-$ ion (m/z 322) produced by ESI of tetryl. Spectrum acquired at a resonant excitation q_z of 0.25, isolation window of 3 amu, and collision energy of 18%.

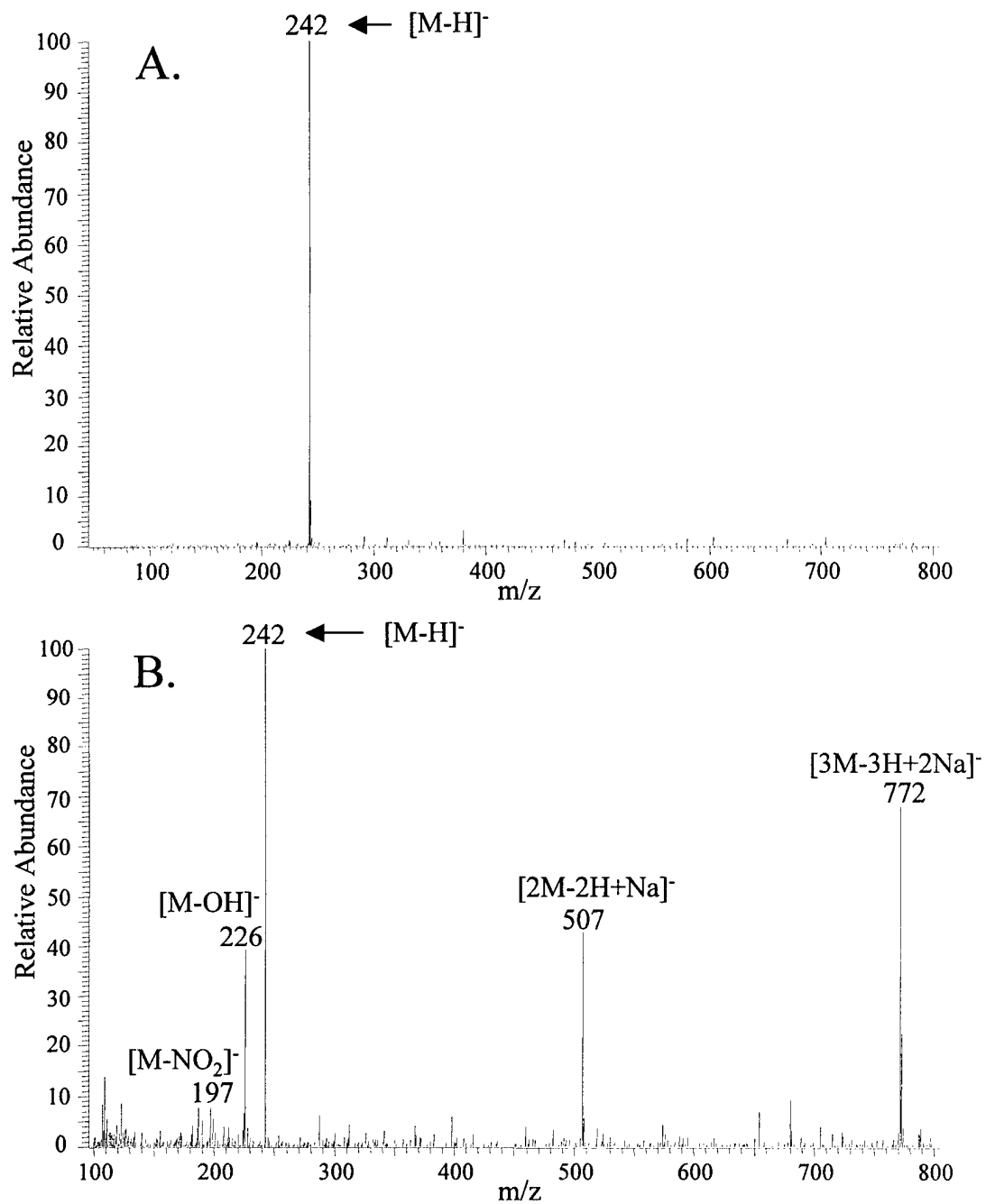
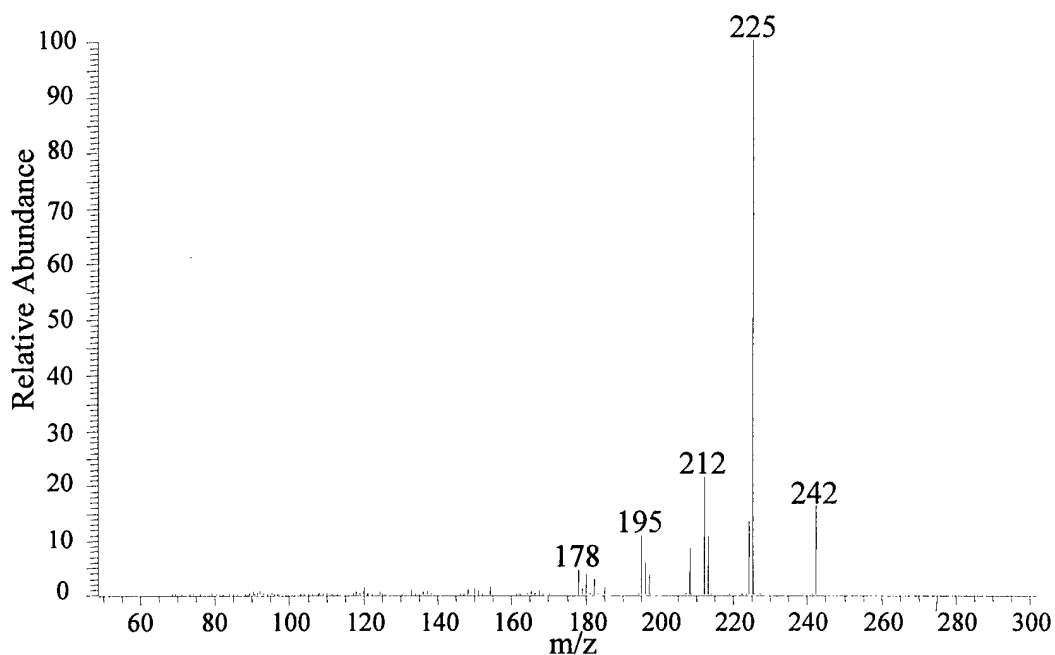


Figure 2-5. Mass spectra of TNC (MW = 243): A. Negative ESI, B. Negative APCI.

at m/z 507 $[2M-2H+Na]^-$, m/z 772 $[3M-3H+2Na]^-$, m/z 226 $[M-OH]^-$, and m/z 197 $[M-NO_2]^-$. The daughter ion spectrum of the $[M-H]^-$ ion (m/z 242) of TNC (Figure 2-6) shows one very intense ion at m/z 225 from the neutral loss of 17 amu (OH), along with three minor daughter ions at m/z 212, 195, and 178 corresponding to neutral losses of 30 amu (NO), 47 amu (NO + OH), and 64 amu (NO + 2OH), respectively.

The ESI-MS spectrum of 2,4,6-trinitroaniline (TNA) (Figure 2-7A) shows the base peak ion to be the acetone adduct $[M+acetone-H]^-$ at m/z 285 with a less intense molecular ion $[M]^-$ at m/z 228. The acetone could come from the stock solutions that were prepared in acetone and from rinsing the syringe with acetone between injections. The APCI-MS spectrum of TNA (Figure 2-7B) shows the most intense ion to be the $[M-H]^-$ ion at m/z 227. The APCI of TNA also produces a couple fragment ions, $[M-NO_2]^-$ at m/z 182 and $[M-OH]^-$ at m/z 211. These fragment ions are also present in the MS/MS spectrum of the $[M]^-$ ion of TNA (Figure 2-8) along with the most intense fragment ion at m/z 198, corresponding to a neutral loss of 30 amu (NO).

TNT is the most widely used military explosive because of its low melting point, its stability, its low sensitivity to impact, friction and high temperature, and its relatively safe methods of manufacture. During the two World Wars, millions of tons of TNT were produced and used mainly as an ingredient in binary explosives [Yinon, 1990]. Because TNT is toxic, as are most explosives, the disposal of obsolete explosives and production waste from munition-manufacturing plants constitutes a serious environmental problem. A single TNT-manufacturing plant can generate as much as 500,000 gallons of wastewater per day, which contain TNT and manufacturing byproducts [Yinon and Zitrin, 1993]. The toxicity of these TNT byproducts is not well known, but they are also of environmental concern.



Daughter Ions of $[M-H]^-$ Ion (m/z 242) of TNC

Daughter Ions (m/z)	Neutral Loss (amu)	Neutral(s) Lost
225	17	OH
212	30	NO
195	47	NO + OH
178	64	NO + 2OH

Figure 2-6. Daughter ion mass spectrum of $[M-H]^-$ ion (m/z 242) produced by ESI of TNC. Spectrum acquired at a resonant excitation q_z of 0.25, isolation window of 1 amu, and collision energy of 34%.

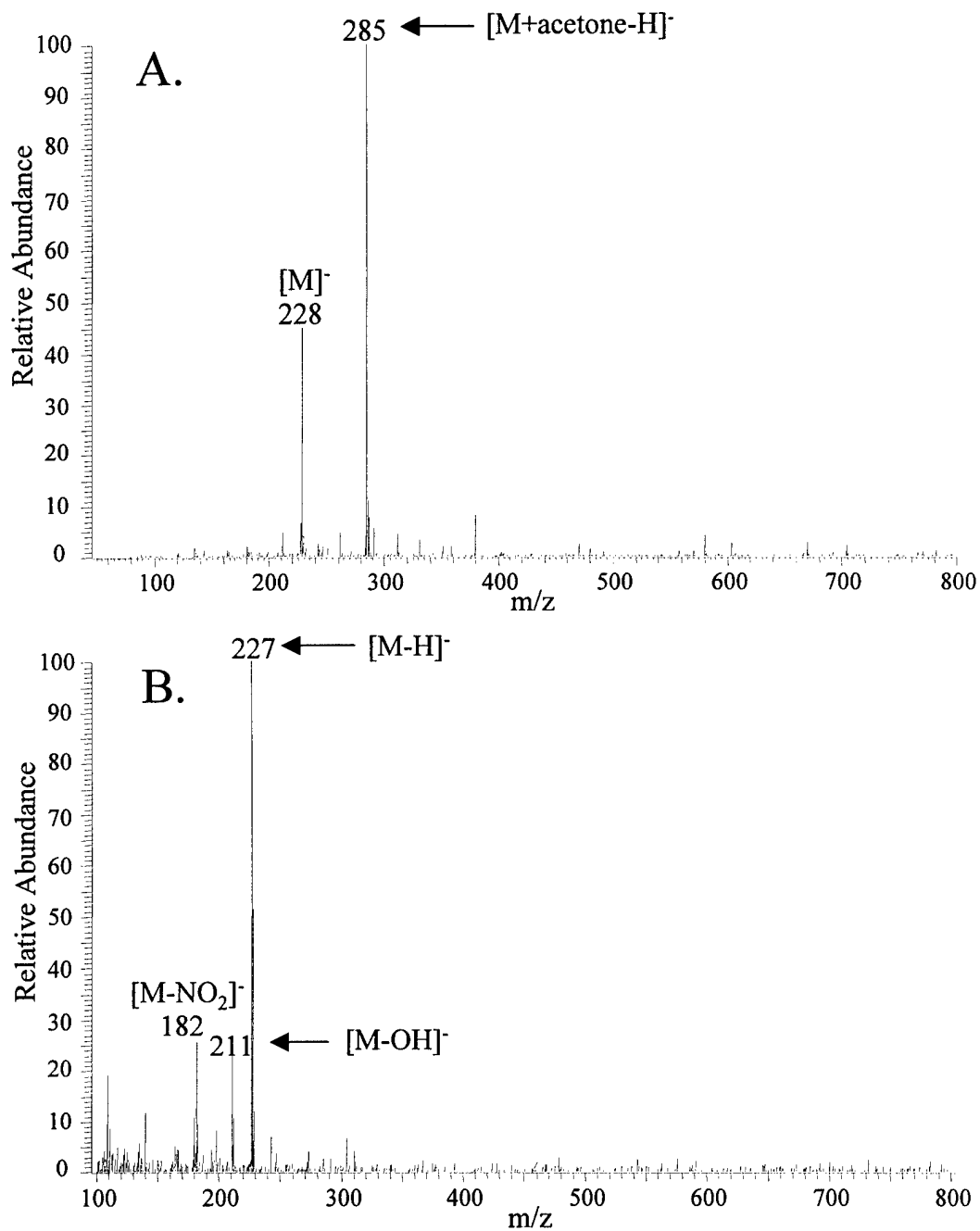
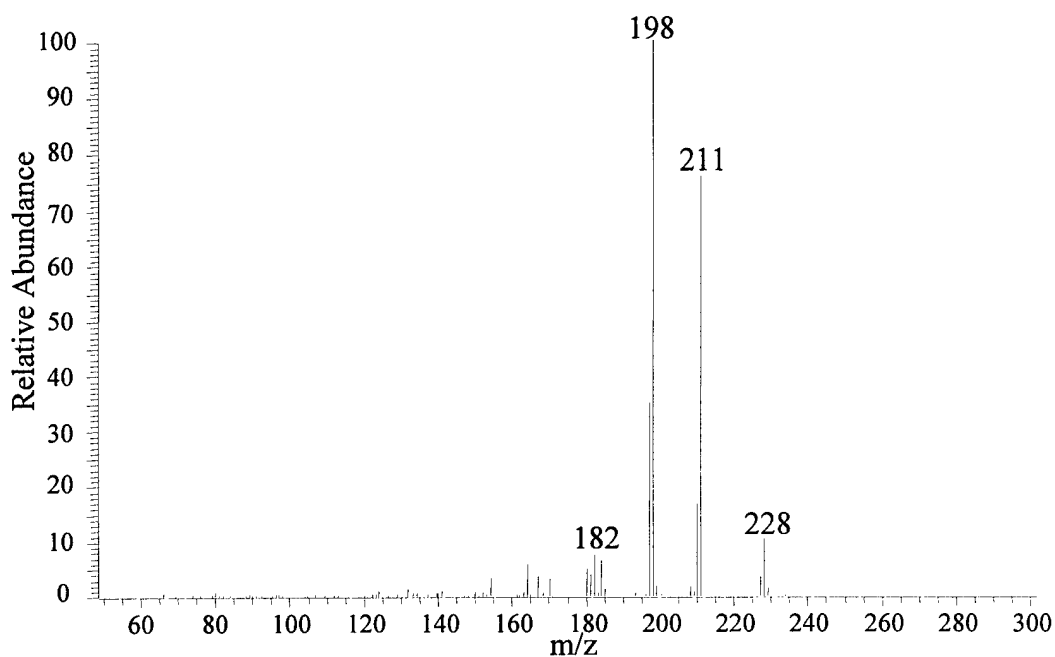


Figure 2-7. Mass spectra of TNA (MW = 228): A. Negative ESI, B. Negative APCI.



Daughter Ions of $[M]^+$ Ion (m/z 228) of TNA

Daughter Ions (m/z)	Neutral Loss (amu)	Neutral(s) Lost
211	17	OH
198	30	NO
182	46	NO ₂

Figure 2-8. Daughter ion mass spectrum of $[M]^+$ ion (m/z 228) produced by ESI of TNA. Spectrum acquired at a resonant excitation q_z of 0.25, isolation window of 2 amu, and collision energy of 28%.

Eight byproducts from the TNT manufacturing process (Figure 1-12) were analyzed with ESI-MS and APCI-MS. ESI-MS was not successful in detecting *o*-nitrotoluene (2-NT), *m*-nitrotoluene (3-NT), *p*-nitrotoluene (4-NT), 2,3-dinitrotoluene (2,3-DNT), 2,4-dinitrotoluene (2,4-DNT), 2,5-dinitrotoluene (2,5-DNT), 2,6-dinitrotoluene (2,6-DNT), and 3,4-dinitrotoluene (3,4-DNT). Since ESI is dependent on the formation of ions in solution, such as deprotonation, these compounds were difficult to detect due to the low acidity of the methyl group. The three nitro groups on TNT are electron-withdrawing and aid in the deprotonation of the methyl group when a base is present in excess of TNT [Bernasconi, 1971]. The acidity of the methyl group decreases with fewer nitro groups on the aromatic ring, which makes ionization via deprotonation difficult. In the literature, these compounds have also proven difficult to detect except for 2,4-DNT, which was successfully detected by preferentially forming an adduct ion from an ammonium salt solution. The acetate adduct $[M+CH_3COO]^-$ of 2,4-DNT (m/z 241) was detected using ESI-MS when 2 mM ammonium acetate was added to an aqueous solution of acetonitrile (ACN) at 50% [Casetta and Garofolo, 1994]. The formate adduct $[M+CHOO]^-$ of 2,4-DNT at m/z 227 was detected using ESI-MS when 0.5 mM ammonium formate was used [Cassada et al, 1999]. The use of additives to form adduct ions holds promise for compounds that are difficult to detect (See Chapter 3).

APCI-MS was not able to detect 3-NT, 2,3-DNT, 2,5-DNT, and 3,4-DNT, but was successful at detecting 2-NT, 4-NT, 2,4-DNT, and 2,6-DNT. Nitro groups on the ortho (e.g. 2-NT) and para (e.g. 4-NT) position of toluene act to stabilize the ion due to the activating and ortho, para-directing properties of the methyl substituent. Nitro groups in the meta position (e.g. 3-NT) destabilize the charge on the ion, making this ion less abundant due to its instability, and therefore compounds of this sort are difficult to detect.

The APCI-MS spectrum of 2-NT (Figure 2-9A) and 4-NT (Figure 2-9B) both contain one ion at m/z 367, which is proposed to be a dimer cluster, adduct ion, or ionized impurity present in both 2-NT and 4-NT. MS/MS of m/z 367 produces one intense daughter ion at m/z 177 with a neutral loss of 190 (data not shown).

The APCI of 2,4-DNT (Figure 2-10A) yields an $[M-H]^-$ ion as the base peak at m/z 181 and an acetone adduct ion $[M+\text{acetone}-H]^-$ at m/z 239. The APCI of 2,6-DNT (Figure 2-10B) produces an acetone adduct ion $[M+\text{acetone}-H]^-$ at m/z 239 as the most intense ion along with ions at m/z 213 and m/z 181, corresponding to $[M+\text{MeOH}-H]^-$ and $[M-H]^-$, respectively. Methanol has been observed to form adducts with other explosives in APCI including 1,3,5,7-tetranitro-1,3,5,7-tetrazacyclooctane (HMX) and pentaerythritol (PETN) [McAvoy et al., 1999]. Proton abstraction from methanol produces a methyloxy (CH_3O^-) ion, which is a strong Brønsted base (almost as strong as OH^-) that reacts readily with many organic compounds with proton affinities lower than 379 kcal/mol [Harrison, 1983]. The MS/MS spectrum of the $[M]^-$ ion of 2,4-DNT (Figure 2-11) shows daughter ions at m/z 165, 152, 137, 122, and 116, corresponding to neutral losses of 17 amu (OH), 30 amu (NO), 45 amu ($\text{NO} + \text{CH}_3$), 60 amu (2NO), and 66 amu ($\text{NO} + 2\text{H}_2\text{O}$), respectively. The 2,6-DNT signal intensity was too weak to obtain a daughter ion spectrum.

The biotransformation products of TNT were readily detected with ESI-MS due to the amine substituents, which are more acidic (by a factor of $\sim 10^{10}$) than the methyl group [Bernasconi, 1971]. The ESI-MS spectra of 2-amino-4,6-dinitrotoluene (2A-4,6-DNT) (Figure 2-12A) and 4-amino-2,6-dinitrotoluene (4A-2,6-DNT) (Figure 2-13A) both show an intense $[M-H]^-$ ion at m/z 196. The APCI-MS spectra of 2A-4,6-DNT (Figure 2-12B) and 4A-2,6-DNT (Figure 2-13A) also show the same $[M-H]^-$ ion at m/z 196 at a

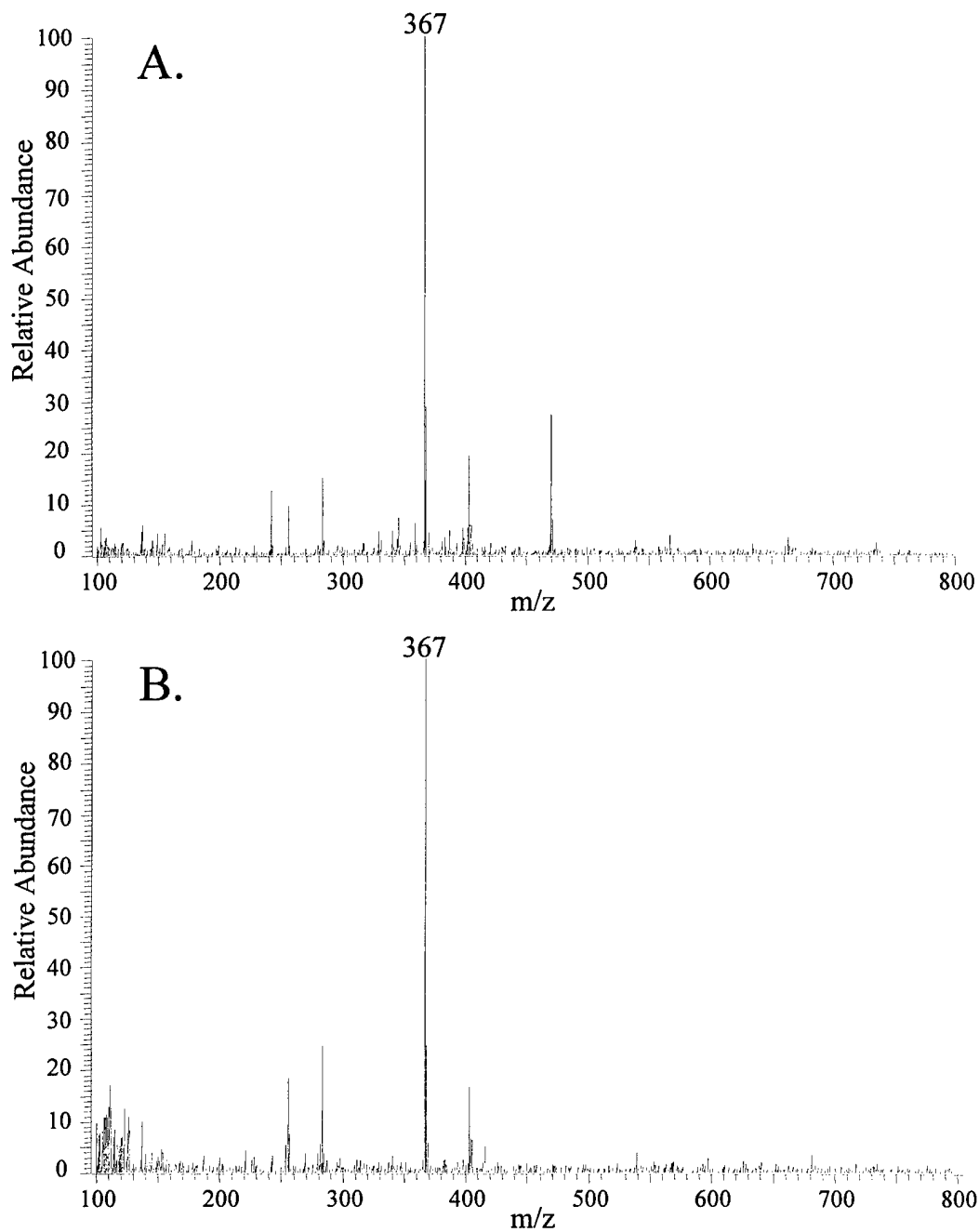


Figure 2-9. A. Negative APCI mass spectrum of 2-NT (MW = 137).
B. Negative APCI mass spectrum of 4-NT (MW = 137).

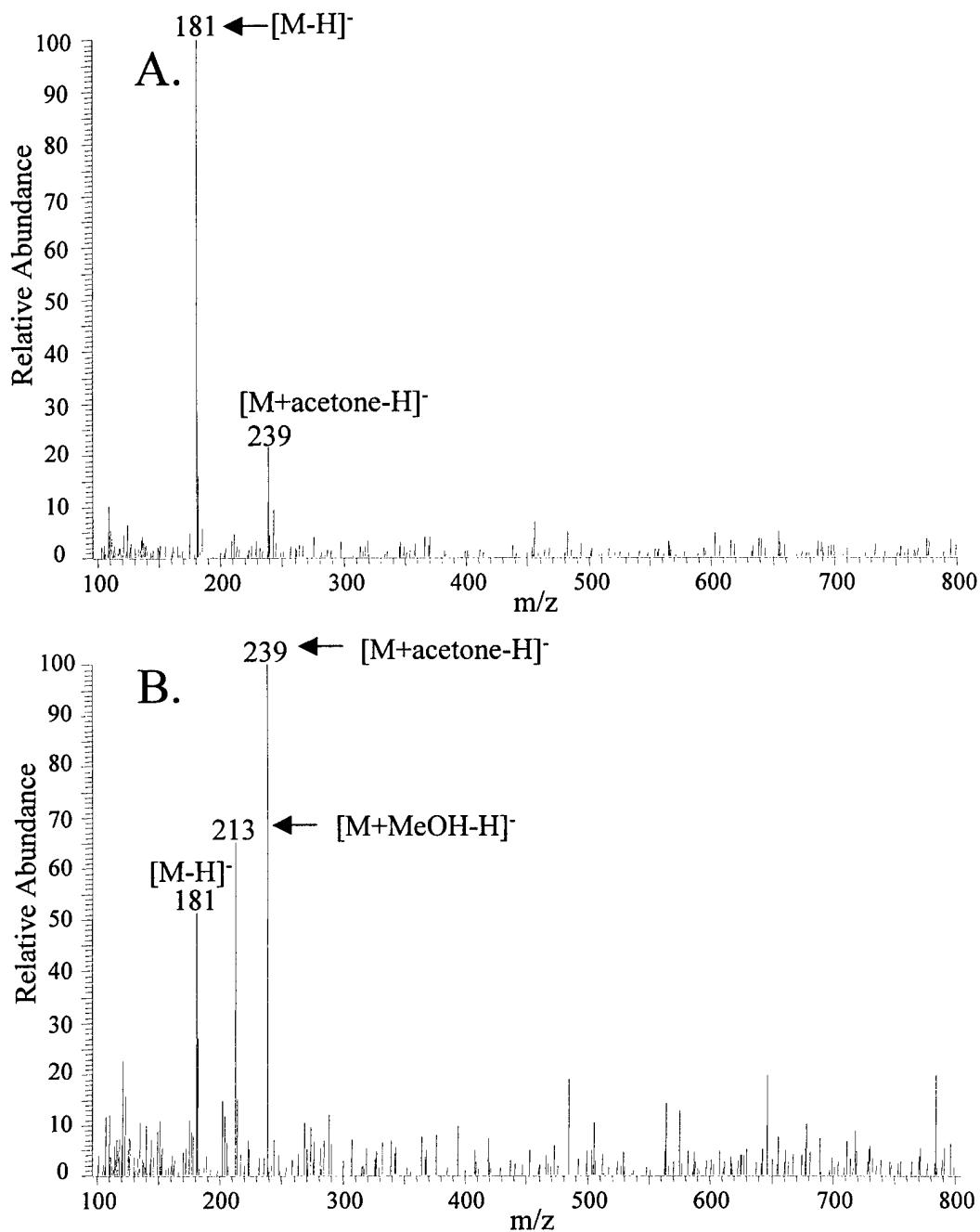
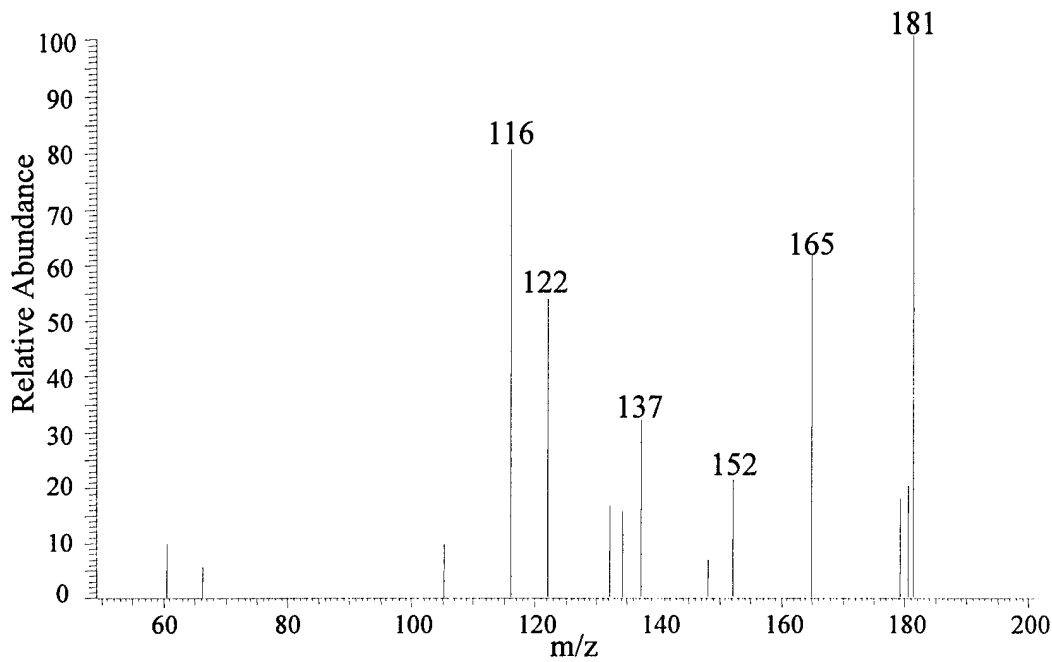


Figure 2-10. A. Negative APCI mass spectrum of 2,4-DNT (MW = 182).
B. Negative APCI mass spectrum of 2,6-DNT (MW = 182).



Daughter Ions of $[M]^+$ Ion (m/z 182) of 2,4-DNT

Daughter Ions (m/z)	Neutral Loss (amu)	Neutral(s) Lost
165	17	OH
152	30	NO
137	45	NO + CH ₃
122	60	2NO
116	66	NO + 2H ₂ O

Figure 2-11. Daughter ion mass spectrum of $[M]^+$ ion (m/z 182) produced by APCI of 2,4-DNT. Spectrum acquired at a resonant excitation q_z of 0.25, isolation window of 3 amu, and collision energy of 30%.

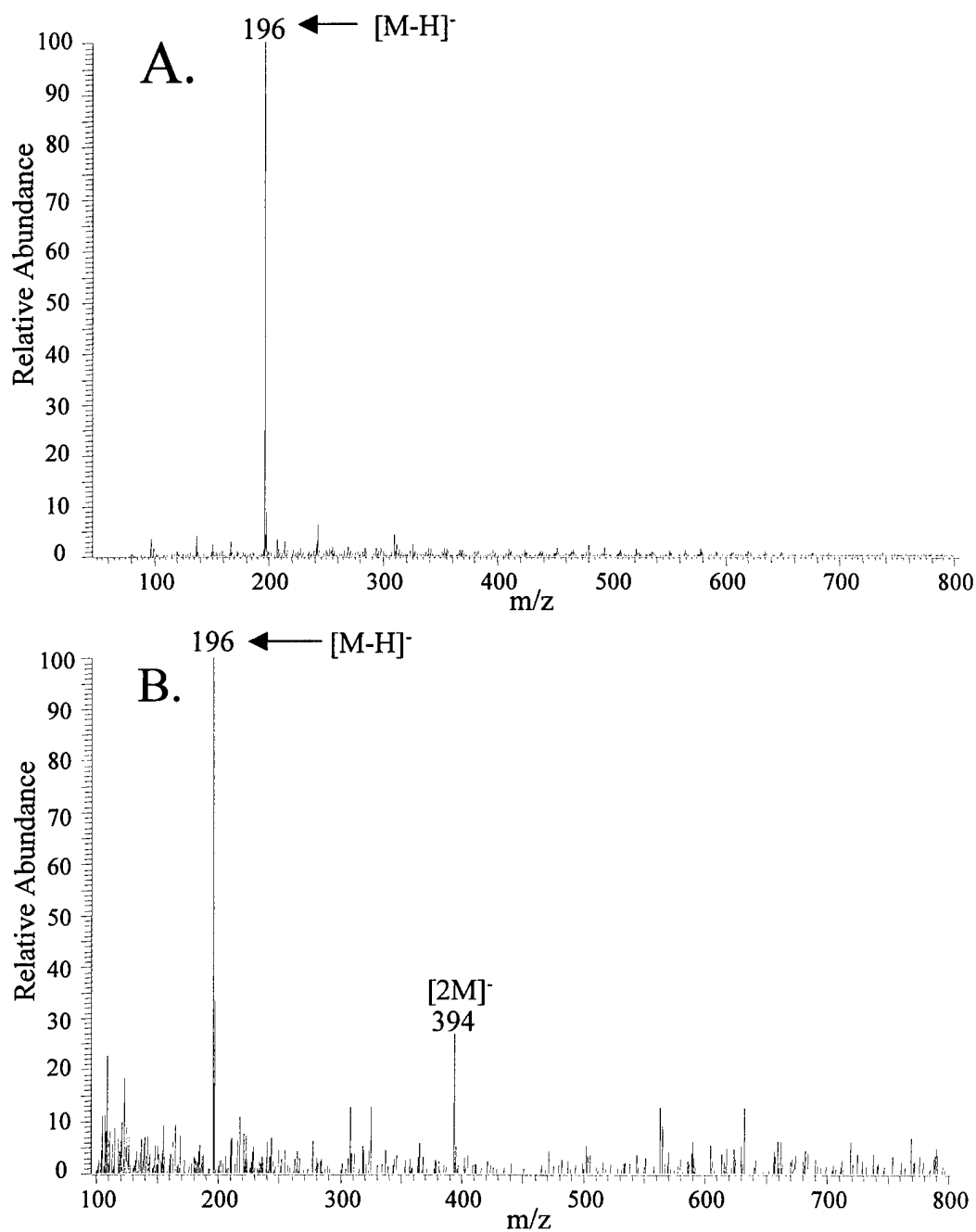


Figure 2-12. Mass spectra of 2A-4,6-DNT (MW = 197): A. Negative ESI, B. Negative APCI.

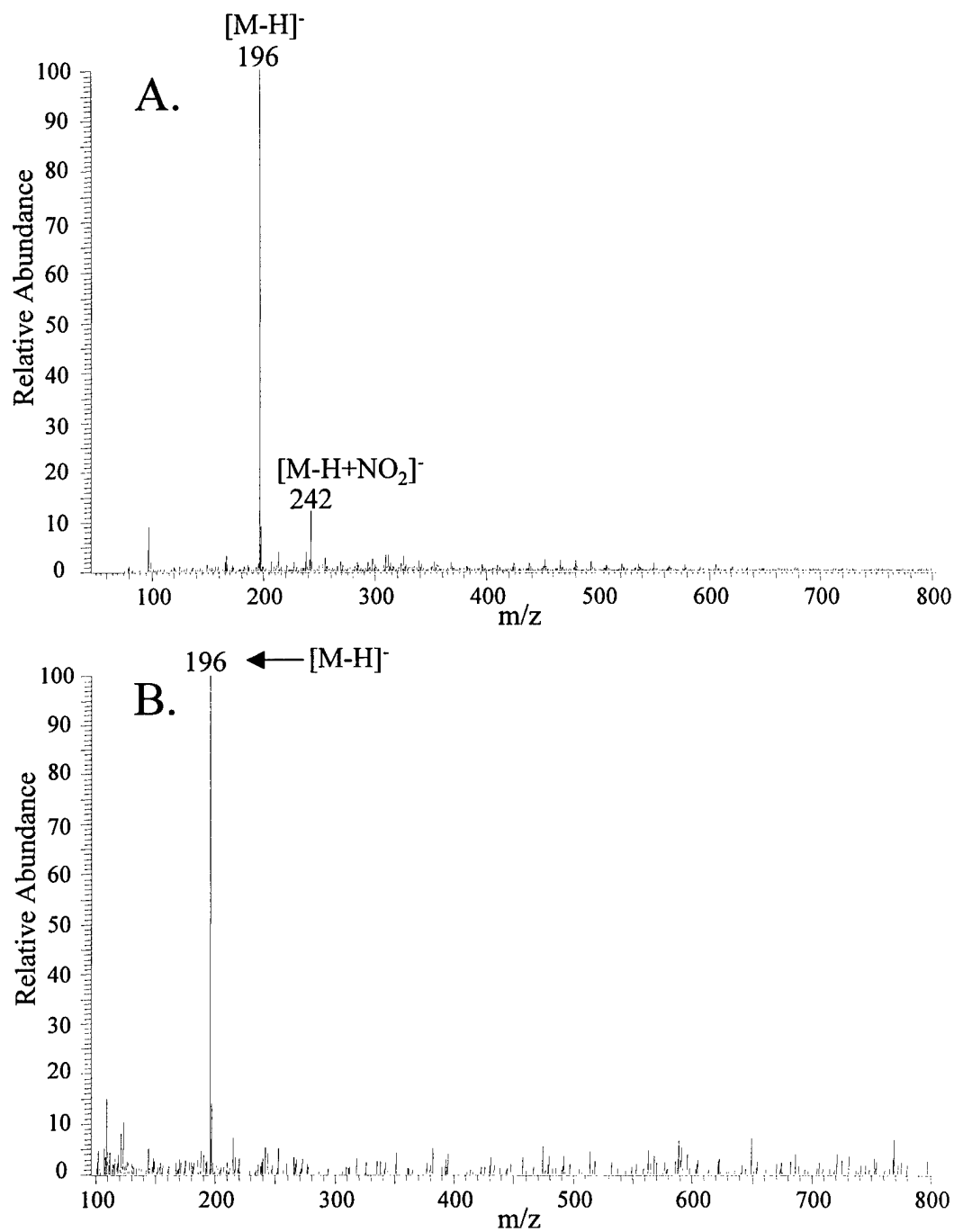
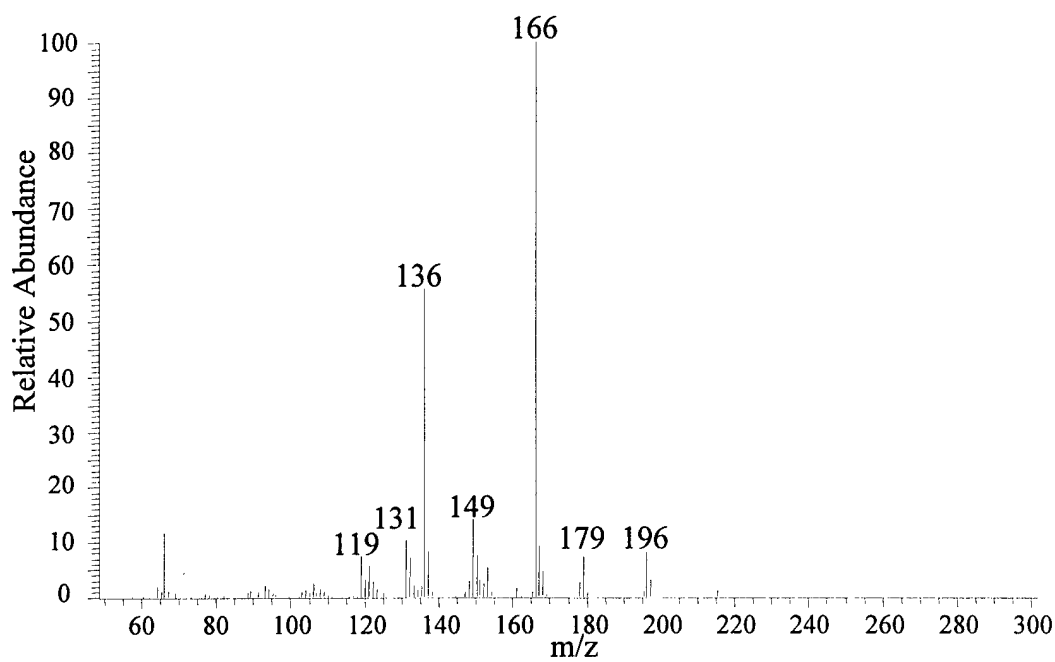


Figure 2-13. Mass spectra of 4A-2,6-DNT (MW = 197): A. Negative ESI, B. Negative APCI.

lower intensity. The MS/MS spectra of the $[M-H]^-$ ion of 2A-4,6-DNT (Figure 2-14) and 4A-2,6-DNT (Figure 2-15) are very similar, with daughter ions at m/z 179, 166, 149, 136, and 119, with corresponding neutral losses of 17 amu (OH), 30 amu (NO), 47 amu (NO + OH), 60 amu (2NO), and 77 amu (NO₂ + OH + CH₂), respectively. The daughter ion spectrum of 2A-4,6-DNT can be differentiated from the daughter ion spectrum of 4A-2,6-DNT by the more intense m/z 136 ion and the presence of m/z 131 ion corresponding to a neutral loss of 65 amu (NO + OH + H₂O).

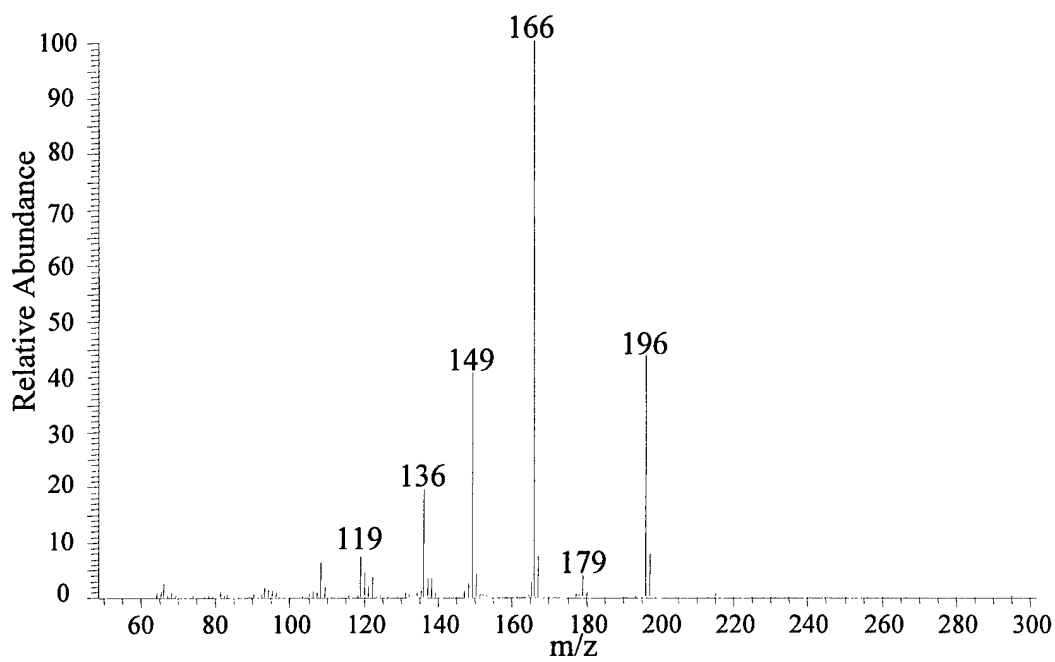
Positive ESI produces more intense molecular ions of 2,4-diamino-6-nitrotoluene (2,4-DA-6-NT) and 2,6-diamino-4-nitrotoluene (2,6-DA-4-NT) than negative ESI due to the basicity of the amino substituents on the aromatic ring. The ESI-MS spectra of 2,4-DA-6-NT (Figure 2-16A) and 2,6-DA-4-NT (Figure 2-17A) are very similar with ions at m/z 168 $[M+H]^+$, 208 $[M+ACN]^+$, and 121 $[M-NO_2]^+$. The positive APCI-MS spectra of 2,4-DA-6-NT (Figure 2-16B) and 2,6-DA-4-NT (Figure 2-17B) show a greater abundance of the acetonitrile (ACN) adduct ion $[M+ACN]^+$ at m/z 208 than the molecular ion $[M+H]^+$ at m/z 168. Acetonitrile comes from the stock solutions of 2,4-DA-6-NT and 2,6-DA-4-NT provided by Dr. Jehuda Yinon. The main difference between the daughter ion mass spectra of the $[M+H]^+$ ions of 2,4-DA-6-NT (Figure 2-18) and 2,6-DA-4-NT (Figure 2-19) is the presence of a predominant m/z 151 daughter ion from the former compound. The m/z 151 ion corresponds to a neutral loss of 17 amu (OH), which is produced from the '*ortho*' effect. The '*ortho*' effect is a rearrangement reaction that involves the hydrogen on the methyl group and the adjacent oxygen on the nitro group in the ortho position [Yinon and Zitrin, 1993]. There are no ortho nitro groups in 2,6-DA-4-NT; therefore, the m/z 151 ion is not present in the daughter ion mass spectrum of its $[M+H]^+$ ion.



Daughter Ions of $[M-H]^-$ Ion (m/z 196) of 2A-4,6-DNT

Daughter Ions (m/z)	Neutral Loss (amu)	Neutral(s) Lost
179	17	OH
166	30	NO
149	47	NO + OH
136	60	2NO
131	65	NO + OH + H ₂ O
119	77	NO ₂ + OH + CH ₂

Figure 2-14. Daughter ion mass spectrum of $[M-H]^-$ ion (m/z 196) produced by ESI of 2A-4,6-DNT. Spectrum acquired at a resonant excitation q_z of 0.25, isolation window of 3 amu, and collision energy of 32%.



Daughter Ions of $[M-H]^-$ Ion (m/z 196) of 4A-2,6-DNT

Daughter Ions (m/z)	Neutral Loss (amu)	Neutral(s) Lost
179	17	OH
166	30	NO
149	47	NO + OH
136	60	2NO
119	77	NO ₂ + OH + CH ₂

Figure 2-15. Daughter ion mass spectrum of $[M-H]^-$ ion (m/z 196) produced by ESI of 4A-2,6-DNT. Spectrum acquired at a resonant excitation q_z of 0.25, isolation window of 3 amu, and collision energy of 30%.

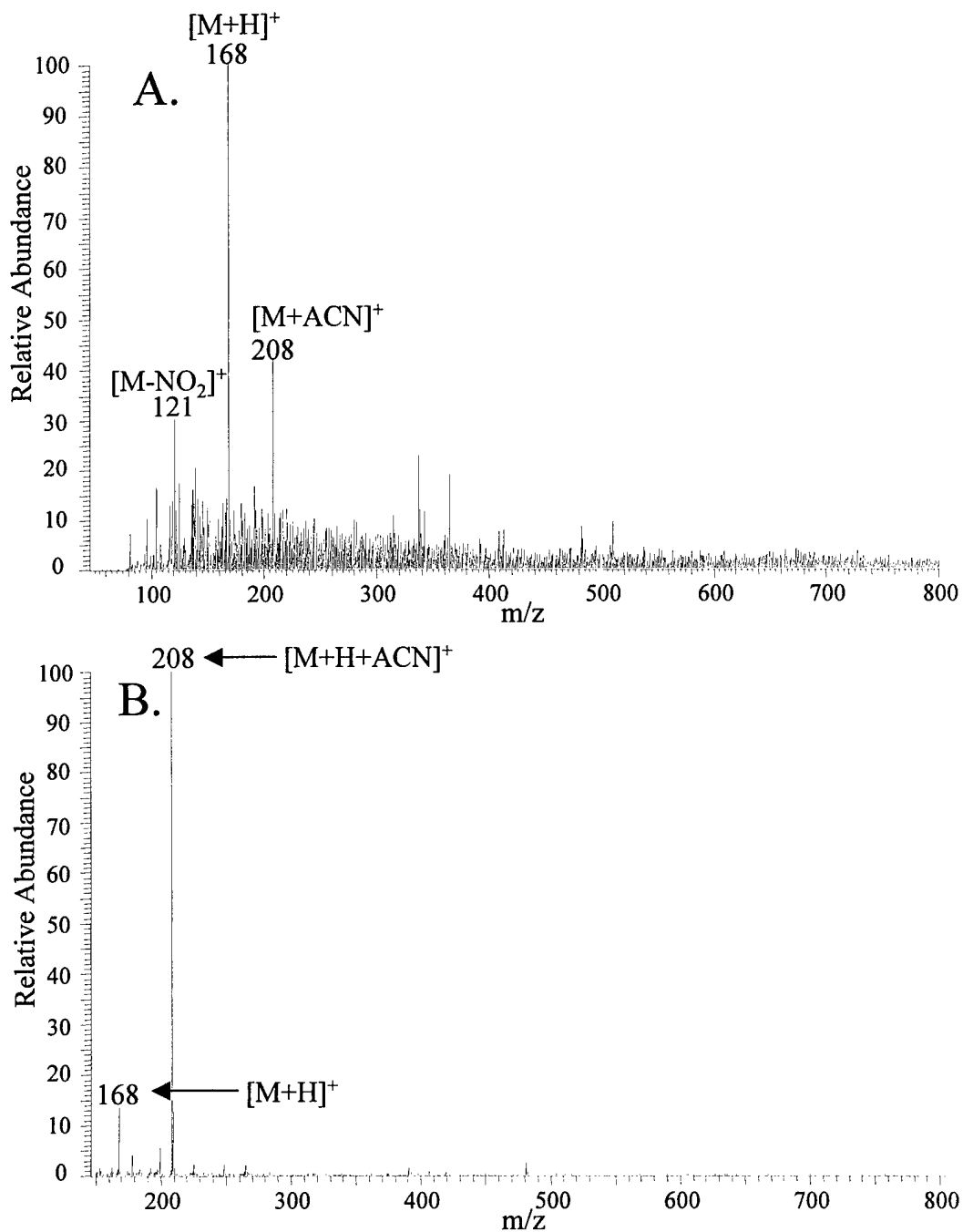


Figure 2-16. Mass spectra of 2,4-DA-6-NT (MW = 167): A. Positive ESI, B. Positive APCI.

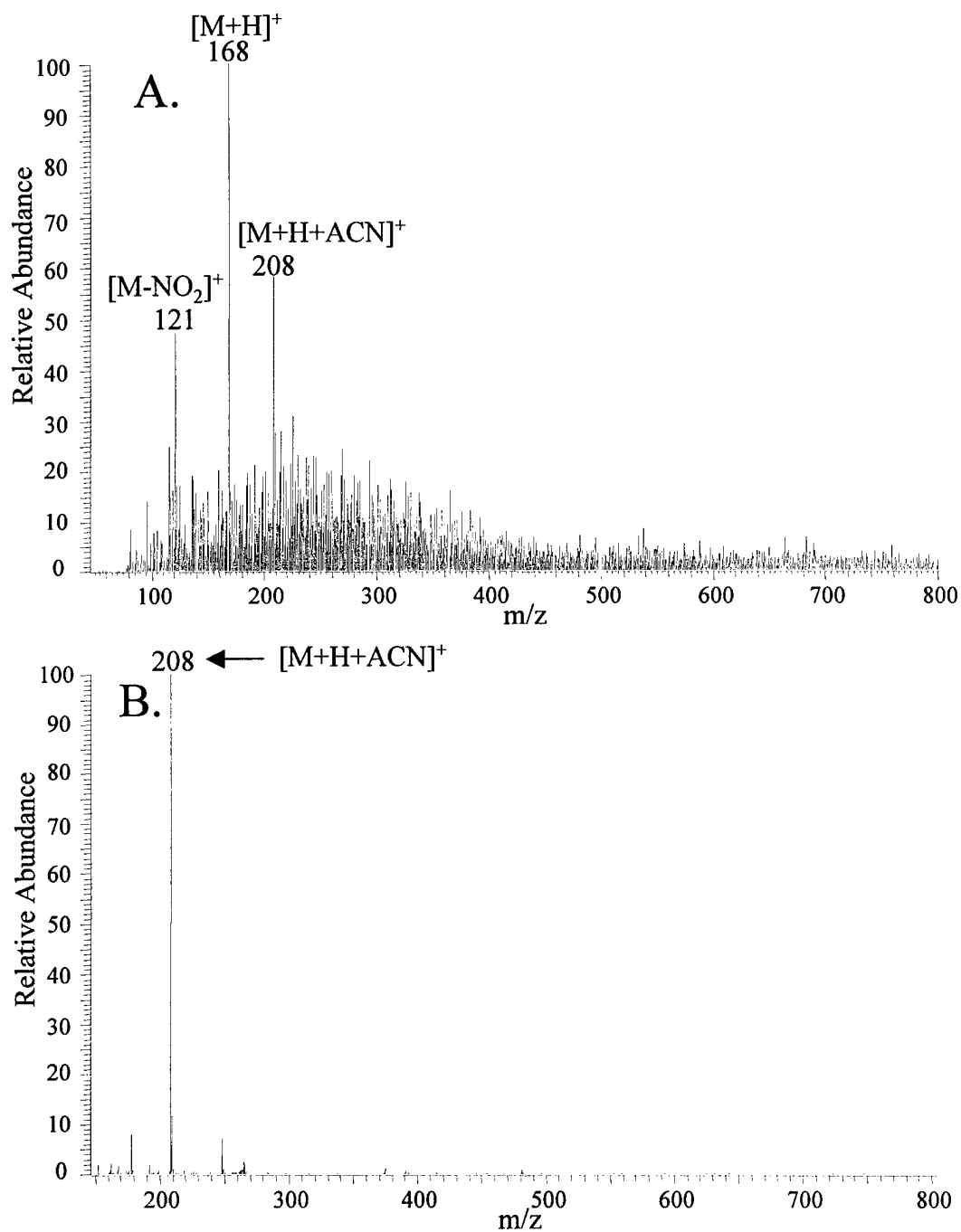
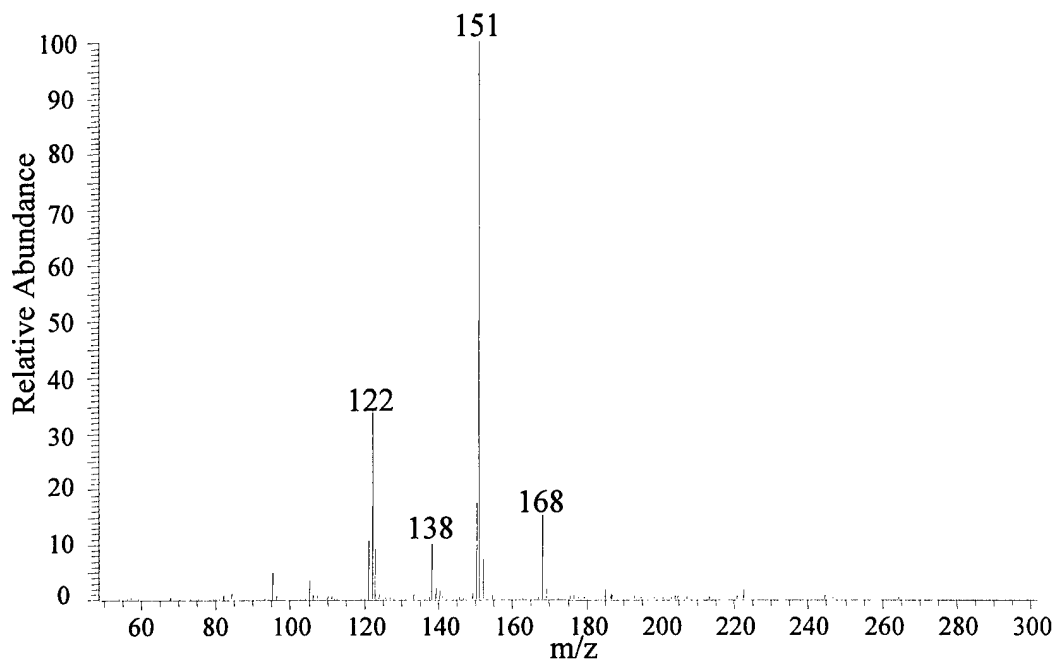


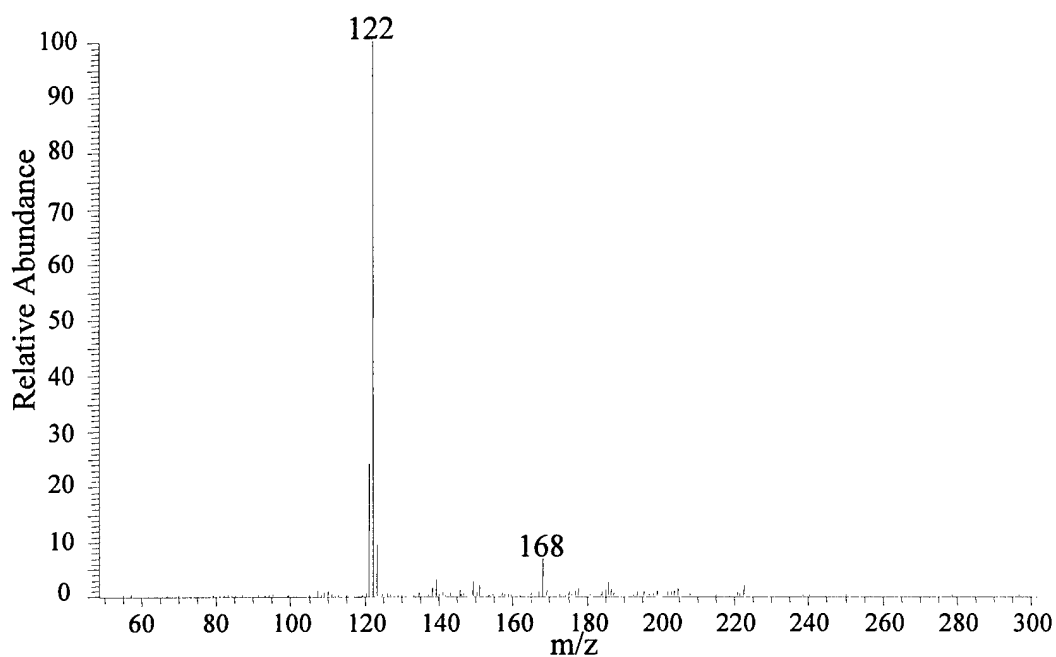
Figure 2-17. Mass spectra of 2,6-DA-4-NT (MW = 167): A. Positive ESI, B. Positive APCI.



Daughter Ions of $[M+H]^+$ Ion (m/z 168) of 2,4-DA-6-NT

Daughter Ions (m/z)	Neutral Loss (amu)	Neutral(s) Lost
151	17	OH
138	30	NO
122	46	NO ₂

Figure 2-18. Daughter ion mass spectrum of $[M+H]^+$ ion (m/z 168) produced by ESI of 2,4-DA-6-NT. Spectrum acquired at a resonant excitation q_z of 0.25, isolation window of 3 amu, and collision energy of 30%.



Daughter Ions of $[M+H]^+$ Ion (m/z 168) of 2,6-DA-4-NT

Daughter Ions (m/z)	Neutral Loss (amu)	Neutral Lost
122	46	NO_2

Figure 2-19. Daughter ion mass spectrum of $[M+H]^+$ ion (m/z 168) produced by ESI of 2,6-DA-4-NT. Spectrum acquired at a resonant excitation q_z of 0.25, isolation window of 3 amu, and collision energy of 32%.

The ESI-MS and APCI-MS spectrum of 1,3,5-trinitrobenzene (TNB) (Figure 2-20A and Figure 2-20B, respectively) have the same ions at m/z 213 $[M]^-$ and m/z 183 $[M-NO]^-$. The APCI of TNB also produces a dimer ion at m/z 395, $[2M-H-NO]^-$. The loss of NO is a common fragmentation of TNB, which is also observed in the daughter ion mass spectrum (Figure 2-21) along with a daughter ion at m/z 137 due to the neutral loss of 76 ($NO + NO_2$). 1,3-Dinitrobenzene (DNB) was only detectable with APCI-MS and produced a spectrum (Figure 2-22) with very weak ions at m/z 168 $[M]^-$, 199 $[M+MeOH-H]^-$, and 138 $[M-NO]^-$. DNB is not susceptible to ESI, because there is no methyl group present for deprotonation. The intensity of the $[M]^-$ ion of DNB is less than TNB, because the nitro groups serve to stabilize the charge on the aromatic ring through resonance. The intensity of the ions of DNB were too weak to acquire an MS/MS spectrum. Nitrobenzene (NB) was not detectable with either ESI-MS or APCI-MS, which is consistent with the literature [Schilling, 1996].

2-Amino-4-nitrotoluene (2A-4-NT) and 4-amino-2-nitrotoluene (4A-2-NT) were not detected with ESI-MS due to the low acidity of the methyl group on the aromatic ring; however, these compounds were detected with positive APCI-MS. The spectrum of 2A-4-NT (Figure 2-23A) has one intense molecular-type ion at m/z 154 $[M+H]^+$, while the APCI of 4A-2-NT (Figure 2-23B) produces ions at m/z 193 $[M-H+ACN]^+$ and m/z 154 $[M+H]^+$. The acetonitrile in the adduct ion comes from the stock solution of 2A-4-NT and 4A-2-NT provided by Dr. Jehuda Yinon. The MS/MS spectra of the $[M+H]^+$ ions of 2A-4-NT (Figure 2-24) and 4A-2-NT (Figure 2-25) are very similar with daughter ions at m/z 153, 136, 123, and 107, corresponding to neutral losses of 1 (H), 18 (H_2O), 31 ($H + NO$), and 47 ($H + NO_2$), respectively. One way to differentiate between 2A-4-NT

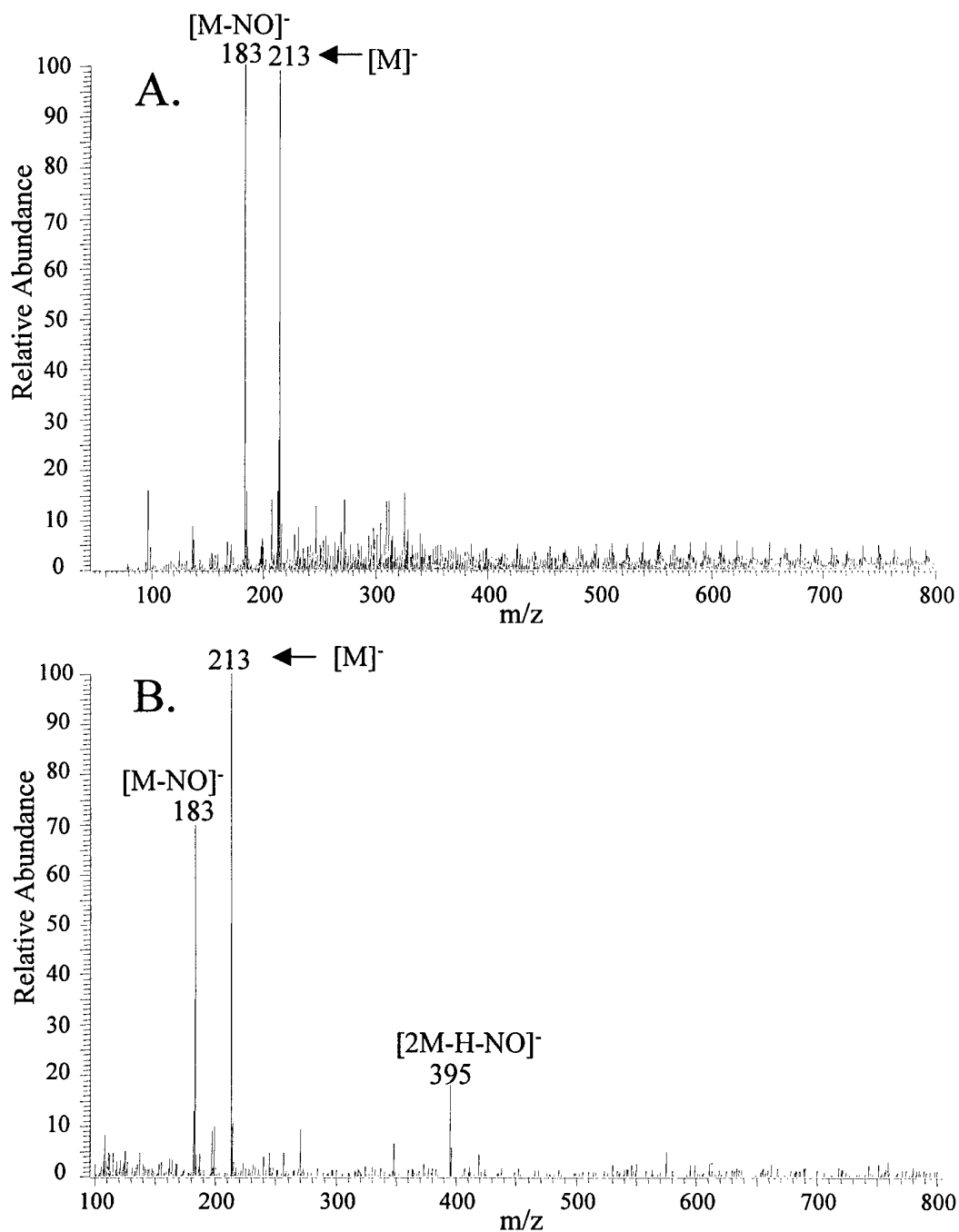
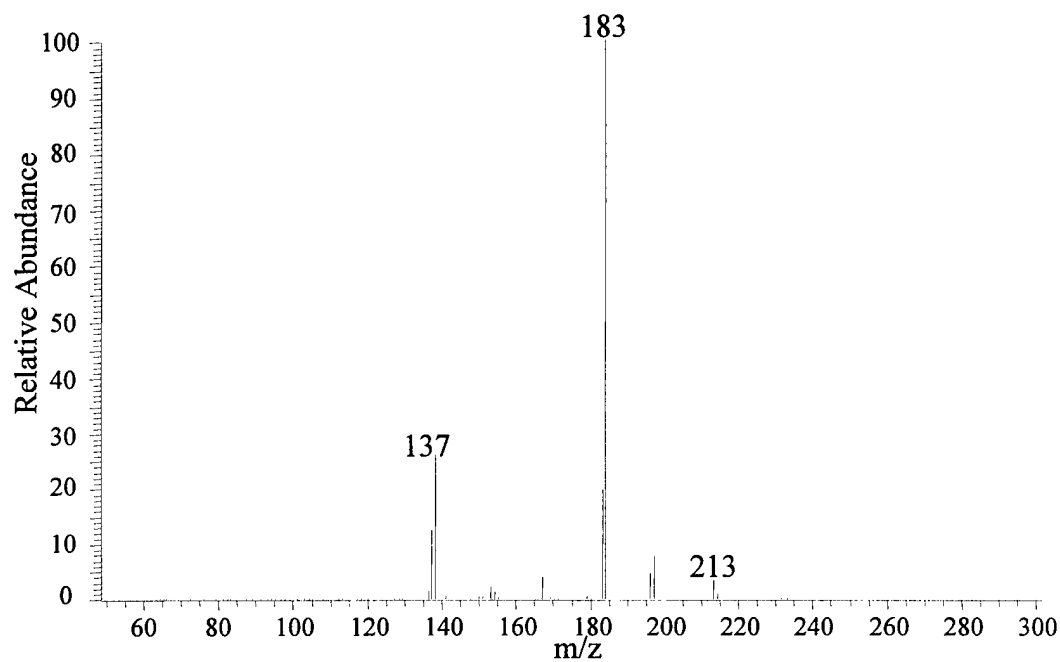


Figure 2-20. Mass spectra of TNB (MW = 213): A. Negative ESI, B. Negative APCI.



Daughter Ions of $[M]^-$ Ion (m/z 213) of TNB

Daughter Ions (m/z)	Neutral Loss (amu)	Neutral(s) Lost
183	30	NO
137	76	NO + NO ₂

Figure 2-21. Daughter ion mass spectrum of $[M]^-$ ion (m/z 213) produced by ESI of TNB. Spectrum acquired at a resonant excitation q_z of 0.25, isolation window of 2 amu, and collision energy of 28%.

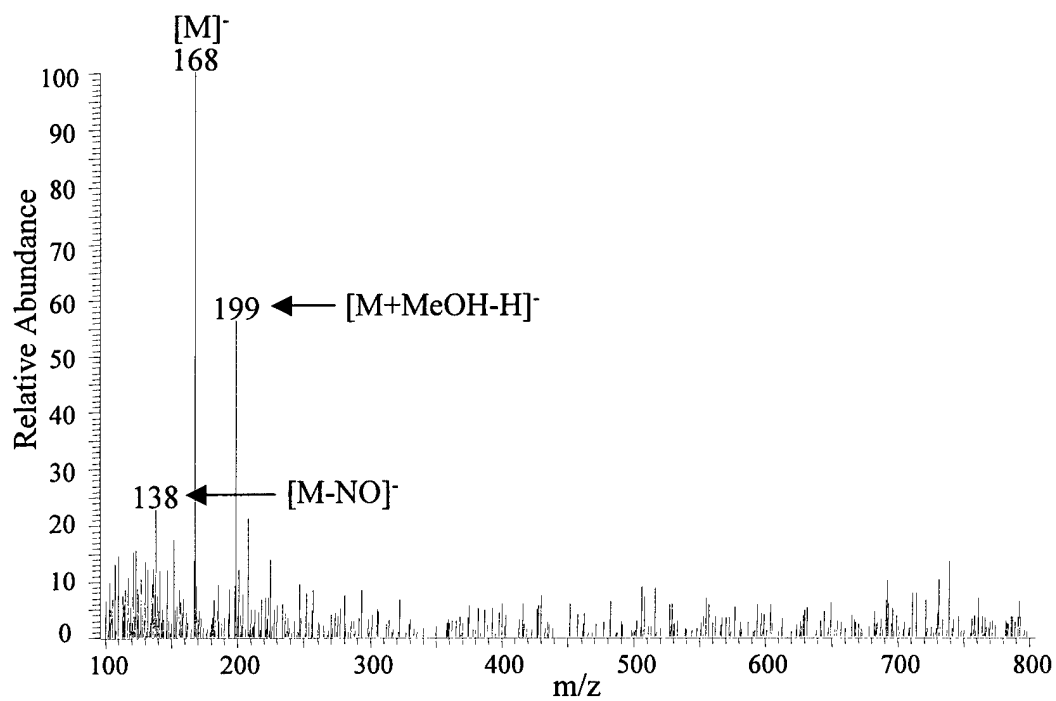


Figure 2-22. Negative APCI mass spectrum of DNB (MW = 168).

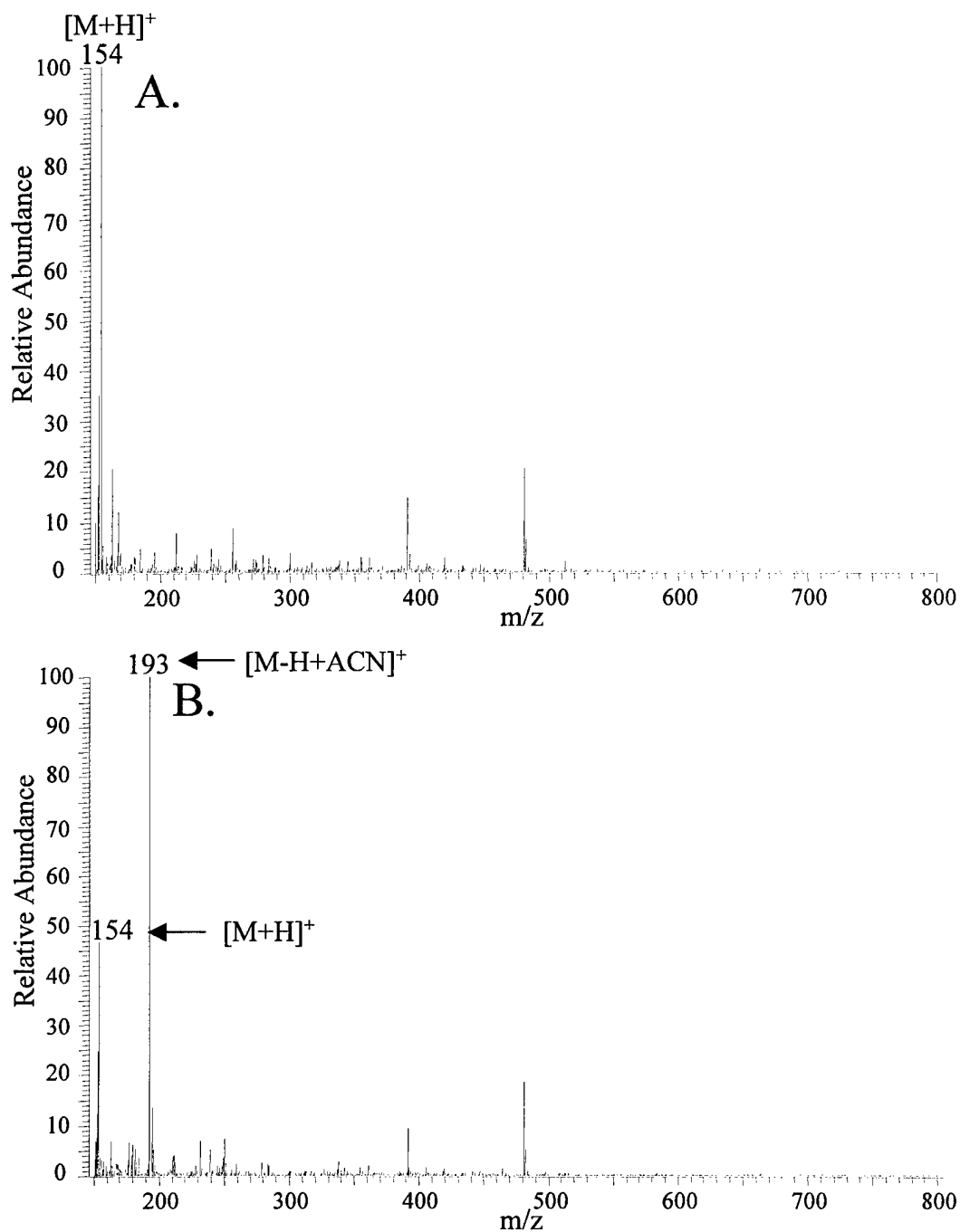
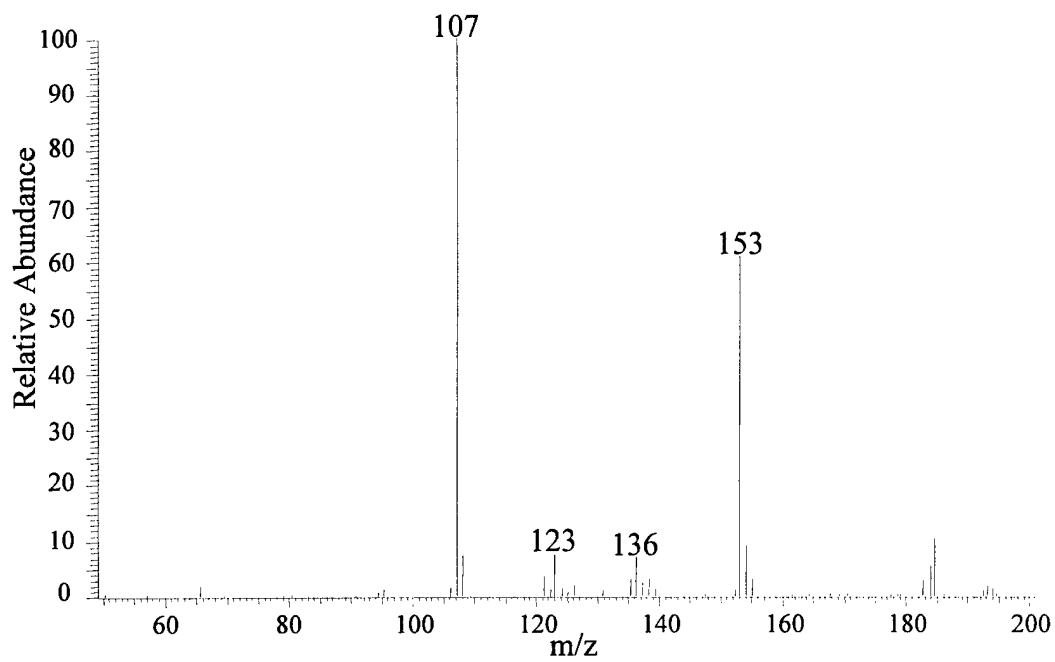


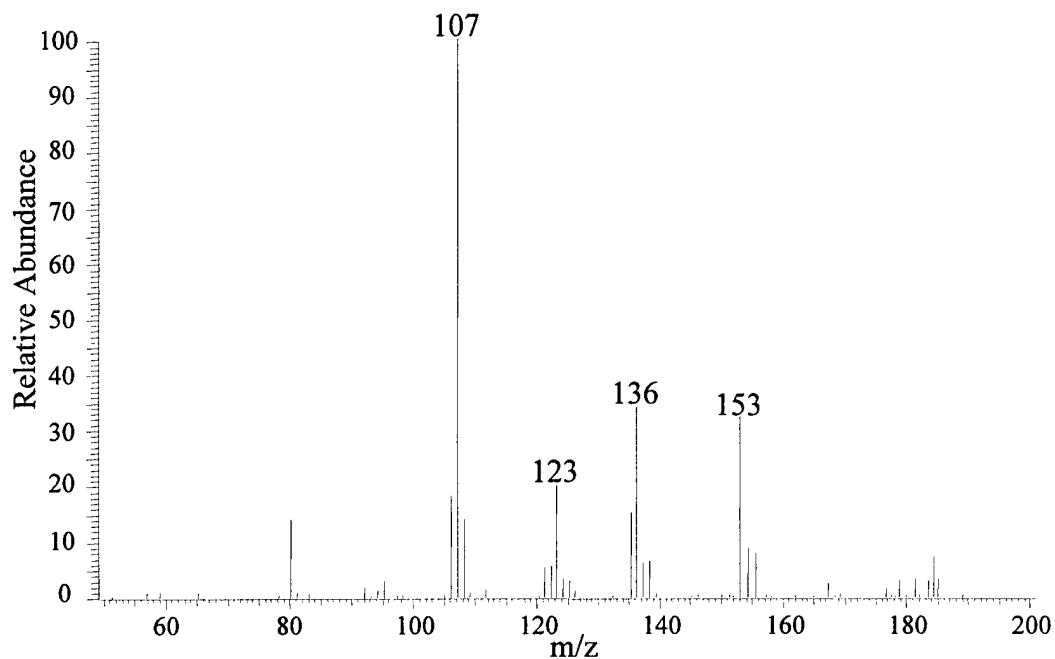
Figure 2-23. A. Positive APCI mass spectrum of 2A-4-NT (MW = 153).
B. Positive APCI mass spectrum of 4A-2-NT (MW = 153).



Daughter Ions of $[M+H]^+$ Ion (m/z 154) of 2A-4-NT

Daughter Ions (m/z)	Neutral Loss (amu)	Neutral(s) Lost
153	1	H
136	18	H ₂ O
123	31	H + NO
107	47	H + NO ₂

Figure 2-24. Daughter ion mass spectrum of $[M+H]^+$ ion (m/z 154) produced by APCI of 2A-4-NT. Spectrum acquired at a resonant excitation q_z of 0.25, isolation window of 3 amu, and collision energy of 30%.



Daughter Ions of $[M+H]^+$ Ion (m/z 154) of 4A-2-NT

Daughter Ions (m/z)	Neutral Loss (amu)	Neutral(s) Lost
153	1	H
136	18	H ₂ O
123	31	H + NO
107	47	H + NO ₂

Figure 2-25. Daughter ion mass spectrum of $[M+H]^+$ ion (m/z 154) produced by APCI of 4A-2-NT. Spectrum acquired at a resonant excitation q_z of 0.25, isolation window of 3 amu, and collision energy of 30%.

and 4A-2-NT is that the daughter ion of the latter compound at m/z 136 (loss of H_2O) is relatively more intense due to the '*ortho*' effect.

Nitrate Esters

Of the three classes of explosives, nitrate esters are the most sensitive to impact and friction due to the weak bond between the oxygen and nitrogen on the nitrate ester group ($RCO-NO_2$) [Yeager, 1996]. This fragility can also be observed in the ESI-MS and APCI-MS of nitrate esters that commonly form nitrate adducts ($[M-H+NO_3]^-$ and $[M+NO_3]^-$) in which the nitrate group is believed to originate from the explosive itself. PETN is the only solid nitrate ester investigated. 1,2,4-Butanetriol trinitrate (BTTN) ($\rho = 1.52$ g/mL), 1,1,1-trimethylolethane trinitrate (TMETN) ($\rho = 1.47$ g/mL), diethyleneglycoldinitrate (DEGDN) ($\rho = 1.38$ g/mL), and triethyleneglycoldinitrate (TEGDN) ($\rho = 1.33$ g/mL) are liquids at room temperature and are often called explosive oils (ρ = density). These oils are used in explosive formulations as energetic plasticizers, which help to provide elasticity to plastic explosives. These compounds are also very fragile and degrade quickly without the use of desensitizers (or stabilizers) such as ethyl centralite, 2-nitrodiphenyl amine, and *N*-methyl-*p*-nitroaniline added at 1% by volume to bind up lost nitro groups [Oehrle, 1977].

The ESI-MS spectrum of PETN (Figure 2-26A) does not have any molecular-type ions, but it does contain dimer and adduct ions of PETN including $[2M-H+Cl]^-$ (m/z 666), $[2M-H+103]^-$ (734), $[M+Cl]^-$ (351), and $[M-H+NO_3]^-$ (377). The adduct formed from 103 has been observed to occur in the negative ESI of nitramines and nitrate esters; the m/z 103 species is suspected to arise from either an impurity or degradation product $[NCH_2N(NO_2)CH_3]^-$ of the explosive [McClellan, 2000]. The APCI of PETN (Figure 2-26B) also produces dimer and adduct ions at m/z 693 $[2M-H+NO_3]^-$, m/z 677

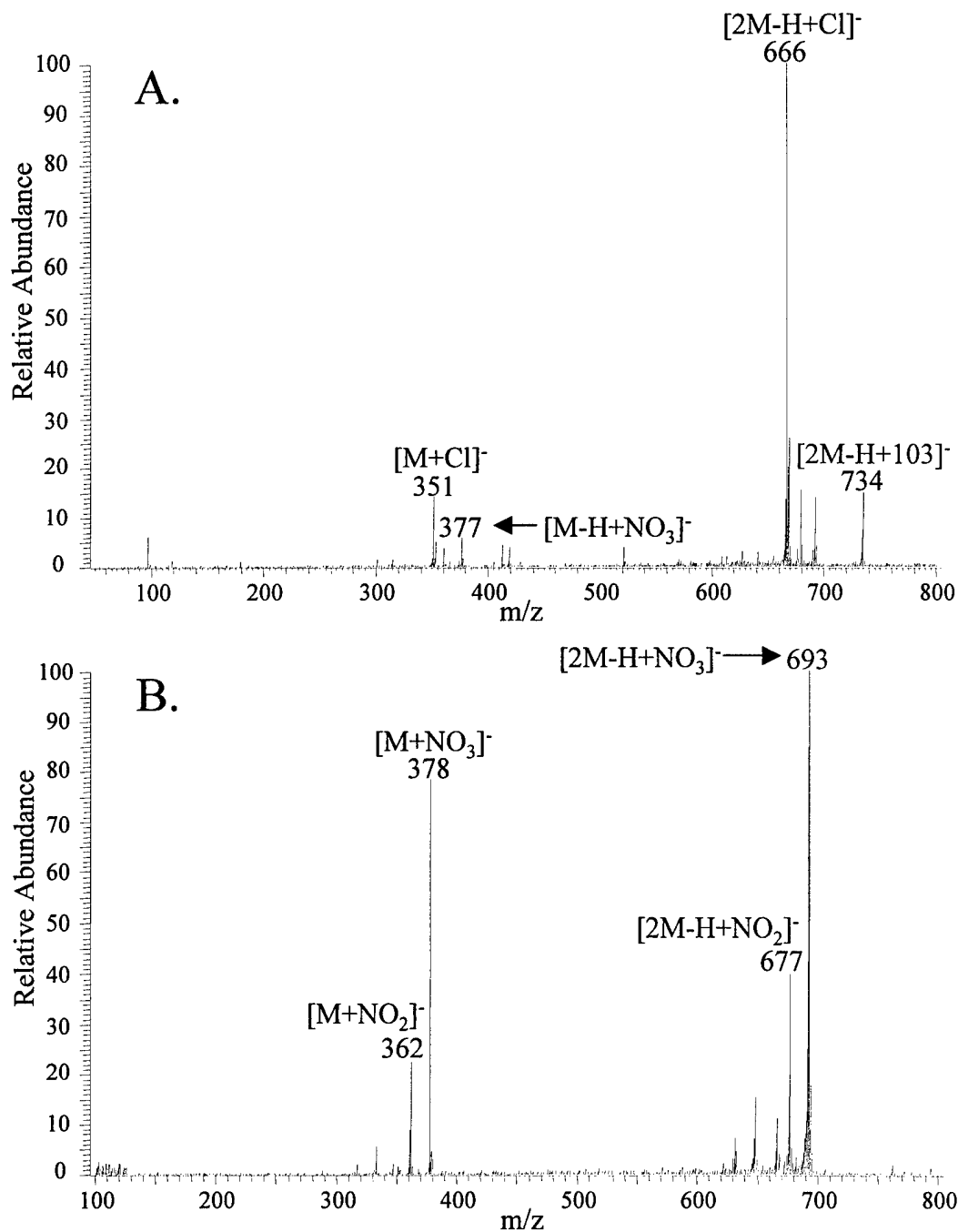
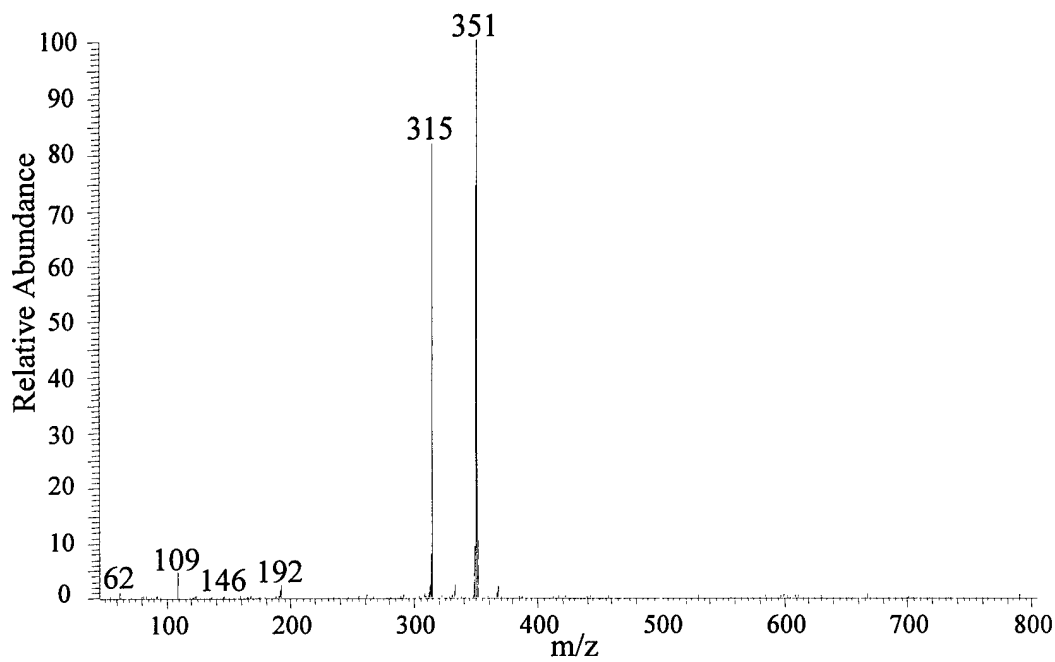


Figure 2-26. Mass spectra of PETN (MW = 316): A. Negative ESI, B. Negative APCI.

$[2M-H+NO_2]^-$, m/z 378 $[M+NO_3]^-$, and m/z 362 $[M+NO_2]^-$. The MS/MS spectrum of the $[M+Cl]^-$ ion (m/z 351) of PETN is shown (Figure 2-27) with one intense daughter ion at m/z 315 corresponding to loss of HCl to form the $[M-H]^-$ ion and less intense ions at m/z 192, 146, 109, and 62, corresponding to the neutral losses of 159 amu ($Cl + 2ONO_2$), 205 amu ($Cl + 2ONO_2 + NO_2$), 242 amu ($Cl + (O_2NOCH_2)_2C(CH)(CH_2O)$), and 289 amu ($Cl + (O_2NOCH_2)_3C(CH_2)$).

The ESI of BTTN (Figure 2-28A) produces two intense adduct ions at m/z 302 $[M-H+NO_3]^-$ and m/z 344 $[M+103]^-$ among many noise spikes, which may be attributed to the desensitizing agent. The APCI of BTTN (Figure 2-28B) produces ions at m/z 303 $[M+NO_3]^-$, m/z 543 $[2M-H+NO_3]^-$, m/z 527 $[2M-H+NO_2]^-$, and m/z 287 $[M+NO_2]^-$. The daughter ion mass spectrum of the $[M-H+NO_3]^-$ ion (m/z 302) of BTTN (Figure 2-29) shows daughter ions at m/z 285, 259, 217, 124, and 109, corresponding to the neutral losses of 17 amu (OH), 43 amu (OH + CHCH), 85 amu ($((OCH)CH(CH_2CHO))$), 178 amu ($((O_2NOCH_2)C(CH_2CH_2ONO_2))$), and 193 amu ($((O_2NOCH_2)CH(CH_2CH_2ONO) + NO)$), respectively.

The ESI-MS spectrum of TMETN (Figure 2-30A) shows two recognizable ions at m/z 358 $[M+103]^-$ and m/z 316 $[M-H+NO_3]^-$, along with noise spikes due to the stabilizers. The APCI-MS spectrum of TMETN (Figure 2-30B) shows three adduct ions at m/z 317 $[M+NO_3]^-$, m/z 301 $[M+NO_2]^-$, and m/z 272 $[M+OH]^-$. The MS/MS spectrum of the $[M-H+NO_3]^-$ ion (m/z 316) ion of TMETN (Figure 2-31) is very rich (due to the branched structure), with daughter ions at m/z 315, 297, 273, 258, 254, 225, 192, 187, and 157. The neutral losses of these daughter ions are listed in Figure 2-31. DEGDN and TEGDN were not detectable using ESI-MS and APCI-MS. This might be



Daughter Ions of $[M+Cl]^-$ Ion (m/z 351) of PETN

Daughter Ions (m/z)	Neutral Loss (amu)	Neutral(s) Lost
315	36	HCl
192	159	Cl + 2ONO ₂
146	205	Cl + 2ONO ₂ + NO ₂
109	242	Cl + (O ₂ NOCH ₂) ₂ C(CH)(CH ₂ O)
62	289	Cl + (O ₂ NOCH ₂) ₃ C(CH ₂)

Figure 2-27. Daughter ion mass spectrum of $[M+Cl]^-$ ion (m/z 351) produced by ESI of PETN. Spectrum acquired at a resonant excitation q_z of 0.25, isolation window of 3 amu, and collision energy of 20%.

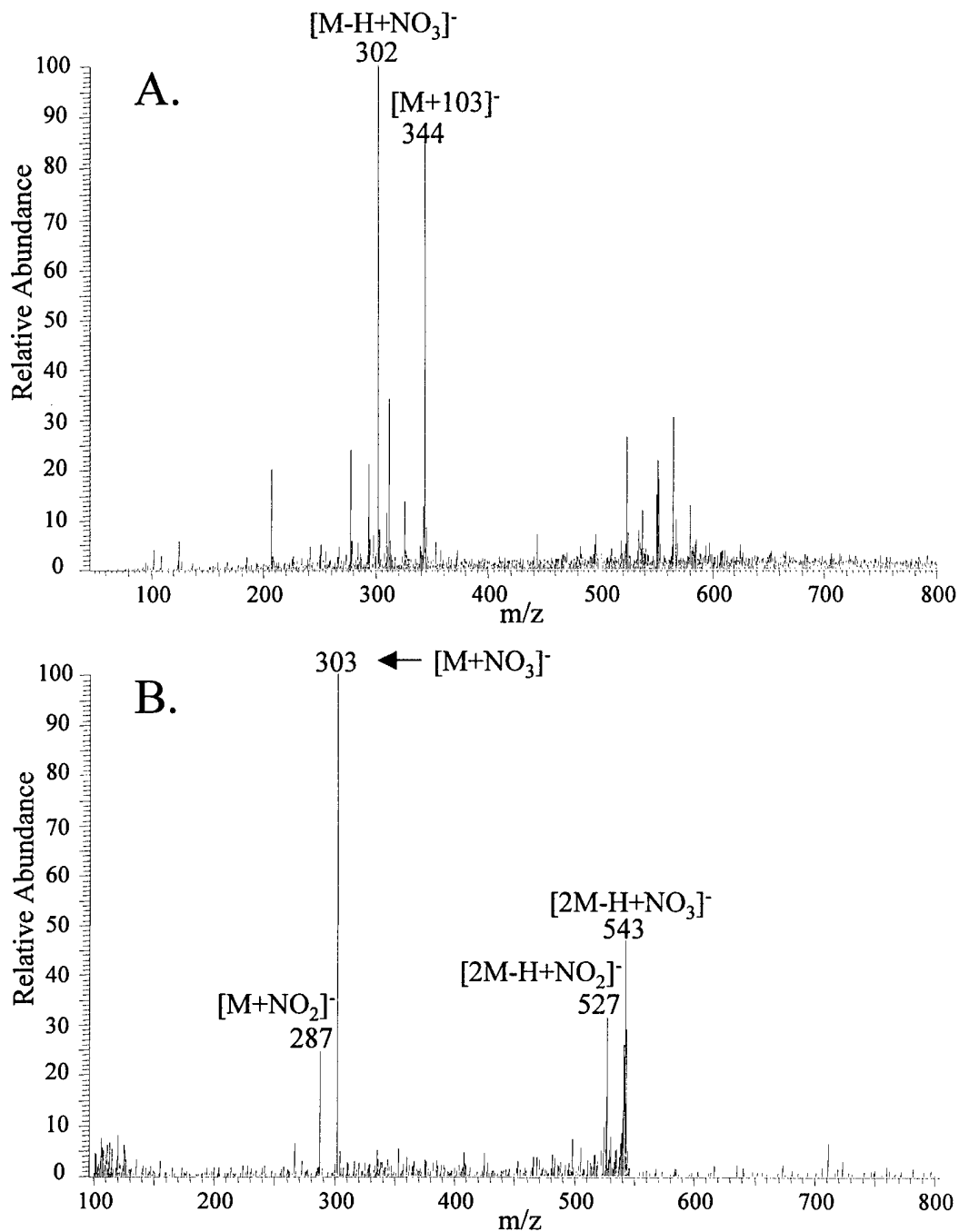
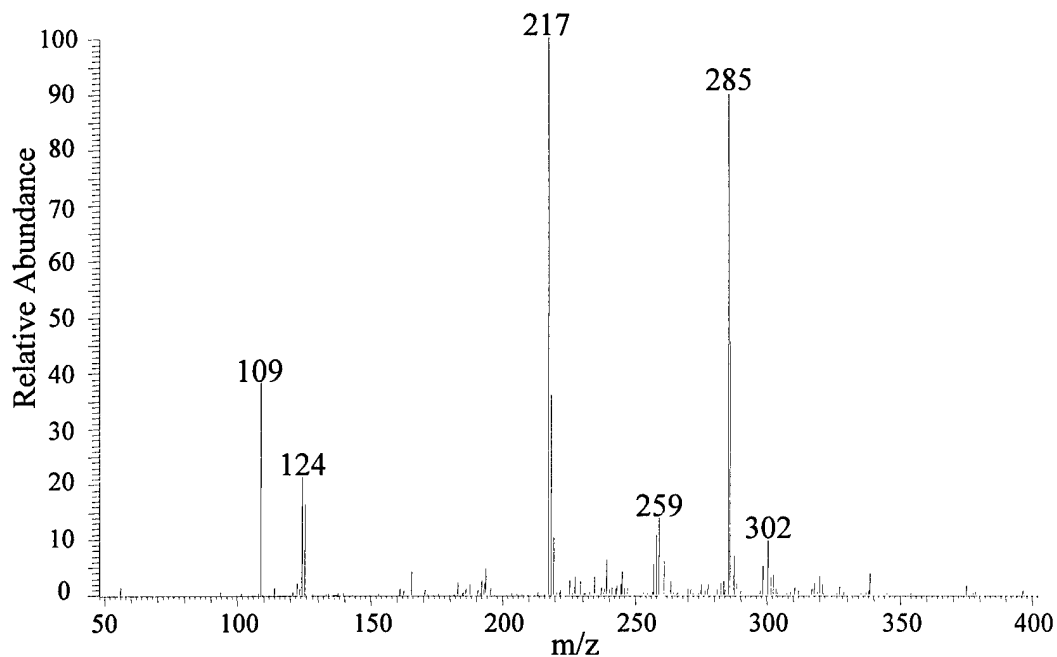


Figure 2-28. Mass spectra of BTTN (MW = 241): A. Negative ESI, B. Negative APCI.



Daughter Ions of $[M-H+NO_3]^-$ Ion (m/z 302) of BTTN

Daughter Ions (m/z)	Neutral Loss (amu)	Neutral(s) Lost
285	17	OH
259	43	OH + CHCH
217	85	(OCH)CH(CH ₂ CHO)
124	178	(O ₂ NOCH ₂)C(CH ₂ CH ₂ ONO ₂)
109	193	(O ₂ NOCH ₂)CH(CH ₂ CH ₂ ONO) + NO

Figure 2-29. Daughter ion mass spectrum of $[M-H+NO_3]^-$ ion (m/z 302) produced by ESI of BTTN. Spectrum acquired at a resonant excitation q_z of 0.25, isolation window of 3 amu, and collision energy of 38%.

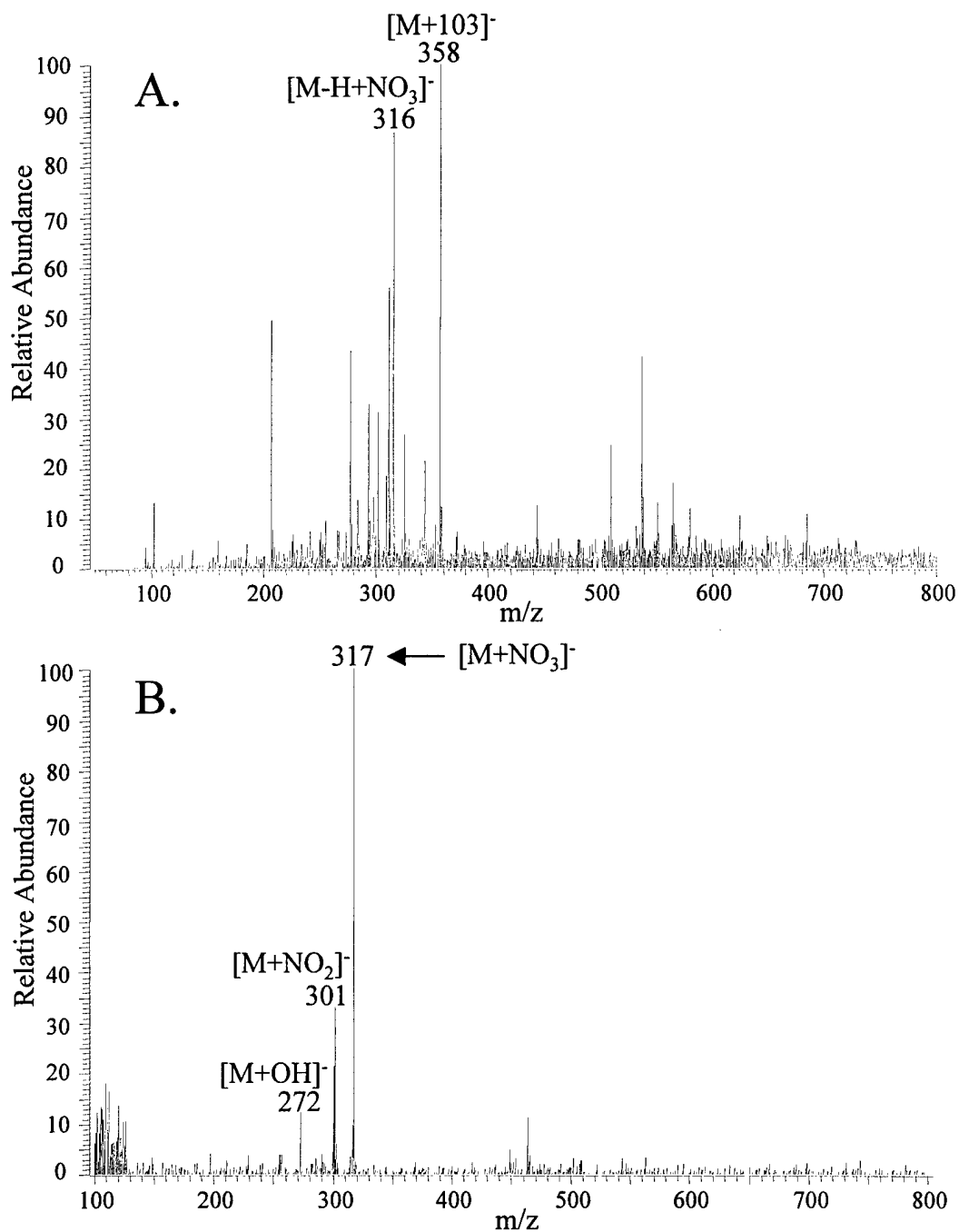
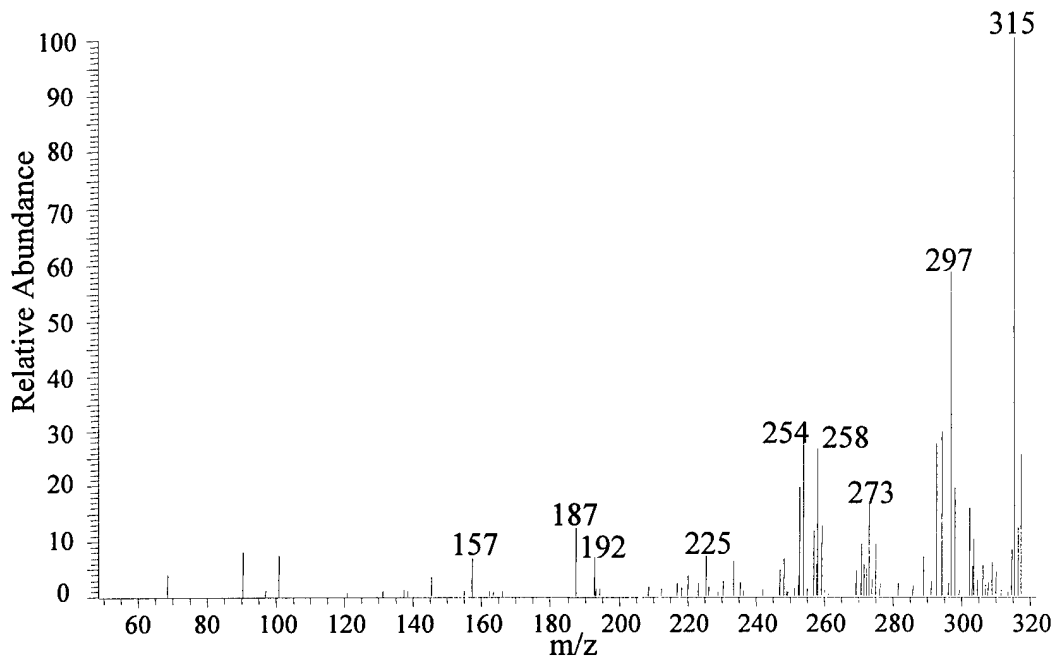


Figure 2-30. Mass spectra of TMETN (MW = 255): A. Negative ESI, B. Negative APCI.



Daughter Ions of $[M-H+NO_3]^-$ Ion (m/z 316) of TMETN

Daughter Ions (m/z)	Neutral Loss (amu)	Neutral(s) Lost
315	1	H
297	19	H + H ₂ O
273	43	CHNO
258	58	CH ₃ + CHNO
254	62	ONO ₂
225	91	CH ₃ CH ₂
192	124	2ONO ₂
187	129	(O ₂ NOCH ₂)C(CH)(CH ₂) ₂
157	159	(O ₂ NOCH ₂)C(CH)(CH ₂) ₂ + NO

Figure 2-31. Daughter ion mass spectrum of $[M-H+NO_3]^-$ ion (m/z 316) produced by ESI of TMETN. Spectrum acquired at a resonant excitation q_z of 0.25, isolation window of 3 amu, and collision energy of 30%.

attributable to the ether functional groups of these explosives, which contributes to the fragility of these compounds.

Nitramines

Nitroguanidine (NQ) has two amino groups besides the nitramine group which are available for deprotonation, making NQ amenable to negative ion ESI. The negative ESI-MS spectrum of NQ (Figure 2-32) has a molecular ion at m/z 103 $[M-H]^-$, a dimer at m/z 207 $[2M-H]^-$, and an adduct ion at m/z 149 $[M-H+NO_2]^-$. The MS/MS spectrum of the $[M-H]^-$ ion (m/z 103) of NQ (Figure 2-33) has only two daughter ions at m/z 61 and m/z 41, corresponding to neutral losses of 42 amu ($NHCNH$) and 62 amu (NH_2NO_2), respectively. NQ is not detectable in negative APCI, but detection is more sensitive in the positive mode of APCI. This is not so however for the positive ESI-MS of NQ (Figure 2-34A), which produces a very weak molecular ion at m/z 105 $[M+H]^+$ and an adduct ion at m/z 121 $[M+OH]^+$. In contrast, the positive APCI-MS of NQ (Figure 2-34B) produces a very intense adduct ion at m/z 137 $[M+H+MeOH]^+$ along with a dimer ion at m/z 209 $[2M+H]^+$. MS/MS of the $[M+H]^+$ ion (m/z 105) of NQ (Figure 2-35) produces daughter ions at m/z 85, 75, and 59, corresponding to the neutral losses of 20 amu (H_2O), 30 amu (NO), and 46 amu (NO_2).

The ESI-MS spectrum of 1,3,5-trinitro-1,3,5-triazacyclohexane (RDX) (Figure 2-36A) shows an assortment of adduct ions and dimer cluster ions at m/z 479 $[2M+Cl]^-$, m/z 489 $[2M-H+NO_2]^-$, m/z 547 $[2M+103]^-$, m/z 257 $[M+Cl]^-$, and m/z 505 $[2M-H+NO_3]^-$. The APCI of RDX (Figure 2-36B) produces adduct and dimer ions at m/z 490 $[2M+NO_2]^-$, m/z 546 $[2M-H+103]^-$, m/z 324 $[M-H+103]^-$, and m/z 268 $[M+NO_2]^-$. The 103 adduct ions show that this type of ion formation is not an ESI phenomenon, but also occurs with APCI. The daughter ion mass spectrum of the $[M+Cl]^-$ ion at m/z 257

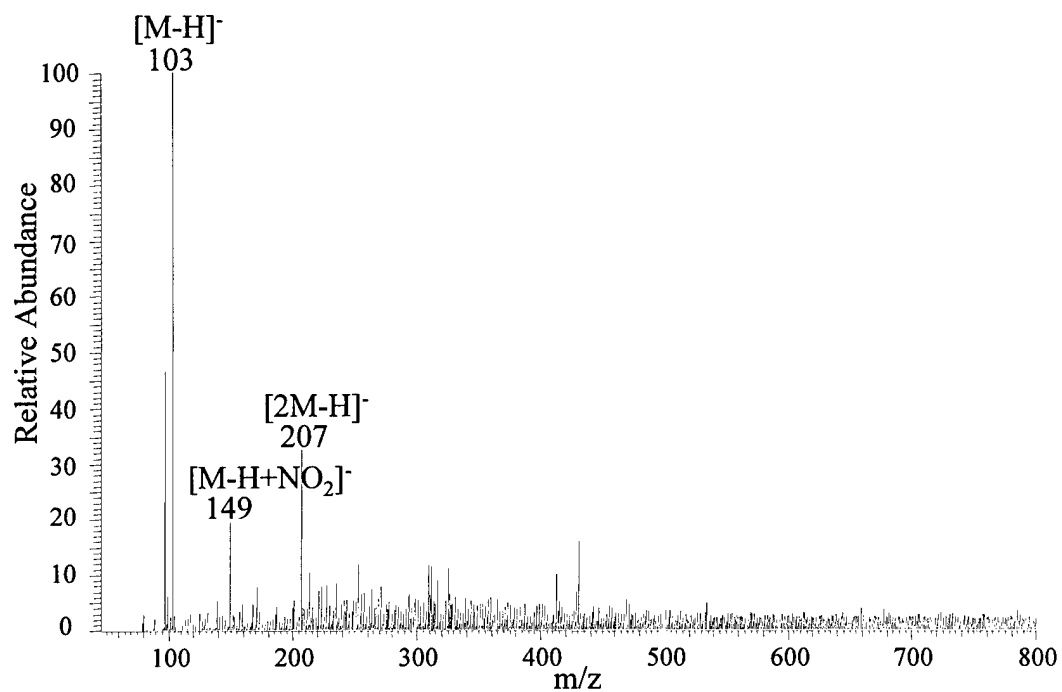
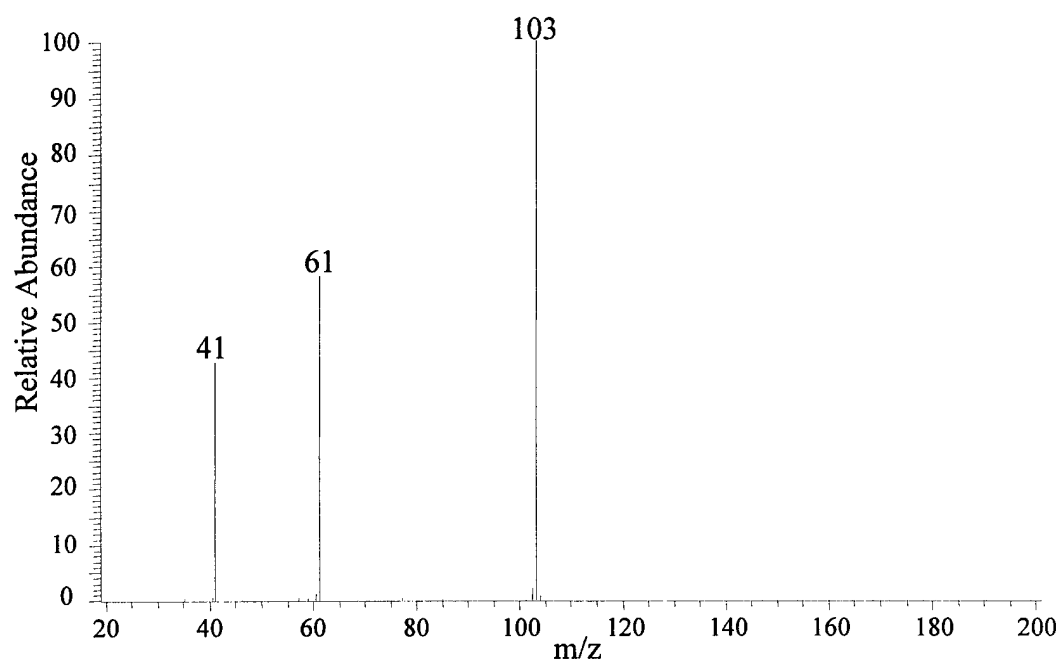


Figure 2-32. Negative ESI mass spectrum of NQ (MW = 104).



Daughter Ions of $[M-H]^-$ Ion (m/z 103) of NQ

Daughter Ions (m/z)	Neutral Loss (amu)	Neutral(s) Lost
61	42	NHCNH
41	62	NH ₂ NO ₂

Figure 2-33. Daughter ion mass spectrum of $[M-H]^-$ ion (m/z 103) produced by ESI of NQ. Spectrum acquired at a resonant excitation q_z of 0.25, isolation window of 3 amu, and collision energy of 22%.

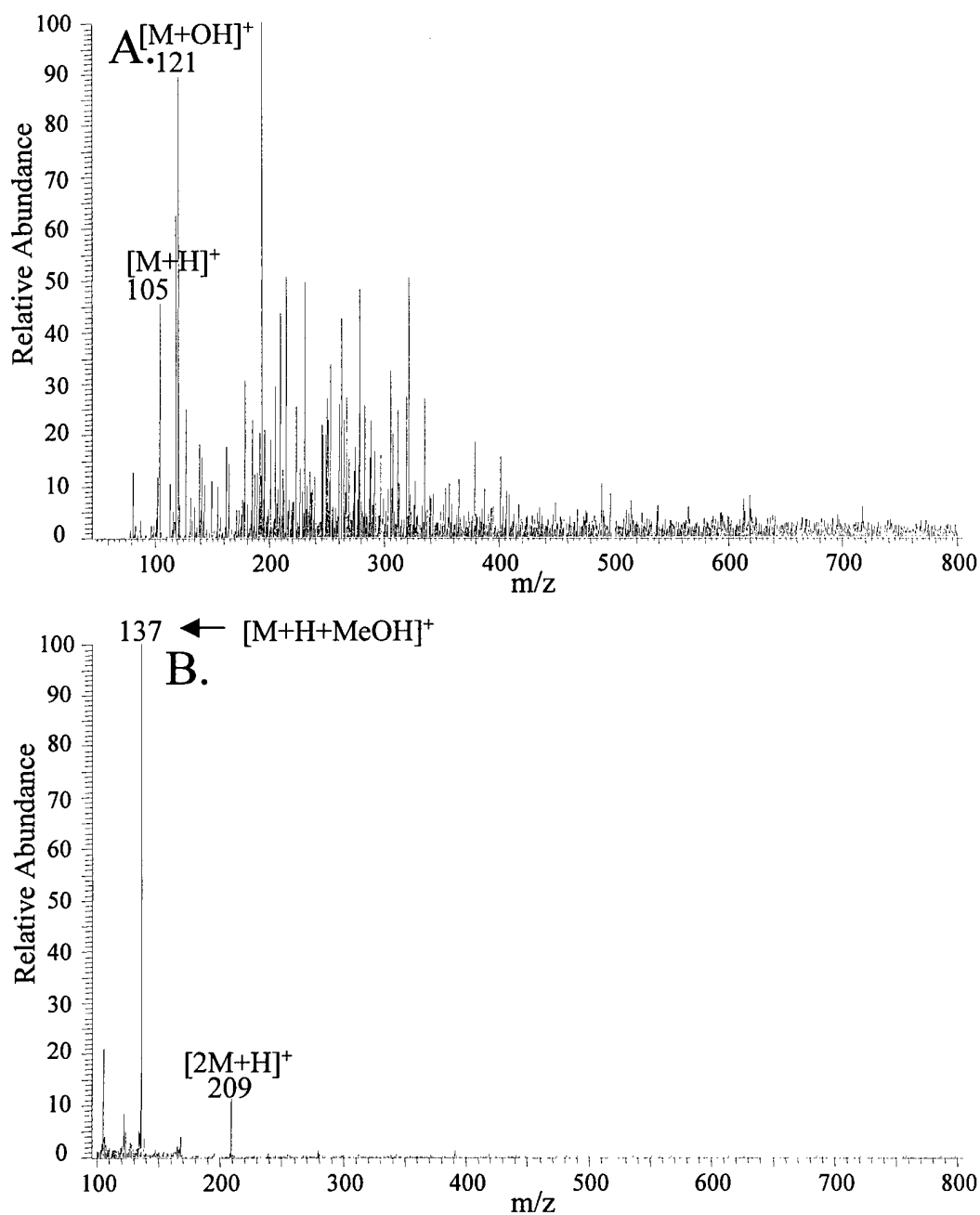
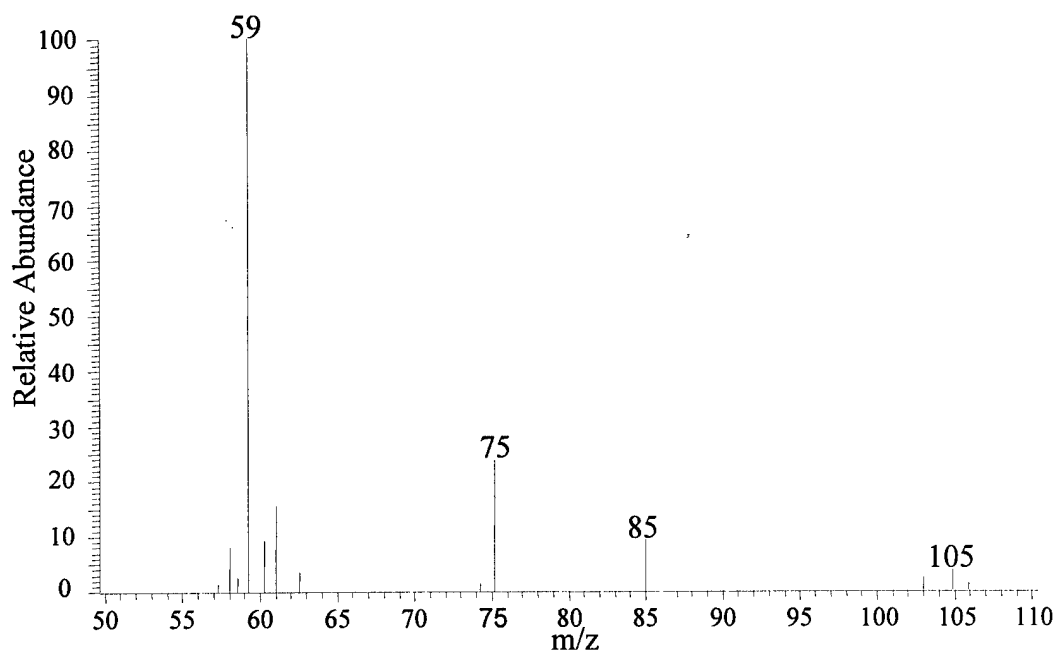


Figure 2-34. Mass spectra of NQ (MW = 104): A. Positive ESI, B. Positive APCI.



Daughter Ions of $[M+H]^+$ Ion (m/z 105) of NQ

Daughter Ions (m/z)	Neutral Loss (amu)	Neutral(s) Lost
85	20	H ₂ O + H ₂
75	30	NO
59	46	NO ₂

Figure 2-35. Daughter ion mass spectrum of $[M+H]^+$ ion (m/z 105) produced by ESI of NQ. Spectrum acquired at a resonant excitation q_z of 0.25, isolation window of 3 amu, and collision energy of 28%.

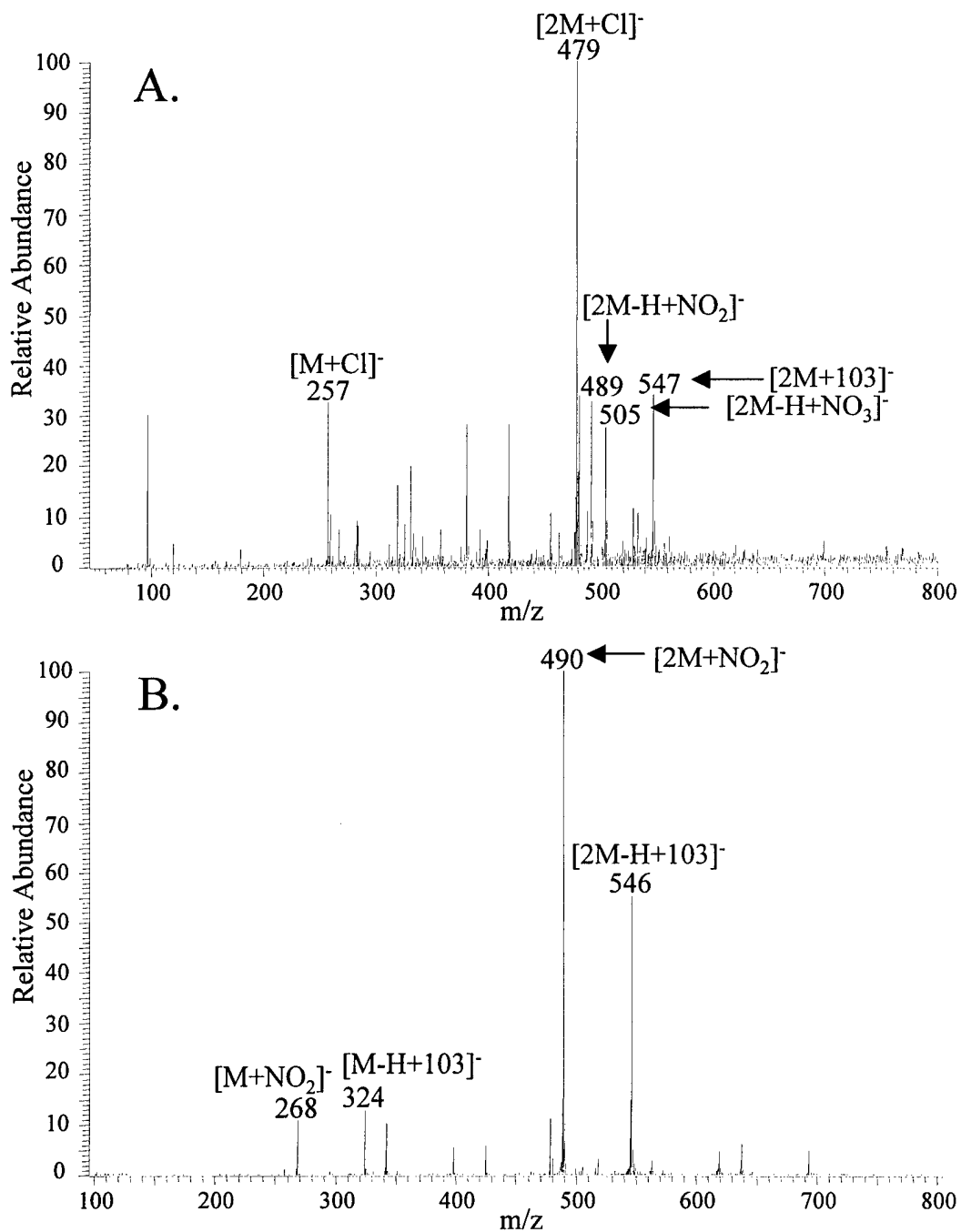
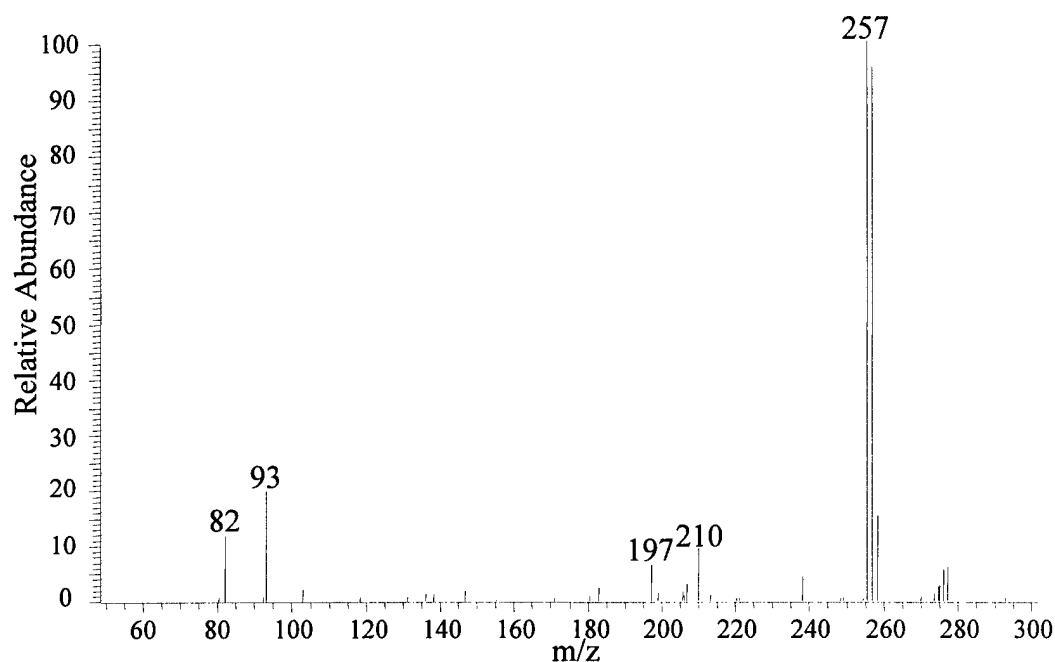


Figure 2-36. Mass spectra of RDX (MW = 222): A. Negative ESI, B. Negative APCI.

(Figure 2-37) was challenging to obtain, because the isolation was very difficult due to its fragility. Very weak daughter ions are observed at m/z 210, 197, 93, and 82, corresponding to the neutral losses of 47 amu (HNO_2), 60 amu (2NO), 164 amu ($\text{CH}_3\text{N}(\text{NO}_2)\text{CH}_2\text{N}(\text{NO}_2)\text{CH}_3$), and 175 amu ($\text{CH}_3\text{N}(\text{NO}_2)\text{CH}_2\text{N}(\text{NO}_2)\text{CN}$).

The ESI-MS spectrum of HMX (Figure 2-38A) contains several adduct and dimer ions at m/z 331 $[\text{M}+\text{Cl}]^-$, m/z 627 $[\text{2M}+\text{Cl}]^-$, m/z 638 $[\text{2M}+\text{NO}_2]^-$, m/z 653 $[\text{2M}-\text{H}+\text{NO}_3]^-$, m/z 357 $[\text{M}-\text{H}+\text{NO}_3]^-$, m/z 695 $[\text{2M}+103]^-$, and m/z 399 $[\text{M}+103]^-$. A weak molecular-type ion is also present at m/z 295 $[\text{M}-\text{H}]^-$. The APCI-MS of HMX (Figure 2-38B) produces adduct ions and dimer clusters at m/z 638 $[\text{2M}+\text{NO}_2]^-$, m/z 694 $[\text{2M}-\text{H}+103]^-$, m/z 342 $[\text{M}+\text{NO}_2]^-$, m/z 398 $[\text{M}-\text{H}+103]^-$, m/z 627 $[\text{2M}+\text{Cl}]^-$, m/z 331 $[\text{M}+\text{Cl}]^-$, and a molecular ion at m/z 295 $[\text{M}-\text{H}]^-$. The MS/MS spectrum of the $[\text{M}-\text{H}]^-$ ion (m/z 295) of HMX (Figure 2-39) is very rich, with daughter ions at m/z 277, 269, 249, 221, 207, 194, 189, 147, and 117. The neutral losses and neutral loss structures from these daughter ions are listed in Figure 2-39.

The ESI-MS spectrum of 2,4,6,8,10,12-hexanitro-2,4,6,8,10,12-hexazaisowurtzitane (CL-20) (Figure 2-40A) shows the presence of adduct ions and dimer cluster ions at m/z 911 $[\text{2M}+\text{Cl}]^-$, m/z 938 $[\text{2M}+\text{NO}_3]^-$, m/z 500 $[\text{M}+\text{NO}_3]^-$, m/z 979 $[\text{2M}+103]^-$, and m/z 473 $[\text{M}+\text{Cl}]^-$ with no apparent molecular ion. CL-20 is barely detectable with APCI, but the APCI-MS spectrum of CL-20 (Figure 2-40B) does show the presence of an $[\text{M}-\text{H}]^-$ ion at m/z 437 $[\text{M}-\text{H}]^-$ and an adduct ion at m/z 473 $[\text{M}+\text{Cl}]^-$. The daughter ion mass spectrum of the $[\text{M}+\text{Cl}]^-$ ion (m/z 473) of CL-20 (Figure 2-41) shows daughter ions at m/z 426, 233, and 208, corresponding to the neutral losses of 47 amu (HNO_2), 240 amu ($\text{Cl} + \text{N}(\text{NO}_2)\text{CHN}(\text{NO}_2)\text{CN}(\text{NO}_2)$), and 265 amu ($\text{N}(\text{NO}_2)\text{CHN}(\text{NO}_2)\text{CN}(\text{NO}_2) + \text{N}(\text{NO}_2)$), respectively. The daughter ion at m/z 233 is



Daughter Ions of $[M+Cl]^-$ Ion (m/z 257) of RDX

Daughter Ions (m/z)	Neutral Loss (amu)	Neutral(s) Lost
210	47	HNO ₂
197	60	2NO
93	164	CH ₃ N(NO ₂)CH ₂ N(NO ₂)CH ₃
82	175	CH ₃ N(NO ₂)CH ₂ N(NO ₂)CN

Figure 2-37. Daughter ion mass spectrum of $[M+Cl]^-$ ion (m/z 257) produced by ESI of RDX. Spectrum acquired at a resonant excitation q_z of 0.25, isolation window of 3 amu, and collision energy of 20%.

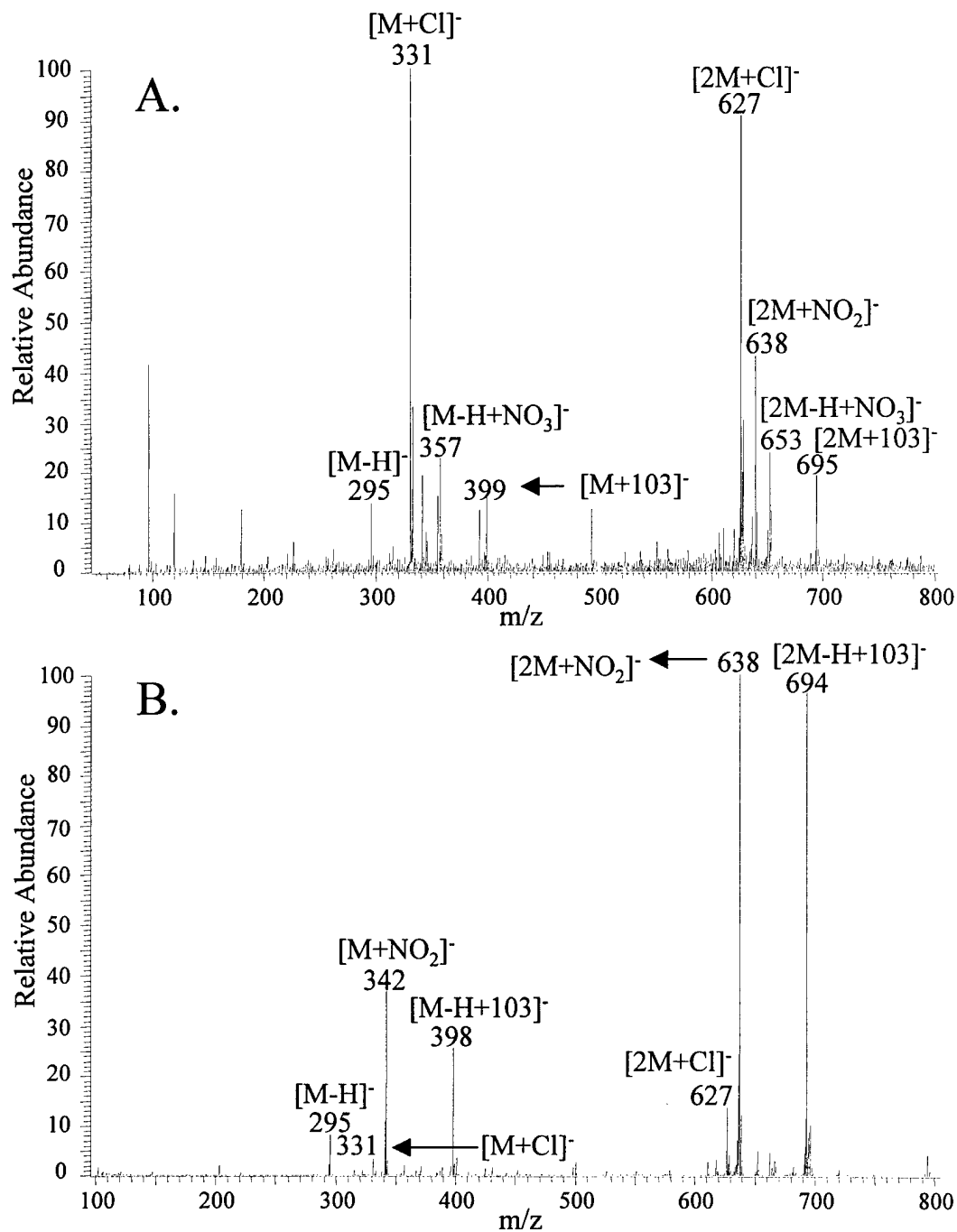
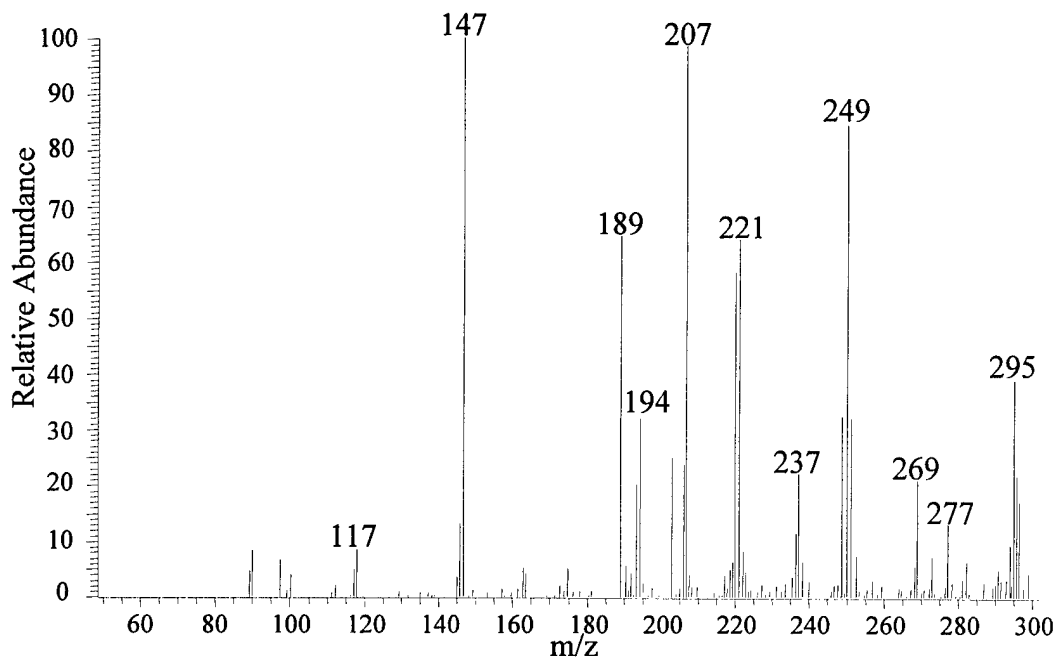


Figure 2-38. Mass spectra of HMX (MW = 296): A. Negative ESI, B. Negative APCI.



Daughter Ions of $[M-H]^-$ Ion (m/z 295) of HMX

Daughter Ions (m/z)	Neutral Loss (amu)	Neutral(s) Lost
277	18	H ₂ O
269	26	CN
249	46	NO ₂
221	74	CH ₂ N(NO ₂)
207	88	NCH ₂ N(NO ₂)
194	101	NCH ₂ N(NO ₂)CH
189	106	NCH ₂ N(NO ₂) + H ₂ O
147	148	CH ₂ N(NO ₂)CH ₂ N(NO ₂)
117	178	CH ₂ N(NO ₂)CH ₂ N(NO ₂) + NO

Figure 2-39. Daughter ion mass spectrum of $[M-H]^-$ ion (m/z 295) produced by ESI of HMX. Spectrum acquired at a resonant excitation q_z of 0.25, isolation window of 3 amu, and collision energy of 24%.

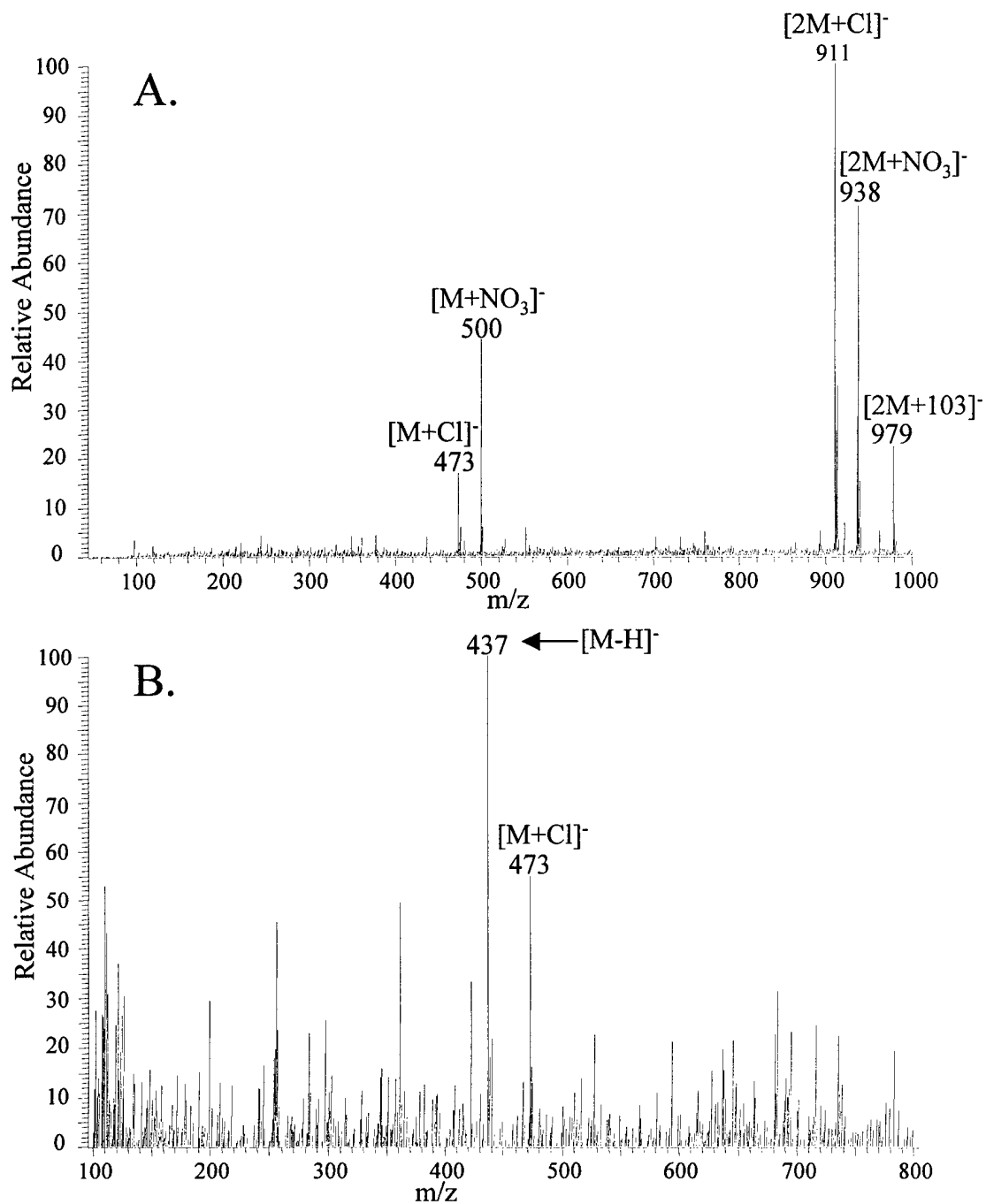
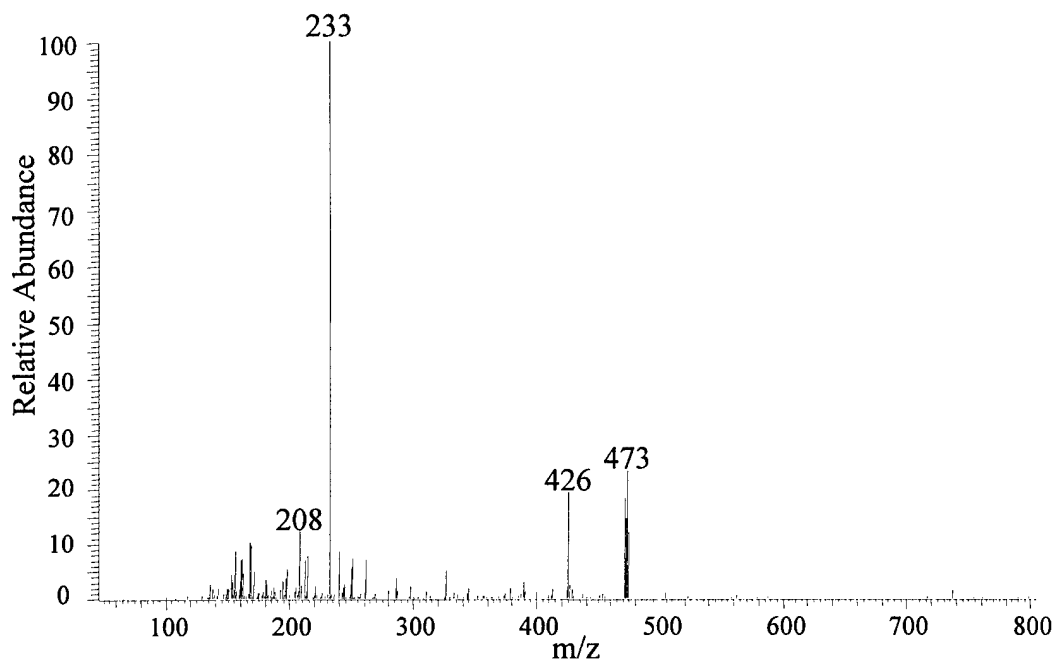


Figure 2-40. Mass spectra of CL-20 (MW = 438): A. Negative ESI, B. Negative APCI.



Daughter Ions of $[M+Cl]^-$ Ion (m/z 473) of CL-20

Daughter Ions (m/z)	Neutral Loss (amu)	Neutral(s) Lost
426	47	HNO_2
233	240	$Cl + N(NO_2)CHN(NO_2)CN(NO_2)$
208	265	$N(NO_2)CHN(NO_2)CN(NO_2) + N(NO_2)$

Figure 2-41. Daughter ion mass spectrum of $[M+Cl]^-$ ion (m/z 473) produced by ESI of CL-20. Spectrum acquired at a resonant excitation q_z of 0.25, isolation window of 4 amu, and collision energy of 20%.

the most intense, because it is a fragment that corresponds to nearly half of the caged molecule and represents the most common fragmentation pathway.

The last of the nitramines investigated is 1,3,3-trinitroazetidine (TNAZ), which was not detectable by APCI-MS and it was barely detected by ESI-MS. This may be attributable to the high shock sensitivity of TNAZ [Reich et al., 1997], which could result in its fragmentation even with the soft ionization of ESI. The ESI-MS spectrum of TNAZ (Figure 2-42) has one recognizable adduct ion at m/z 227 $[M+Cl]^-$. MS/MS of the $[M+Cl]^-$ ion (m/z 227) of TNAZ (Figure 2-43) produces two daughter ions at m/z 153 and m/z 121, corresponding to the neutral losses of 74 amu ($Cl + CHCHCH$) and 106 amu ($Cl + NO_2CCH$).

Nitro Aliphatic Compound

The only nitro aliphatic compound interrogated for this study was 5-nitro-2,4-dihydro-3*H*-1,2,4-triazol-3-one (NTO). NTO was not detectable with APCI-MS, but produced a very strong $[M-H]^-$ ion at m/z 129 with ESI-MS (Figure 2-44). The ESI-MS of NTO also produced a dimer ion at m/z 259 $[2M-H]^-$ and a series of sodiated adduct clusters at m/z 281 $[2M-2H+Na]^-$, m/z 433 $[3M-3H+2Na]^-$, m/z 585 $[4M-4H+3Na]^-$, and m/z 737 $[5M-5H+4Na]^-$. The daughter ion mass spectrum of $[M-H]^-$ ion (m/z 129) of NTO (Figure 2-45) shows one intense ion at m/z 55, which corresponds to a neutral loss of 74 amu ($CO + NO_2$).

Conclusion

In this chapter, thirty-two different explosives have been investigated with ESI-MS and APCI-MS to determine their ability to be detected using these atmospheric pressure ionization methods. Table 2-1 lists the explosives, along with the most intense

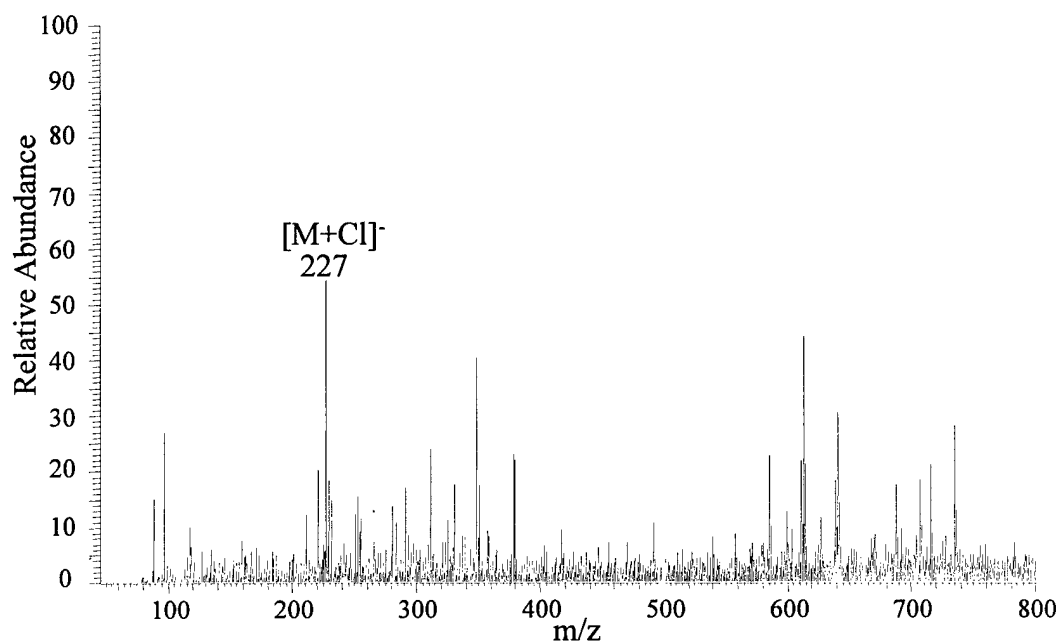
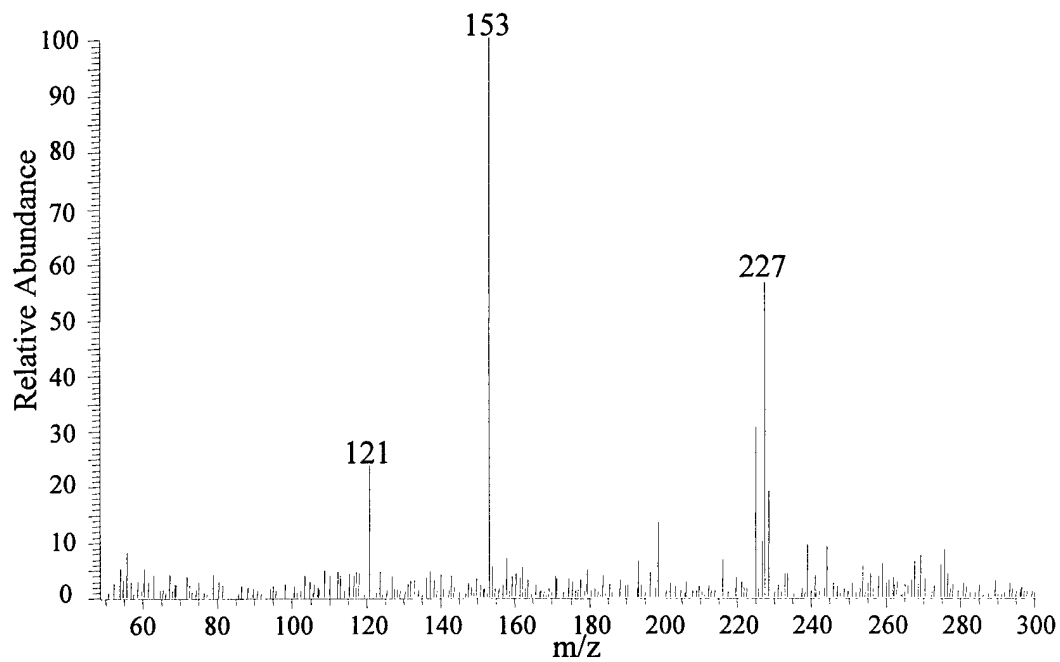


Figure 2-42. Negative ESI mass spectrum of TNAZ (MW = 192).



Daughter Ions of $[M+Cl]^-$ Ion (m/z 227) of TNAZ

Daughter Ions (m/z)	Neutral Loss (amu)	Neutral(s) Lost
153	74	Cl + CHCHCH
121	106	Cl + NO ₂ CCH

Figure 2-43. Daughter ion mass spectrum of $[M+Cl]^-$ ion (m/z 227) produced by ESI of TNAZ. Spectrum acquired at a resonant excitation q_z of 0.25, isolation window of 4 amu, and collision energy of 20%.

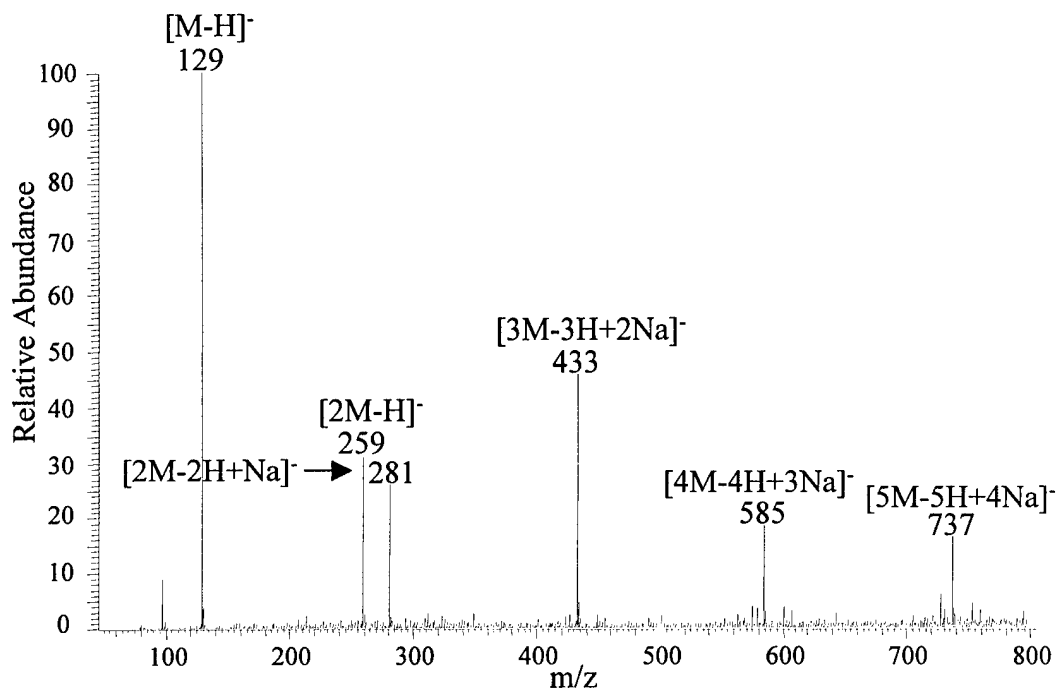
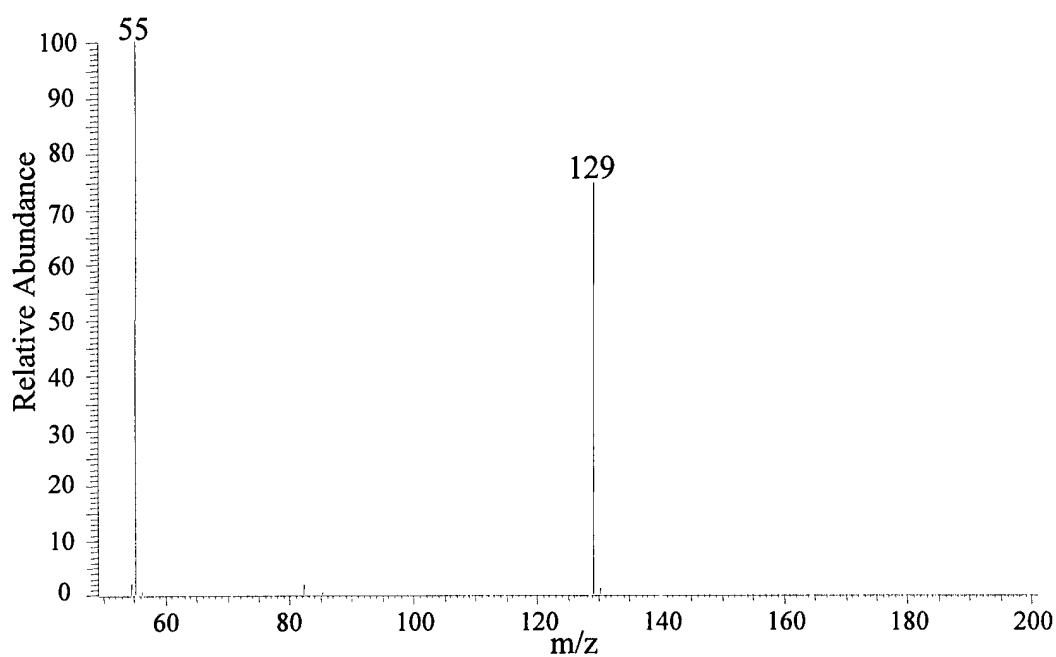


Figure 2-44. Negative ESI mass spectrum of NTO (MW = 130).



Daughter Ions of $[M-H]^-$ Ion (m/z 129) of NTO

Daughter Ions (m/z)	Neutral Loss (amu)	Neutral(s) Lost
55	74	CO + NO ₂

Figure 2-45. Daughter ion mass spectrum of $[M-H]^-$ ion (m/z 129) produced by ESI of NTO. Spectrum acquired at a resonant excitation q_z of 0.25, isolation window of 3 amu, and collision energy of 24%.

Table 2-1: ESI and APCI of Explosives

Explosive (20 ppm)	ESI		APCI	
	Base Peak (m/z)	Intensity	Base Peak (m/z)	Intensity
TNT	[M-H] ⁻ , 226	1.98 x 10 ⁶	[M] ⁻ , 227	1.01 x 10 ⁸
Tetryl	[2M+Cl] ⁻ , 609	2.05 x 10 ⁶	[M*-H] ⁻ , 241	2.17 x 10 ⁷
TNC	[M-H] ⁻ , 242	4.86 x 10 ⁷	[M-H] ⁻ , 242	1.22 x 10 ⁵
TNA	[M+acetone-H] ⁻ , 285	1.96 x 10 ⁷	[M-H] ⁻ , 227	1.50 x 10 ⁵
2-NT	Not Detected	--	367	1.49 x 10 ⁵
3-NT	Not Detected	--	Not Detected	--
4-NT	Not Detected	--	367	1.28 x 10 ⁶
2,3-DNT	Not Detected	--	Not Detected	--
2,4-DNT	Not Detected	--	[M-H] ⁻ , 181	1.21 x 10 ⁵
2,5-DNT	Not Detected	--	Not Detected	--
2,6-DNT	Not Detected	--	[M+acetone-H] ⁻ , 239	3.95 x 10 ⁴
3,4-DNT	Not Detected	--	Not Detected	--
2A-4,6-DNT	[M-H] ⁻ , 196	1.02 x 10 ⁷	[M-H] ⁻ , 196	5.12 x 10 ⁴
4A-2,6-DNT	[M-H] ⁻ , 196	6.57 x 10 ⁶	[M-H] ⁻ , 196	9.38 x 10 ⁴
2,4-DA-6-NT	[M+H] ⁺ , 168	5.00 x 10 ⁶	[M+ACN] ⁺ , 208	4.53 x 10 ⁸
2,6-DA-4-NT	[M+H] ⁺ , 168	6.38 x 10 ⁶	[M+ACN] ⁺ , 208	9.29 x 10 ⁸
TNB	[M] ⁻ , 213	1.44 x 10 ⁶	[M] ⁻ , 213	1.59 x 10 ³
DNB	Not Detected	--	[M] ⁻ , 168	4.91 x 10 ⁴
NB	Not Detected	--	Not Detected	--
2A-4-NT	Not Detected	--	[M+H] ⁺ , 154	5.04 x 10 ⁷
4A-2-NT	Not Detected	--	[M-H+ACN] ⁺ , 193	7.99 x 10 ⁷
PETN	[2M-H+Cl] ⁻ , 666	6.98 x 10 ⁶	[2M-H+NO ₃] ⁻ , 693	1.23 x 10 ⁶
BTTN	[M-H+NO ₃] ⁻ , 302	3.71 x 10 ⁶	[M+NO ₃] ⁻ , 303	2.74 x 10 ⁵
TMETN	[M+103] ⁻ , 358	2.42 x 10 ⁶	[M+NO ₃] ⁻ , 317	2.75 x 10 ⁵
DEGDN	Not Detected	--	Not Detected	--
TEGDN	Not Detected	--	Not Detected	--
NQ	[M-H] ⁻ , 103	7.93 x 10 ⁵	[M+H+MeOH] ⁺ , 137	1.69 x 10 ⁸
RDX	[2M+Cl] ⁻ , 479	1.70 x 10 ⁶	[2M+NO ₂] ⁻ , 490	5.63 x 10 ⁶
HMX	[M+Cl] ⁻ , 331	1.62 x 10 ⁶	[2M+NO ₂] ⁻ , 638	4.42 x 10 ⁷
CL-20	[2M+Cl] ⁻ , 911	2.95 x 10 ⁵	[M-H] ⁻ , 437	6.75 x 10 ⁴
TNAZ	[M+Cl] ⁻ , 227	2.74 x 10 ⁴	Not Detected	--
NTO	[M-H] ⁻ , 129	1.71 x 10 ⁶	Not Detected	--

M* = *N*-methylpicramide

ion formed with ESI and APCI as well as the relative intensity of the base peak ion. This table allows for the determination of the most appropriate ionization method for each explosive. Some explosives are only detectable only with ESI or APCI, and others are not detectable with either method.

Only seven of the thirty-two explosives were not detectable by either method. 3-NT, 2,3-DNT, 2,5-DNT, 3,4-DNT contain a nitro group in the meta position of the aromatic ring, which destabilizes the charge. Nitrobenzene does not contain any basic or acidic sites, and does not have enough nitro groups on the aromatic ring to stabilize a charge through resonance. The explosive oils, DEGDN and TEGDN, contain ether groups, which contribute to the instability of these nitrate esters. APCI appears to be better suited for detecting compounds with weak acidic sites such as 2-NT, 4-NT, 2,4-DNT, 2,6-DNT, DNB, 2A-4-NT, and 4A-2-NT. ESI is better suited for ionizing compounds that are very fragile including CL-20, TNAZ, and NTO.

With such a wide variety of different compounds, characteristic ionization patterns can be determined for the different classes of explosives. In general, nitroaromatics do not readily form adduct ions due to the high electron density in their rings [Miller et al., 1996]. However, they have been shown to form adduct ions with acetone and acetonitrile. All of the explosive solutions were prepared from acetone stock solutions except for 2,4-DA-6-NT, 2,6-DA-4-NT, 2A-4-NT, and 4A-2-NT, which were prepared from acetonitrile stock solutions. The spectra of TNT and tetryl did not show any acetone adduct ions, but they have been observed previously [Reich et al., 2000]. The acetone adduct ion $[M+\text{acetone}-H]^+$ (m/z 284) of TNT is formed from the deprotonation of acetone, which has been confirmed by the deuterated acetone adduct ion (m/z 289) of TNT (Figure 2-46).

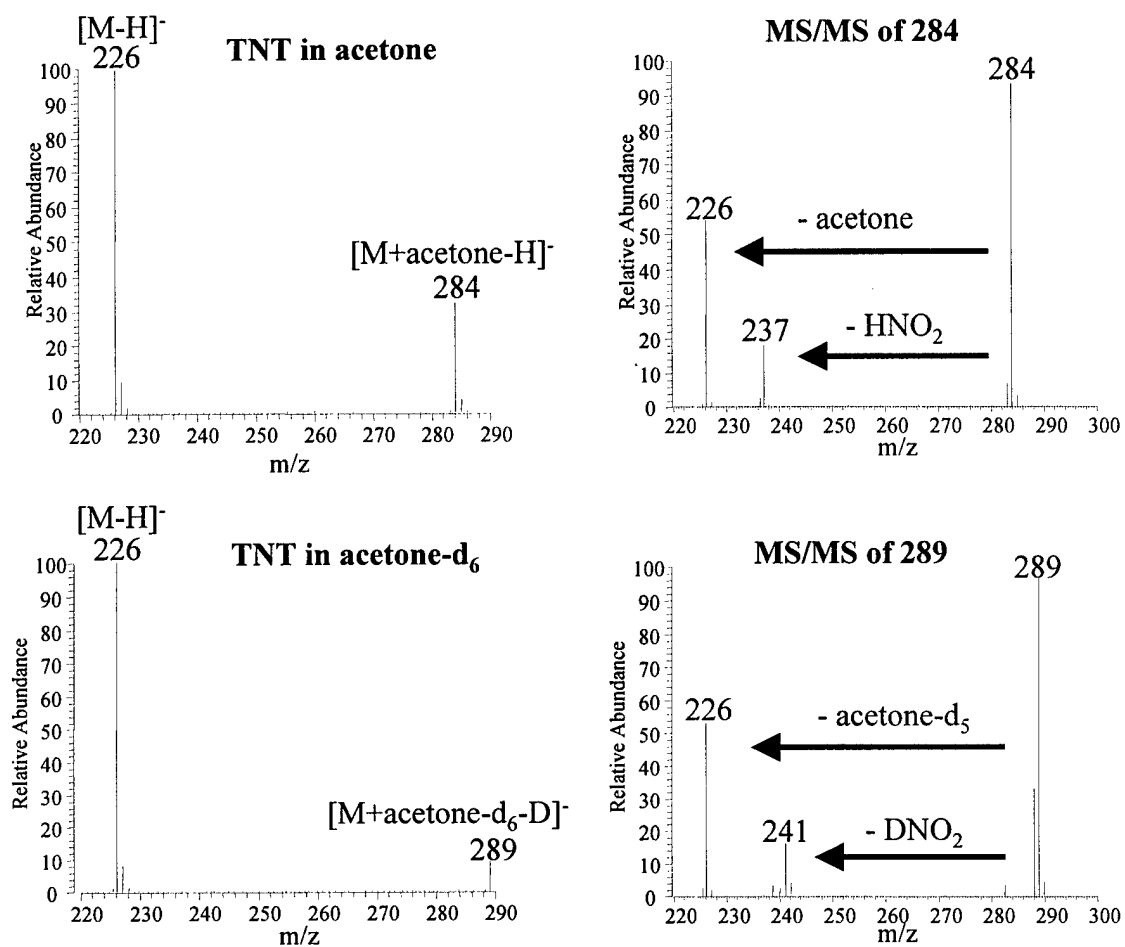


Figure 2-46. Negative ion ESI of acetone and deuterated acetone (acetone- d_6) adduct ions of TNT.

Tetryl is the only nitroaromatic explosive investigated that readily forms adduct ions with anions present in solution. This may be due to the nitramine functional group on the aromatic ring. Nitramines and nitrate esters have been previously reported to readily form adduct ions and can also be observed in the ESI-MS and APCI-MS spectra shown here. The nitro groups on these compounds have a strong inductive field effect (electron-withdrawing), which is sufficient for the attachment of nucleophilic anions on sites of low electron density [Miller et al., 1996].

The ESI and APCI of nitramines, nitrate esters, and tetryl are particularly susceptible to any impurities in the solvent system. Therefore, in order to predict which adduct ions will form, it is advisable to first acquire a low mass scan (m/z 20-200) of just the solvent ions produced with ESI and APCI. The solvent spectrum from ESI (Figure 2-47A) and APCI (Figure 2-47B) both contain chloride (Cl^-) and formate (CHO_2^-) ions. The anions that formed adducts with the explosives included chloride, nitrite (NO_2^-), nitrate (NO_3^-), and 103 (presumably $\text{NCH}_2\text{N}(\text{NO}_2)\text{CH}_3^-$). Chloride is present in both ESI and APCI solvent systems, which most likely comes from the glassware used in solution preparation. The 103 anion is only present in the ESI solvent spectrum; however, 103 also forms adducts with the explosives in APCI. Due to the lack of nitrite, nitrate, and 103 in the solvent systems, it can be concluded that these anions originate from the explosives.

Dimerization is another ionization pattern that is characteristic to certain explosive classes. Again, nitramines, nitrate esters, and tetryl are susceptible to dimer formation as they were to adduct ion formation, because of the low electron density sites of their structures. Excluding tetryl, 2A-4,6-DNT and TNB were the only nitroaromatics to form dimers, and this occurred only with APCI. Tetryl and the nitramines and nitrate

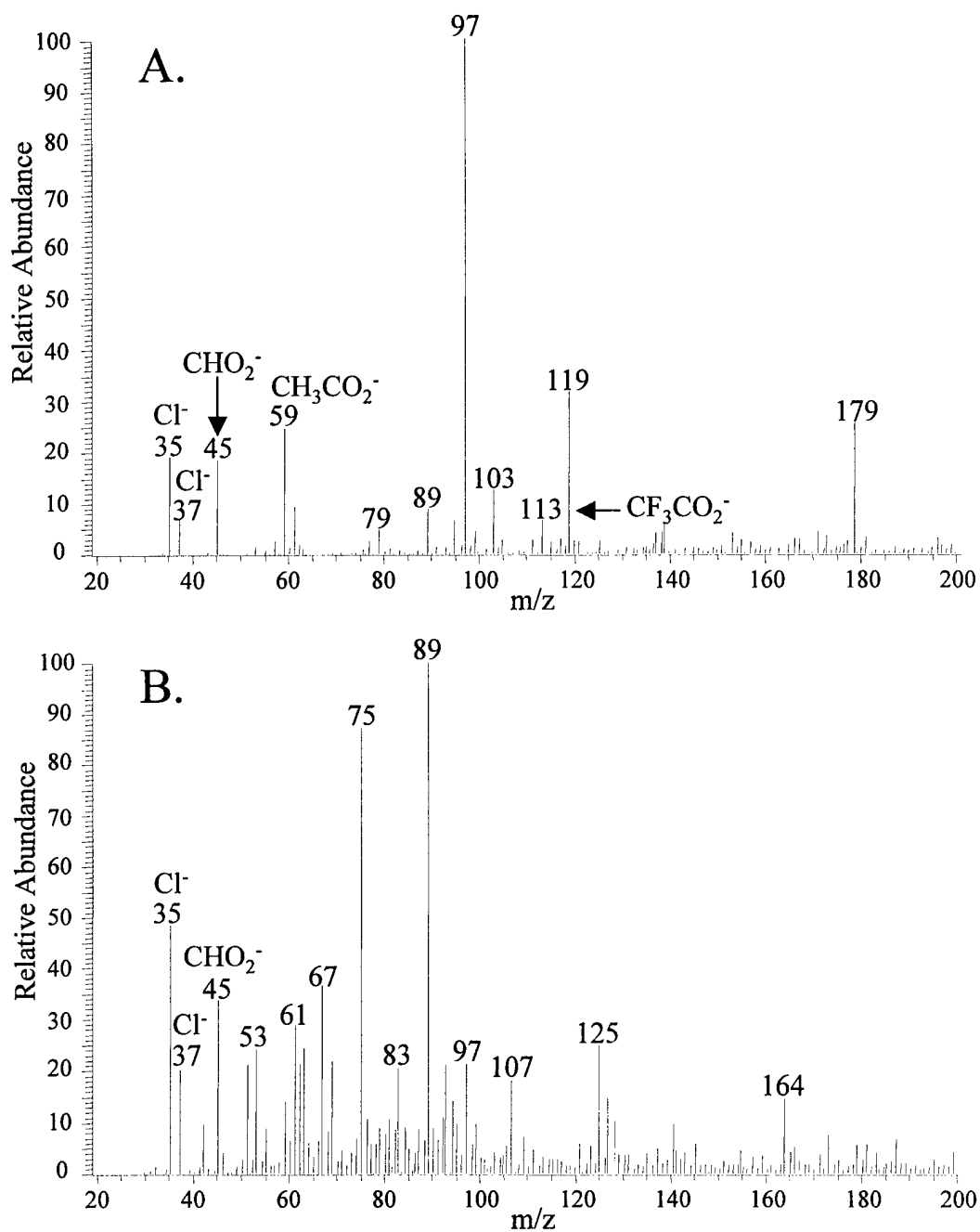


Figure 2-47. A. Negative ESI-MS spectrum of solvent ions formed with 50/50 IPA/ H_2O with 0.1% NH_4OH . B. Negative APCI-MS spectrum of solvent ions formed with 35/65 H_2O /MeOH (v/v).

esters investigated, readily form dimers with the same anions used to form adduct ions. The dimer ions formed are commonly the most intense ions in the spectra. Dimer formation is a serious concern, which needs to be corrected if any quantitation is going to be performed. TNC and NTO undergo sodiated polymerization in which a series of cluster ions are formed (e.g. $[2M-2H+Na]^+$, $[3M-3H+2Na]^+$, $[4M-4H+3Na]^+$, $[5M-5H+4Na]^+$). The sodium ion is probably present from the water and readily clusters with TNC and NTO. TNC and NTO contain one similar structural characteristic, which might influence the formation of these sodiated clusters. They both contain an oxygenated functional group (e.g. $R-C-OH$ and $R-C=O$) with lone pair electrons, which could easily allow for the attachment of a commonly present cation like sodium (Na^+).

CHAPTER 3 ADDUCT ION FORMATION OF EXPLOSIVES

As shown in Chapter 2, explosives produce identifiable ESI and APCI mass spectra which include adduct ions, molecular-type ions, fragment ions, and dimer ions. One of the main problems with using these ionization techniques, however, is the inconsistency in the spectra of the explosives. Adduct ions with chloride, nitrate, and nitrite have been observed in the spectra at times even though these anions were not intentionally added to the solvent system. It is believed that these anions are present as impurities in the solvent, sample, and/or instrument; in order to obtain reproducible spectra for each explosive, the conditions of the experiment must remain free of any impurities [McClellan, 2000]. This becomes nearly impossible when analyzing “real-world” samples such as soil, waste water and detonation soot, which include omnipresent interferants that can add to the spectral inconsistencies.

Previous research has shown that additives can be used to enhance ESI intensities and spectral consistencies for explosives detection [Miller et al., 1996; Schilling, 1996; Miller et al., 1997; McClellan et al., 1999]. Additives that are readily deprotonated in solution, such as trifluoroacetic acid (TFA), acetic acid (AA), formic acid (FA), and propionic acid (PA), or additives that form intense anions in negative-ESI, such as nitrate, nitrite and chloride, have been shown to be effective at preferentially forming one type of adduct ion for each explosive. This has resulted in improved sensitivity by increasing the relative intensities of the ions, and simplifies MS/MS experiments by forming only one intense characteristic parent ion for CID.

The daughter ion spectra of different adduct ions of explosives has been investigated, and it has been determined the daughter ion spectra of some adduct ions (e.g. $[M+TFA-H]^-$ and $[M+NO_3]^-$) do not yield relevant structural information about the analyte [Reich et al., 2000], while others (e.g. $[M+NO_2]^-$, $[M+PA-H]^-$, $[M+FA-H]^-$, $[M+AA-H]^-$, and $[M+Cl]^-$) provide rich daughter ion spectra. In this chapter, the ability of different additives to form adduct ions with explosives in ESI and APCI was studied, along with their ability to produce structurally informative daughter ion spectra. One explosive was chosen in order to simplify the study and make it possible to correlate physical properties with adduct ion formation characteristics. HMX, a nitramine explosive, was chosen because its ions readily forms adduct ions and undergoes efficient CID resulting in rich daughter ion spectra.

Experimental

Instrumentation

All experiments were performed on the Finnigan LCQ (San Jose, CA), a commercial, bench-top QITMS instrument with the ability to perform both ESI and APCI. For investigations of adduct ion formation and MS/MS in ESI, samples were infused into the mass spectrometer at a flow rate of 5 $\mu\text{L}/\text{min}$ using the LCQ syringe pump. For APCI experiments, samples were introduced into the mass spectrometer via flow injection analysis. Sample solutions were loaded into a 100 μL sample loop, and then flushed into the APCI source at 1 mL/min with the solvent from an LC. Each ESI spectrum presented is the average of 50 analytical scans. The number of analytical scans averaged for each APCI spectrum presented was dependent on the width of the flow

injection peak. For both ESI and APCI, each analytical scan consisted of 3 microscans, maximum injection time was set to 50 ms, and the AGC target values for full scan and MS/MS scans were 2×10^7 and 2×10^6 , respectively.

Samples

HMX was the only explosive used for the studies in this chapter. HMX was provided by Dr. Jehuda Yinon of the Weizmann Institute of Science, and were obtained from the Analytical Laboratory of the Israeli Police Headquarters. The sample solutions for the ESI experiments were prepared by diluting the acetone stock solutions to a concentration of 20 ppm with 50% HPLC-grade IPA: 50% HPLC-grade H_2O (v/v), with 0.1% NH_4OH . The sample solutions for the APCI experiments were prepared by diluting the acetone stock solutions to a concentration of 20 ppm with 35% HPLC-grade H_2O : 50% HPLC-grade MeOH (v/v).

The effects of different anions on adduct ion formation were studied and for trifluoroacetate (TFA-H), propionate (PA-H), acetate (AA-H), formate (FA-H), nitrite (NO_2^-), nitrate (NO_3^-), chloride (Cl^-), bisulfite (HSO_3^-), bioxalate (HOCOCO_2^-), dihydrogenphosphate (H_2PO_4^-), hydrogensulfate (HSO_4^-), bicarbonate (HCO_3^-), iodide (I^-), bromide (Br^-), bisulfide (HS^-), and fluoride (F^-). For the introduction of these ions, the following additives were employed: trifluoroacetic acid (TFA), 99% Pure (Acros); propionic acid (PA), ACS certified (Aldrich); acetic acid (AA), ACS certified (Aldrich); formic acid (FA), ACS certified (Aldrich); sodium nitrite (NaNO_2), ACS certified (Fisher Scientific); ammonium nitrate (NH_4NO_3), ACS certified (Fisher Scientific); ammonium chloride (NH_4Cl), Puratonic Grade (Alfa Aesar); sodium sulfite (Na_2SO_3), ACS certified (Aldrich); sodium oxalate ($\text{Na}_2\text{C}_2\text{O}_4$), ACS certified (Aldrich); sodium

dihydrogenphosphate (NaH_2PO_4), ACS certified (Aldrich); sodium hydrogensulfate (NaHSO_4), ACS certified (Aldrich); sodium bicarbonate (NaHCO_3), ACS certified (Aldrich); sodium iodide (NaI), ACS certified (Aldrich); ammonium bromide (NH_4Br), ACS certified (Aldrich); sodium sulfide (Na_2S), ACS certified (Aldrich); sodium fluoride (NaF), ACS certified (Aldrich).

For the ESI experiments, additives were added directly to the sample solution at a concentration that resulted in a sufficient adduct ion intensity with minimal chemical noise due to cluster ions. For the APCI experiments, additives were added to the mobile phase rather than the sample solution in order to achieve a high enough concentration of gas-phase ions for ion-molecule reactions. Again, the additive concentration was optimized to minimize cluster formation from the additives.

Results and Discussion

Effects of Additives on ESI-MS and APCI-MS

Additives that readily form negative ions in solution (ESI), or in the gas phase (APCI), can be used to form adduct ions with explosives to enhance signal intensities and spectral consistencies. Additives that form strong adduct ions in the positive mode have also been investigated [Crellin, et al., 1997; Faye, et al., 2000], but the research in this thesis will cover negative adduct ion formation only, since the majority of explosives are more amenable to negative ESI and APCI. HMX is a nitramine that forms a variety of different adduct and dimer ions with impurities in the solvent when no additives are intentionally added (Figure 3-1A). With the addition of 0.1 mM NaNO_2 , the ESI-MS of HMX forms two intense adduct ions at m/z 342 $[\text{M}+\text{NO}_2]^-$ and m/z 358 $[\text{M}+\text{NO}_3]^-$ with

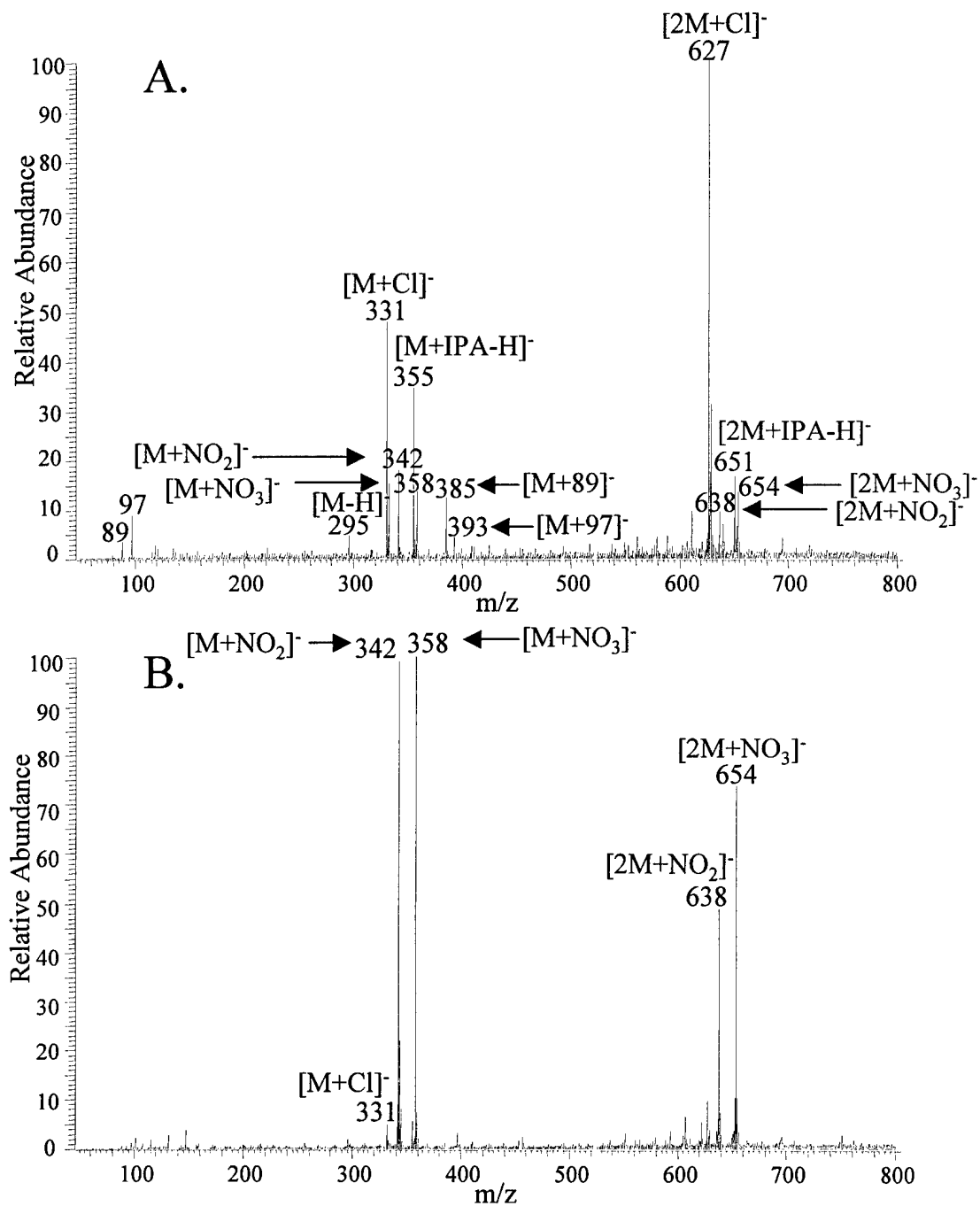


Figure 3-1. Negative ESI Mass Spectra of HMX (MW = 296): A. No $NaNO_2$ or other additives, B. 0.1 mM $NaNO_2$.

their corresponding dimer cluster ions at m/z 638 $[2M+NO_2]^-$ and m/z 654 $[2M+NO_3]^-$ (Figure 3-1B). Although the nitrate ion (NO_3^-) was not introduced to the solution, the increase in intensity of this specific adduct ion is probably due to the oxidation of nitrite (NO_2^-) to NO_3^- , as a result of the electrochemical processes that often play a part in the ion production of ESI [Van Berkel, 1997]. With increasing concentrations of $NaNO_2$ (Figure 3-2A, 1.0 mM; Figure 3-2B, 2.0 mM), the formation of nitrite adduct ions ($[M+NO_2]^-$ and $[2M+NO_2]^-$) dominates over formation of nitrate adduct ions ($[M+NO_3]^-$ and $[2M+NO_3]^-$). Salt clusters also begin to form that follow a regular pattern ($[NO_2(NaNO_2)_n]^-$, where $n = 1, 2, 3, 4 \dots n+1$). ESI has a remarkable ability to produce ion clusters via a phenomenon called ‘fractional charging’, in which the cluster ion contains one or several neutral species attached to an anion or a cation [Gamero-Castaño and de la Mora, 1999]. This pattern of salt clusters has been observed for other additives as well (e.g., $[NO_3(NaNO_3)_n]^-$ for NH_4NO_3 ; $[NaSO_4(Na_2SO_4)_n]^-$ for Na_2SO_4 ; $[H_2PO_4(NaH_2PO_4)_n]^-$ for NaH_2PO_4 ; $[NaSO_3(Na_2SO_3)_n]^-$ for Na_2SO_3 ; $[CO_2(NaO_2C)_n]^-$ for $NaOCOCO_2Na$). With the addition of even higher concentrations of $NaNO_2$ (Figure 3-3A, 5.0 mM; Figure 3-3B, 10.0 mM), salt cluster intensities increase with the appearance of a new pattern of clusters that contain a hydroxide ion (OH^-) as the core $[OH(NaNO_2)_n]^-$. The intensity of the ion at m/z 638 is from the combined relative abundance of the $[2M+NO_2]^-$ adduct ion and $[OH(NaNO_2)_9]^-$ salt cluster ion.

Addition of any ionic species (i.e., electrolytes) to the electrospray solution, other than the analyte (or small amounts of acids or bases to ionize the analyte), is usually avoided when possible, because their presence in solution tends to suppress the formation of gas-phase ions from the analytes of interest [Van Berkel, 1997]. The suppression of

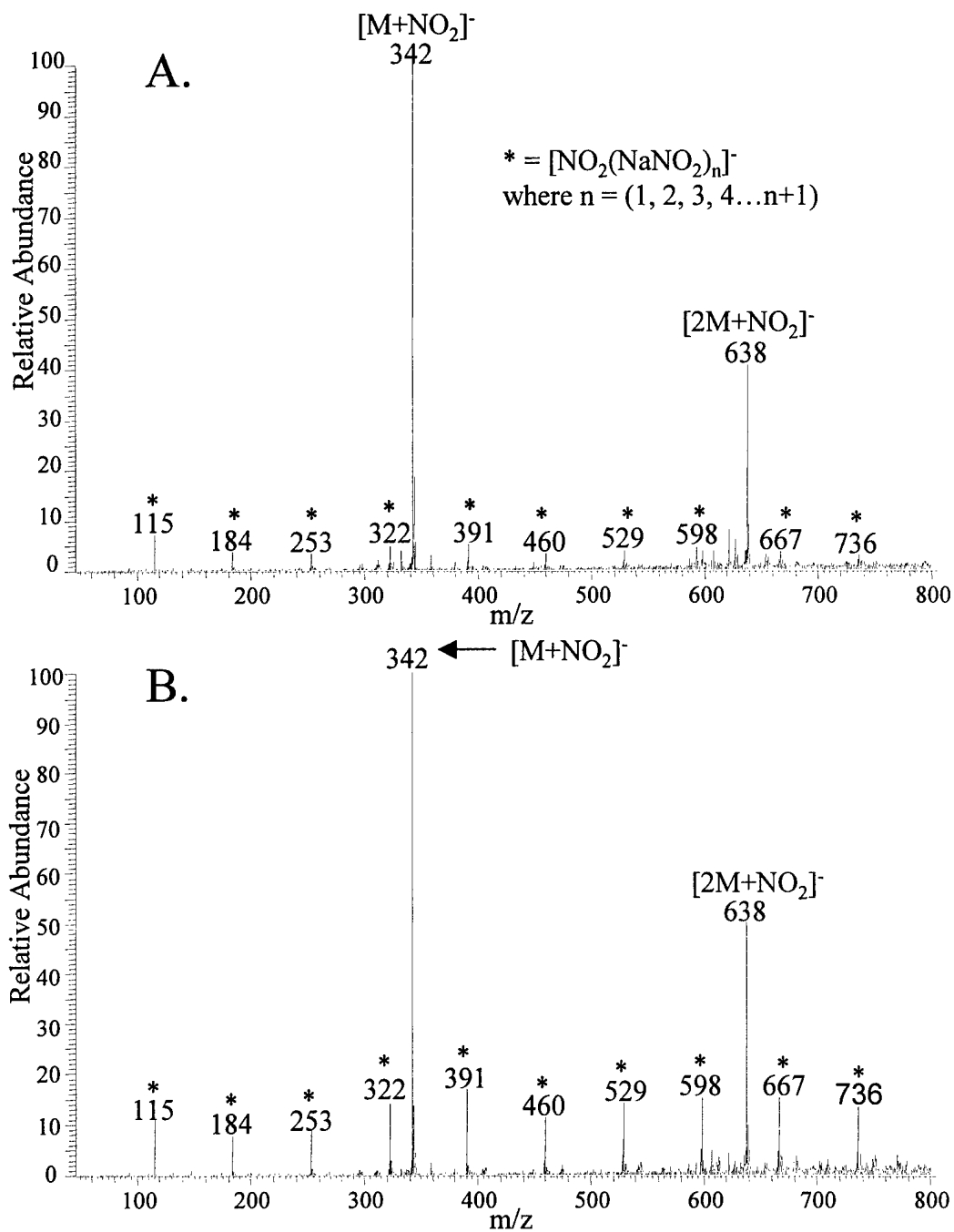


Figure 3-2. Negative ESI Mass Spectra of HMX (MW = 296): A. 1.0 mM $NaNO_2$, B. 2.0 mM $NaNO_2$.

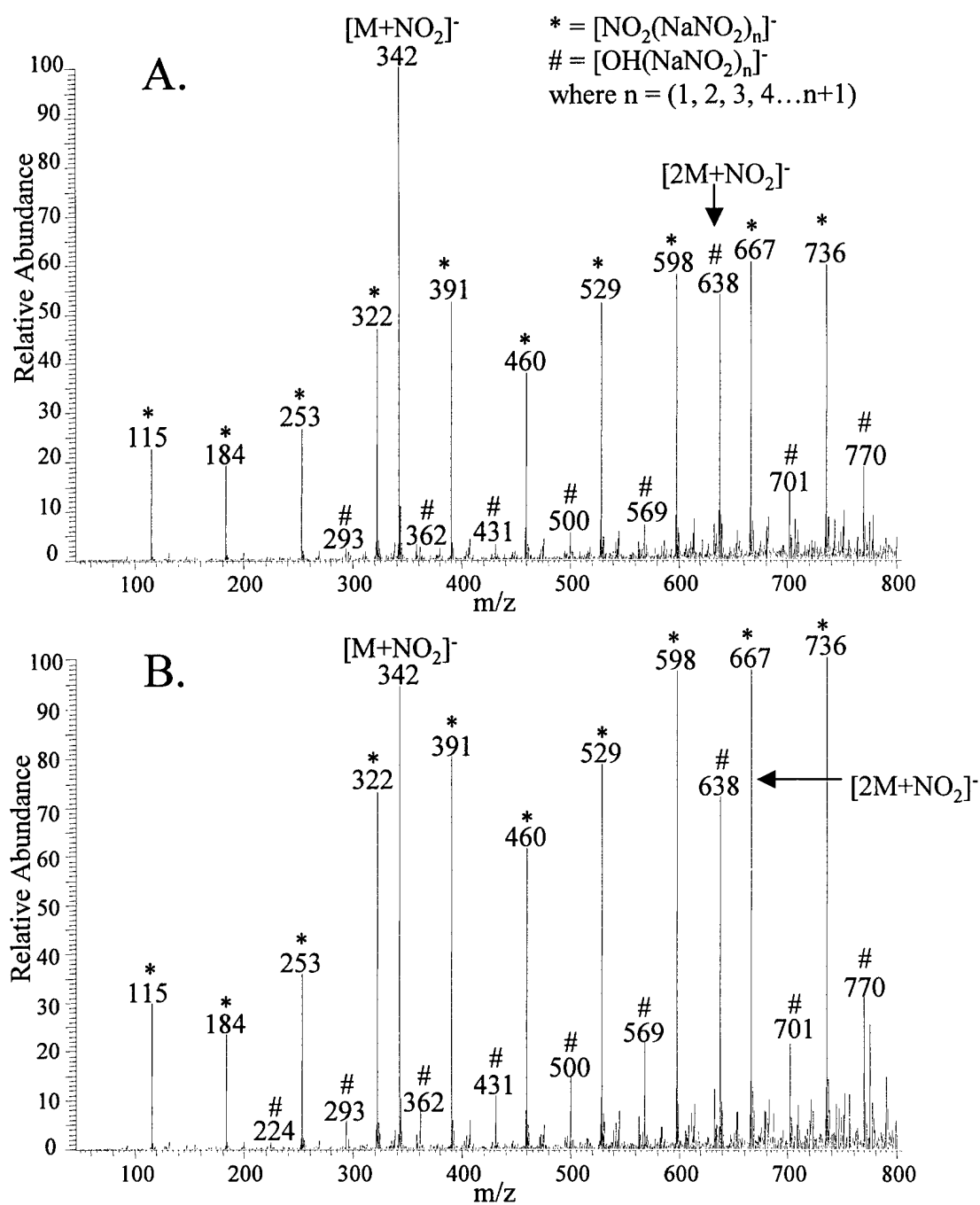


Figure 3-3. Negative ESI Mass Spectra of HMX (MW = 296): A. 5.0 mM NaNO₂, B. 10.0 mM NaNO₂.

the explosive adduct ions ($[M+NO_2]^-$ and $[2M+NO_2]^-$) with increasing additive concentration is observed in Figure 3-4. The intensity of the salt clusters steadily increases with the increase in $NaNO_2$ concentration. The $[M+NO_2]^-$ ion increases rapidly with the addition of $NaNO_2$ up to the optimal concentration of 1-2 mM $NaNO_2$. The $[M+NO_2]^-$ ion signal then decreases as it is suppressed by the salt clusters until the salt clusters have a greater intensity at 10.0 mM $NaNO_2$. At the optimal concentration of 1-2 mM $NaNO_2$, the intensity of the dimer adduct ion $[2M+NO_2]^-$ is also optimized. The slight increase in intensity between 5-10 mM $NaNO_2$ for the $[2M+NO_2]^-$ ion is due to the signal contribution of the salt cluster having the same m/z . Dimer formation is detrimental to quantitation, and should be minimized if possible. At 1 mM $NaNO_2$, the ratio of the intensities of the $[M+NO_2]^-$ to $[2M+NO_2]^-$ ion is the greatest, and therefore this concentration of $NaNO_2$ should be used.

The addition of other ionic species in ESI-MS also forms adduct ions as well as cluster ions spread throughout the mass spectrum (Figure 3-5A). The addition of NH_4NO_3 , for instance, follows the same salt cluster pattern $[X(NaX)_n]^-$ even though the additive does not contain any sodium. As observed in Chapter 2 with the sodiated clusters of TNA and NTO, sodium is always present in the solvent system and readily binds with negative sites. APCI-MS is also capable of forming adduct ions when additives are used, with the exception that salt clusters are not formed; for example, Figure 3-5B shows the APCI spectrum of HMX with NH_4NO_3 . Instead of salt cluster ions, dimer ions $[NO_3(HNO_3)]^-$ and trimer ions $[NO_3(HNO_3)_2]^-$ are formed that are very intense at m/z 125 and 188, respectively.

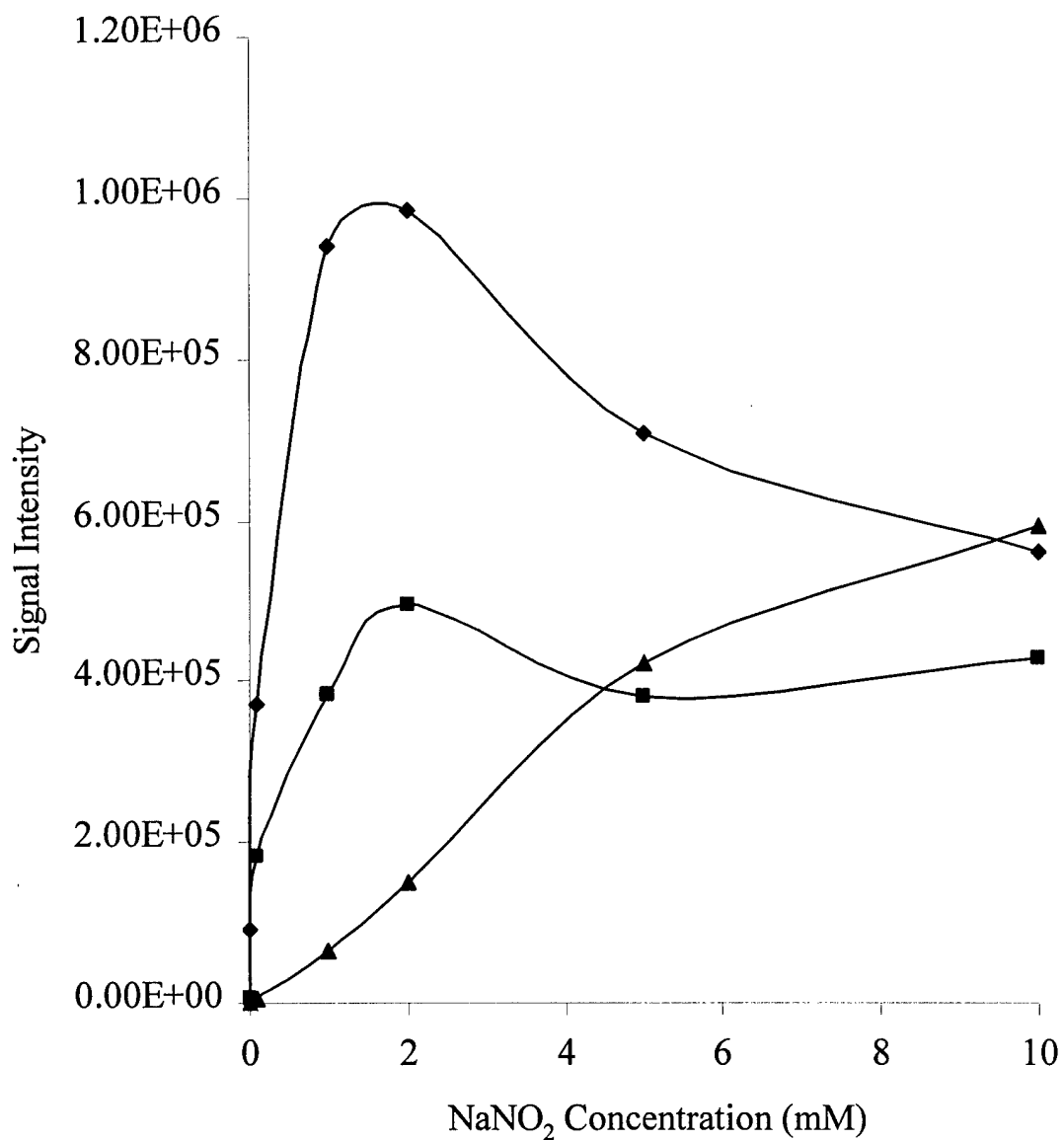


Figure 3-4. Effects of NaNO₂ concentration on [M+NO₂]⁻ ion (m/z 342) [◆], [2M+NO₂]⁻ ion (m/z 638) [■], and cluster ion [NO₂(NaNO₂)_n]⁻ [▲] formation. Negative ESI-MS of HMX (10 ppm) in 50/50 IPA/H₂O (v/v). Each point represents the average of 50 analytical scans.

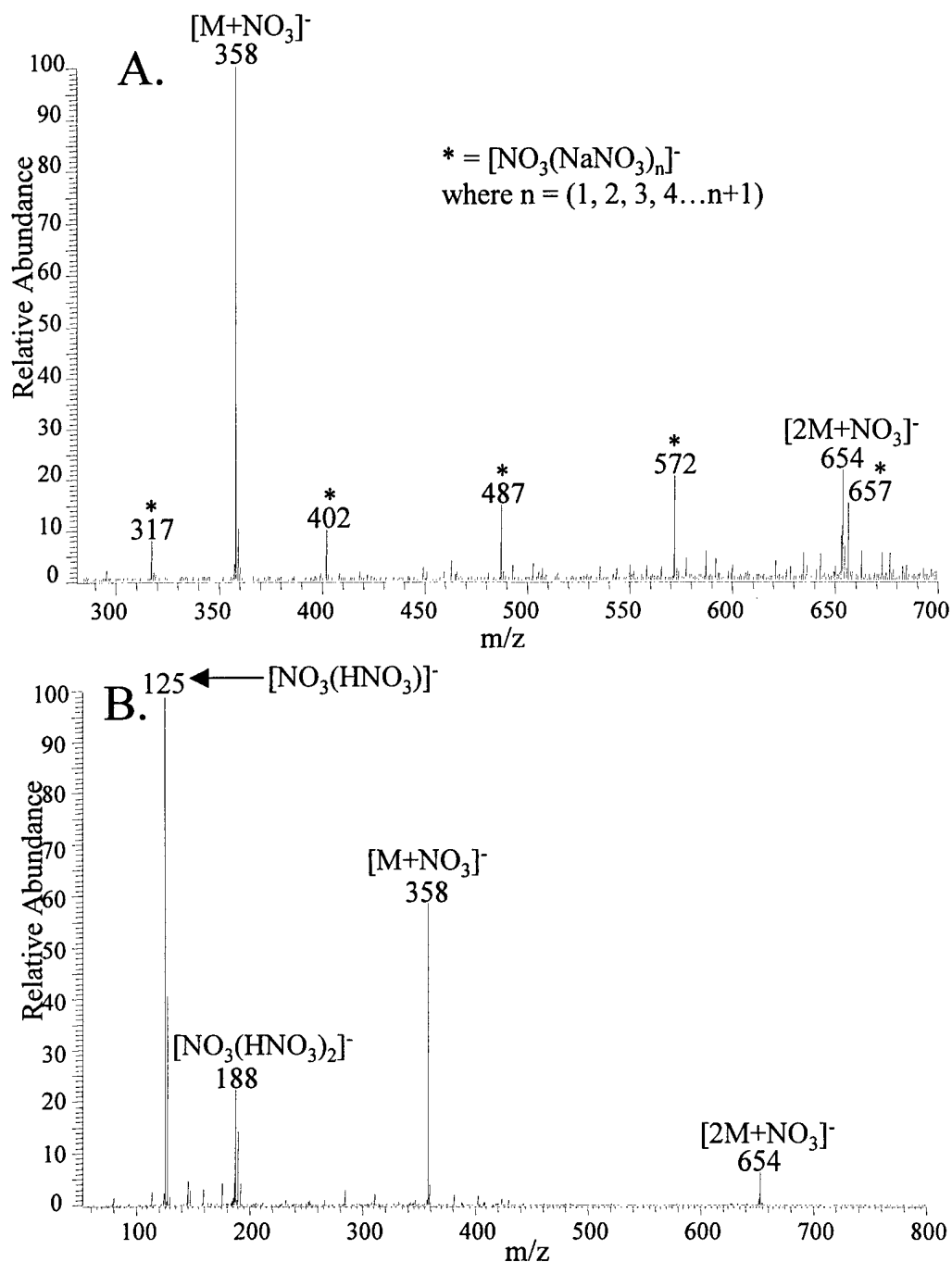


Figure 3-5. Mass spectra of NH_4NO_3 (1 mM) adduct ions of HMX (MW = 296): A. ESI-MS, B. APCI-MS.

MS/MS of Adduct Ions

Additives have been shown to improve the ionization efficiency of explosives through adduct ion formation; however, the additives used may affect the number and intensity of daughter ions produced in MS/MS. Several additives were investigated to determine their effects on the daughter ion mass spectra of HMX. When available, ammonium salts (which are more volatile than their sodium counterparts) were used in order to prevent contamination of the API chamber or plugging of the sampling orifice. Phosphate and sulfate additives are not suitable for API-MS, and were only used in this study to assist in finding a correlation between anion properties and daughter ions formed. The additives investigated are listed in Table 3-1 with the concentrations used, m/z of anions formed in solution, and the identity and m/z of the most intense adduct ion formed. The concentrations used varied for each additive depending on the amount necessary to produce only one type of adduct ion. The MS/MS spectrum of the most intense adduct ion was then acquired; the m/z of the daughter ions produced are listed in Table 3-1 in order of decreasing abundance. Although ESI-MS is capable of producing and detecting multiply-charged ions, only singly-charged anions were observed. When the additive used was dibasic (e.g., Na_2S , Na_2SO_3 , Na_2SO_4 , and $\text{NaOCOCO}_2\text{Na}$), a proton was transferred to the doubly charged anion from the analyte or the solvent to make it singly-charged (e.g., HS^- , HSO_3^- , HSO_4^- , and HOCOCO_2^-).

The adduct ions studied can be divided into three different classes depending on the type of daughter ions produced from MS/MS. The first type of adduct ion produces daughter ions that are consistent with those produced from MS/MS of the $[\text{M-H}]^-$ ion of HMX (m/z 295) that was reported in Chapter 2 (Figure 2-39). These daughter ions

Table 3-1: HMX Adduct Ion Formation and Resulting Daughter Ions from MS/MS

Additive	Concentration (mM)	Anion Formed (m/z)	Major HMX (MW = 296) Adduct Ion Formed (m/z)	Daughter Ions (m/z)
Trifluoroacetic Acid (TFA)	1.0	CF ₃ CO ₂ ⁻ 113	[M+TFA-H] ⁻ 409	113 [TFA-H] ⁻
Propionic Acid (PA)	1.0	CH ₃ CH ₂ CO ₂ ⁻ 73	[M+PA-H] ⁻ 369	147, 174, 192, 221, 117, 249
Acetic Acid (AA)	1.0	CH ₃ CO ₂ ⁻ 59	[M+AA-H] ⁻ 355	147, 174, 192, 221, 117, 249
Formic Acid (FA)	1.0	HCO ₂ ⁻ 45	[M+FA-H] ⁻ 341	147, 174, 192, 221, 117, 249
NaF	1.3	F ⁻ 19	[M+F] ⁻ 315	221, 147, 249
NH ₄ Cl	1.0	Cl ⁻ 35/37	[M+Cl] ⁻ 331	183, 257
NH ₄ Br	1.6	Br ⁻ 79/81	[M+Br] ⁻ 375	153, 275, 277
NaI	0.1	I ⁻ 127	[M+I] ⁻ 423	127 [I] ⁻
Na ₂ S	0.4	HS ⁻ 33	[M+HS] ⁻ 329	147, 174, 192, 221, 117, 249
Na ₂ SO ₃	2.2	HSO ₃ ⁻ 81	[M+acetone+HSO ₃] ⁻ 435	377 (MS ³ 377): 147, 174, 192, 221, 117, 249
Na ₂ SO ₄	0.1	HSO ₄ ⁻ 97	[M+H ₂ O+H ₂ SO ₃ +HSO ₄] ⁻ 493	393 (MS ³ 393): 147, 174, 192, 221, 117, 249
NaNO ₂	1.0	NO ₂ ⁻ 46	[M+NO ₂] ⁻ 342	147, 174, 192, 221, 117, 249
NH ₄ NO ₃	1.0	NO ₃ ⁻ 62	[M+NO ₃] ⁻ 358	62 [NO ₃] ⁻
NaHCO ₃	1.0	HCO ₃ ⁻ 61	[M+HCO ₃] ⁻ 357	147, 221, 192, 249, 117
NaOCOCO ₂ Na	0.1	HOCOCO ₂ ⁻ 89	[M+103+HOCOCO ₂] ⁻ 488	385, 342, 147, 221, 249 (MS ³ 385): 190, 237, 147
NaH ₂ PO ₄	0.1	H ₂ PO ₄ ⁻ 97	[M+H ₂ PO ₄] ⁻ 393	272, 198, 171, 245, 124, 147, 117

include m/z 147, 174, 192, 221, 117, and 249. These ions sometimes vary in intensity depending on the anion used to form the adduct. Two examples of this class of adduct ions are $[M+FA-H]^-$ formed from formate (Figure 3-6A) and $[M+AA-H]^-$ formed from acetate (Figure 3-6B). Sodium sulfite (Na_2SO_3), sodium sulfate (Na_2SO_4), and sodium oxalate ($NaOCOCO_2Na$) formed adduct ions that were solvated with solvent molecules (acetone and H_2O), or a fragment (m/z 103). These adduct ions required an additional MS stage (MS^3) first to remove the neutral molecule and then to fragment that ion to produce characteristic daughter ions of HMX.

The second class of adduct ions includes the adducts formed from chloride $[M+Cl]^-$ and bromide $[M+Br]^-$. These adduct ions are unique in that their MS/MS produce only a few intense daughter ions that contain large fragments of the analyte molecule. The MS/MS of the $[M+^{35}Cl]^-$ ion (Figure 3-7A), for example, produces daughter ions at m/z 257 and m/z 183, corresponding to one or two neutral losses of 74 amu ($CH_2N(NO_2)$). The MS/MS of $[M+Br]^-$ ion (Figure 3-7B) produces daughter ions at m/z 374/376 (from $^{79}Br/^{81}Br$), 301, 295, 275/277, and 153, which correspond to the neutral losses of 1 amu (H), 74 amu ($CH_2N(NO_2)$), 80 or 82 amu (HBr), 100 amu ($CH_2N(NO_2)CN$), and 222 or 224 amu (HBr + NO + $2CN(NO)$), respectively.

The third class of adduct ions includes the adducts formed from trifluoroacetate $[M+TFA-H]^-$, iodide $[M+I]^-$, and nitrate $[M+NO_3]^-$. The MS/MS of these adduct ions is different than the other classes, because it does not produce any structural information about HMX. These adduct ions fragment to lose the entire analyte molecule with the adduct retaining the charge. The MS/MS of $[M+NO_3]^-$ (Figure 3-8A), for example, produces one daughter ion at m/z 62 $[NO_3]^-$ corresponding to the neutral loss of 296 amu

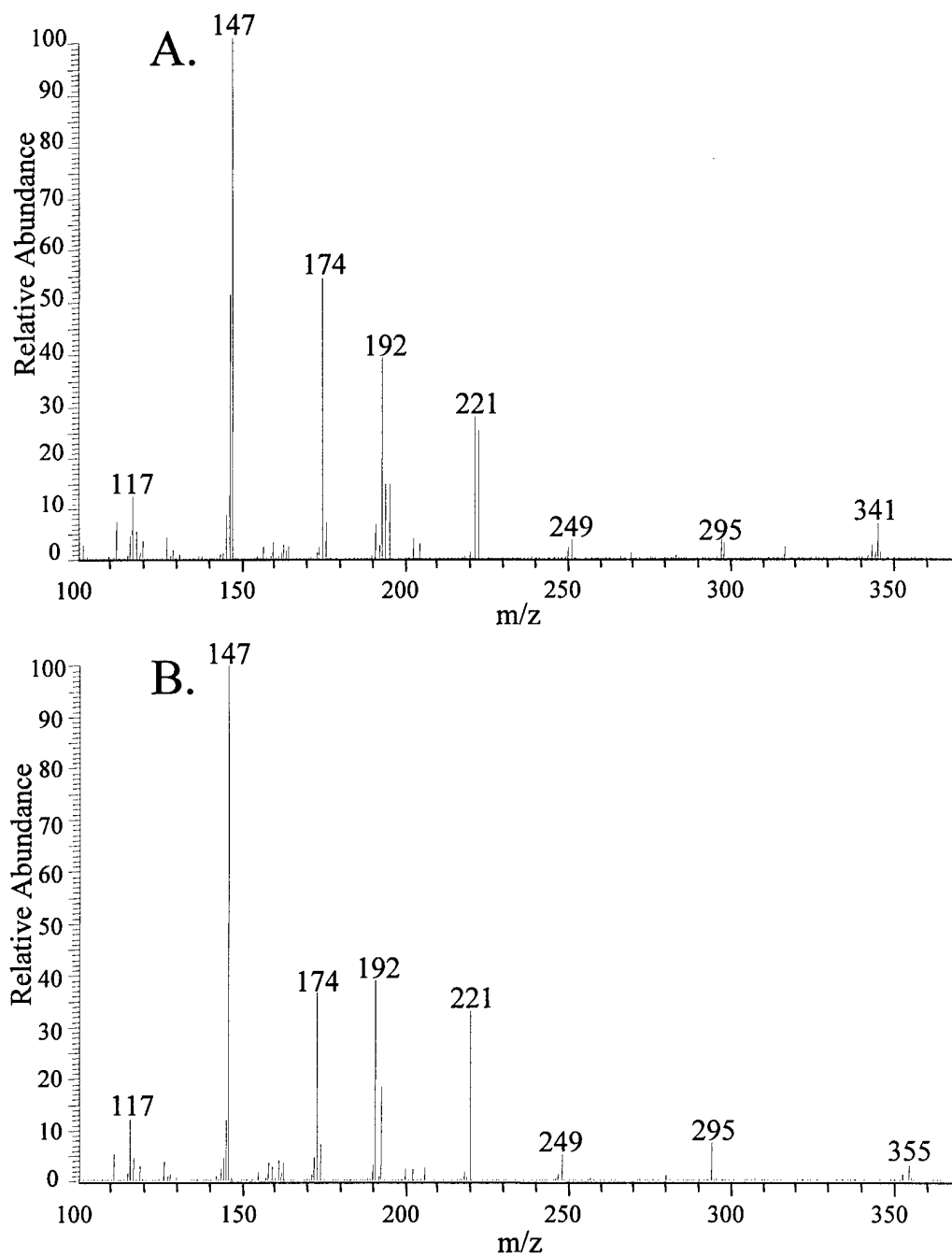


Figure 3-6. MS/MS spectra of HMX (MW = 296) adduct ions:
A. MS/MS of formic acid (FA) adduct ion $[M+FA-H]^-$ (m/z 341),
B. MS/MS of acetic acid (AA) adduct ion $[M+AA-H]^-$ (m/z 355).

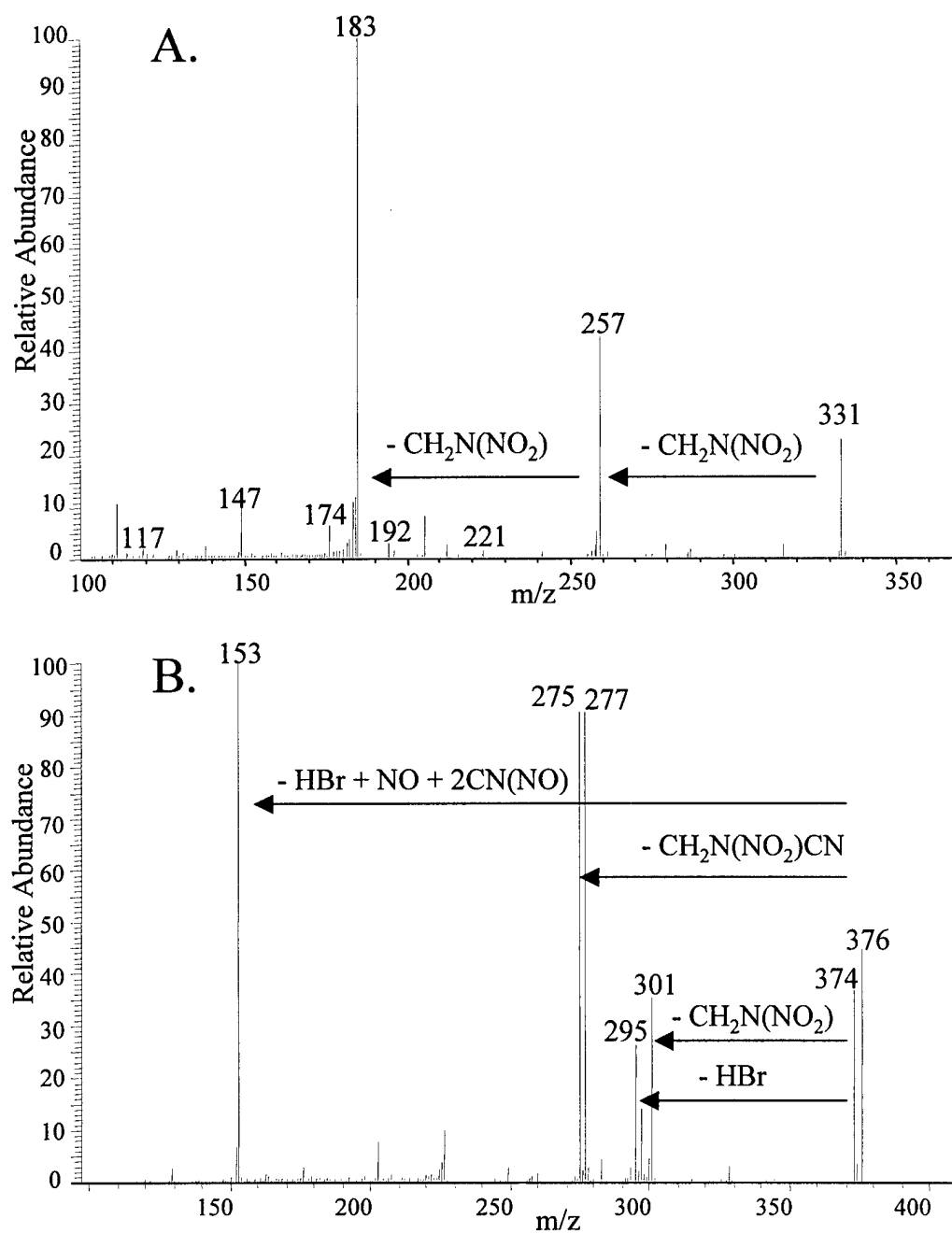


Figure 3-7. MS/MS spectra of HMX (MW = 296) adduct ions:
 A. MS/MS of NH_4Cl adduct ion $[\text{M}+\text{Cl}]^-$ (m/z 331),
 B. MS/MS of NH_4Br adduct ion $[\text{M}+\text{Br}]^-$ (m/z 375).

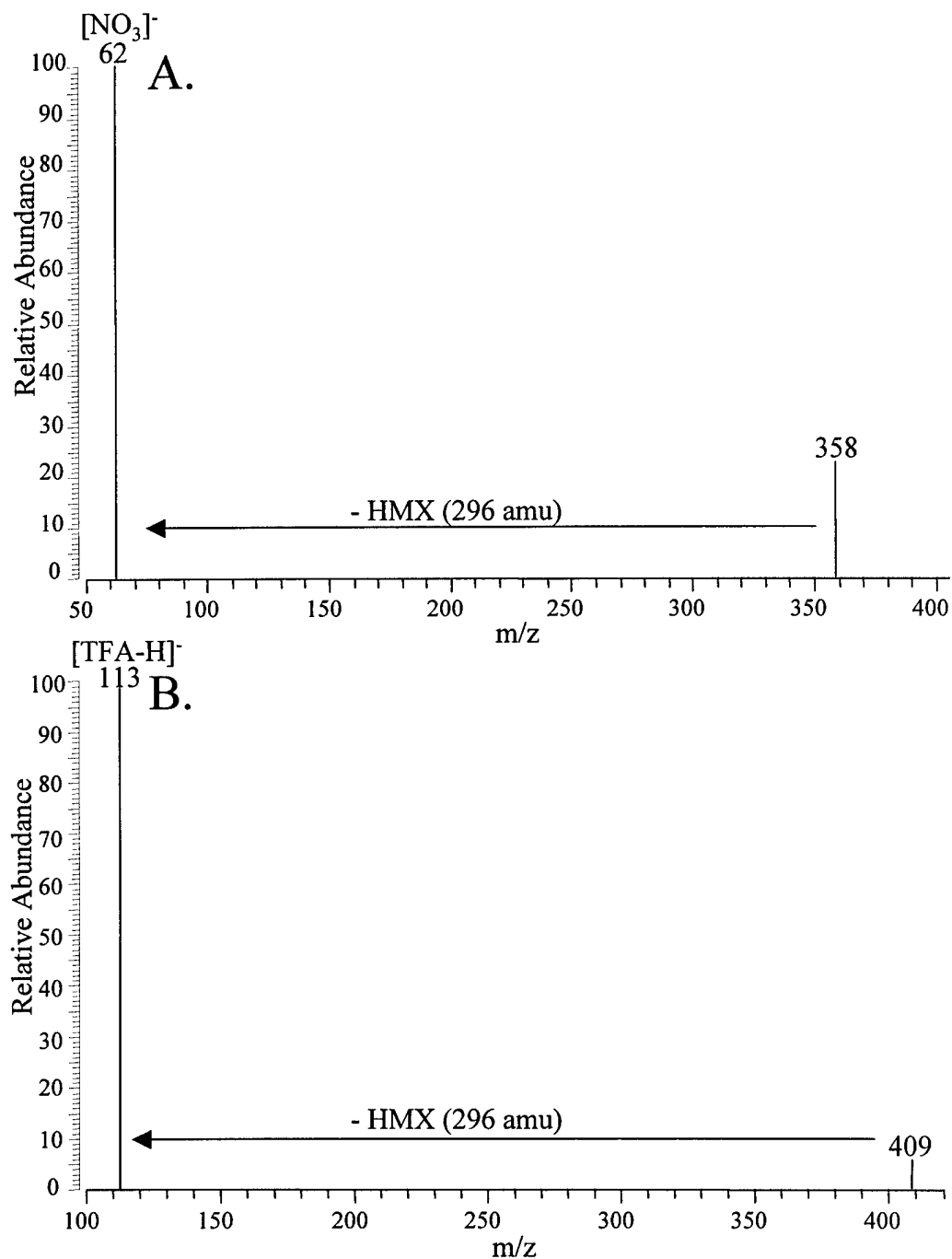


Figure 3-8. MS/MS spectra of HMX (MW = 296) adduct ions:
A. MS/MS of NaNO_3 adduct ion $[\text{M}+\text{NO}_3]^-$ (m/z 358).
B. MS/MS of trifluoroacetic acid (TFA) adduct ion $[\text{M}+\text{TFA-H}]^-$ (m/z 409),

(HMX). Similarly, the MS/MS of $[M+TFA-H]^-$ (Figure 3-8B) produces one daughter ion at m/z 113 $[TFA-H]^-$ corresponding to the neutral loss of 296 amu (HMX). When choosing additives for adduct ion formation, these particular additives should be avoided since their MS/MS spectra do not produce any relevant structural information about the analyte.

Conclusion

In this chapter, the effects of additives on the negative-ESI and negative-APCI mass spectra of HMX were explored. It was shown that additives could enhance the signal intensity and spectral consistency of the explosive. It was also observed in ESI-MS that increasing concentrations of additive result in the formation of salt clusters that suppress the analyte signal. These salt clusters have a regular pattern that make their m/z assignment easy. APCI is also capable of forming adduct ions; with increasing concentrations of additive, dimers and trimers of the anion are formed.

Through MS/MS investigations, it was determined that there are three characteristic classes of adduct ions that are defined by the structural information provided by their daughter ions. The type of fragments formed during MS/MS is presumably dependent on the size and electronegativity of the anion and its ability to stabilize and hold a charge. A proposed structure of an adduct ion of HMX is shown in Figure 3-9A. The electron-withdrawing properties of the four nitro groups produce low electron density sites within the ring. These electropositive regions are proposed to form van der Waals bonds with the anion, which sits on top of, or within the structural ring of HMX.

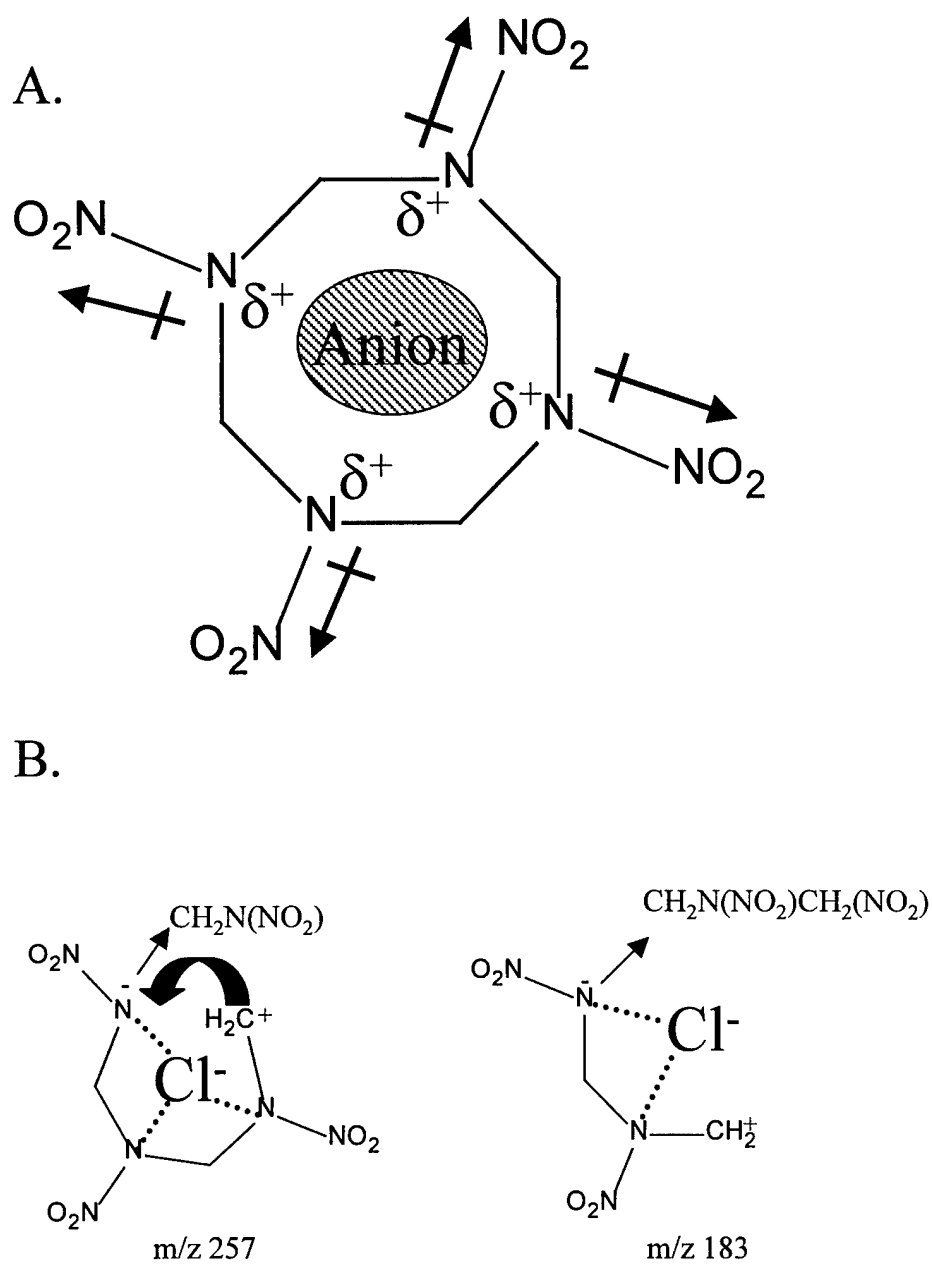


Figure 3-9. A. Proposed structure of HMX adduct ions, B. Proposed structures of daughter ions m/z 257 and m/z 183 of $[M+Cl]^-$ (m/z 331) of HMX.

Chloride and bromide form a class of adduct ions with HMX whose daughter spectra are very different than those of the $[M-H]^-$ ion of HMX. Chlorine and bromine have relatively high electron affinities (-349 kJ/mol and -325 kJ/mol, respectively) compared with other atoms in the periodic table. Their high affinity for electrons allows chlorine and bromine to strongly bind to electropositive sites. This provides stability to the adduct ion and allows for the loss of large neutral fragments such as $CH_2N(NO_2)$, which is a very common neutral loss from adduct ions of RDX and HMX [Doyle and Campana, 1985]. The proposed structures of the daughter ions at m/z 257 and m/z 183 of the $[M+Cl]^-$ (m/z 331) adduct ion of HMX are shown in Figure 3-9B.

Another class of adduct ions do not form structurally relevant daughter ions of HMX; instead, the anion holds the charge, resulting in a neutral loss of HMX. Trifluoroacetate is capable of taking the charge from HMX, for example, because the carbon atom that is attached to three very electronegative fluoride atoms is very electropositive. Therefore, a negative charge is needed on the anion to stabilize the ion. Nitrate may be capable of retaining the charge due to its ability to stabilize through resonance. Surprisingly, due to the high electronegativity of halogens, iodide is the only halide observed to pull the charge from HMX. The reason for this may be from unusually large electron-electron repulsions within the monoatomic ions. Iodide has a very large atomic volume, which minimizes the effects of electron repulsions, possibly allowing for a stable ion to be formed.

When choosing an additive to form adduct ions with explosives, it is important to consider the type of daughter ions that MS/MS will produce. The majority of additives investigated produce structurally informative daughter ions of HMX. Only a few

additives (TFA, NaI, and NH_4NO_3) produced daughter ions with no structural information about the analyte, and these additives need to be avoided if MS/MS is going to be used to perform trace detection of explosives.

Another important issue for selection of an additive is the formation of one intense adduct ion that does not require more than two stages of MS to produce structurally informative daughter ions. The intensity of daughter ions typically decreases with each sequential stage of MS. The dibasic additives Na_2SO_3 , Na_2SO_4 , and $\text{NaOCOCO}_2\text{Na}$ form adduct ions with HMX that require three stages of MS to produce structurally informative daughter ions about the analyte. The additive NaF formed a molecular-type ion $[\text{M}-\text{H}]^-$ of HMX and a series of adduct ions; $[\text{M}+\text{F}]^-$, $[\text{M}+\text{HF}+\text{F}]^-$, $[\text{M}+2\text{HF}+\text{F}]^-$, and $[2\text{M}+\text{F}]^-$. The additive NaHCO_3 also formed a molecular-type ion $[\text{M}-\text{H}]^-$ of HMX and several adduct ions; $[\text{M}+\text{HCO}_3]^-$, $[\text{M}+103]^-$, and $[2\text{M}+103]^-$. The additive NaH_2PO_4 forms very weak adduct ions ($[\text{M}+\text{H}_2\text{PO}_4]^-$ and $[2\text{M}+\text{H}_2\text{PO}_4]^-$) of HMX whose intensities are suppressed by a series of salt cluster ions. The additives Na_2S and NH_4Br form very intense adduct ions of HMX that show promise for developing an analytical method; however, these additives were not investigated with other explosives. The adduct formation of PETN, RDX, and HMX with a series of additives (AA, PA, NaNO_2 , FA, NH_4Cl , NH_4NO_3 , and TFA) were previously investigated, and showed that the chloride ion produced the most intense adduct ions for the explosives studied [Reich et al., 2000].

CHAPTER 4

LC/APCI-MS METHOD DEVELOPMENT FOR THE ANALYSIS OF EXPLOSIVES

In Chapter 2 it was observed that ESI-MS and APCI-MS of nitramines and nitrate esters yield complex spectra full of various adduct ions and dimer clusters, whose presence and intensity is dependent on impurities in the solvent, sample, and/or instrument. In Chapter 3 it was discussed that the use of additives in ESI-MS and APCI-MS can be used to preferentially form one type of adduct ion, which improves the sensitivity for the explosive and the consistency of the spectrum. A number of additive studies have been reported in the literature for the ESI-MS of explosives [Miller et al., 1996; Schilling, 1996; Miller et al., 1997; McClellan et al., 1999], but there have been no studies on the use of additives to enhance the detection of explosives using APCI-MS.

APCI uses higher flow rates from 0.5 to 2.0 mL/min compared to ESI, which uses effluent flows from 1 to 10 μ L/min. APCI is a mass-sensitive technique, whose sensitivity increases with flow rate; therefore it would be beneficial to use the highest flow rate possible. Due to the pumping capacity of the LCQ, however, an eluent flow rate of 1.0 mL/min or less is optimal for APCI. Due to the high flow rates of APCI, signal suppression and API chamber contamination caused by salt additives is of greater concern for APCI than for ESI. Use of a volatile additive will reduce contamination and provide for more efficient gas-phase ionization.

The use of chlorinated solvents to form chloride adducts, $[M+Cl]^-$, of analytes that lack acidic sites has proven to be effective for ESI-MS [Cole, 1999]. The addition of chlorine-containing additives has also proven effective in promoting formation of

[M+Cl]⁻ adduct species in LC/MS applications employing ECNCI [Tannenbaum et al., 1975; Dougherty et al., 1975; Parker et al., 1985; Barcelo et al., 1987; Geerdink et al., 1987; Kuksis et al., 1991; Kato et al., 1991; Marai et al., 1992]. APCI-MS is very similar to ECNCI-MS with the exception that APCI occurs at higher pressures (760 Torr compared to 1 Torr) than ECNCI. Therefore, the use of chlorinated solvents should prove effective for forming chloride adducts in APCI. Since most chlorinated solvents are volatile and chloride adducts of explosives have been shown to produce structurally informative daughter ions (see Chapter 3), different chlorinated solvents should be investigated for use with APCI-MS for the trace detection of explosives.

Although MS/MS is capable of separating mixtures of explosives, co-eluting compounds in the APCI source will undergo competition for ionization. Compounds with the highest chloride ion affinity will form chloride adducts via nucleophilic addition (Chapter 1) and will have more efficient ionization (higher intensity) than the other co-eluting compounds, making quantitation difficult. This is why chromatographic separation is an important aspect of trace detection of explosives using APCI-MS. LC also serves to remove interfering substances from other components of such complex mixtures as soil samples and post-explosion residues, which can also compete for ionization.

Experimental

Instrumentation

All experiments were performed on the Finnigan LCQ (San Jose, CA) in the negative-APCI mode. A Hewlett Packard 1090 HPLC pump coupled to a Haisil 100 C18

column (150 mm in length x 4.6 mm i.d., 5 μ m particle size) from Higgins Analytical, Inc. (Mountain View, CA) was used for all LC/MS experiments. The mobile phase was 35% HPLC grade water (H_2O): 65% HPLC grade methanol (MeOH), which was sufficient at separating the explosives isocratically with a flow rate of 1 mL/min. It is important that the composition of the mobile phase remain constant (i.e. no gradient), because the APCI settings are dependent on the volatility of the eluent and ramping these parameters would not prove effective. Samples were injected from a 24.6 μ L sample loop. For the variable sample loop experiment, 10, 24.6, 50, 75, and 100 μ L sample loops were used to introduce samples. Sample loops and tubing between the pump, column, and APCI source were composed of polyetheretherketone (PEEK) material. The pressure of the system was 140 \pm 3 bar. The number of analytical scans averaged for each APCI mass spectrum presented was dependent on the width of the mass chromatographic peak. Each analytical scan consisted of 3 microscans, maximum injection time was set to 200 ms to optimize ion injection for each point in the chromatographic peak, and the AGC target values for full scan and MS/MS scans were 2×10^7 and 2×10^6 , respectively.

Samples

The effects of different chlorinated solvents on adduct ion formation were investigated, including the following: methylene chloride (CH_2Cl_2), ACS certified (Fisher Scientific), MW = 84.93; chloroform (CHCl_3), ACS certified (Fisher Scientific), MW = 119.38; and carbon tetrachloride (CCl_4), ACS certified (Fisher Scientific), MW = 153.82. Chlorinated solvents were added directly to the mobile phase at various concentrations (volume percent).

For the chlorinated solvent study and APCI tune method development, the five most often used and manufactured military explosives [Yinon, 1999] were investigated. These explosives are HMX, RDX, tetryl, TNT, and PETN. Three additional explosives which are commonly used in military explosive formulations, NTO, NQ, and CL-20, were used in the variable sample loop volume experiment and in the LC/APCI-MS and LC/APCI-MS/MS method development. Explosive mixtures were prepared by diluting the acetone stock solutions with HPLC-grade H₂O. A 1 ppm explosive mixture was used for all experiments except for in the development of the calibration curve, in which variable concentrations were prepared by serial dilution ranging from 1 ppt to 1 ppm. A 1 ppm solution consists of 1 µg/mL of each explosive in the mixture.

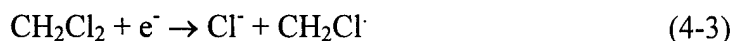
Results and Discussion

Chlorinated Solvent Study

The chloride ion (Cl⁻) is produced under APCI conditions by dissociative electron capture [Harrison, 1983]. The major reaction of the chloride ion is to form the adduct ion [M+Cl]⁻, therefore it is important to maximize the amount of gas-phase chloride ions present for reaction. One parameter that can be used to determine the propensity of a chlorinated solvent to produce chloride ions is its electron attachment rate constant [Harrison, 1983]. A faster electron attachment rate constant should result in a faster production of chloride ions and a higher efficiency for the formation of adduct ions, [M+Cl]⁻. The electron attachment rate constants for methylene chloride, chloroform, and carbon tetrachloride are 1.4×10^{-11} , 3.6×10^{-9} , and 2.5×10^{-7} cm³ molecule⁻¹ sec⁻¹, respectively [Harrison, 1983].

The intensities of five different explosives (HMX, RDX, tetryl, TNT, and PETN) were plotted as a function of methylene chloride concentration (0%, 0.01%, and 0.1% by volume) in Figure 4-1. The intensity of the $[M+Cl]^-$ adduct ion was monitored for each explosive except for TNT, in which the $[M-H]^-$ ion was used because TNT does not form adduct ions with chloride. With increasing concentration of methylene chloride, the intensity of the $[M+Cl]^-$ ion of RDX and PETN gradually increases, while that of HMX increases rapidly with concentrations above 0.01%. Tetryl forms adducts with chloride, but its $[M+Cl]^-$ ion intensity appeared to remain constant with increasing concentrations of methylene chloride.

TNT's $[M-H]^-$ ion signal decreased dramatically with increasing methylene chloride concentration, presumably, due to signal suppression caused by competitive ionization processes. The $[M-H]^-$ ion is produced by proton abstraction of TNT by the O^- reagent ion (equation 4-1). Electron capture by nitrous oxide (N_2O), using a nonreactive moderating gas such as N_2 (sheath and auxiliary gas of API source), produces the O^- reagent ion via dissociation (equation 4-2). The chloride reagent ion Cl^- is produced by a similar reaction with the electron capture by methylene chloride (equation 4-3).



Since the chlorine atom has a higher electron affinity (83.4 kcal/mol) than the oxygen atom (33.7 kcal/mol), the formation of oxide reagent ions O^- is reduced, resulting in the signal suppression of the $[M-H]^-$ ion of TNT.

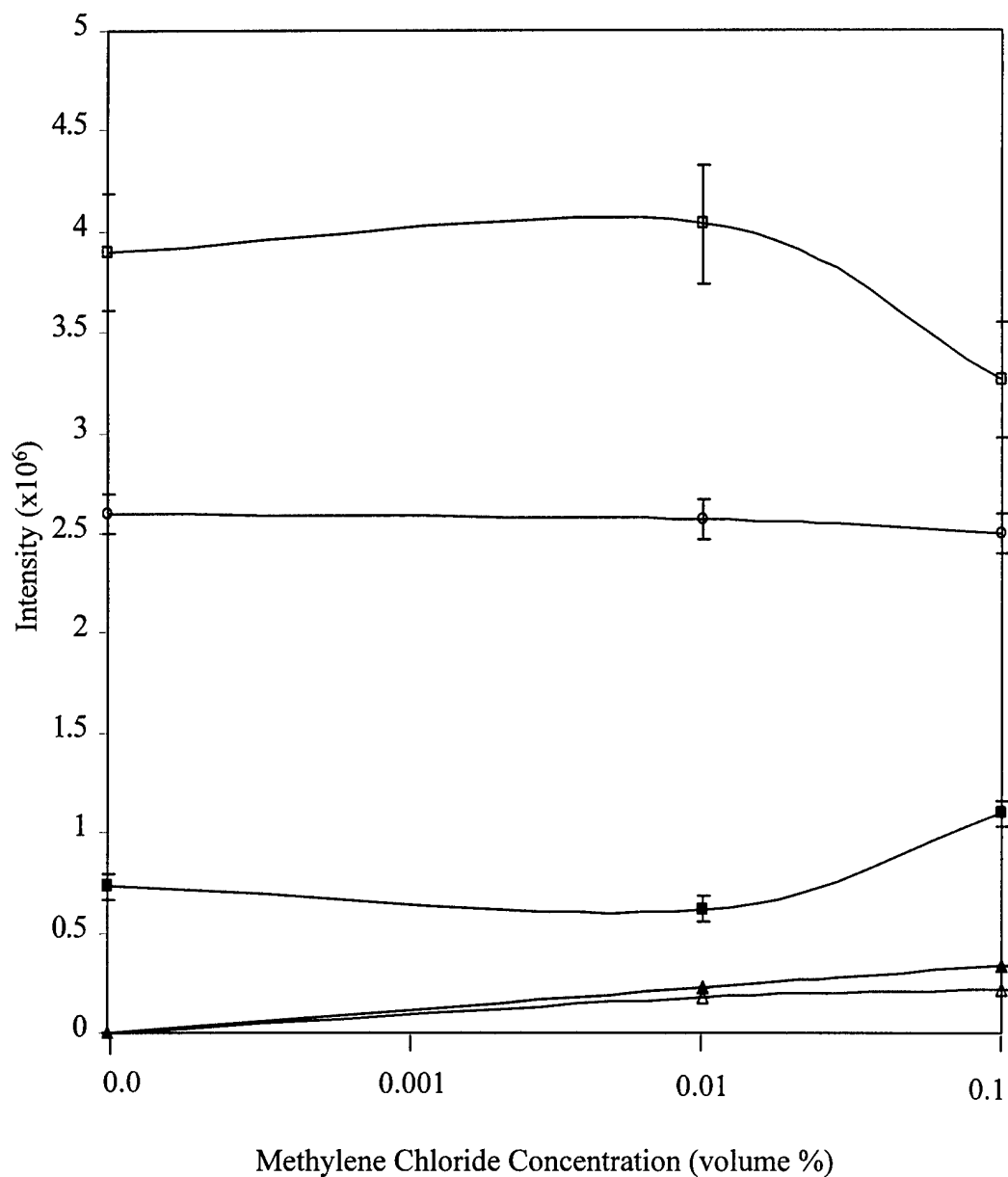


Figure 4-1. The effects of methylene chloride concentration (volume %) on the APCI-MS intensities of $[M+Cl]^-$ of HMX (■), $[M+Cl]^-$ of RDX (▲), $[M+Cl]^-$ and $[M^*-H]^-$ of tetraol (○), $[M-H]^-$ of TNT (□), and $[M+Cl]^-$ of PETN (△). M^* is *N*-methylpicramide. Error bars are +/- one standard deviation of the mean for three replicates.

Another change in TNT ionization as a result of methylene chloride addition is the formation of the $[M-H]^-$ rather than the $[M]^-$ ion observed in Chapter 2 (Figure 2-1B). The $[M]^-$ ion is formed by charge exchange from the reagent gas ion N_2^+ that is formed by electron capture of thermal electrons. The addition of methylene chloride reduces the number of thermal electrons present in the API source available for reaction.

The addition of increasing concentrations of carbon tetrachloride (Figure 4-2) and chloroform (Figure 4-3) both show similar ionization patterns as methylene chloride. Carbon tetrachloride shows the greatest increase in intensities of the $[M+Cl]^-$ ion of HMX, RDX, tetryl, and PETN, followed by chloroform and then methylene chloride. This observation is in agreement with the relative electron attachment rate constants of these chlorinated solvents. TNT shows a similar signal suppression at 0.01% followed by a gradual increase in intensity.

For the remaining studies, 0.1% chloroform was added to the mobile phase consisting of 35% H_2O and 65% MeOH by volume. Carbon tetrachloride would have been a better additive; however, after continued use of this solvent it was observed that ion burns were produced on the skimmer cone that resulted in signal suppression. Although the signal intensities of the $[M+Cl]^-$ ions of the explosives increase with increasing concentration of chloroform, only 0.1% was used in further studies because of its limited miscibility with water. The APCI-MS spectrum of low-mass solvent ions produced from 1 mL/min flow of 35/65 H_2O /MeOH (v/v%) with 0.1% chloroform is shown in Figure 4-4. It is apparent how reactive the chloride ion is by the various adduct

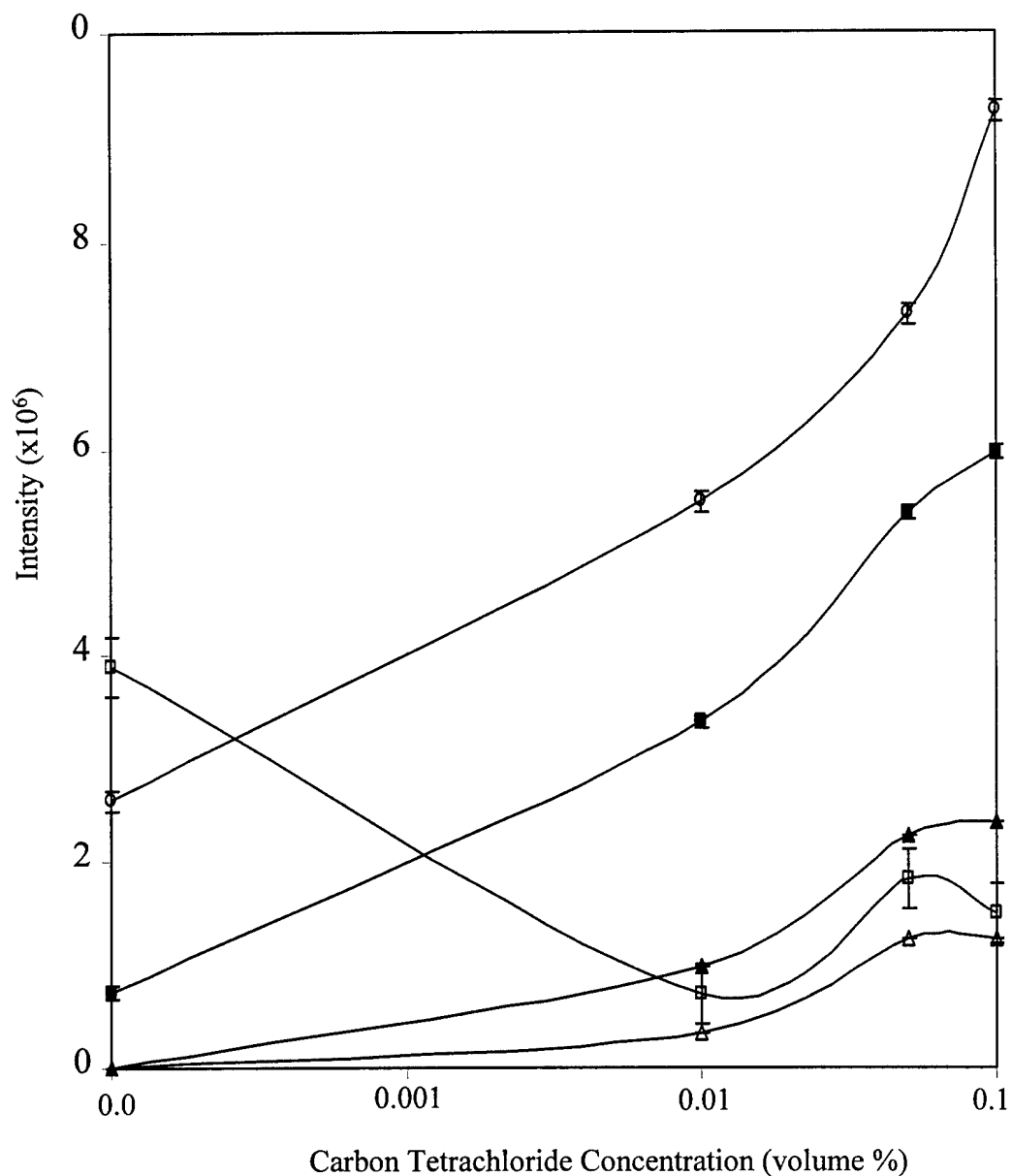


Figure 4-2. The effects of carbon tetrachloride concentration (volume %) on the APCI-MS intensities of $[M+Cl]^-$ of HMX (■), $[M+Cl]^-$ of RDX (▲), $[M+Cl]^-$ and $[M^*-H]^-$ of tetraol (O), $[M-H]^-$ of TNT (□), and $[M+Cl]^-$ of PETN (△). M^* is *N*-methylpicramide. Error bars are \pm one standard deviation of the mean for three replicates.

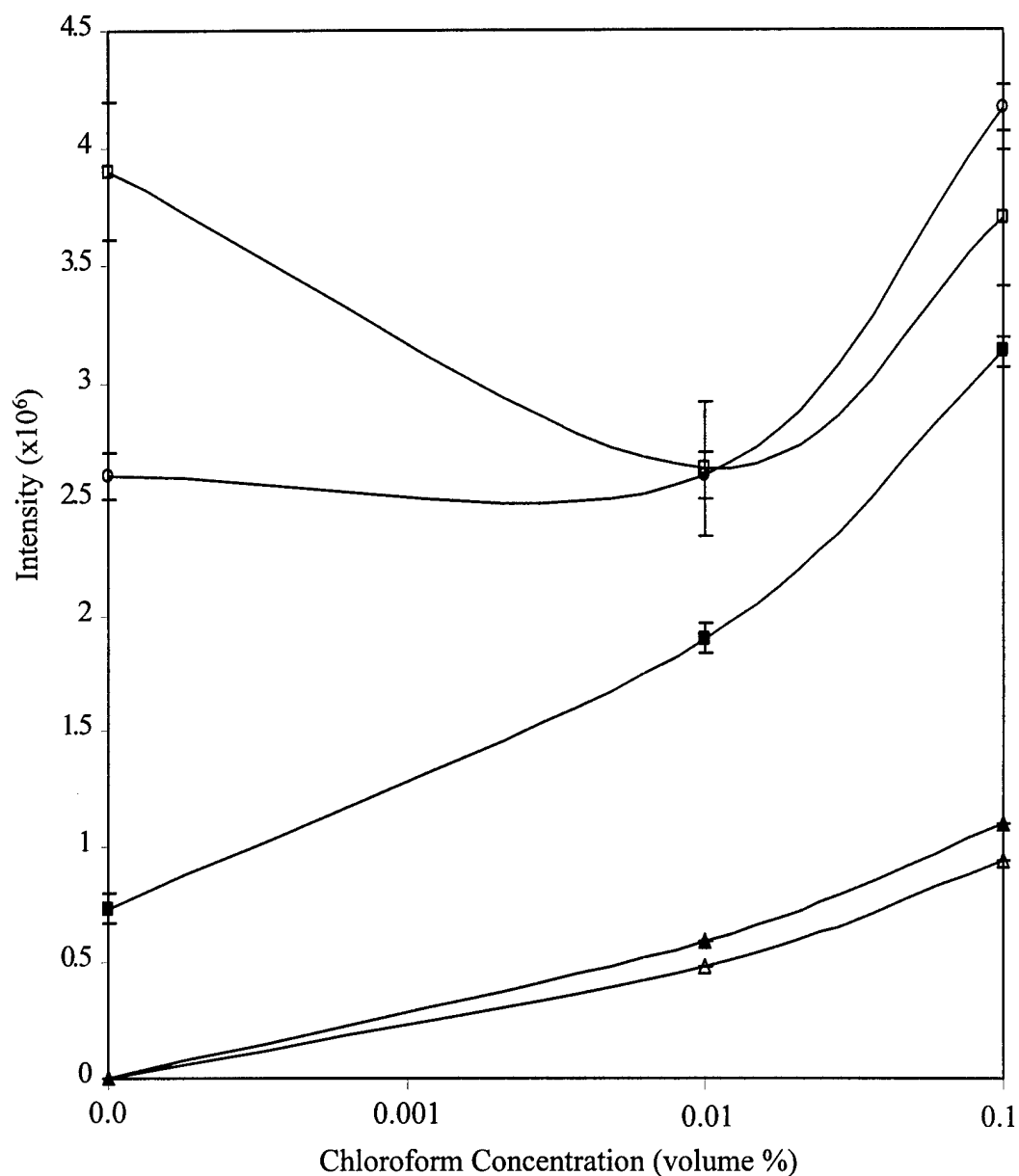


Figure 4-3. The effects of chloroform concentration (volume %) on the APCI-MS intensities of $[M+Cl]^-$ of HMX (■), $[M+Cl]^-$ of RDX (▲), $[M+Cl]^-$ and $[M^*-H]^-$ of tetryl (○), $[M-H]^-$ of TNT (□), and $[M+Cl]^-$ of PETN (△). M^* is *N*-methylnpicramide. Error bars are \pm one standard deviation of the mean for three replicates.

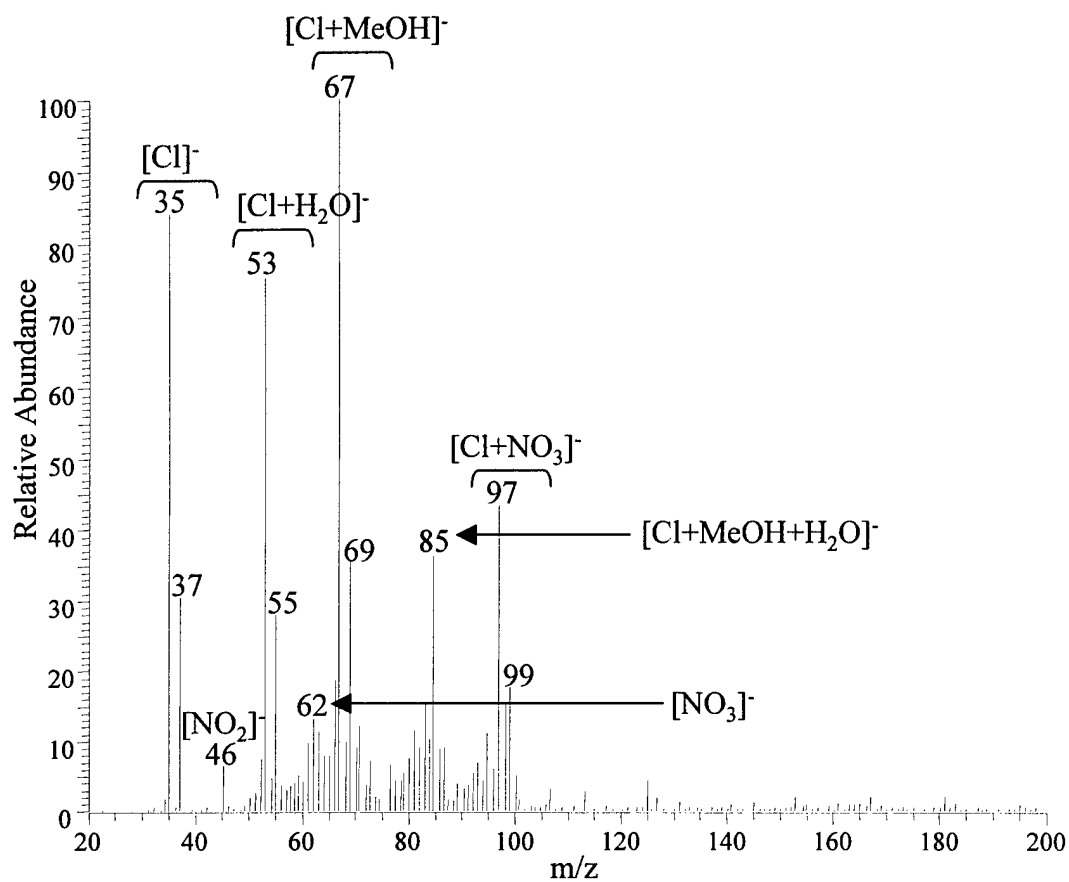


Figure 4-4. APCI-MS spectrum of low-mass solvent ions produced from 1 mL/min flow of 35/65 $\text{H}_2\text{O}/\text{MeOH}$ (v/v %) with 0.1% chloroform.

ions it forms with the solvent molecules and with impurities in the solvent. Note as well that there are no dimer or trimer ions of the chloride ion to interfere as observed for other additives with APCI (Figure 3-5B).

APCI Tune Method Development

The vaporizer temperature is one of the most important APCI parameters. A fine spray is directed into the vaporizer, which is heated at temperatures ranging from 300 to 600 °C. The high temperature is used to desolvate the droplets and subsequently evaporate the solutes into the vapor phase. Although high temperature is required to supply the heat of vaporization to the flowing solvent, the analyte is not directly exposed to these high temperatures. However, thermally labile species may decompose at higher vaporizer temperatures, as can be observed in Figure 4-5. This figure plots the relative intensities of the ions formed for each explosive as a function of vaporizer temperature. Tetryl has proven to be a difficult explosive to analyze with GC/MS at oven temperatures above 250 °C due to its thermal lability [Yinon, 1993]. The signal intensity of tetryl rapidly decreases with increasing vaporizer temperatures due to thermal decomposition. TNT, RDX, and PETN show a gradual decrease in signal with increasing temperature, whereas the signal intensity of HMX plateaus around 400 to 500 °C. The optimal vaporizer temperature was determined to be 350 °C, where the total ion current of the five explosives is the greatest.

The nitrogen sheath gas and auxiliary gas assist in pneumatically nebulizing the eluent into a fine mist, which aids in solvent vaporization. The ion intensities of the five explosives as a function of sheath gas and auxiliary gas flow are shown in Figure 4-6 and

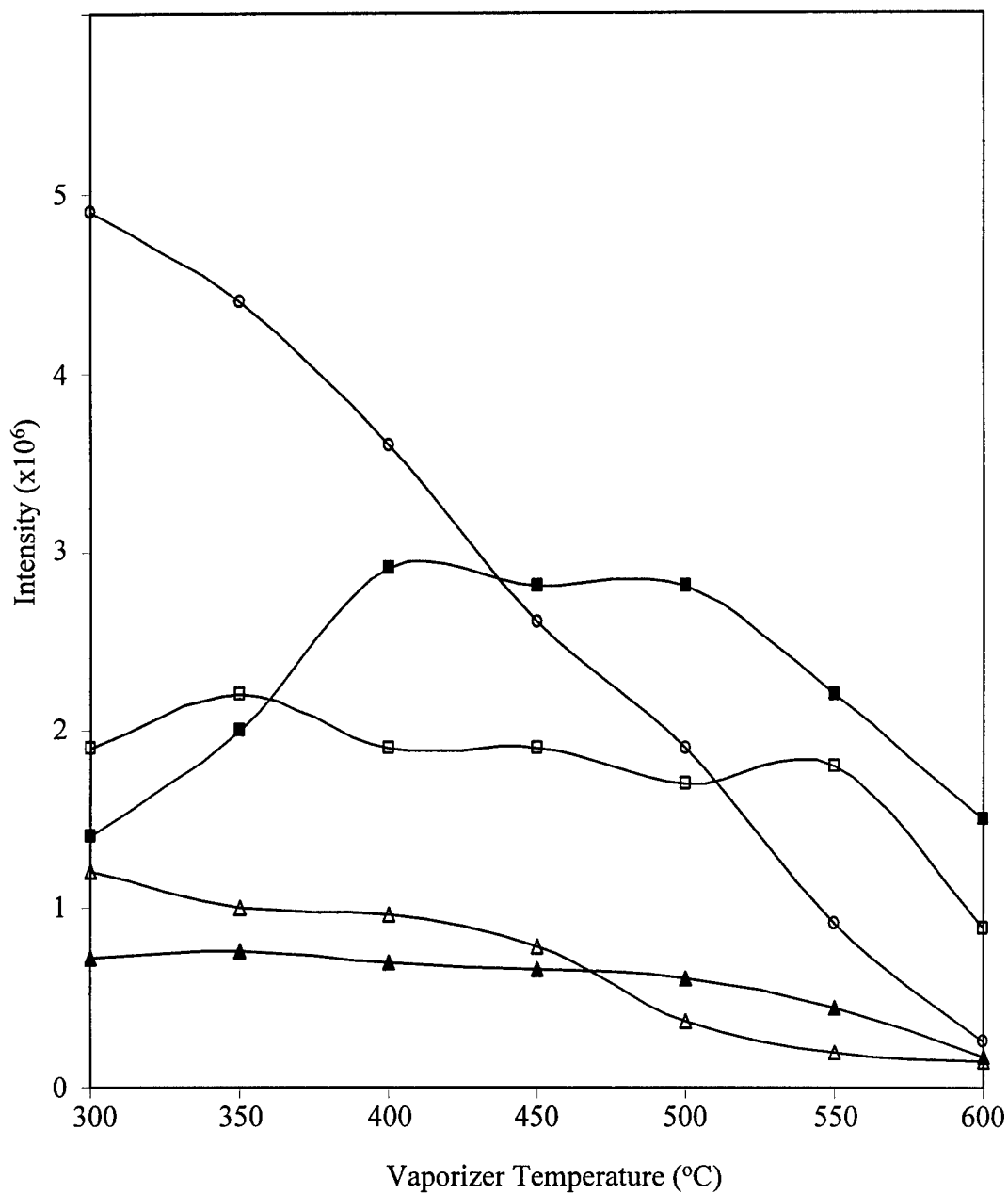


Figure 4-5. The effects of vaporizer temperature (°C) on the APCI-MS intensities of $[M+Cl]^-$ of HMX (■), $[M+Cl]^-$ of RDX (▲), $[M+Cl]^-$ and $[M^*-H]$ of tetryl (○), $[M-H]^-$ of TNT (□), and $[M+Cl]^-$ of PETN (△). M^* is *N*-methylnpicramide.

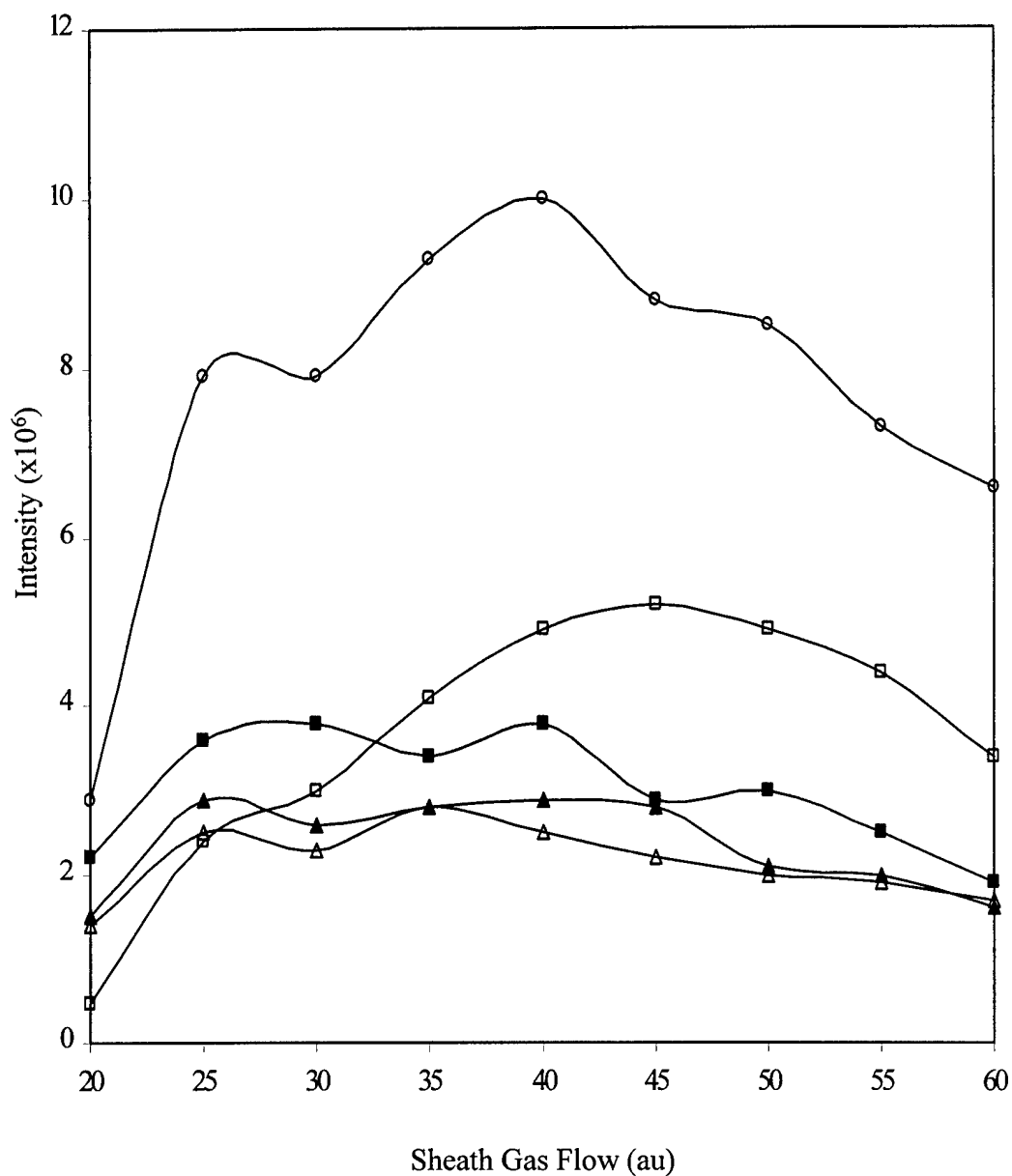


Figure 4-6. The effects of sheath gas flow (au = arbitrary units) on the APCI-MS intensities of $[M+Cl]^-$ of HMX (■), $[M+Cl]^-$ of RDX (▲), $[M+Cl]^-$ and $[M^*-H]$ of tetryl (○), $[M-H]^-$ of TNT (□), and $[M+Cl]^-$ of PETN (△). M^* is *N*-methylnicotinamide.

Figure 4-7, respectively. The nitrogen sheath gas is released parallel to the solvent flow, whereas the nitrogen auxiliary gas is directed at an angle towards the eluent stream (Figure 1-2). The optimal sheath gas flow determined by the combined intensities of the explosives was 45 arbitrary units. It was determined that no auxiliary gas should be used, because it leads to increased desolvation and exposes the thermally labile analyte molecules to the high temperatures of the vaporizer.

A source of electrons produced from a corona discharge needle (5.00 μA discharge current) is introduced on-axis with the heated spray, which results in a rich plasma of reagent ions in the API chamber. A series of ion-molecule reactions occur until the partially desolvated ions and neutrals are sampled by the heated capillary. The heated capillary assists in desolvating the ions at temperatures ranging from 100 to 300 $^{\circ}\text{C}$. The effect of capillary temperature on the ion intensities of the five explosives is illustrated in Figure 4-8. The partially desolvated ions were more sensitive to temperatures in the heated capillary than they were in the vaporizer, and the optimal capillary temperature was determined to be 140 $^{\circ}\text{C}$.

A negative potential is typically applied to the heated capillary, which assists in repelling negative ions from the capillary to the tube lens. However, it can be observed that the optimal capillary voltage determined from the plot in Figure 4-9 is +10 V. This can be explained by a phenomenon called up-front collision-induced dissociation (CID) [Bruins, 1997], in which fragmentation is induced in one of the higher-pressure regions of the ion path from the source into the mass analyzer. A negative potential applied to the capillary would accelerate the fragile negative ions of the explosives into neutrals, resulting in fragmentation and reduced ion signal.

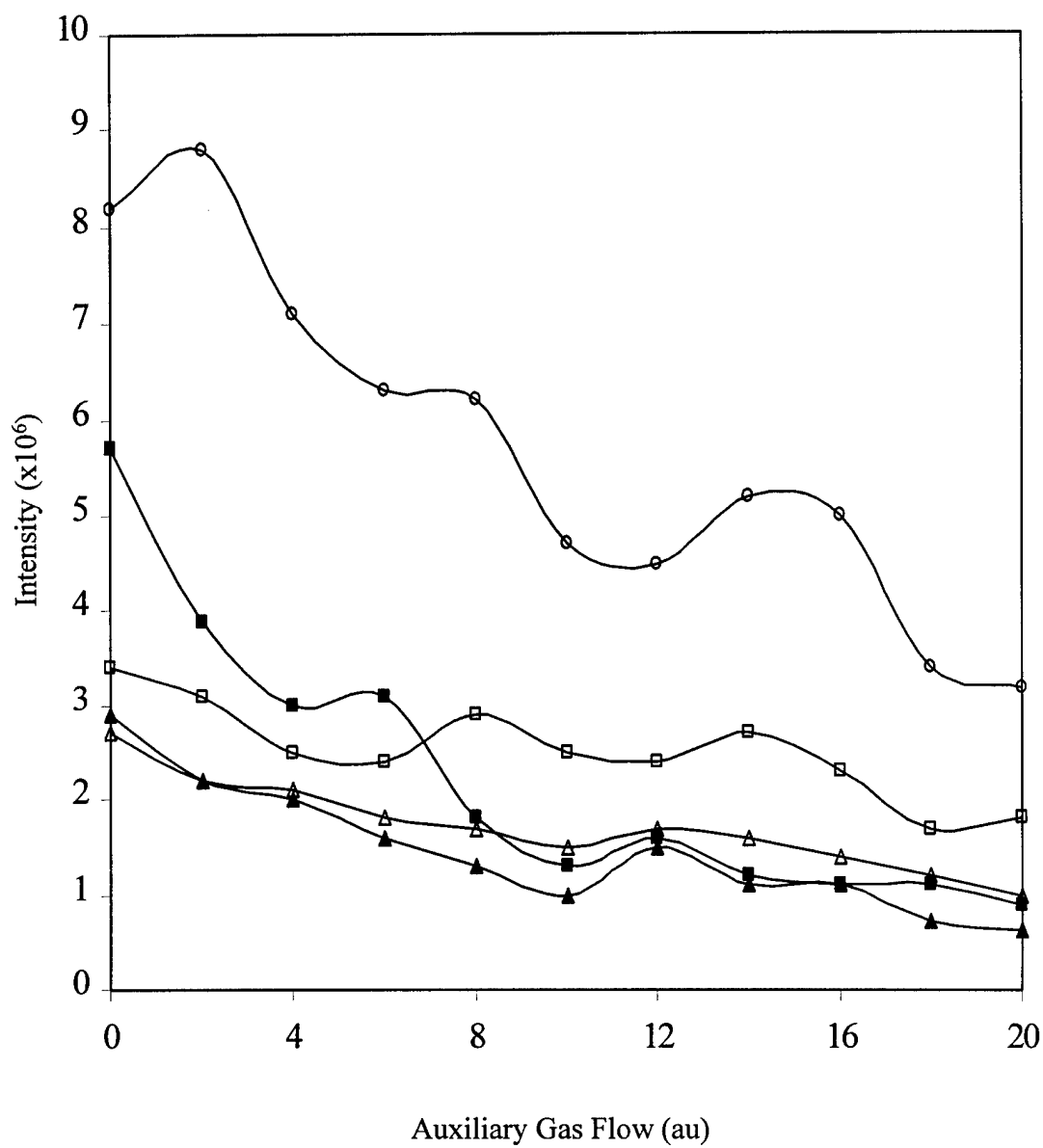


Figure 4-7. The effects of auxiliary gas flow (au = arbitrary units) on the APCI-MS intensities of $[M+Cl]^+$ of HMX (■), $[M+Cl]^+$ of RDX (▲), $[M+Cl]^+$ and $[M-H]^+$ of tetryl (○), $[M-H]^+$ of TNT (□), and $[M+Cl]^+$ of PETN (△). M* is *N*-methylnicotinamide.

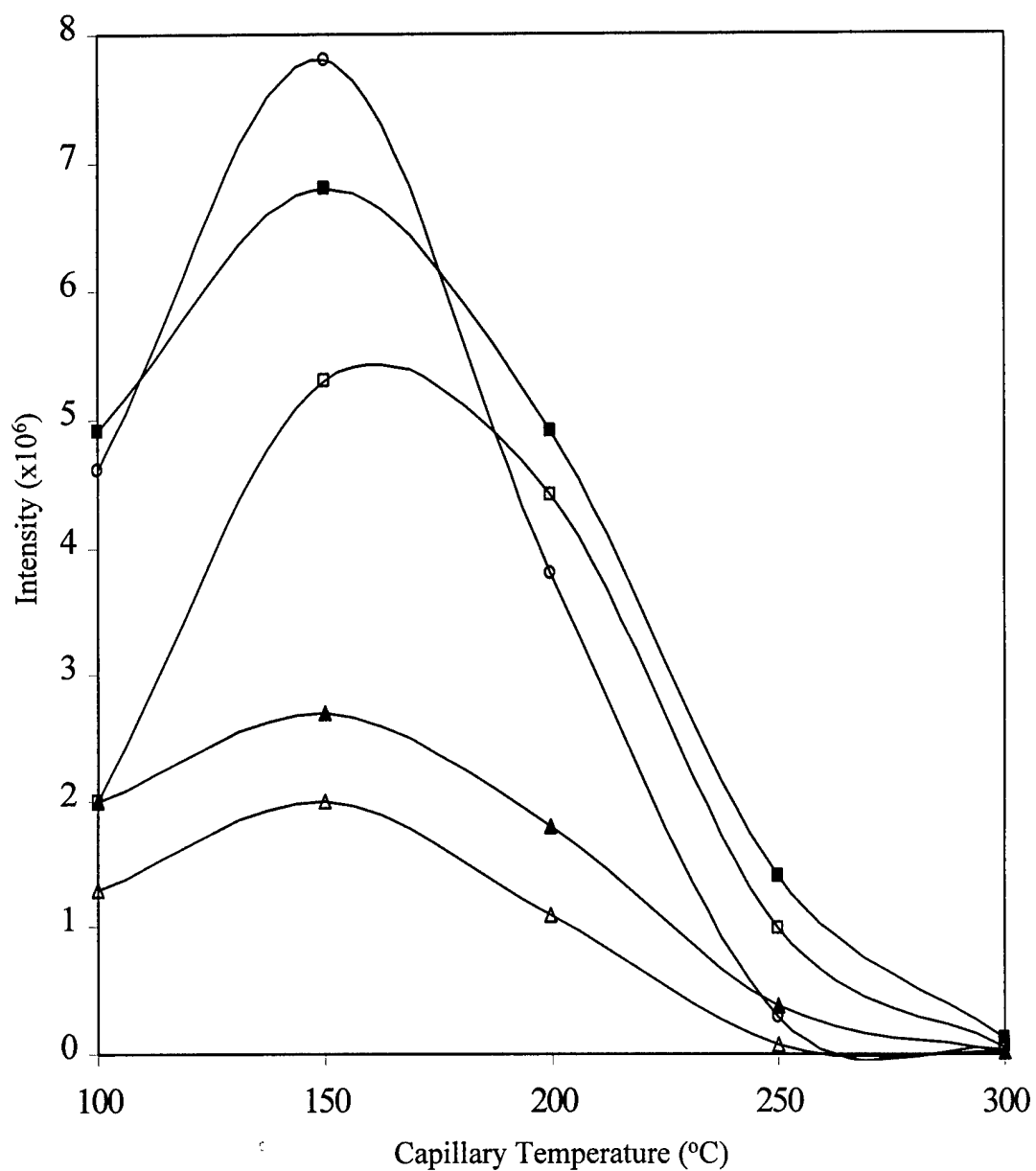


Figure 4-8. The effects of capillary temperature (°C) on the APCI-MS intensities of $[M+Cl]^-$ of HMX (■), $[M+Cl]^-$ of RDX (▲), $[M+Cl]^-$ and $[M^*-H]^-$ of tetryl (○), $[M-H]^-$ of TNT (□), and $[M+Cl]^-$ of PETN (△). M^* is *N*-methylnpicramide.

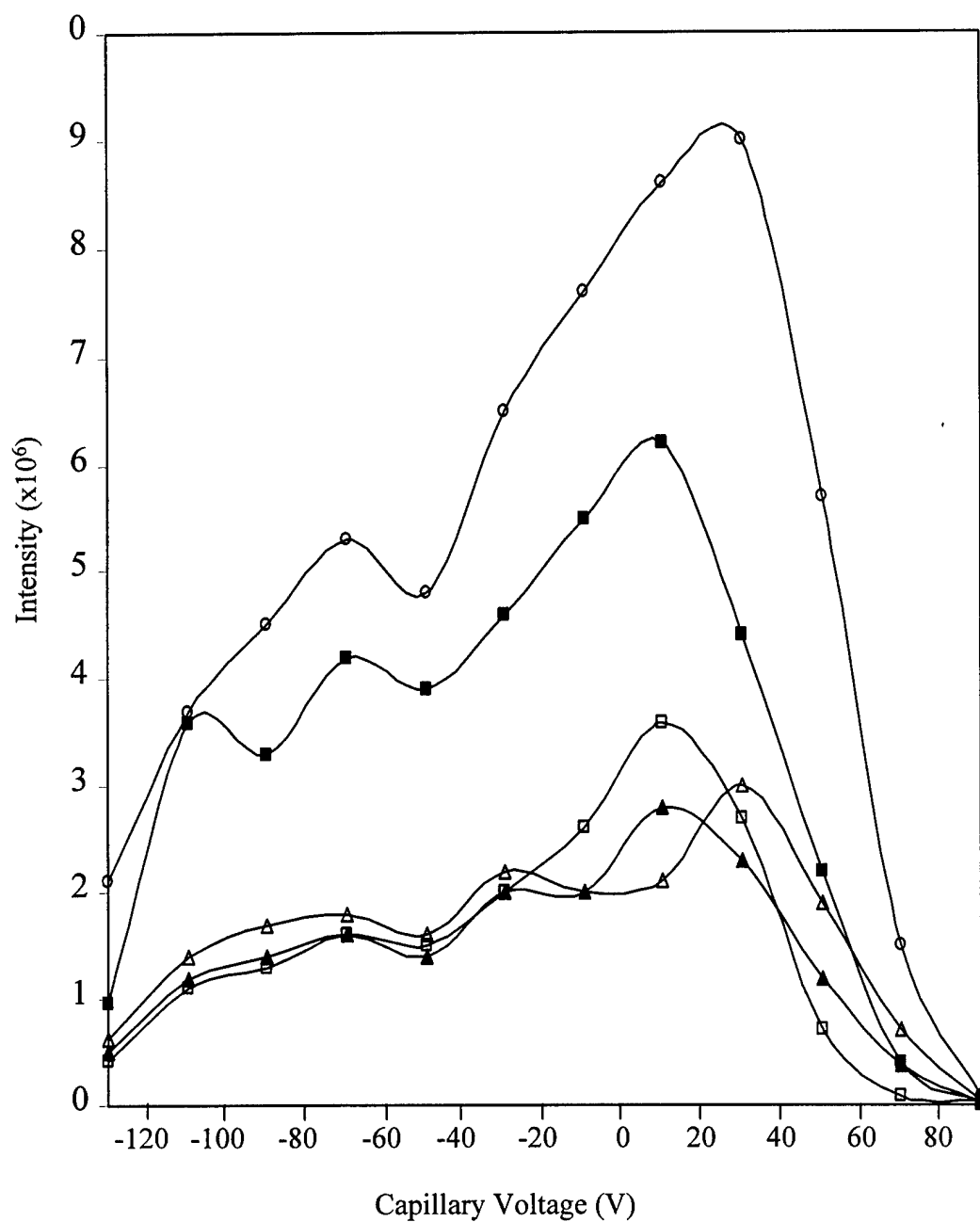


Figure 4-9. The effects of variable capillary voltages on the APCI-MS intensities of $[M+Cl]^-$ of HMX (■), $[M+Cl]^-$ of RDX (▲), $[M+Cl]^-$ and $[M^*-H]^-$ of tetryl (○), $[M-H]^-$ of TNT (□), and $[M+Cl]^-$ of PETN (△).

Ions and neutrals exiting the heated capillary undergo free-jet expansion as they are transported from an atmospheric pressure region (760 Torr) to the lower pressure region (1 Torr) of the API stack (Figure 1-3). Focusing of the negative ions expanding in the vacuum towards the opening of the skimmer cone requires a negative potential on the tube lens. The effect of tube lens voltages on the ion intensities of the five explosives is illustrated in Figure 4-10; the optimal tube lens offset was determined to be -15 V. Table 4-1 summarizes the optimal APCI source parameters used in the tune method to analyze the explosives. Also included in the table is a list of optimal ion optics parameters determined by calibration of the mass spectrometer with a tuning solution of caffeine, MRFA, and Ultramark 1621.

Improved Explosive Detection with Chloroform

The use of 0.1% chloroform with APCI-MS has allowed for the detection of certain explosive compounds that were found to be undetectable with APCI in Chapter 2. The dinitrotoluene isomers 2,5-DNT, 2,3-DNT, and 3,4-DNT are not ionized efficiently due to the destabilizing properties of nitro groups in the meta position of the aromatic ring. In the presence of chloroform, these compounds form the $[M]^-$ ion by charge exchange from the chloride ion Cl^- . This is contrary from what was observed with TNT in which the $[M-H]^-$ ion was formed rather than the $[M]^-$ ion in the presence of chloroform. This may be due to the lower acidity of the methyl group on the dinitrotoluenes, because of the destabilizing meta nitro groups. The APCI-MS spectrum of 2,5-DNT with 0.1% chloroform (Figure 4-11A) has a molecular ion $[M]^-$ at m/z 182 and a fragment ion $[M-NO]^-$ at m/z 152. The APCI-MS/MS spectrum of the $[M]^-$ ion (m/z 182) of 2,5-DNT (Figure 4-11B) shows one dominant daughter ion at m/z 152

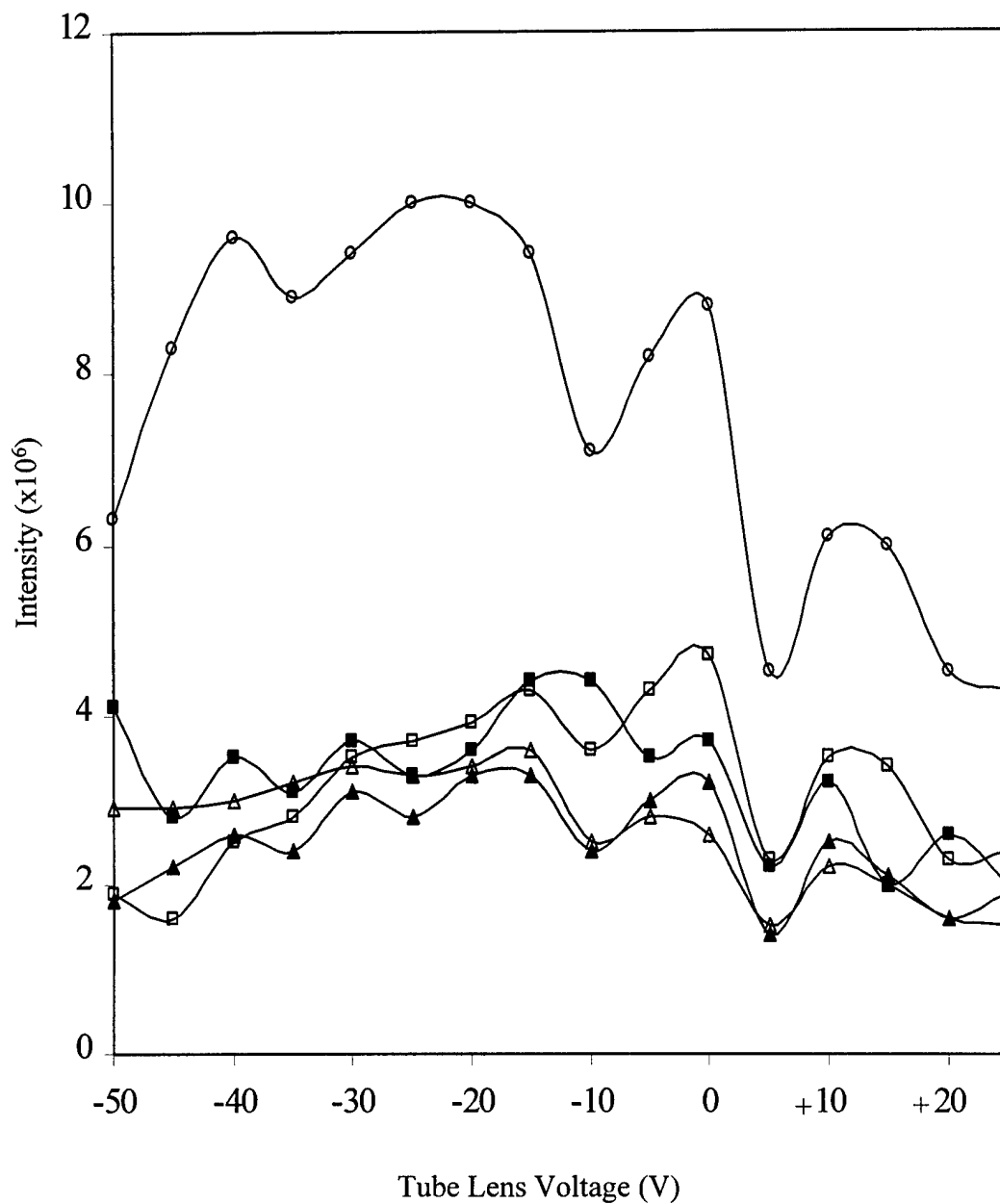


Figure 4-10. The effects of variable tube lens voltages on the APCI-MS intensities of $[M+Cl]^-$ of HMX (■), $[M+Cl]^-$ of RDX (▲), $[M+Cl]^-$ and $[M^*-H]^-$ of tetryl (○), $[M-H]^-$ of TNT (□), and $[M+Cl]^-$ of PETN (△). M^* is *N*-methylpicramide. Capillary voltage is held constant at 10 V.

Table 4-1: APCI Tune Method

APCI Source Parameter	Tune Method Setting
Vaporizer Temperature (°C)	350
Sheath Gas Flow Rate (arbitrary units)	45
Auxiliary Gas Flow Rate (arbitrary units)	0
Corona Discharge Current (μA)	5.00
Capillary Temperature (°C)	140
Capillary Voltage (V)	10.00
Tube Lens Offset (V)	-15.00
Ion Optics Parameter	Tune Method Setting
Octopole 1 Offset (V)	3.00
Lens Voltage (V)	18.00
Octopole 2 Offset (V)	5.50
Octopole RF Amplitude (V _{p-p})	400.00

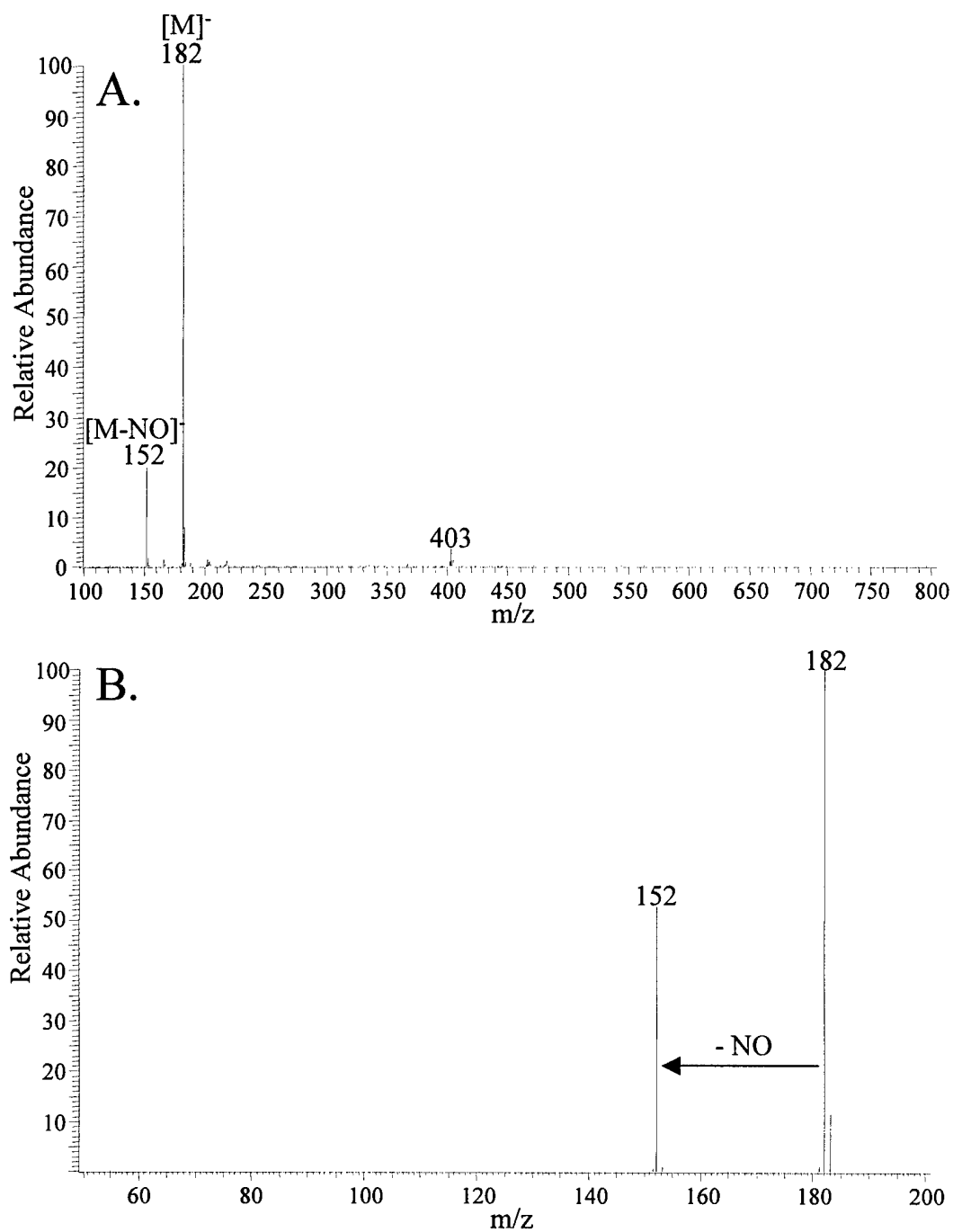


Figure 4-11. A. APCI-MS spectrum of 2,5-DNT (MW = 182) with 0.1% chloroform. B. Daughter ion spectrum of $[M]^-$ ion (m/z 182) of 2,5-DNT.

corresponding to a neutral loss of 30 amu (NO). The APCI-MS spectra of 2,3-DNT (Figure 4-12A) and 3,4-DNT (Figure 4-13A) also have a molecular ion $[M]^-$ at m/z 182 and a fragment ion $[M-NO]^-$ at m/z 152. In addition to these ions, 2,3-DNT and 3,4-DNT also have an HCl adduct ion $[M+HCl]^-$ at m/z 218 and other unidentified ions that may be solvent adduct ions. The ability for 2,3-DNT and 3,4-DNT to form adduct ions may be due to the adjacent nitro groups on the aromatic ring. The daughter ion spectra of the $[M]^-$ ions of 2,3-DNT (Figure 4-12B) and 3,4-DNT (Figure 4-13B) have one dominant product ion at m/z 152 corresponding to a neutral loss of 30 amu (NO), which is a common fragment ion of dinitrotoluene anions.

TEGDN and DEGDN were not detectable in the experiments reported in Chapter 2, but are detectable with APCI-MS with 0.1% chloroform. The APCI-MS of TEGDN with 0.1% chloroform (Figure 4-14A) shows two adduct ions at m/z 275 $[M+Cl]^-$ and m/z 307 $[M+MeOH+Cl]^-$. The APCI-MS of DEGDN with 0.1% chloroform (Figure 4-14B) shows two adduct ions at m/z 231 $[M+Cl]^-$ and m/z 258 $[M+NO_3]^-$. The chloride ion may assist in the ionization of the fragile nitrate esters, TEGDN and DEGDN, by forming adduct ions, which help to delocalize the kinetic energy that arises from ion-molecule reactions in the API region. The MS/MS of the $[M+Cl]^-$ ion of TEGDN and DEGDN did not produce any observable daughter ions.

The chloride ion may also assist in a similar manner with the ionization of the fragile compounds NTO and TNAZ, which were not detectable with APCI in Chapter 2. In the presence of 0.1% chloroform, these compounds form chloride adducts as well as other ions, as shown in Figure 4-15A and Figure 4-15B. The dominant ion in the APCI-MS spectrum of NTO is the dimer $[2M-H]^-$ at m/z 259. Nitramines and nitrate esters

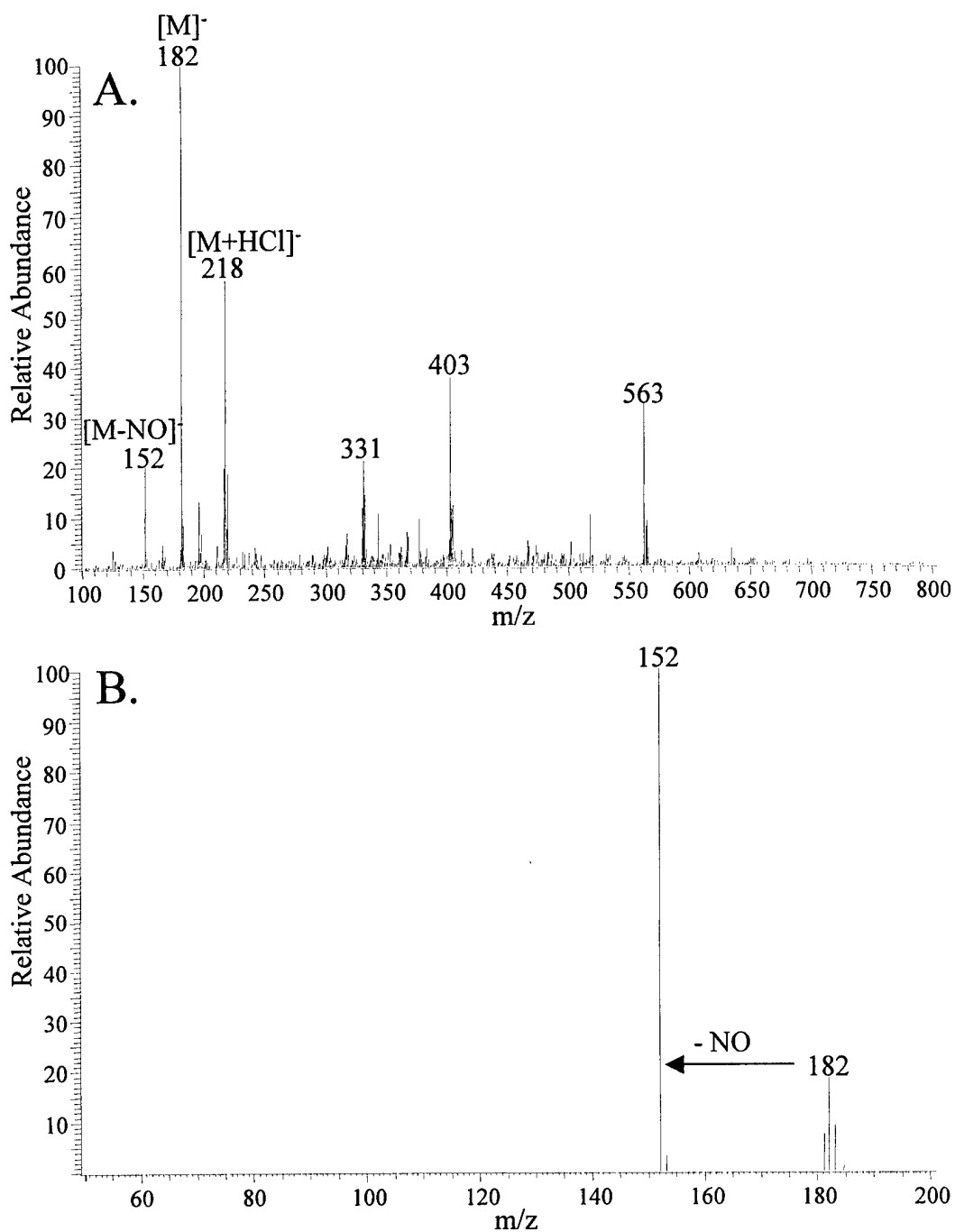


Figure 4-12. A. APCI-MS spectrum of 2,3-DNT (MW = 182) with 0.1% chloroform. B. Daughter ion spectrum of $[M]^-$ ion (m/z 182) of 2,3-DNT.

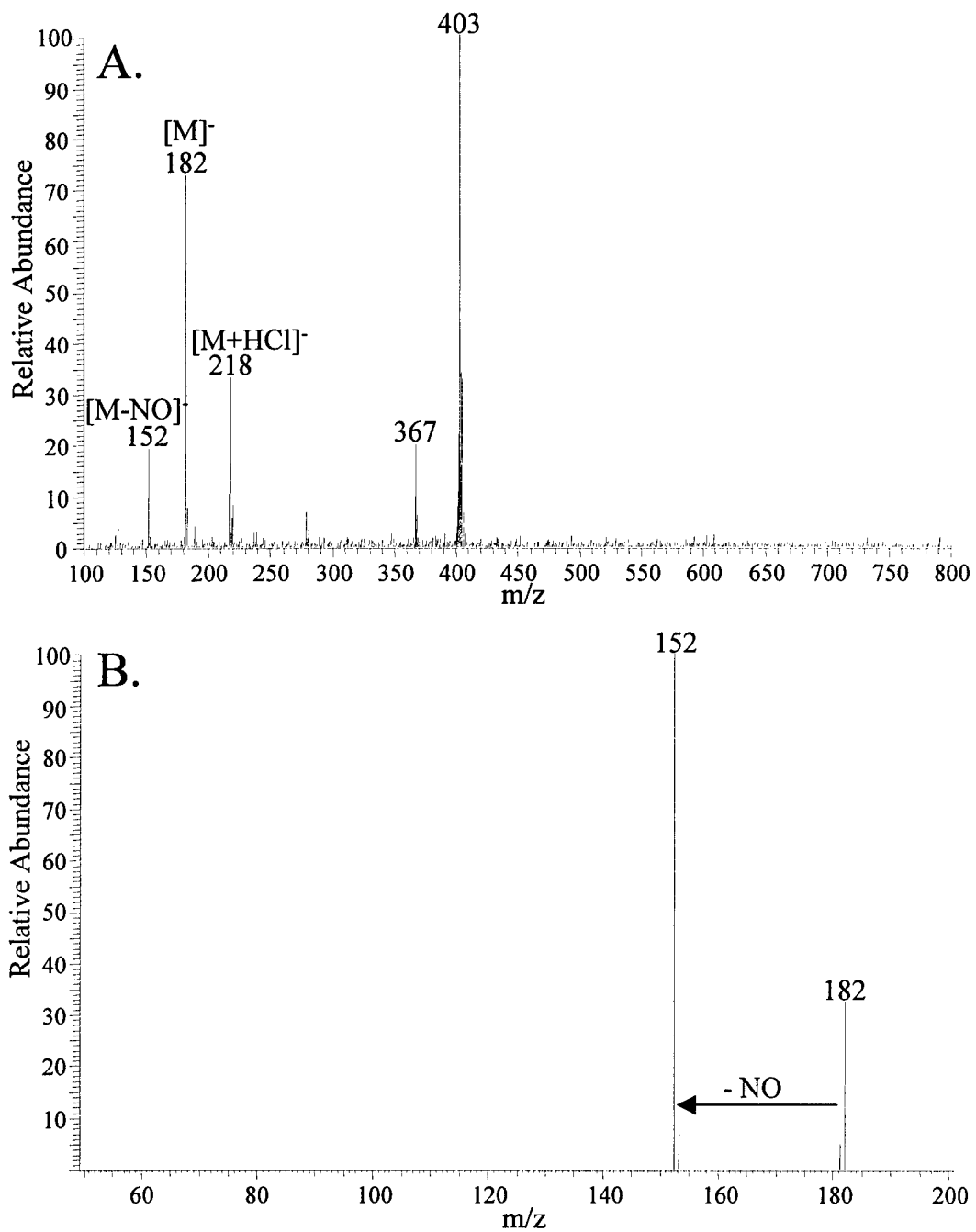


Figure 4-13. A. APCI-MS spectrum of 3,4-DNT (MW = 182) with 0.1% chloroform. B. Daughter ion spectrum of $[M]^-$ ion (m/z 182) of 3,4-DNT.

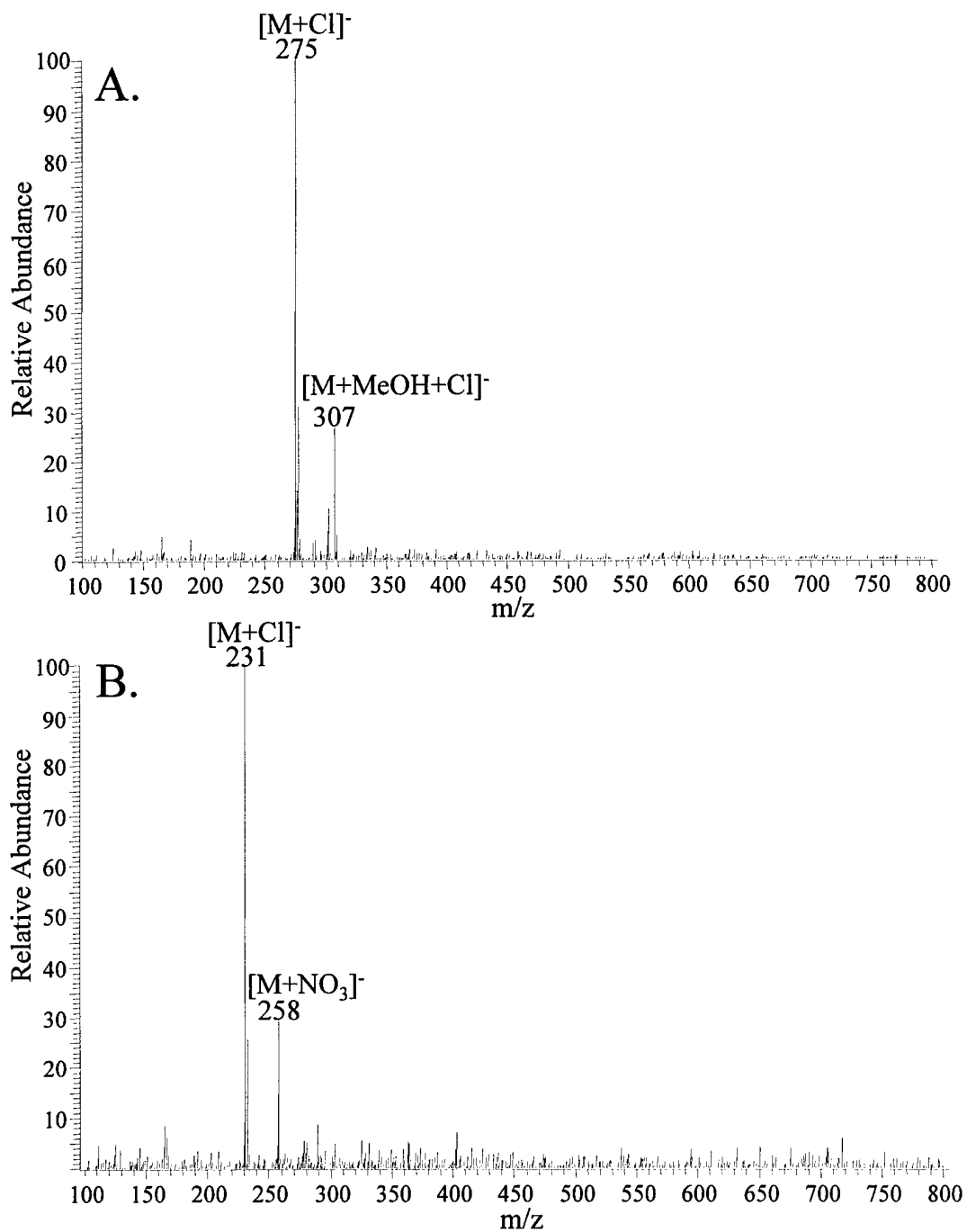


Figure 4-14. APCI-MS spectra with 0.1% chloroform: A. TEGDN (MW = 240)
B. DEGDN (MW = 196).

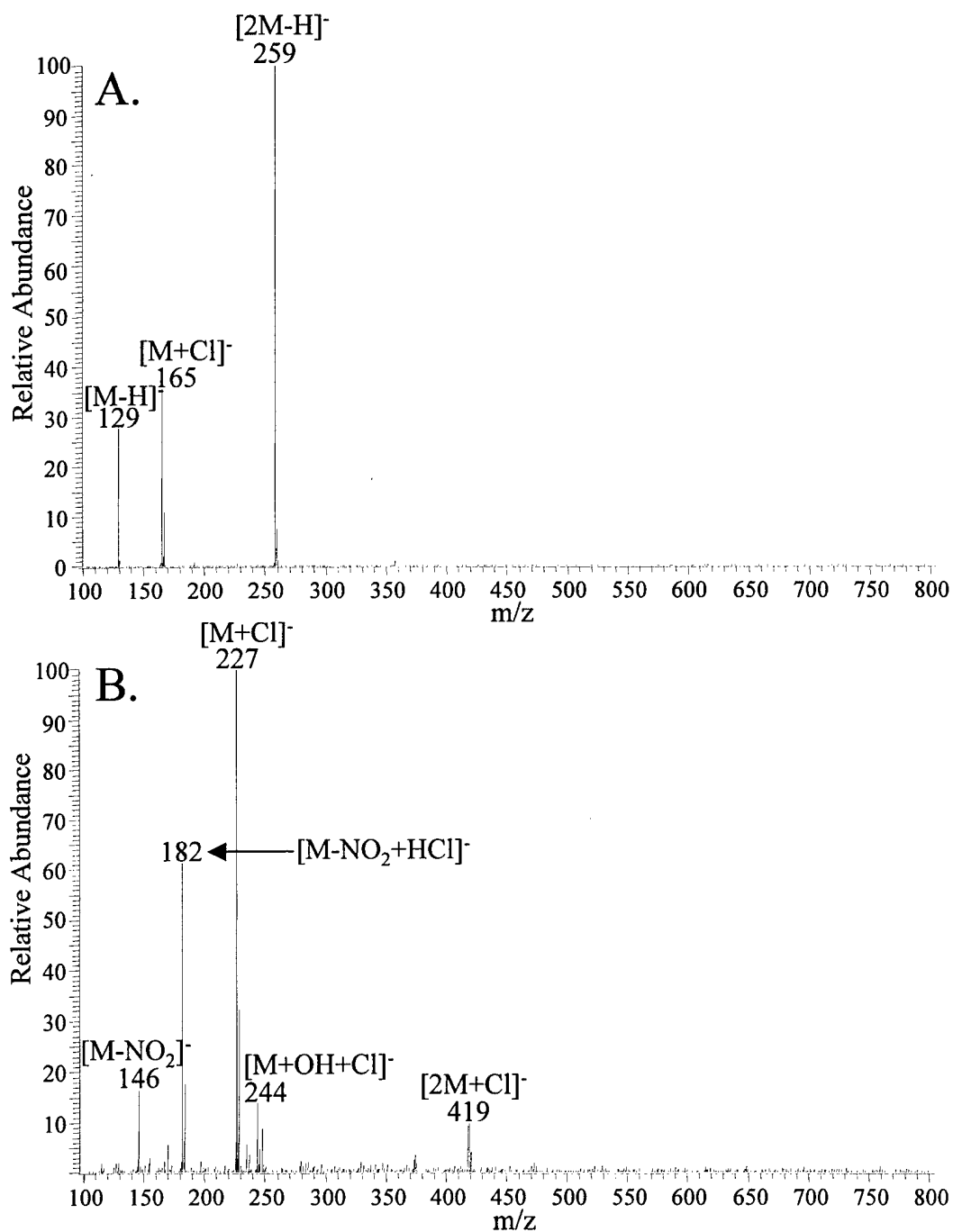


Figure 4-15. APCI-MS spectra with 0.1% chloroform: A. NTO (MW = 130) B. TNAZ (MW = 192).

commonly form dimers similar to this nitro aliphatic compound that are dependent on explosive concentration. Figure 4-16 illustrates the effects of NTO concentration on dimer formation. At NTO concentrations higher than 1 ppm, the dimer ion $[2M-H]^-$ (m/z 259) begins to form and suppress the signal intensity of the $[M-H]^-$ ion (m/z 129) and $[M+Cl]^-$ ion (m/z 165) of NTO. This signal suppression as a result of dimer formation limits the linear dynamic range of explosives to a maximum concentration of approximately 1 ppm. The linear dynamic range of a series of explosives will be illustrated later in this chapter.

LC/APCI-MS and LC/APCI-MS/MS of Explosives

APCI is a mass-sensitive ionization method, whose sensitivity towards an analyte is directly dependent on the amount of material present for ionization. Therefore, if the sample quantity is not limited, it is beneficial to introduce as much of the analyte to the APCI source as possible (i.e., operate at as high of a flow rate as possible). To illustrate the mass-sensitive characteristics of APCI, a 1 ppm mixture of eight different explosives (NTO, NQ, HMX, RDX, CL-20, tetryl, TNT, and PETN) was introduced with five different sample loops of increasing volume (10, 24.6, 50, 75, and 100 μ L corresponding to 10, 24.6, 50, 75, and 100 ng of material, respectively). The chromatographic peak area of each explosive formed by monitoring specific ions of each compound (NTO: m/z 175, m/z 129, and m/z 192; NQ: m/z 139; HMX: m/z 331; RDX: m/z 257; CL-20: m/z 473; tetryl: m/z 322 and m/z 241; TNT: m/z 226; and PETN: m/z 351) was plotted as a function of sample loop volume, and is shown in Figure 4-17. There appears to be a linear relationship between the sensitivity of APCI for each explosive and the amount of material introduced. The correlation coefficients (R^2) for NTO, NQ, HMX, RDX, CL-20,

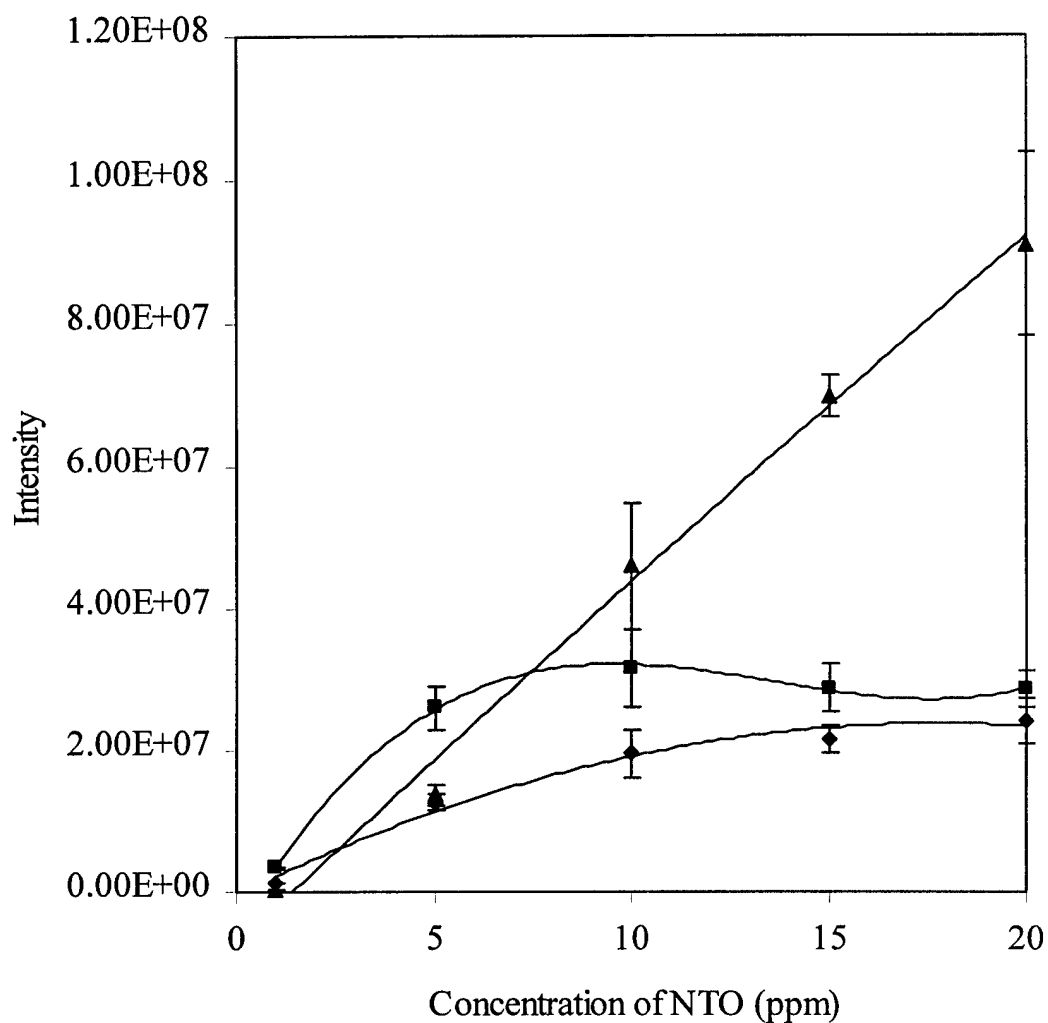


Figure 4-16. Effects of NTO concentration on dimer ion formation: (◆) $[M-H]^-$ of NTO (m/z 129), (■) $[M+Cl]^-$ of NTO (m/z 165), and (▲) $[2M-H]^-$ of NTO (m/z 259). Error bars are +/- one standard deviation of the mean for three replicates.

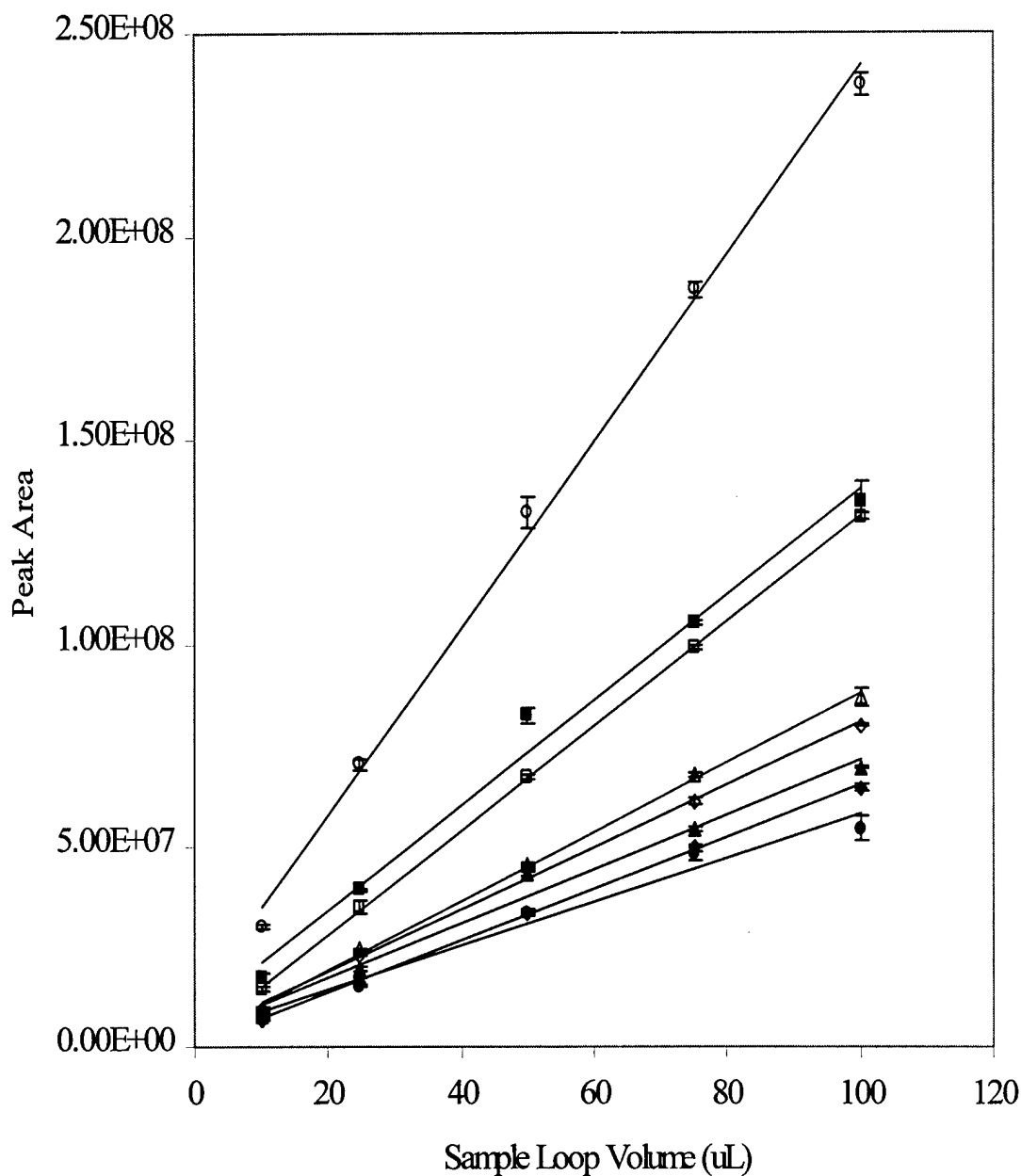


Figure 4-17. LC-APCI-MS of 1 ppm loop injections of NTO (◆), NQ (●), HMX (■), RDX (▲), CL-20 (◇), tetryl (○), TNT (□), and PETN (△) with sample loop volumes of 10, 24.6, 50, 75, and 100 μ L. The following ions were monitored for each explosive: $[M+Cl]^-$, $[M-H]^-$, and $[M+NO_3]^-$ of NTO; $[M+Cl]^-$ of NQ; $[M+Cl]^-$ of HMX; $[M+Cl]^-$ of RDX; $[M+Cl]^-$ of CL-20; $[M+Cl]^-$ and $[M^*-H]^-$ of tetryl; $[M-H]^-$ of TNT; and $[M+Cl]^-$ of PETN. M^* is *N*-methylpicramide.

tetryl, TNT, and PETN were 0.9993, 0.9760, 0.9985, 0.9999, 0.9999, 0.9998, 0.9998, and 0.9999, respectively. Although larger sample loop volumes provide for a greater sensitivity for explosives, the 24.6 μL sample loop was used for the remaining studies to avoid the possibility of peak broadening as a result of overloading the column (saturation of binding sites) when real samples are investigated.

The LC/APCI-MS chromatograms of a 1 ppm explosive mixture consisting of NTO (eluting at 1.13 min), NQ (eluting at 1.54 min), HMX (eluting at 1.76 min), RDX (eluting at 2.24 min), CL-20 (eluting at 2.72 min), tetryl (eluting at 2.95 min), TNT (eluting at 3.64 min), and PETN (eluting at 4.44 min) are shown in Figure 4-18. Each chromatogram is constructed from a mass scan filter, which shows the relative abundance of specific m/z ions as a function of retention time. The NTO peak is constructed from the intensities of the $[\text{M}+\text{Cl}]^-$ ion (m/z 175), $[\text{M}-\text{H}]^-$ ion (m/z 129), and $[\text{M}+\text{NO}_3]^-$ ion (m/z 192), which are the most intense ions produced for NTO. The NQ peak is constructed from the intensity of the $[\text{M}+\text{Cl}]^-$ ion (m/z 139). The HMX peak is constructed from the intensity of the $[\text{M}+\text{Cl}]^-$ ion (m/z 331). The RDX peak is constructed from the intensity of the $[\text{M}+\text{Cl}]^-$ ion (m/z 257). The mass filter for m/z 257 also includes the $[\text{M}-\text{NO}]^-$ ion (m/z 257) of tetryl. The CL-20 peak is constructed from the intensity of the $[\text{M}+\text{Cl}]^-$ ion (m/z 473). The tetryl peak is constructed from the intensities of the $[\text{M}+\text{Cl}]^-$ ion (m/z 322) and $[\text{M}^*-\text{H}]^-$ ion (m/z 241) ($\text{M}^* = N$ -methylnitramide, the hydrolysis product of tetryl). The TNT peak is constructed from the intensity of the $[\text{M}-\text{H}]^-$ ion (m/z 226). The PETN peak is constructed from the intensity of the $[\text{M}+\text{Cl}]^-$ ion (m/z 351). The APCI-MS (A) and APCI-MS/MS (B) spectra are shown from the chromatographic peaks of NTO (Figure 4-19), NQ (Figure 4-20),

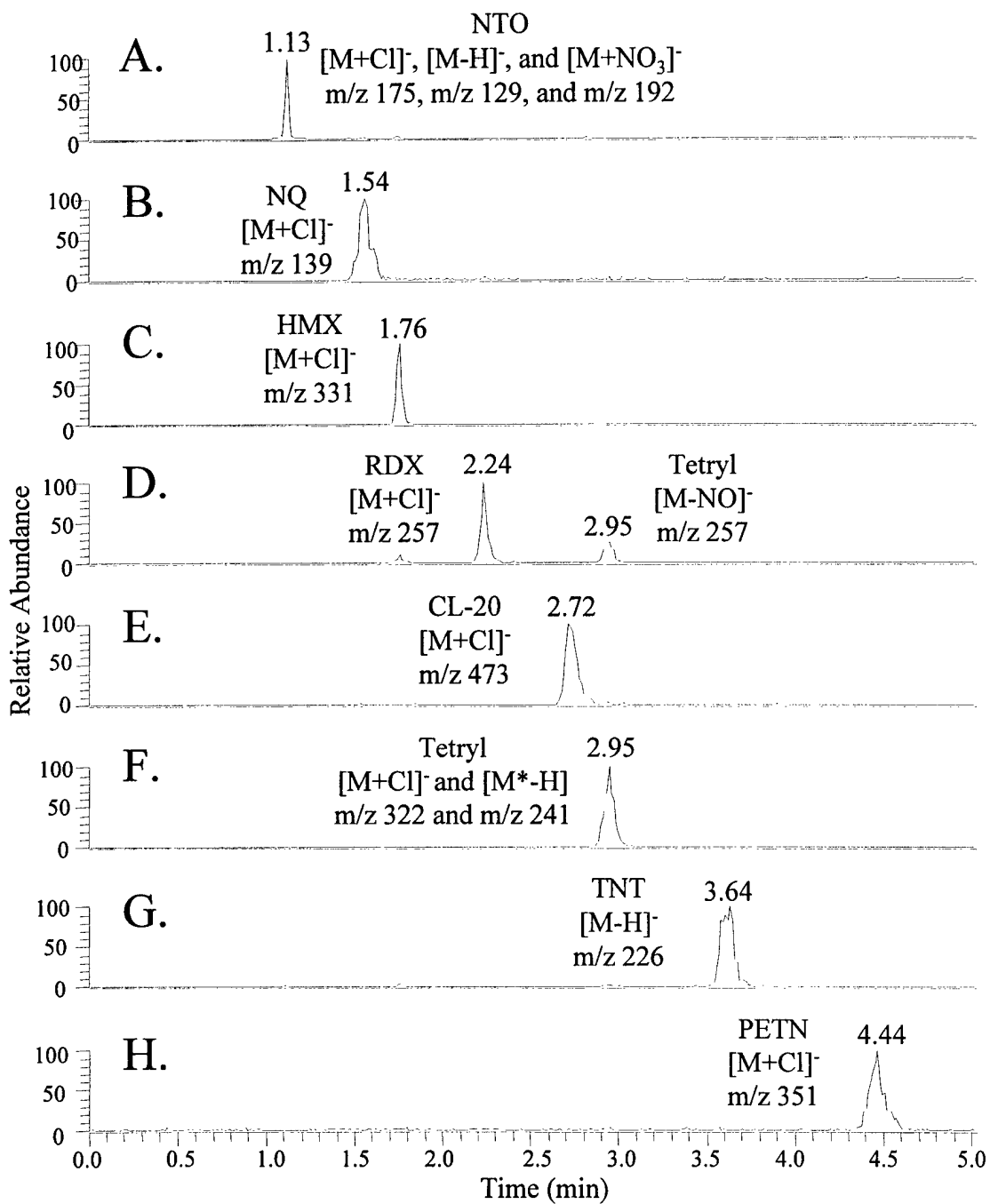


Figure 4-18. LC-APCI-MS chromatogram of 1 ppm explosive mixture consisting of (A) NTO eluting at 1.13 min, (B) NQ eluting at 1.54 min, (C) HMX eluting at 1.76 min, (D) RDX eluting at 2.24 min, (E) CL-20 eluting at 2.72 min, (F) tetryl eluting at 2.95 min, (G) TNT eluting at 3.64 min, and (H) PETN eluting at 4.44 min.

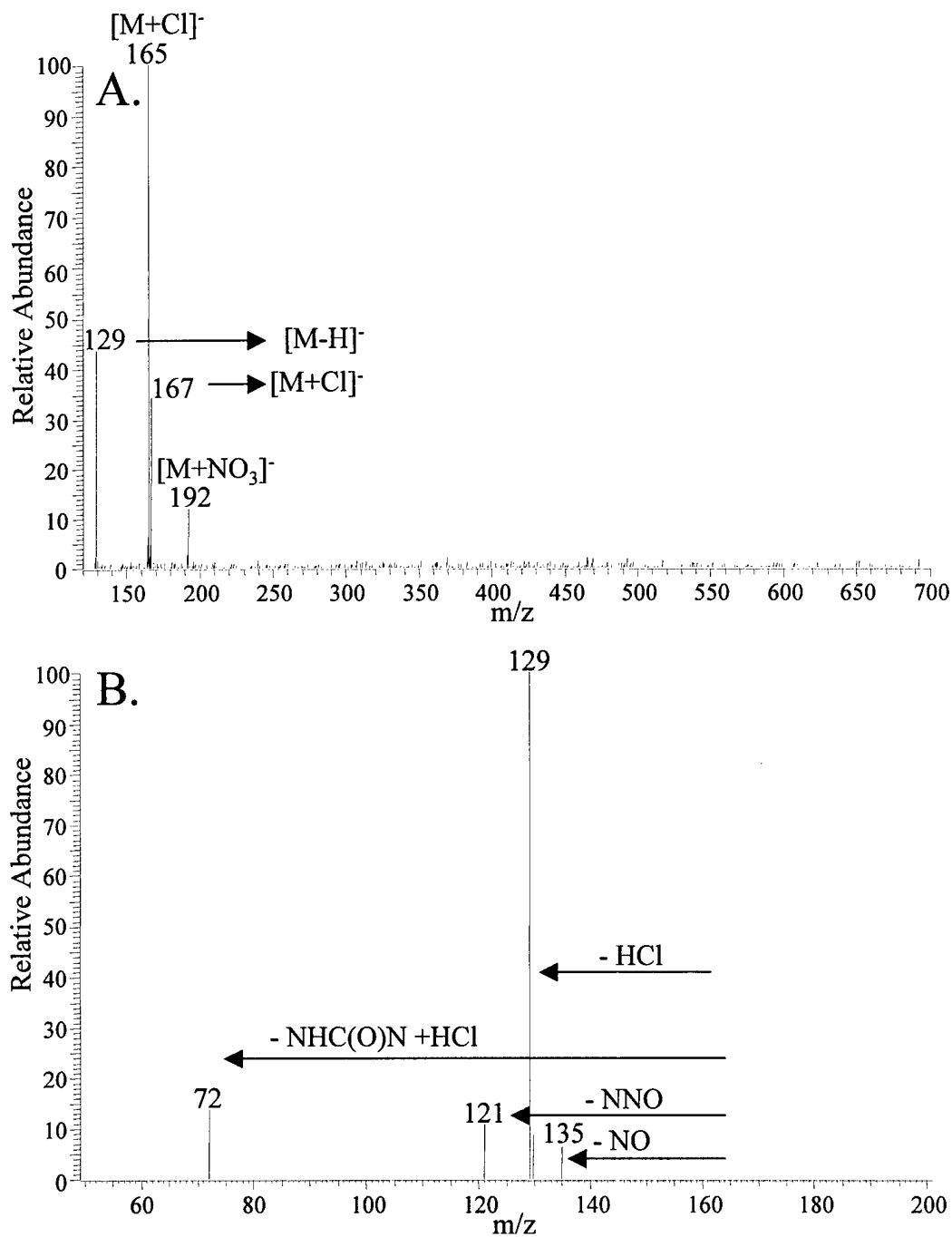


Figure 4-19. A. APCI-MS spectrum of NTO peak. B. Daughter ion spectrum of $[M+Cl]^-$ ion (m/z 165) of NTO.

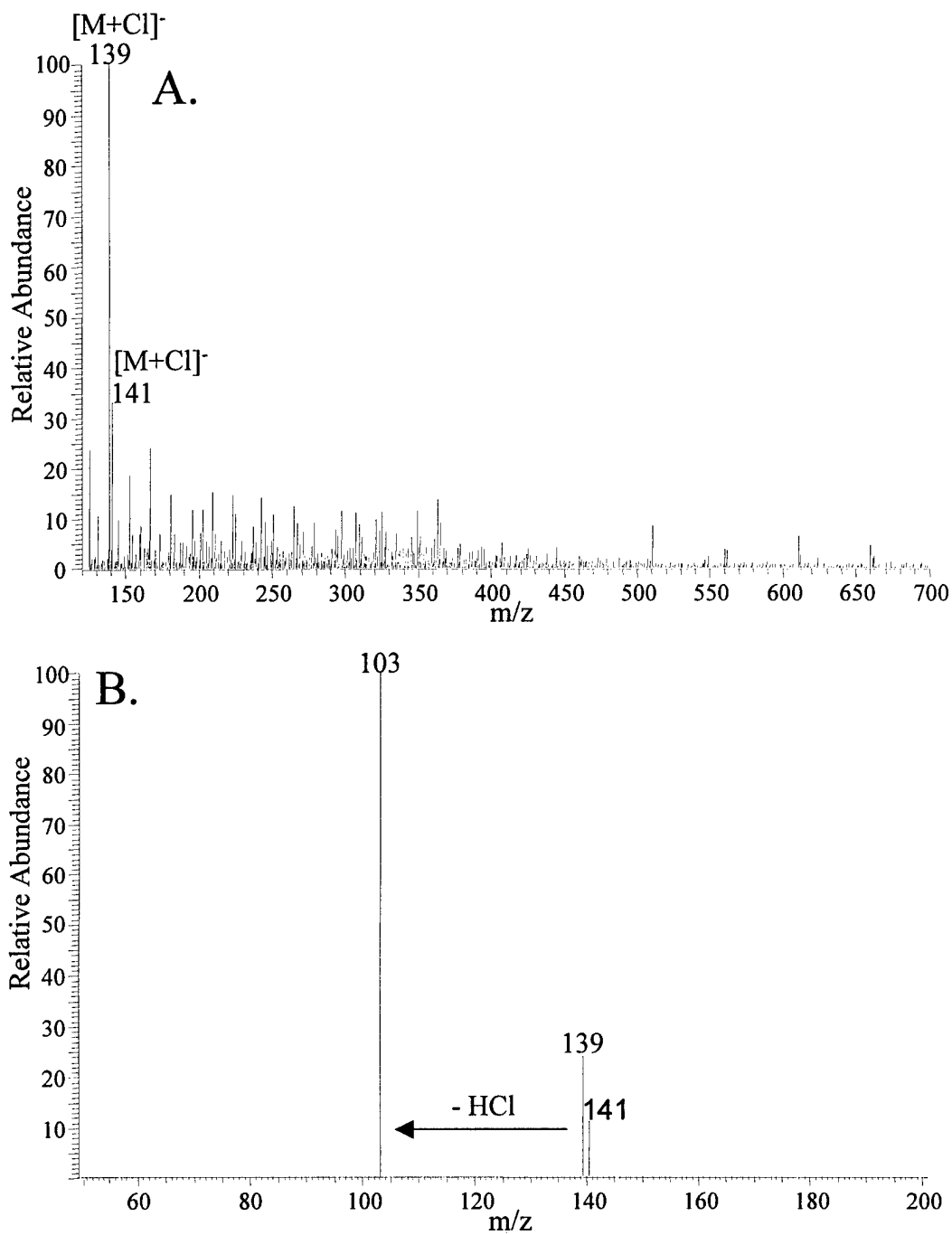


Figure 4-20. A. APCI-MS spectrum of NQ peak. B. Daughter ion spectrum of $[M+Cl]^-$ ion (m/z 139) of NQ.

HMX (Figure 4-21), RDX (Figure 4-22), CL-20 (Figure 4-23), tetryl (Figure 4-24), TNT (Figure 4-25), and PETN (Figure 4-26). Table 4-2 summarizes the most intense parent ion (m/z), isolation window (amu), CID efficiency (%), optimum collision energy (%), and most intense daughter ion (m/z) from the APCI-MS/MS experiments. CID efficiency (E_{CID}) is defined by equation 4-4 as the summation of daughter ion intensities (D_i) divided by the intensity of the parent ion (P_o) prior to CID. The CID efficiency was determined by the instrument software, and the collision energy was optimized for the maximum intensity of the most intense daughter ion from the CID spectrum.

$$E_{CID} = \Sigma D_i / P_o \quad (4-4)$$

A calibration curve is presented for NTO, NQ, HMX, RDX, CL-20, tetryl, TNT, and PETN (Figure 4-27). The peak areas for each explosive were constructed from the same mass scan filters used in the chromatograms in Figure 4-18. The linear dynamic range (LDR) for each explosive, defined as the range over which linearity can be assumed [Miller and Miller, 1984], was 5 to 1000 ppb. The limit of detection (LOD) for each explosive, described in general terms as the concentration which gives an instrument signal significantly different from the blank or background signal [Miller and Miller, 1984], was 5 ppb. A more sensible definition of LOD that minimizes the possibility of false positives is the analyte concentration giving a signal equal to the blank signal, y_B , plus three standard deviations of the blank, s_B (equation 4-5). The limit of quantitation (LOQ) is a lower limit for precise quantitative measurements as opposed to qualitative detection, and is described by equation 4-6.

$$y = y_B + 3s_B \quad (4-5)$$

$$y = y_B + 10s_B \quad (4-6)$$

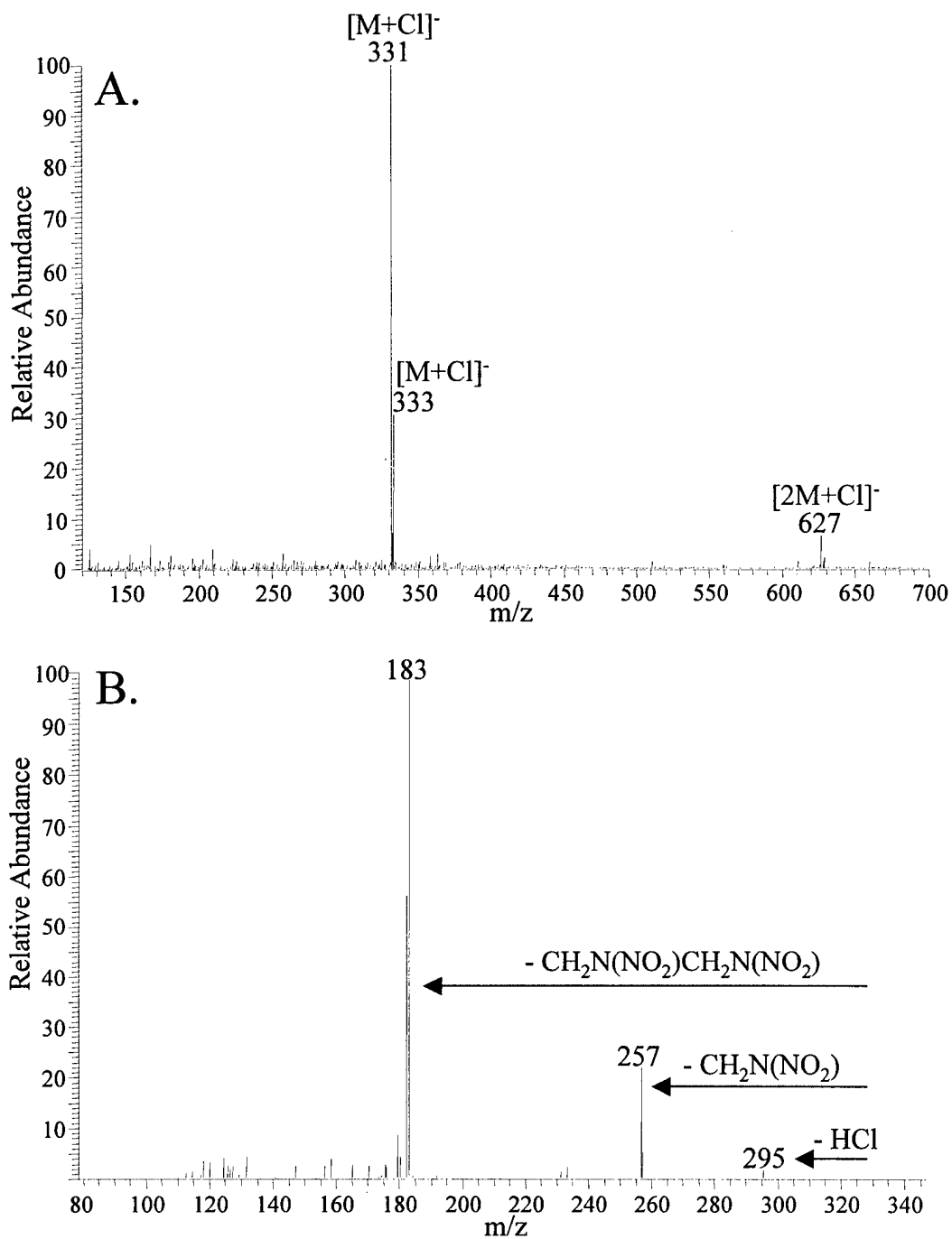


Figure 4-21. A. APCI-MS spectrum of HMX peak. B. Daughter ion spectrum of $[M+Cl]^-$ ion (m/z 331) of HMX.

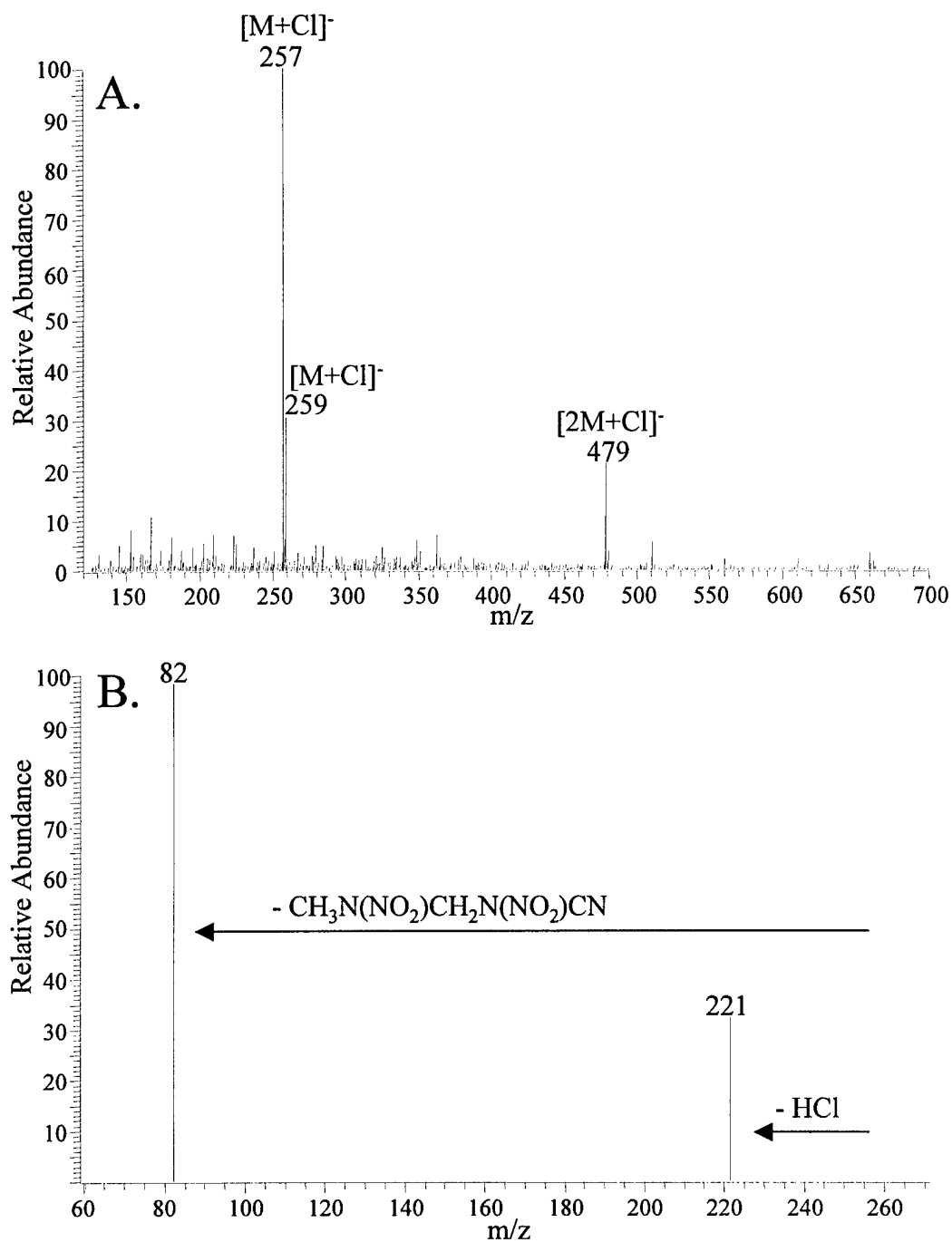


Figure 4-22. A. APCI-MS spectrum of RDX peak. B. Daughter ion spectrum of $[M+Cl]^-$ ion (m/z 257) of RDX.

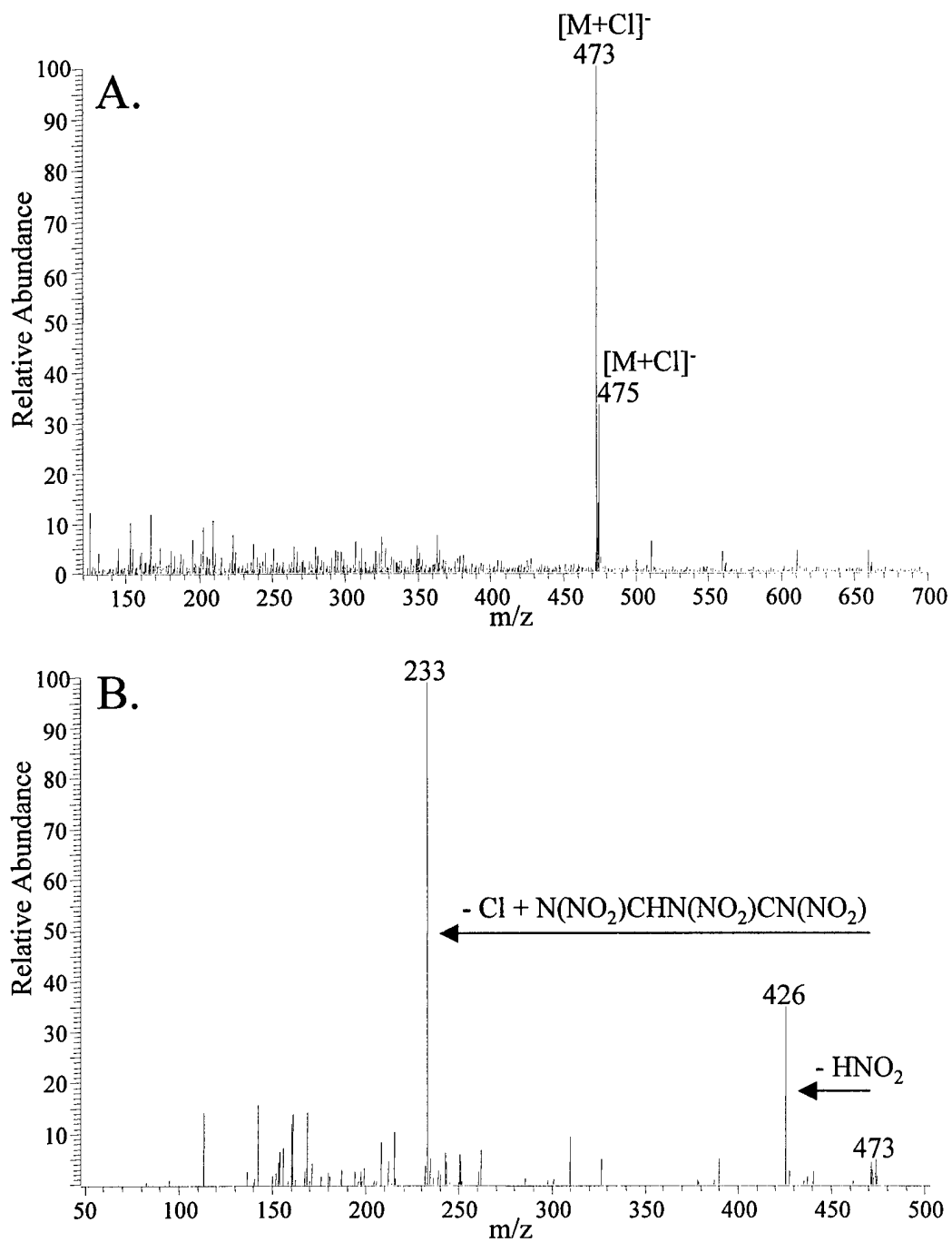


Figure 4-23. A. APCI-MS spectrum of CL-20 peak. B. Daughter ion spectrum of $[M+Cl]^-$ ion (m/z 473) of CL-20.

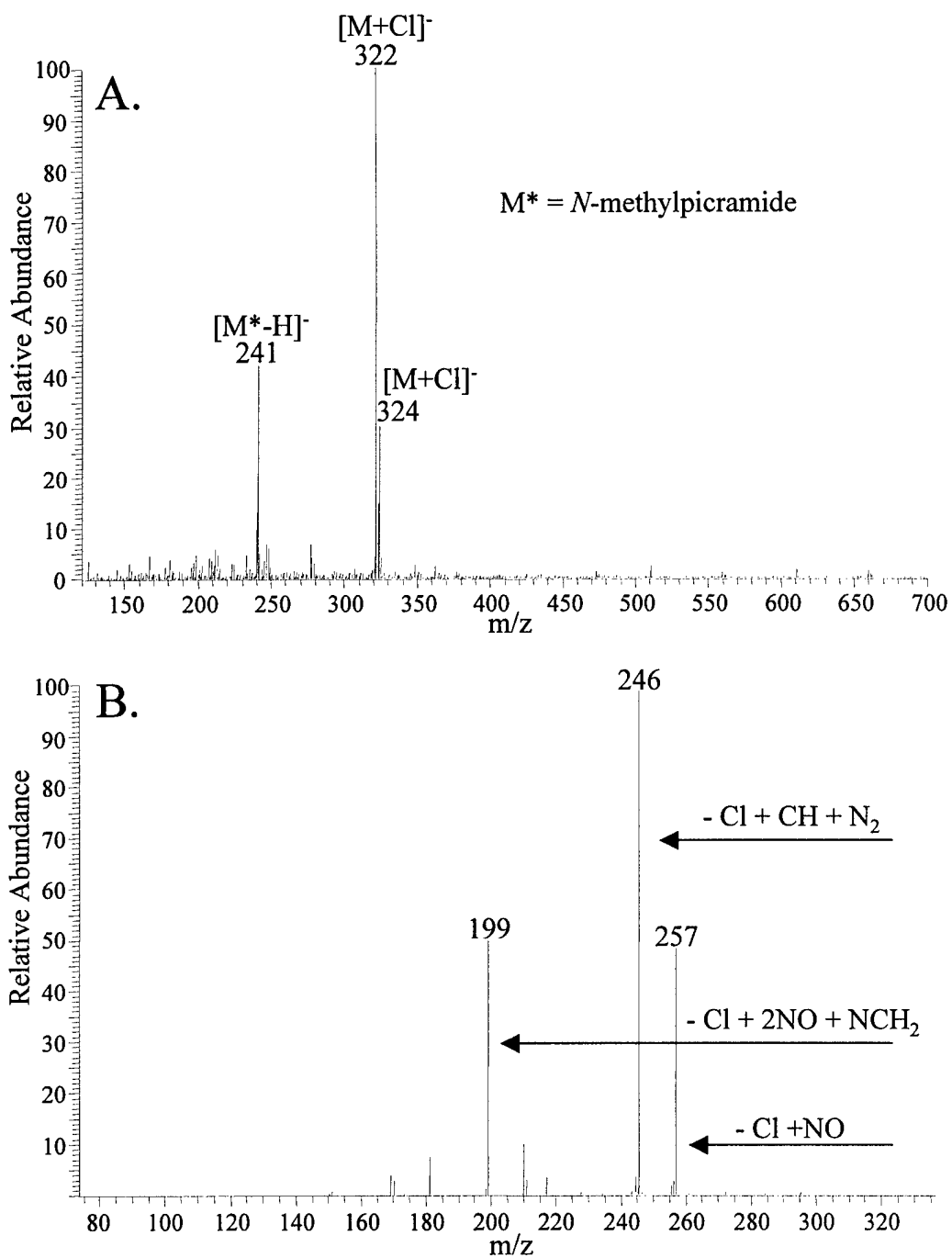


Figure 4-24. A. APCI-MS spectrum of tetryl peak. B. Daughter ion spectrum of $[M+Cl]^-$ ion (m/z 322) of tetryl.

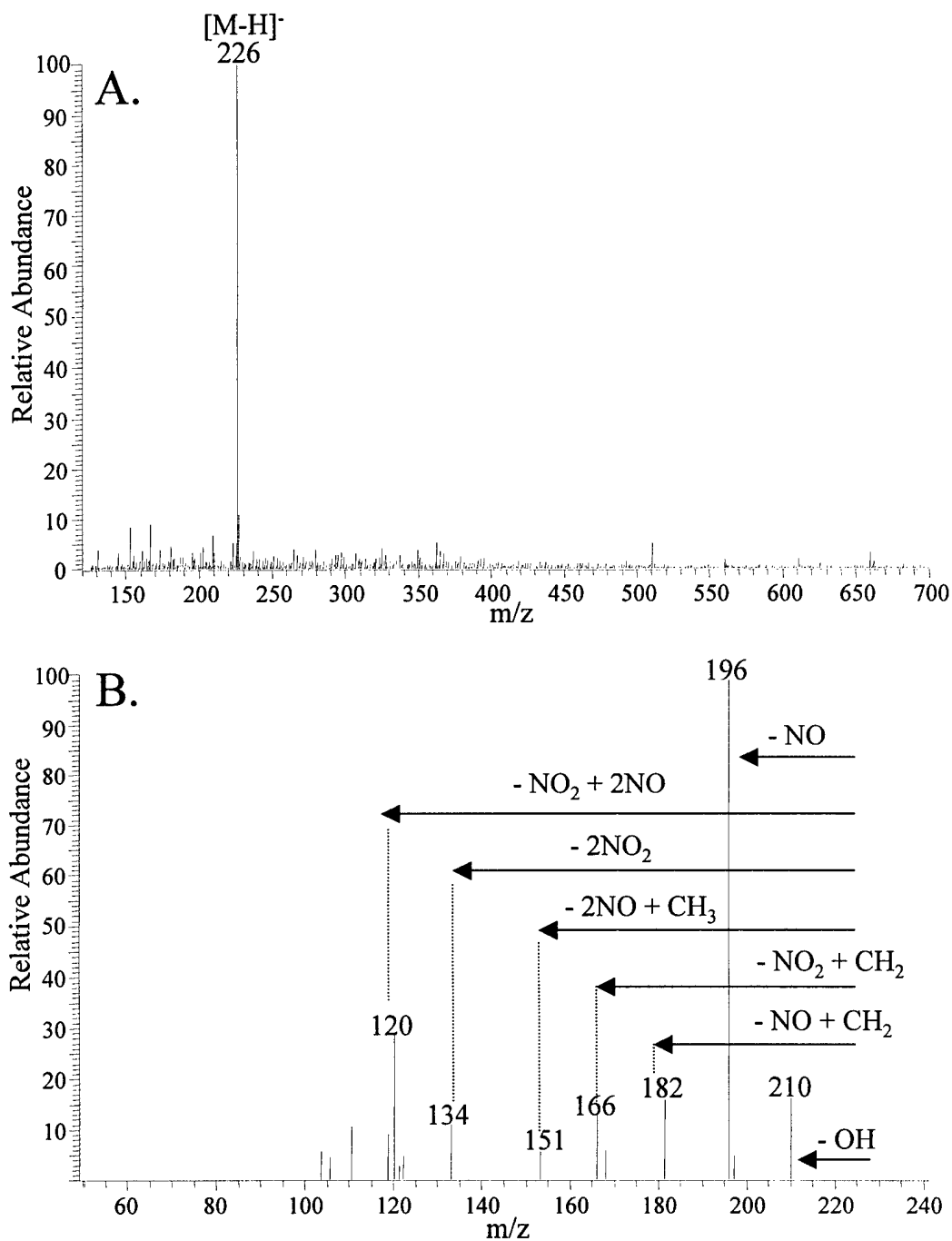


Figure 4-25. A. APCI-MS spectrum of TNT peak. B. Daughter ion spectrum of $[M-H]^-$ ion (m/z 226) of TNT.

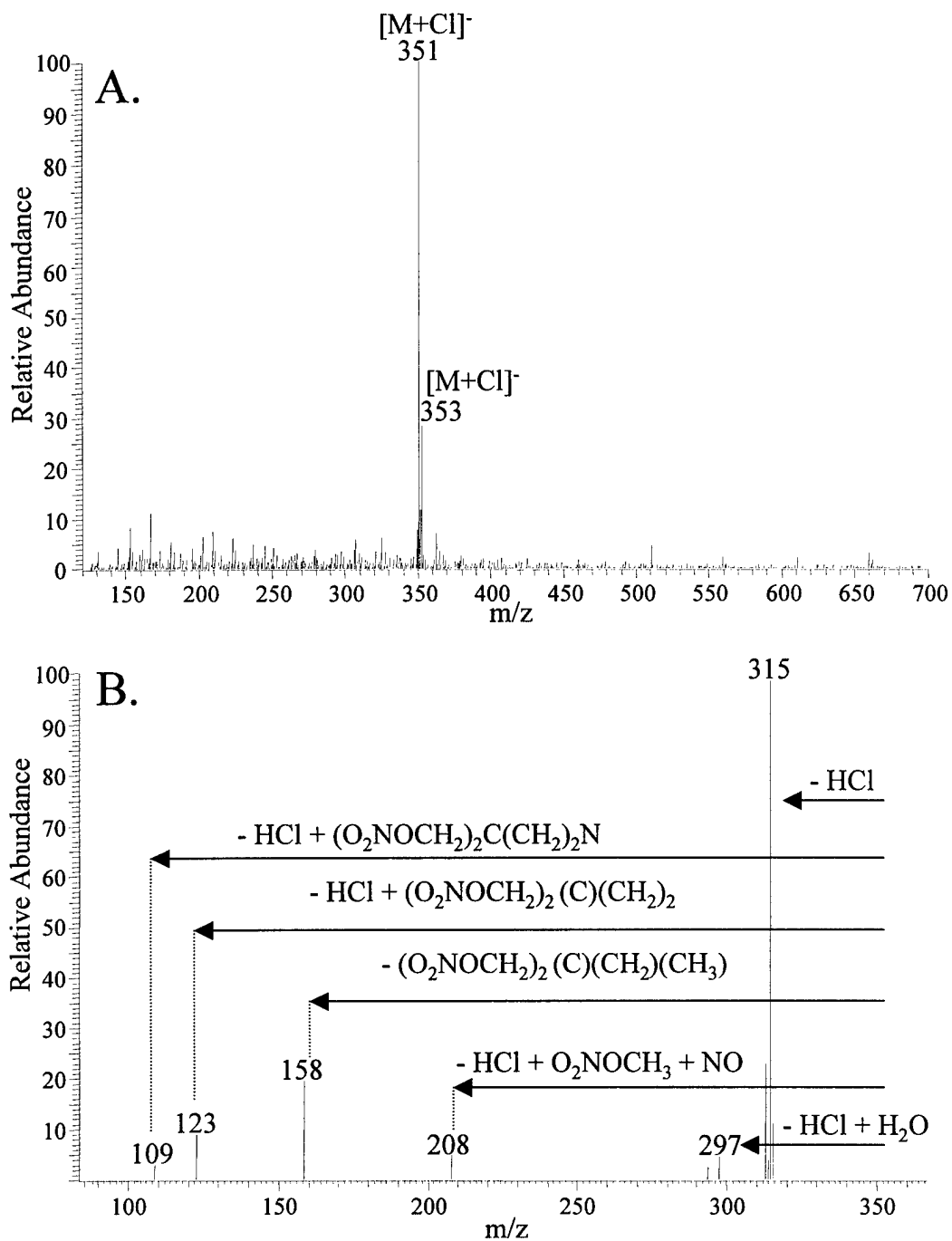


Figure 4-26. A. APCI-MS spectrum of PETN peak. B. Daughter ion spectrum of $[M+Cl]^-$ ion (m/z 351) of PETN.

Table 4-2: APCI-MS/MS Properties

Explosive	Parent Ion (m/z)	Isolation Width (amu)	CID Efficiency (%)	Collision Energy (%)	Most Intense Daughter Ion (m/z)
NTO	165	3	14.8	26	129
NQ	139	3	6.0	28	103
HMX	331	3	10.6	24	183
RDX	257	3	1.7	20	82
CL-20	473	4	8.1	20	233
Tetryl	322	3	73.8	18	246
TNT	226	2	6.6	30	196
PETN	351	3	10.5	20	315

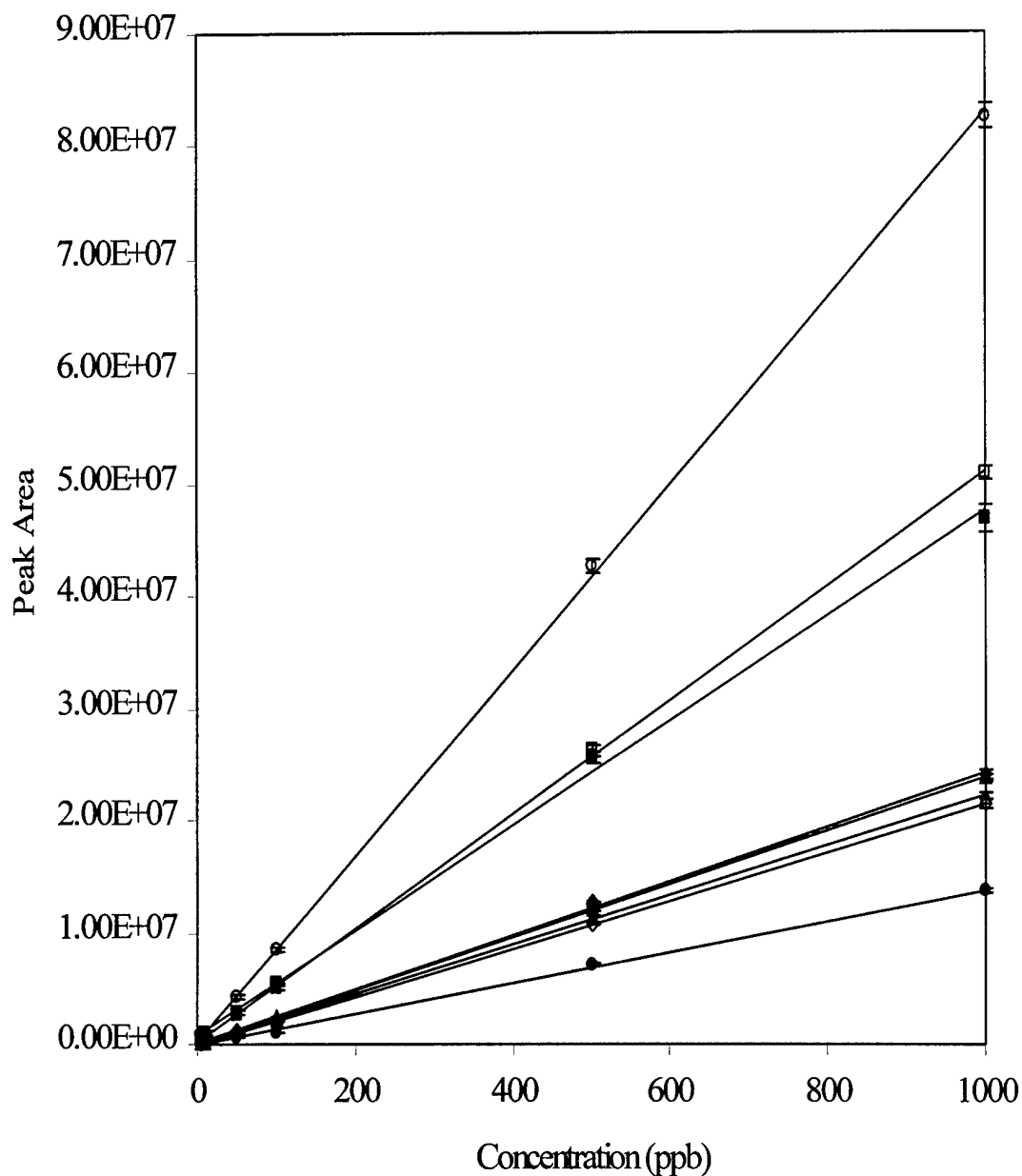


Figure 4-27. Calibration curves for LC-APCI-MS volume injections of 0, 5, 10, 50, 100, 500, and 1000 ppb of NTO (◆), NQ (●), HMX (■), RDX (▲), CL-20 (◈), tetryl (◐), TNT (◑), and PETN (◒). The following ions were monitored for each explosive: $[M+Cl]^-$, $[M-H]^-$, and $[M+NO_3]^-$ of NTO; $[M+Cl]^-$ of NQ; $[M+Cl]^-$ of HMX; $[M+Cl]^-$ of RDX; $[M+Cl]^-$ of CL-20; $[M+Cl]^-$ and $[M^*-H]^-$ of tetryl; $[M-H]^-$ of TNT; and $[M+Cl]^-$ of PETN. M^* is *N*-methylpicramide.

The LODs and LOQs for NTO, NQ, HMX, RDX, CL-20, tetryl, TNT, and PETN are listed in Table 4-3. Regression error bands were plotted at the 95% confidence level for NTO (Figure 4-28A), NQ (Figure 4-28B), HMX (Figure 4-29A), RDX (Figure 4-29B), CL-20 (Figure 4-30A), tetryl (Figure 4-30B), TNT (Figure 4-31A), and PETN (Figure 4-31B). These confidence bands take into consideration the random errors in the values for the slope and intercept of the regression lines used to interpolate the concentrations of the explosives.

Conclusion

In this chapter, the effects of chlorinated solvents on the APCI-MS of explosives were presented. Increasing concentrations of chlorinated solvent increase the intensity of HMX, RDX, tetryl, and PETN, but suppress the $[M]^+$ ion signal of TNT due to competitive ionization processes. Carbon tetrachloride showed the best improvement in signal; however, chloroform was used in the APCI method development because it did not cause signal suppression due to ion burns. An APCI tune method was developed by optimizing the signal intensities of HMX, RDX, tetryl, TNT, and PETN with various parameter settings. An LC/APCI-MS and LC/APCI-MS/MS method was developed using the APCI tune method. The methods developed are capable of isocratically separating NTO, NQ, HMX, RDX, CL-20, tetryl, TNT, and PETN under five minutes with the identification of major parent ions and daughter ions of each explosive. The method proved to be sensitive for each explosive down to 5 ppb with a linear dynamic range that reaches up to 1000 ppb.

Table 4-3: Limit of Detection and Limit of Quantitation

Explosive	Limit of Detection (ppb)	Limit of Quantitation (ppb)
NTO	40	132
NQ	60	201
HMX	52	173
RDX	12	38
CL-20	10	33
Tetryl	25	74
TNT	19	64
PETN	12	42

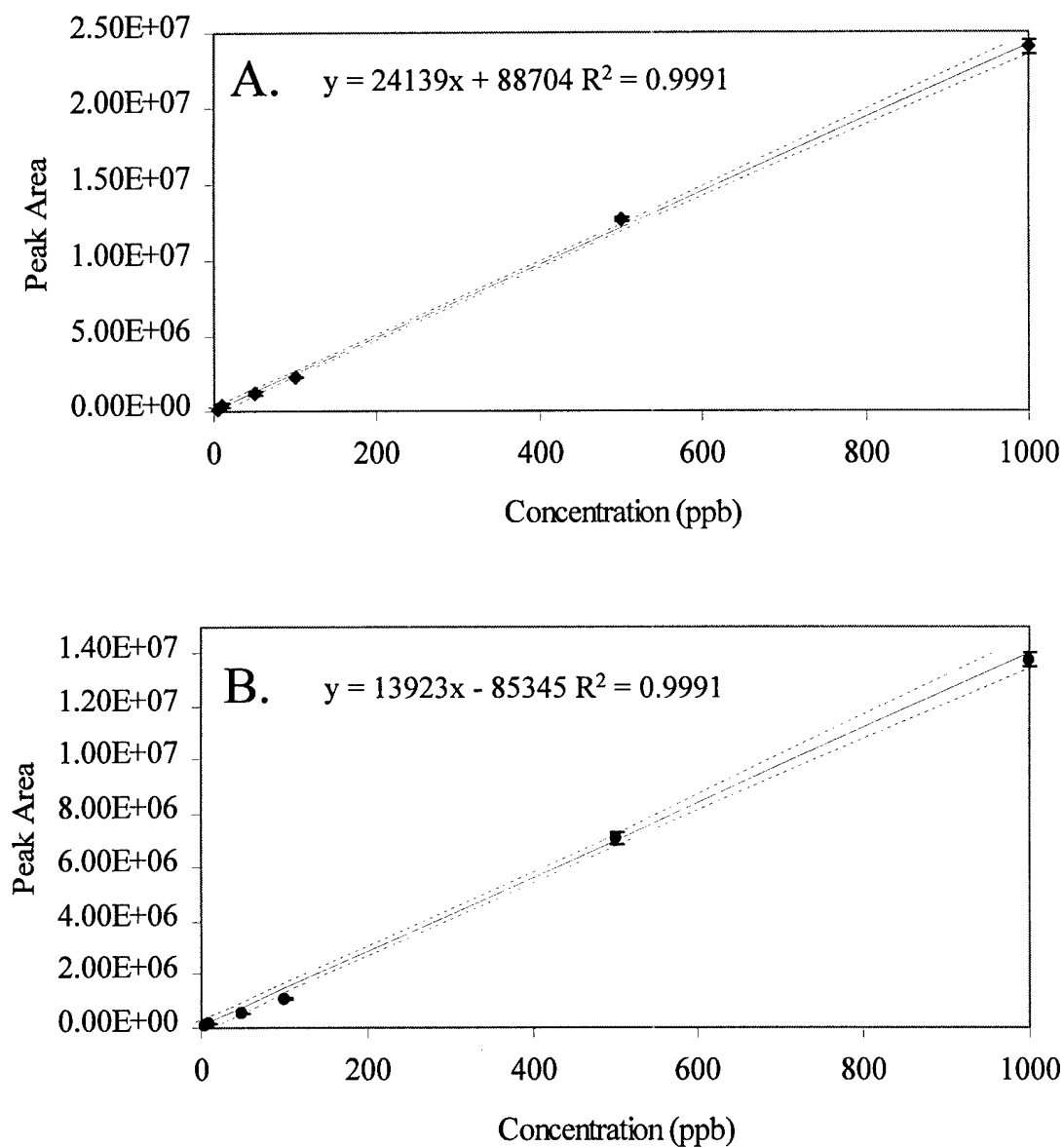


Figure 4-28. LC-APCI-MS of 5, 10, 50, 100, 500, and 1000 ppb loop injections of (A) NTO and (B) NQ. Regression error bands plotted at the 95% confidence level.

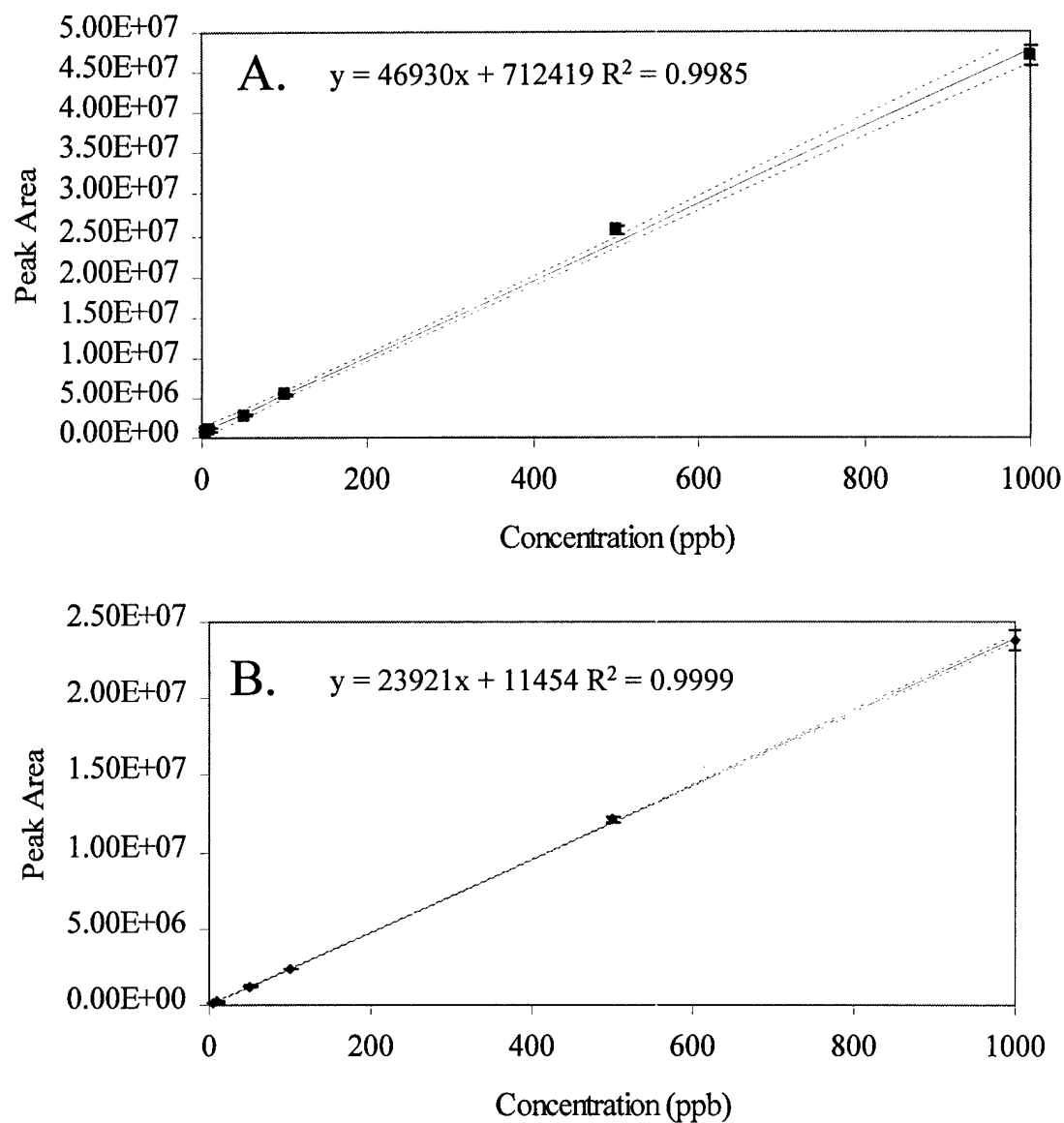


Figure 4-29. LC-APCI-MS of 5, 10, 50, 100, 500, and 1000 ppb loop injections of (A) HMX and (B) RDX. Regression error bands plotted at the 95% confidence level.

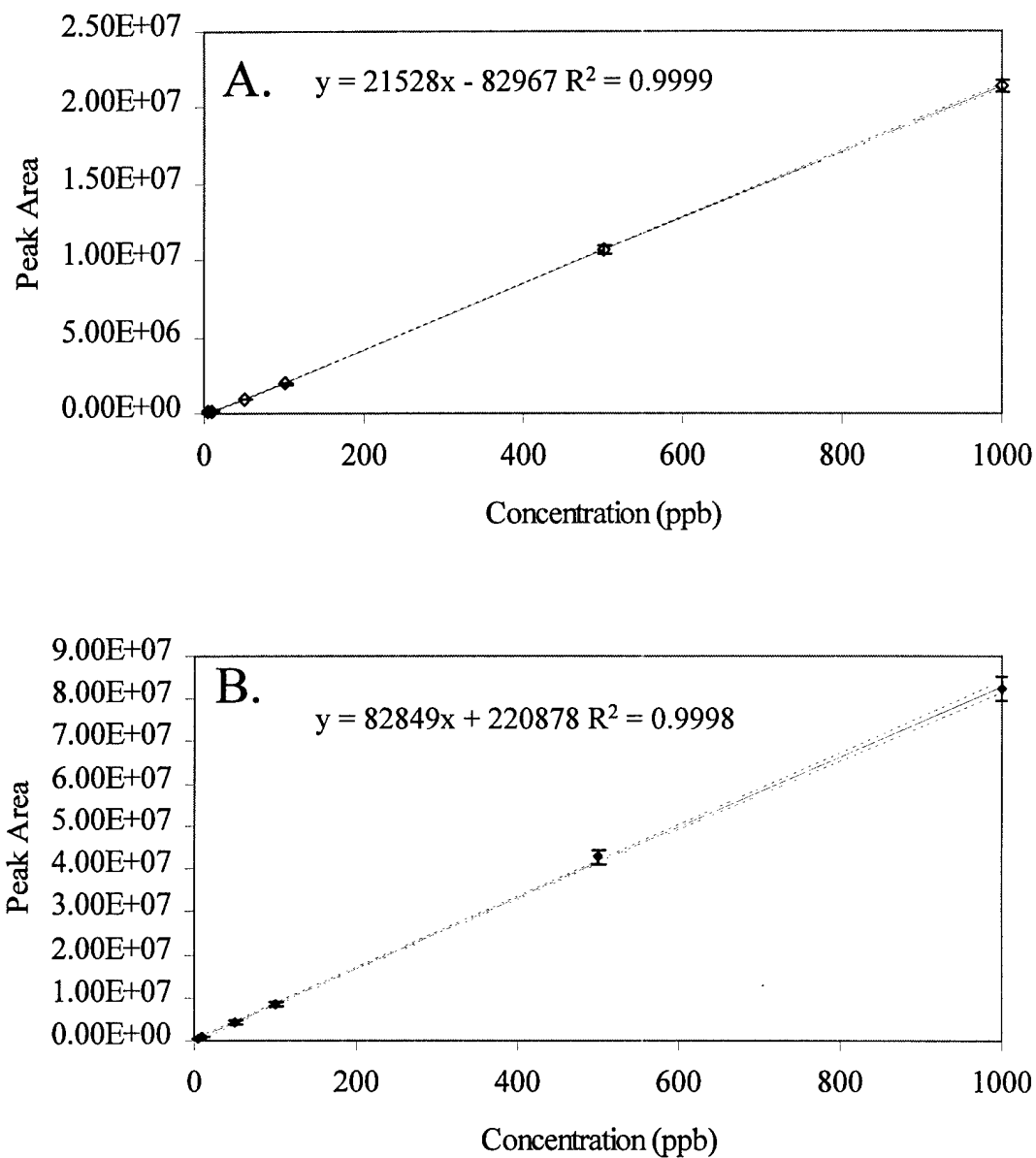


Figure 4-30. LC-APCI-MS of 5, 10, 50, 100, 500, and 1000 ppb loop injections of (A) CL-20 and (B) Tetryl. Regression error bands plotted at the 95% confidence level.

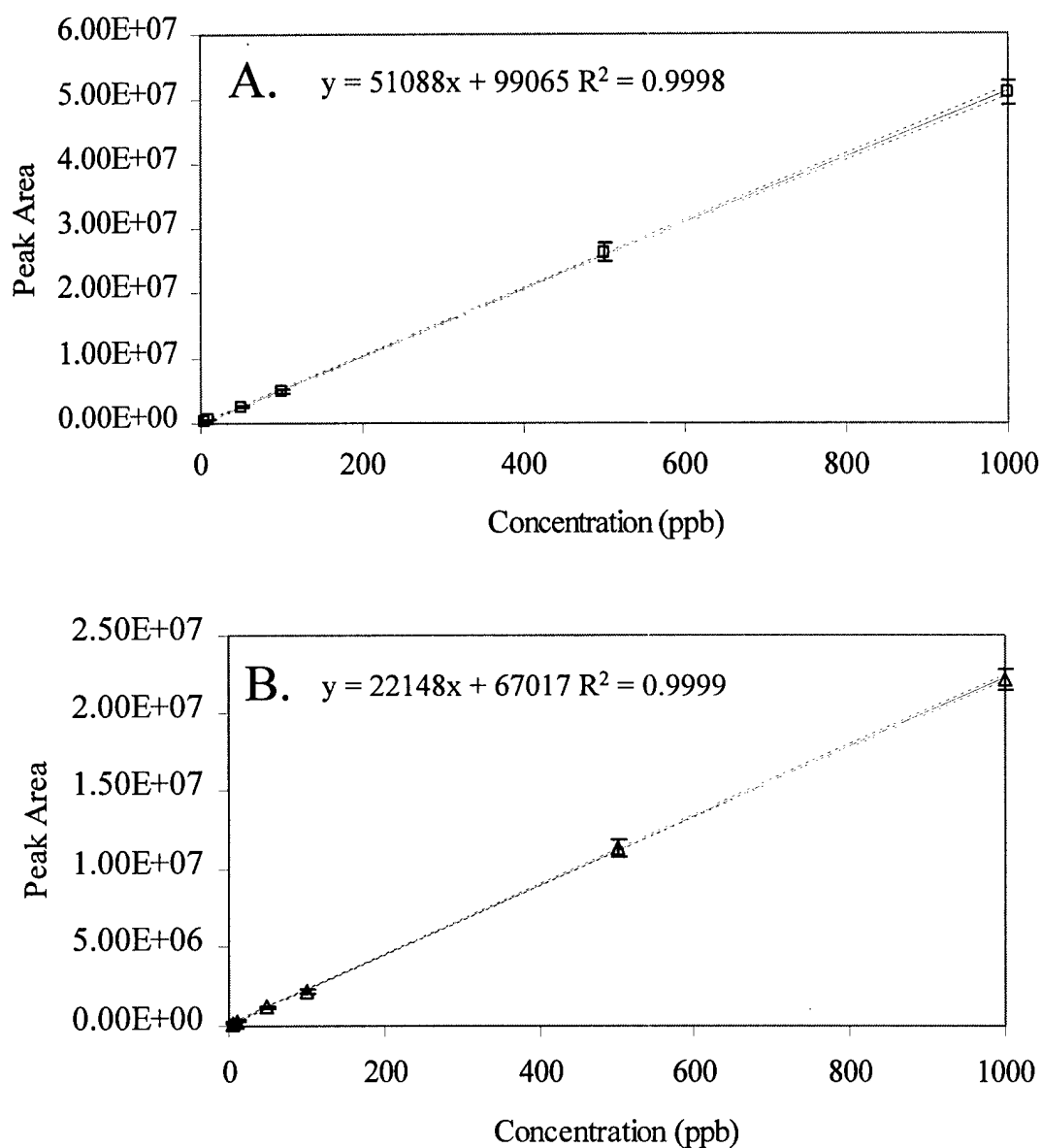


Figure 4-31. LC-APCI-MS of 5, 10, 50, 100, 500, and 1000 ppb loop injections of (A) TNT and (B) PETN. Regression error bands plotted at the 95% confidence level.

CHAPTER 5

APPLICATION OF LC/APCI-MS METHOD FOR ANALYSIS OF REAL SAMPLES

In Chapter 4, an LC/APCI-MS method developed for the analysis of explosives was described. In this chapter, the use of this method to identify and quantitate trace amounts of explosives from real samples will be detailed. The real samples include two soil samples, two detonation soot samples, a water sample, and SEMTEX, a type of plastic explosive used during the terrorist bombing of Pan Am flight 103 over Scotland in 1988. The soil samples come from an explosive factory in the Czech Republic, and they were suspected to be contaminated with RDX, TNT, and PETN. The detonation soot samples come from the detonation of an explosive formulation known to contain NQ and TNT; these samples were analyzed to determine the presence of unreacted explosive. The water sample comes from a holding tank from an explosive processing facility, which contains the rinse water from cleaning the processing melt kettles and equipment.

The ability to detect trace amounts (less than 1 ppm) of explosives in water and soil is environmentally important due to the health risks that these compounds pose. Over the last decade, the U.S. EPA has issued Health Advisories for many of these compounds in drinking water, with proposed limits in the low parts-per-billion (ppb = $\mu\text{g/L}$) range. Also the ability to ascertain the presence of specific explosives from detonation soot from a terrorist bombing is vital to forensic work, and could lead to the information needed to solve a case.

Experimental

Instrumentation

All experiments were performed on the Finnigan LCQ (San Jose, CA) in the negative-APCI mode. A Hewlett Packard 1090 HPLC pump coupled to a Haisil 100 C18 column (150 mm in length x 4.6 mm i.d., 5 μ m particle size) from Higgins Analytical, Inc. (Mountain View, CA) was used for all LC/MS experiments. The mobile phase was 35% HPLC grade water (H₂O): 65% HPLC grade methanol (MeOH) with 0.1% chloroform. Samples were separated isocratically with a flow rate of 1 mL/min. Samples were injected from a 24.6 μ L sample loop. Sample loops and tubing between the pump, column, and APCI source were composed of polyetheretherketone (PEEK) material. The pressure of the system was 140 \pm 3 bar. The number of analytical scans averaged for each APCI mass spectrum was dependent on the width of the mass chromatographic peak. Each analytical scan consisted of 3 microscans, the maximum injection time was set to 200 ms to optimize ion injection for each point in the chromatographic peak, and the AGC target values for full scan and MS/MS were 2×10^7 and 2×10^6 , respectively.

Samples

Soil and detonation soot samples were provided by Dr. Fred Volk of the Fraunhofer Institute of Chemical Technology, Germany. Soil samples were prepared by placing 1 g of ground soil into a sealed glass vial with 5 mL of methanol. The samples were vortex swirled for one minute, and then placed in a cooled ultrasonic bath for 18 hr. Ice was periodically added to the non-circulated ultrasonic bath to maintain a temperature below 30°C. After sonication, the samples were centrifuged for one minute at 3000 rpm. Then 3 mL of the supernatant were removed and filtered through a 0.45- μ m Teflon

disposable syringe filter (Osmonics, Inc.). This extraction process is similar to that in EPA Method 8330, which is used for trace analysis of explosives, with the exception that methanol is used instead of acetonitrile and the salting-out step with calcium chloride solution is omitted. Methanol was used instead of acetonitrile because it was previously demonstrated that it was more effective at extracting TNT, RDX, and HMX from soil and more suitable for reverse-phase chromatography due to its lower solvent strength [Cragin et al., 1985]. The calcium chloride solution was avoided to prevent salt cluster formation and signal suppression during APCI. 2.6 mL of the methanol soil extracts were diluted with 1.4 mL of water to form a solution similar to the mobile phase.

The detonation soot samples were prepared by placing 10 mg of soot into a sealed glass vial with 4 mL of acetone. The samples were vortex swirled for one minute, and then centrifuged for one minute at 3000 rpm. Then 3 mL of the supernatant were removed and filtered through a 0.45- μ m Teflon disposable syringe filter (Osmonics, Inc.). The acetone soot extracts were diluted with 35/65 H₂O/MeOH.

The High Explosive Research and Development (HERD) Facility at Eglin AFB, Florida, provided the water sample. The sample was not filtered nor was a salting-out procedure as in EPA Method 8330 employed. The sample was diluted with HPLC grade water. SEMTEX was provided by Dr. Jehuda Yinon of the Weizmann Institute of Science, and obtained from the Analytical Laboratory of the Israeli Police Headquarters. An acetone stock solution of SEMTEX was prepared by placing 2.7 mg of the plastic explosive in 1 mL of acetone. The solution was vortex swirled for one minute and the supernatant was diluted with 35/65 H₂O/MeOH. All samples were stored in a refrigerator at 4°C to prevent decomposition.

Results and Discussion

Calibration Curve

All samples were initially screened to determine which explosives were detected and their relative signal intensities. It was determined that NQ, HMX, RDX, TNT, and PETN were present in the different samples; therefore, calibration curves for these explosives were produced using standards. Increasing concentrations of NQ, HMX, RDX, TNT, and PETN (50 ppb, 100 ppb, 200 ppb, 400 ppb, 600 ppb, 800 ppb, and 1000 ppb) were individually injected and detected using the LC/APCI-MS method developed in Chapter 4. The calibration curves produced are shown in Figure 5-1. The calibration curves are less linear than the curves in Figure 4-27, at least at concentrations > 400 ppb. The calibration curves of NQ, HMX, RDX, and PETN showed a closer fit to second order equations than a first order equation. TNT was the only explosive detected that showed a linear response, and coincidentally it does not form a chloride adduct. More critically, however, is that the sensitivity (slope) for TNT here (Figure 5-1) is ten times lower than before (Figure 4-27), whereas the other compounds have the same sensitivity. The observed change in calibration curves might be due to changes in the skimmer cone, which was damaged during cleaning and was subsequently replaced after the first calibration curve (Figure 4-21) was produced and before the second calibration curve (Figure 5-1) was generated. It may also arise from changes in solution composition since only the sensitivity of TNT was affected.

Due to the nonlinearity of the calibration curves at higher concentrations, only the linear portion of the curves were utilized for quantitation. The calibration curves used for

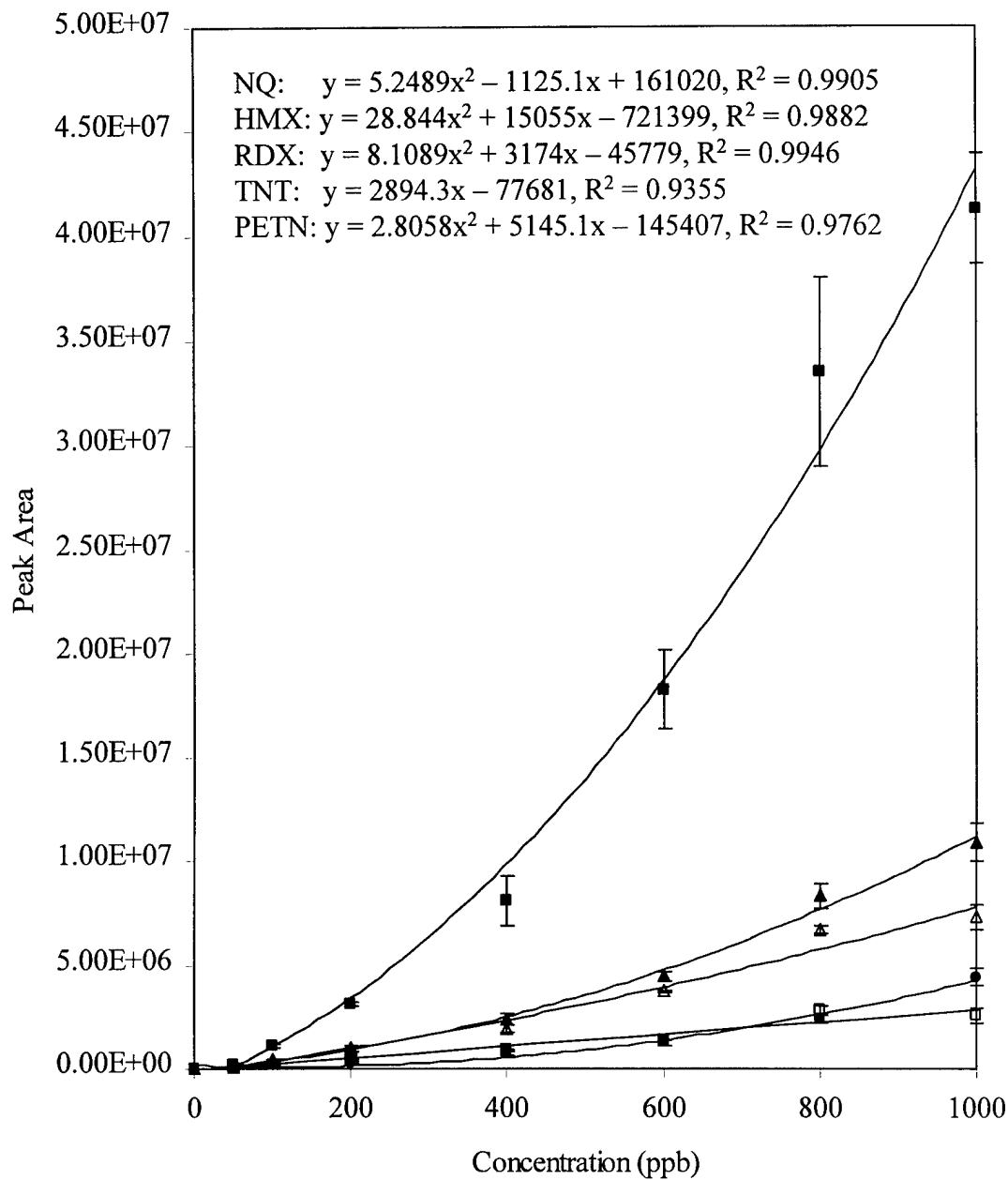


Figure 5-1. LC/APCI-MS calibration curve of $[M+Cl]^-$ of NQ (●), $[M+Cl]^-$ of HMX (■), $[M+Cl]^-$ of RDX (▲), $[M-H]^-$ of TNT (□), and $[M+Cl]^-$ of PETN (△). Error bars are +/- one standard deviation of the mean for three replicates.

quantitation of NQ, HMX, RDX, TNT, and PETN are shown in Figure 5-2A, 5-2B, 5-3A, 5-3B, and 5-4, respectively, with corresponding 95% confidence bands. The samples had to be diluted because they were determined to be too concentrated with explosives. The samples were diluted so that the peak areas of the detected explosives remained bracketed by standards on the calibration curve. Some samples contained a broad range of explosive concentrations, and had to be diluted several times to keep each explosive within its linear range.

Water Sample

The LC/APCI-MS chromatogram of the unfiltered water sample is shown in Figure 5-5. The two major peaks observed in the total ion current (TIC) chromatogram are TNT and RDX. Ions were detected at m/z 465 (unknown) at 1.54 min, m/z 331 ($[M+Cl]^-$ of HMX) at 1.73 min, m/z 257 ($[M+Cl]^-$ of RDX) at 2.20 min, m/z 226 ($[M-H]^-$ of TNT) at 3.50 min, and m/z 351 ($[M+Cl]^-$ of PETN) at 4.33 min. The sample dilution, peak areas, and concentrations of each detected explosive are listed in Table 5-1. The concentrations of HMX, RDX, TNT, and PETN in the water were determined to be 2.0 ± 0.4 $\mu\text{g/ml}$, 9.4 ± 1.3 $\mu\text{g/ml}$, 1.4 ± 0.0 mg/ml , and 392 ± 90 ng/ml , respectively (Table 5-2). These relative concentrations are reasonable considering the types of explosive formulations that are processed at the HERD. Octol (75/25% by weight TNT/HMX), Comp B (60/40% by weight RDX/TNT), pentolite (75/25% by weight TNT/PETN), and various RDX- and HMX-based plastic explosives are commonly processed at this facility on a daily basis. One- to thirty-gallon batches of the explosives are mixed in steam jacketed melt kettles that are cleaned with acetone and water after their use.

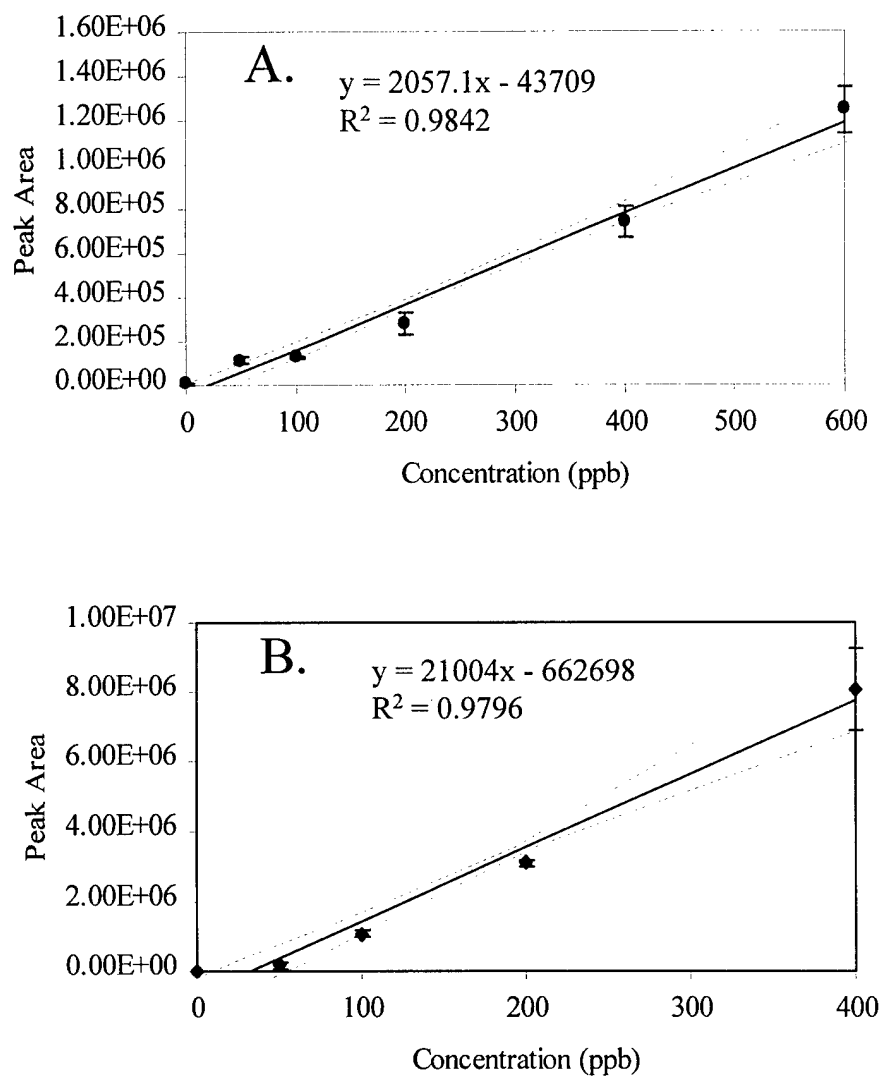


Figure 5-2. LC/APCI-MS calibration curve acquired with 25 μ L sample loop: A. $[M+Cl]^-$ of NQ (\bullet), B. $[M+Cl]^-$ of HMX (\blacksquare). Error bars are \pm one standard deviation of the mean for three replicates.

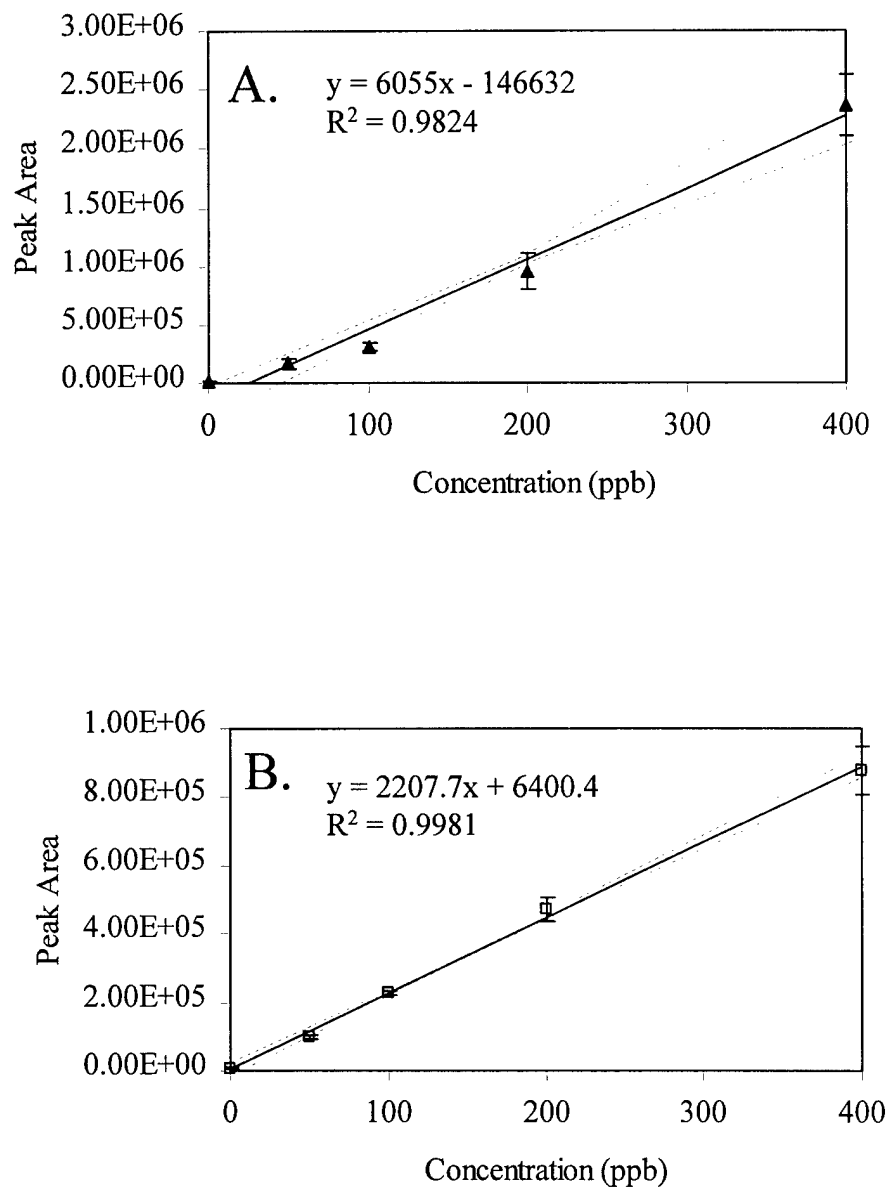


Figure 5-3. LC/APCI-MS calibration curve acquired with 25 μ L sample loop: A. $[M+Cl]^-$ of RDX (\blacktriangle), B. $[M-H]^-$ of TNT (\square). Error bars are \pm one standard deviation of the mean for three replicates.

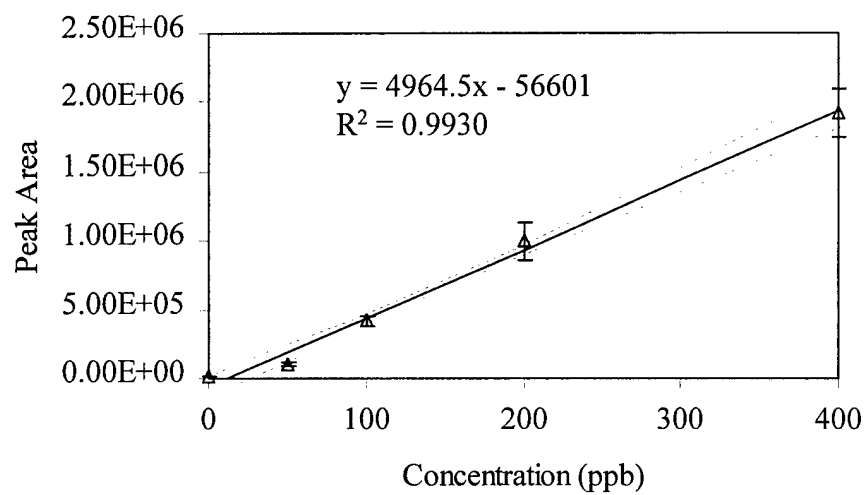


Figure 5-4. LC/APCI-MS calibration curve acquired with 25 μ L sample loop for $[M+Cl]^-$ of PETN (Δ). Error bars are +/- one standard deviation of the mean for three replicates.

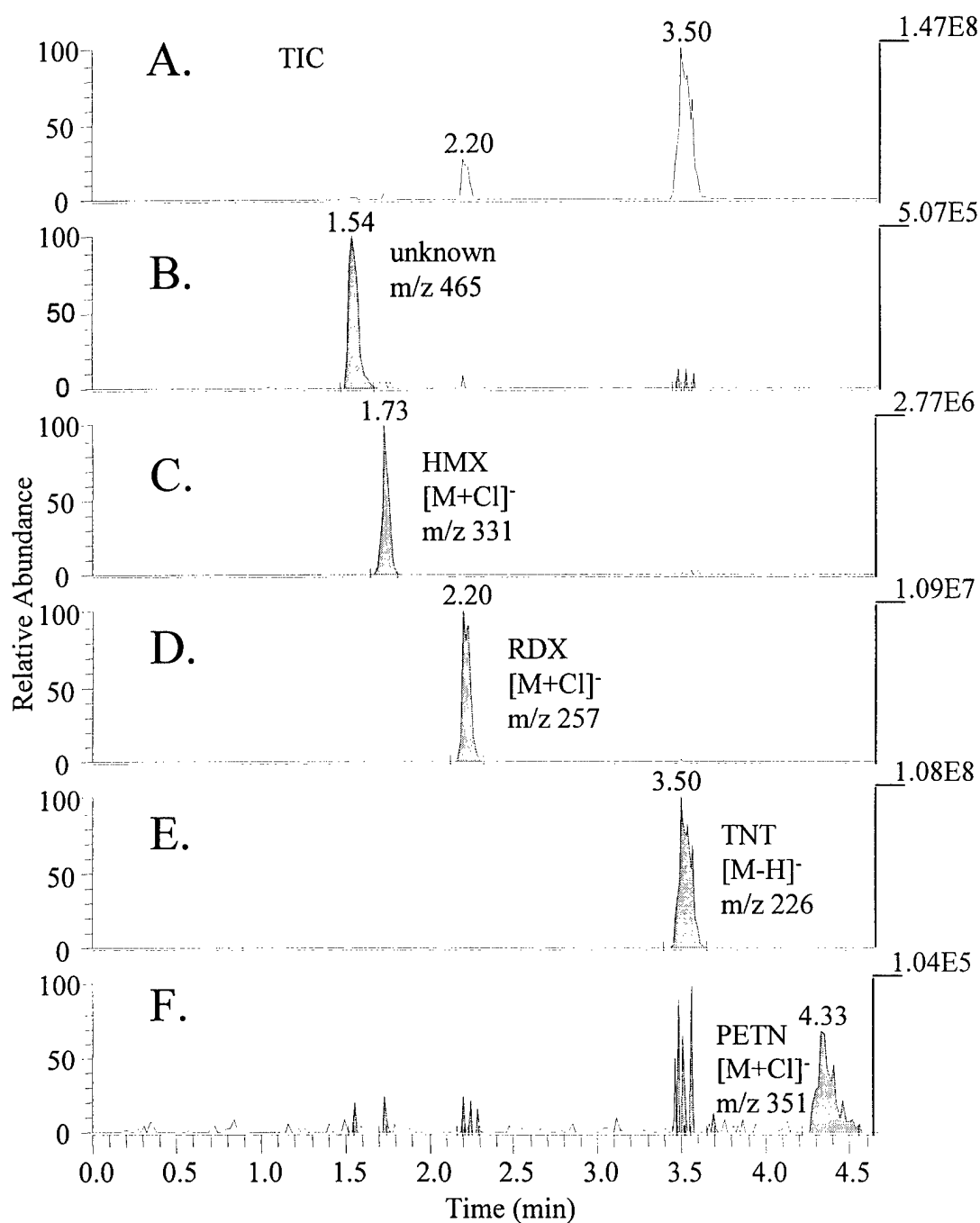


Figure 5-5. LC/APCI-MS chromatograms of water sample, diluted by 1:10: (A) total ion current (TIC) from m/z 120 to 700, (B) m/z 465 (unknown) eluting at 1.54 min, (C) m/z 331 ($[M+Cl]^-$ of HMX) eluting at 1.73 min, (D) m/z 257 ($[M+Cl]^-$ of RDX) eluting at 2.20 min, (E) m/z 226 ($[M-H]^-$ of TNT) eluting at 3.50 min, and (F) m/z 351 ($[M+Cl]^-$ of PETN) at 4.33 min.

Table 5-1 Analysis of Real Samples

Sample	Dilution Factor (v/v)	Explosive Detected	Peak Area Replicate Measurements			Mean Peak Area	Standard Deviation of the Mean	Concentration in Diluted Sample (ppb)
Soil #1	1/2.6	RDX	933652	1082248	1217922	1077941	82090	202 +/- 38
	1/2.6	PETN	1209660	1795016	1702591	1569089	181684	327 +/- 48
Soil #2	1/14	RDX	920730	894887	927191	914269	9869	175 +/- 26
	1/1.5	TNT	777264	761772	704232	747756	22217	336 +/- 7
	1/14	PETN	1558820	1949057	1635840	1714572	119332	357 +/- 35
Soot #1	1/62	NQ	417954	610522	769107	599194	101527	312 +/- 71
	1/25	TNT	569232	584724	555954	569970	8313	255 +/- 1
Soot #2 Water	1/209	NQ	689814	572008	662628	641483	35613	333 +/- 38
	1/5.6	HMX	8102800	6805651	5576773	6828408	729290	357 +/- 66
	1/26	RDX	2322702	1799385	1999667	2040585	152448	361 +/- 49
	1/3540	TNT	850296	879066	890132	873165	11872	393 +/- 2
SEMTEX	1/5.6	PETN	259741	336761	270010	288837	24144	70 +/- 16
	1/6780	RDX	66630	66060	47587	60092	6255	34 +/- 25
	1/6780	PETN	213289	387473	453829	351864	71405	82 +/- 26

Table 5-2 Explosive Concentrations

Sample	Explosive Detected	Concentration
Soil #1	RDX	1.4 +/- 0.0 µg/g of soil sample
	PETN	2.2 +/- 0.1 µg/g of soil sample
Soil #2	RDX	6.4 +/- 0.9 µg/g of soil sample
	TNT	1.3 +/- 0.0 µg/g of soil sample
	PETN	13 +/- 1 µg/g of soil sample
Soot #1	NQ	5.5 +/- 1.2 mg/g of soot sample
	TNT	1.8 +/- 0.0 mg/g of soot sample
Soot #2	NQ	23 +/- 3 mg/g of soot sample
Water	HMX	2.0 +/- 0.4 µg/ml of water sample
	RDX	9.4 +/- 1.3 µg/ml of water sample
	TNT	1.4 +/- 0.0 mg/ml of water sample
	PETN	392 +/- 90 ng/ml of water sample
SEMTEX	RDX	8.5 +/- 0.1% by weight
	PETN	20.6 +/- 0.1% by weight

Soil Samples

The soil and detonation soot samples were filtered through a 0.45- μm Teflon disposable syringe filter (Osmonics, Inc.) to remove particulate material. The recovery of explosives from these syringe filters were determined by filtering a 1 ppm standard explosive mixture consisting of NTO, NQ, HMX, RDX, CL-20, tetryl, TNT, and PETN, and comparing peak areas from the LC/APCI-MS chromatogram to that of an unfiltered 1 ppm explosive mixture (Figure 5-6). It was determined that there is no significant loss in samples within statistical error due to filtering with the Teflon filter.

The LC/APCI-MS chromatogram of an extract of the filtered soil sample #1 is shown in Figure 5-7. Note that the TIC trace is far more complex than that for the water sample. Indeed no explosive peaks are apparent in the TIC chromatogram. Ions were detected at m/z 189 (unknown) at 1.06 min, m/z 377 (unknown) at 1.35 min, m/z 257 ($[\text{M}+\text{Cl}]^-$ of RDX) at 2.16 min, m/z 349 (unknown) at 2.33 min, m/z 351 ($[\text{M}+\text{Cl}]^-$ of PETN) at 4.33 min, and m/z 353 (unknown) at 8.44 min. The unknown ions at m/z 189, 377, 349, and 353 are each part of a typical chlorine isotopic pattern, which indicates that these ions are either formed from chlorinated compounds or are chloride adduct ions. The sample dilution, peak areas, and concentrations of each explosive detected are listed in Table 5-1. From these calibrations, the concentrations of RDX and PETN in soil sample #1 are 1.4 ± 0.0 $\mu\text{g/g}$ and 2.2 ± 0.1 $\mu\text{g/g}$, respectively (Table 5-2).

The LC/APCI-MS chromatogram of an extract of the filtered soil sample #2 is shown in Figure 5-8. Note that in this case, the TIC trace shows two dominant peaks, corresponding to RDX and PETN. Ions were detected at m/z 257 ($[\text{M}+\text{Cl}]^-$ of RDX) at 2.14 min, m/z 306 (unknown) at 3.03 min, m/z 306 ($[\text{M}+\text{HCl}-\text{NO}_2]^-$ of PETN) at 4.30

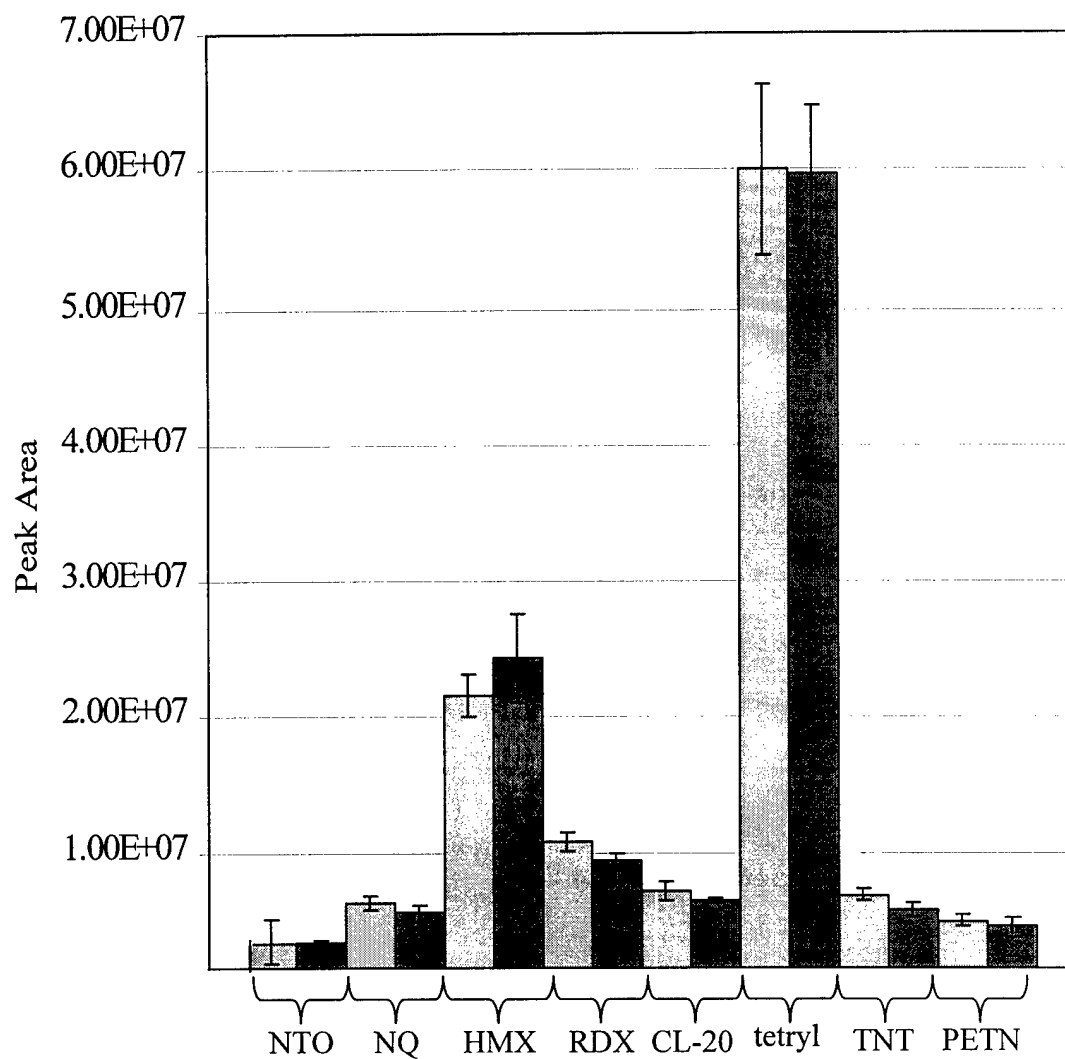




Figure 5-6. Sample recovery after filtering with 0.45 μm Teflon disposable syringe filters as determined by LC/APCI-MS peak areas;  filtered and  unfiltered.

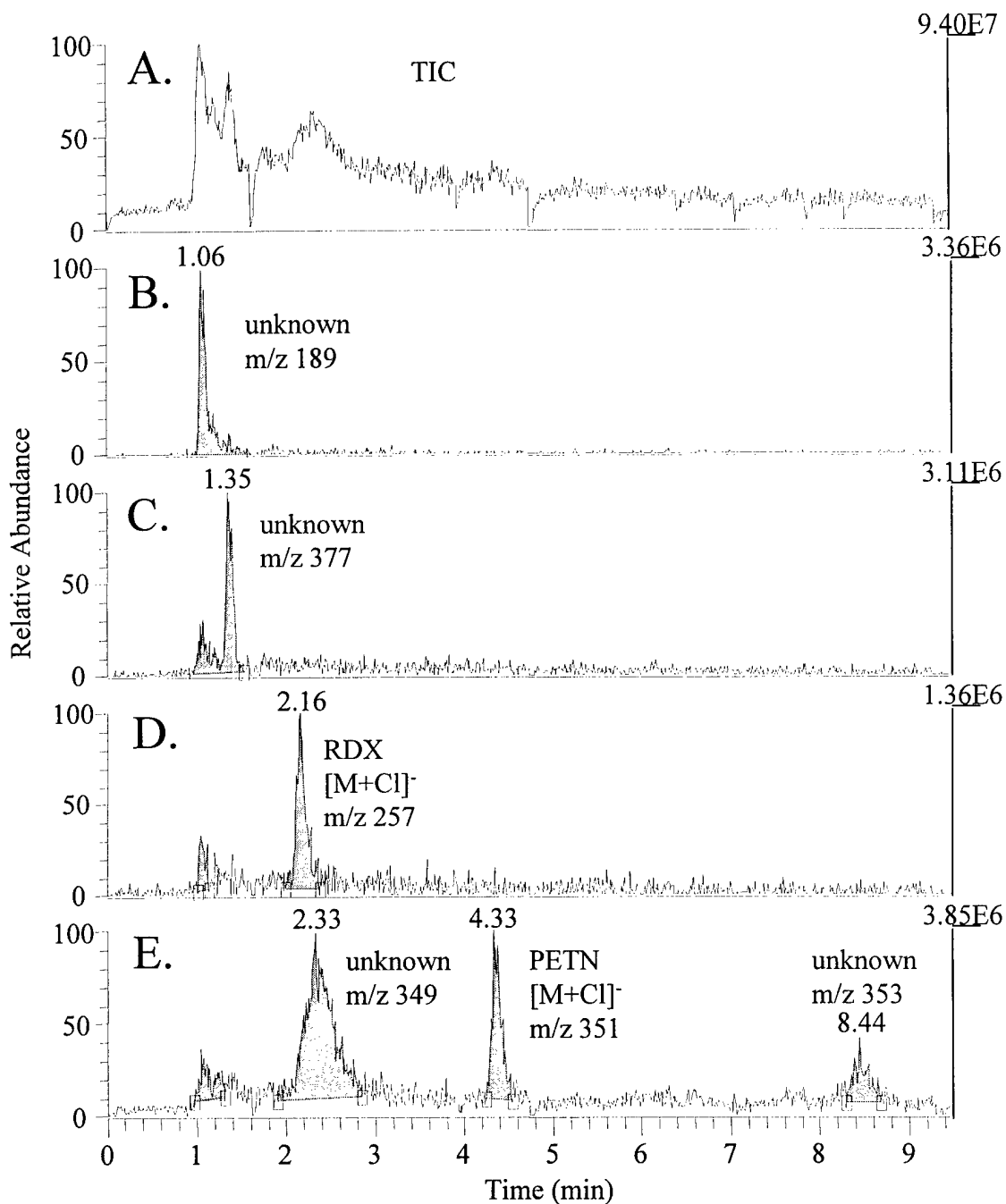


Figure 5-7. LC/APCI-MS chromatograms of soil sample #1 extract, diluted by 1:10: (A) total ion current (TIC) from m/z 120 to 700, (B) m/z 189 (unknown) eluting at 1.06 min, (C) m/z 377 (unknown) eluting at 1.35 min, (D) m/z 257 ([M+Cl]⁻ of RDX) eluting at 2.16 min, (E) m/z 349 (unknown) eluting at 2.33 min, m/z 351 ([M+Cl]⁻ of PETN) eluting at 4.33 min, and m/z 353 (unknown) at 8.44 min.

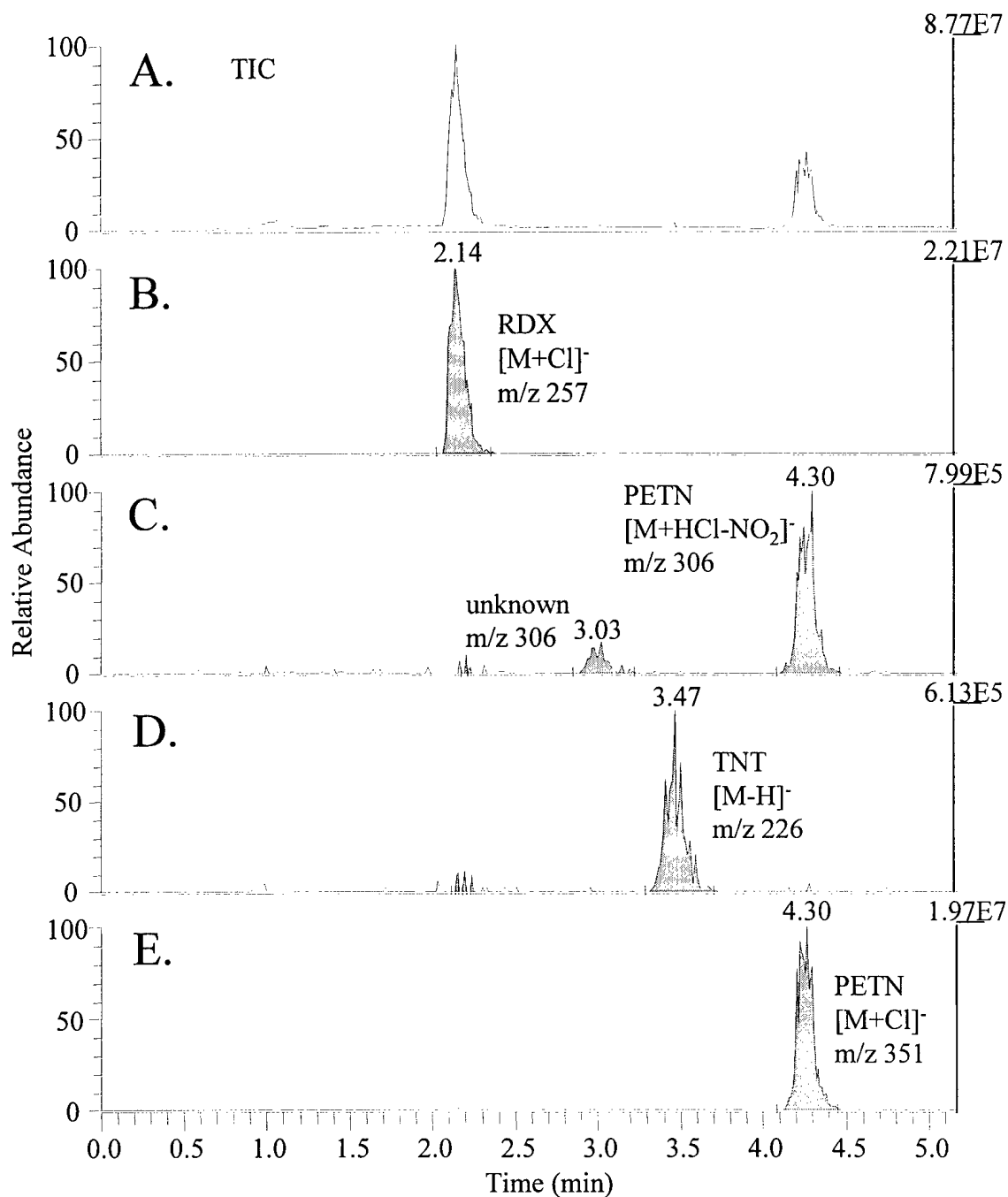


Figure 5-8. LC/APCI-MS chromatograms of soil sample #2 extract, diluted by 1:10: (A) total ion current (TIC) from m/z 120 to 700, (B) m/z 257 ($[M+Cl]^-$ of RDX) eluting at 2.14 min, (C) m/z 306 (unknown) eluting at 3.03 min, m/z 306 ($[M+HCl-NO_2]^-$ of PETN) eluting at 4.30 min, (D) m/z 226 ($[M-H]^-$ of TNT) eluting at 3.47 min, and (F) m/z 351 ($[M+Cl]^-$ of PETN) at 4.27 min.

min, m/z 226 ($[M-H]^-$ of TNT) at 3.47 min, and m/z 351 ($[M+Cl]^-$ of PETN) at 4.30 min. The unknown ion at m/z 306 is part of a chlorine isotopic pattern. The sample dilution, peak areas, and concentrations of each explosive detected are listed in Table 5-1. The concentrations of RDX, TNT, and PETN in soil sample #2 are 6.4 ± 0.9 $\mu\text{g/g}$, 1.3 ± 0.0 $\mu\text{g/g}$, and 13 ± 1 $\mu\text{g/g}$, respectively (Table 5-2), about five times higher than in soil #1.

Soot Samples

The LC/APCI-MS chromatogram of an extract of the filtered soot sample #1 is shown in Figure 5-9. One major peak is observed in the TIC trace, corresponding to NQ. Ions were detected at m/z 139 ($[M+Cl]^-$ of NQ) at 1.63 min, m/z 291 (unknown) at 1.78 min, m/z 261 (unknown) at 1.81 min, m/z 305 (unknown) at 2.11 min, m/z 227 (unknown) at 2.95 min, and m/z 226 ($[M-H]^-$ of TNT) at 3.31 min. The unknown ions at m/z 291, 261, 305, and 227 are part of a chlorine isotopic pattern. The sample dilution, peak areas, and concentrations of each explosive detected are listed in Table 5-1. The concentrations of NQ and TNT in soot sample #1 are 5.5 ± 1.2 mg/g and 1.8 ± 0.0 mg/g , respectively (Table 5-2).

The LC/APCI-MS chromatogram of the filtered soot sample #2 is shown in Figure 5-10. As in soot sample #1, the TIC trace contains one major LC peak, corresponding to NQ. Ions were detected at m/z 139 ($[M+Cl]^-$ of NQ) at 1.47 min, m/z 261 (unknown) at 1.82 min, and m/z 227 (unknown) at 2.94 min. The unknown ions at m/z 261 and m/z 227 were also present in soot sample #1. The sample dilution, peak areas, and concentration of NQ is listed in Table 5-1. The concentration of NQ in soot sample #2 is 23 ± 3 mg/g (Table 5-2). No TNT was detected in soot sample #2 even though it was expected to contain both NQ and TNT.

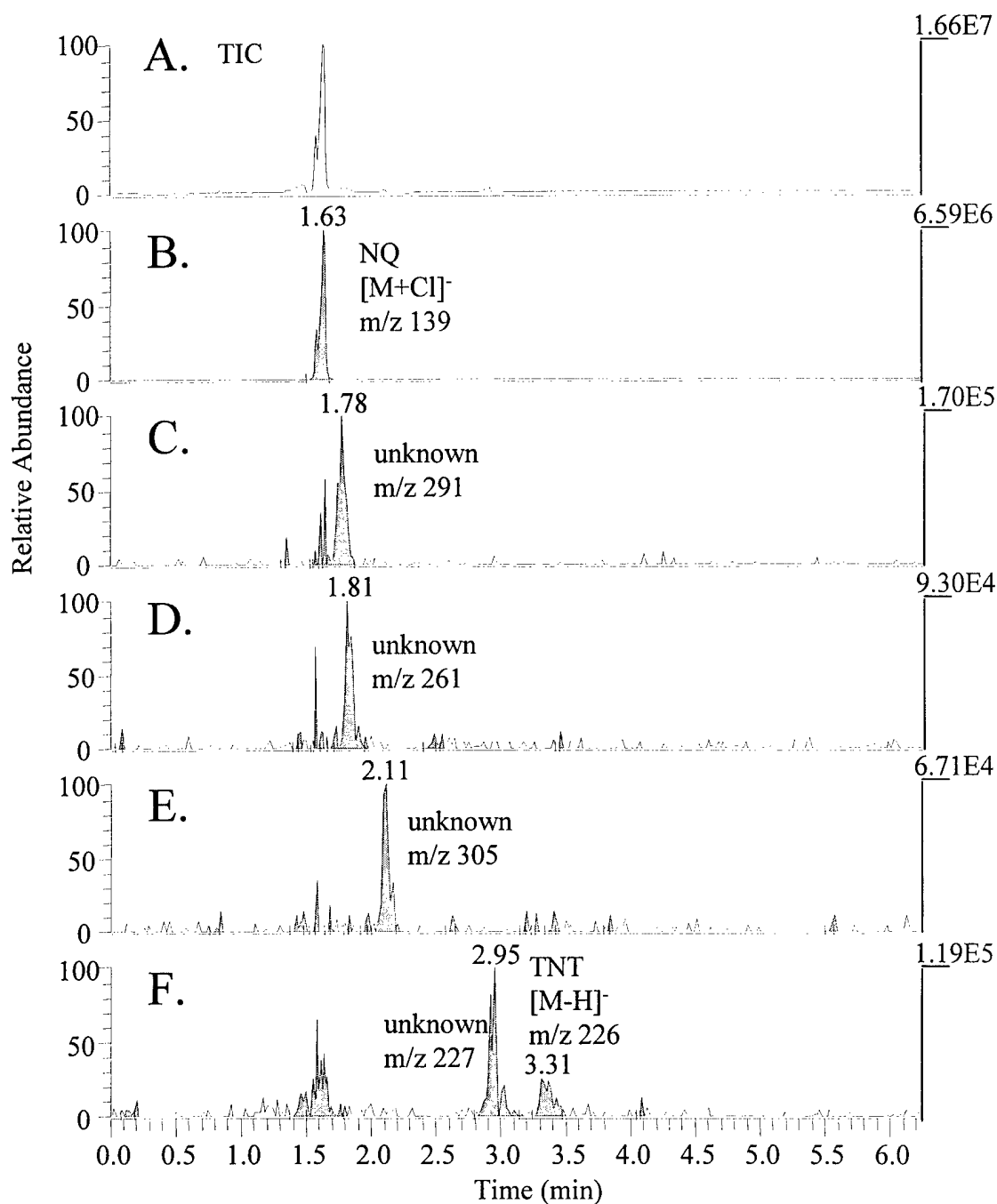


Figure 5-9. LC/APCI-MS chromatograms of extract of soot sample #1, diluted by 1:10: (A) total ion current (TIC) from m/z 120 to 700, (B) m/z 139 ([M+Cl]⁻ of NQ) eluting at 1.63 min, (C) m/z 291 (unknown) eluting at 1.78 min, (D) m/z 261 (unknown) eluting at 1.81 min, (E) m/z 305 (unknown) eluting at 2.11 min, and (F) m/z 227 (unknown) eluting at 2.95 min, and m/z 226 ([M-H]⁻ of TNT) eluting at 3.31 min.

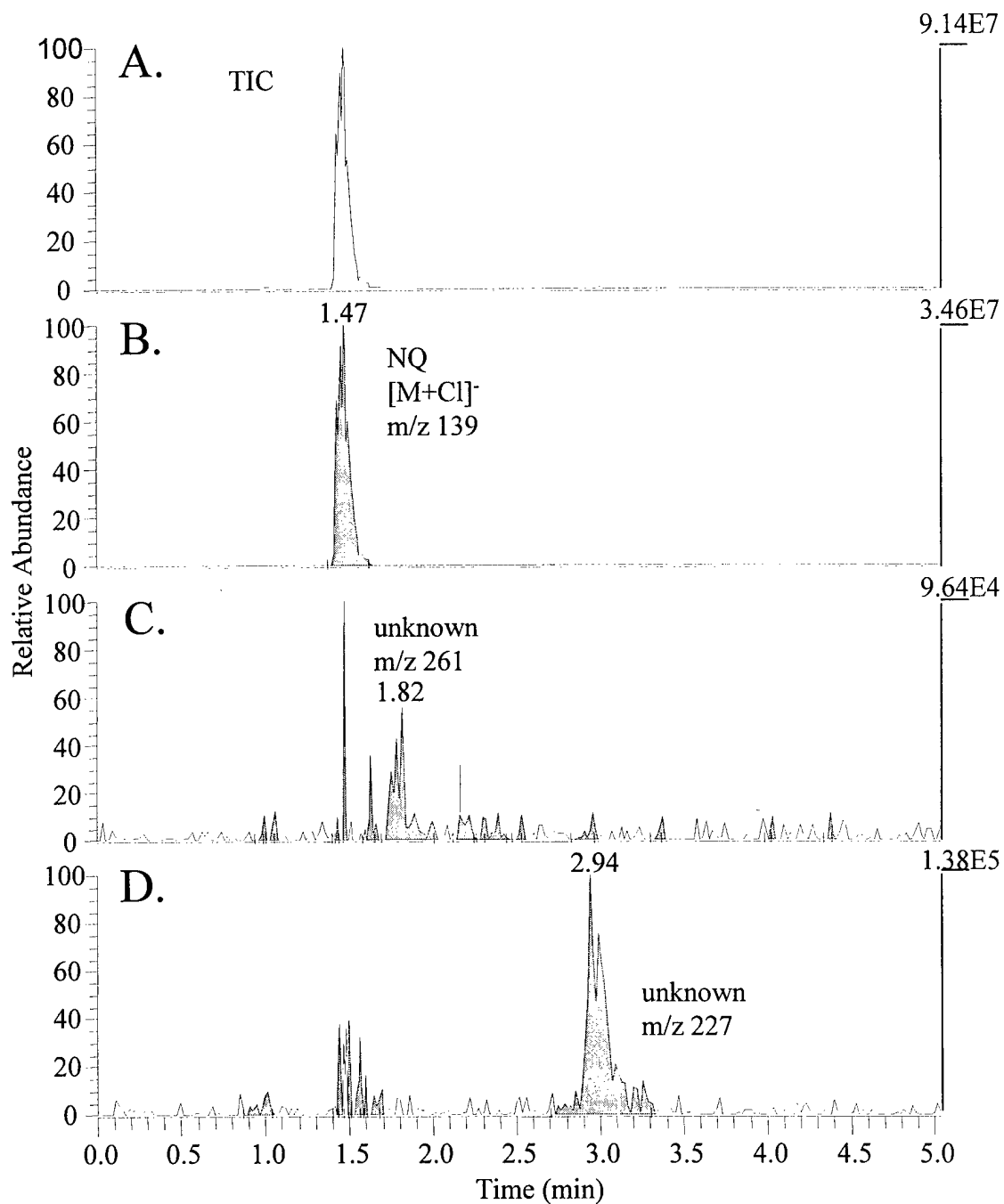


Figure 5-10. LC/APCI-MS chromatograms of extract of soot sample #2, diluted by 1:10: (A) total ion current (TIC) from m/z 120 to 700, (B) m/z 139 ($[M+Cl]^-$ of NQ) eluting at 1.47 min, (C) m/z 261 (unknown) eluting at 1.82 min, (D) m/z 227 (unknown) eluting at 2.94 min.

SEMTEX

The LC/APCI-MS chromatogram of the acetone extract of SEMTEX is shown in Figure 5-11. Ions were detected at m/z 257 ($[M+Cl]^-$ of RDX) at 2.13 min and m/z 351 ($[M+Cl]^-$ of PETN). The sample dilution, peak areas, and concentrations of RDX and PETN are listed in Table 5-1. The concentrations of RDX and PETN detected in SEMTEX are 8.5 \pm 0.1% and 20.6 \pm 0.1% by weight, respectively. SEMTEX is a plastic explosive that is composed of 45% RDX, 45% PETN, and 10% oil based binder by weight. The difference in the concentrations of RDX and PETN detected in SEMTEX can be attributed to the difference in solubilities of these two explosives in the acetone extract. PETN is about twice as soluble in acetone (20.3 g/100g at 20°C) than RDX (8.3 g/100g at 25°C) [Yinon, 1999], which corresponds to the relative weight percents of PETN and RDX detected.

Conclusion

In this chapter, the LC/APCI-MS method developed in Chapter 4 was applied to the detection of explosives in water, soil, detonation soot, and SEMTEX. It was shown that this is an effective method for detecting and quantifying trace amounts of explosives in complex matrices. At the level of explosives observed in these samples (~1-10 ppm in soil, ~2000-24,000 ppm in detonation soot, and ~0.4-1400 ppm in water), the negative ion APCI TIC chromatograms typically show major peaks for the explosives with few if any background peaks. Clearly, the selectivity of the analytical method (extraction, LC,

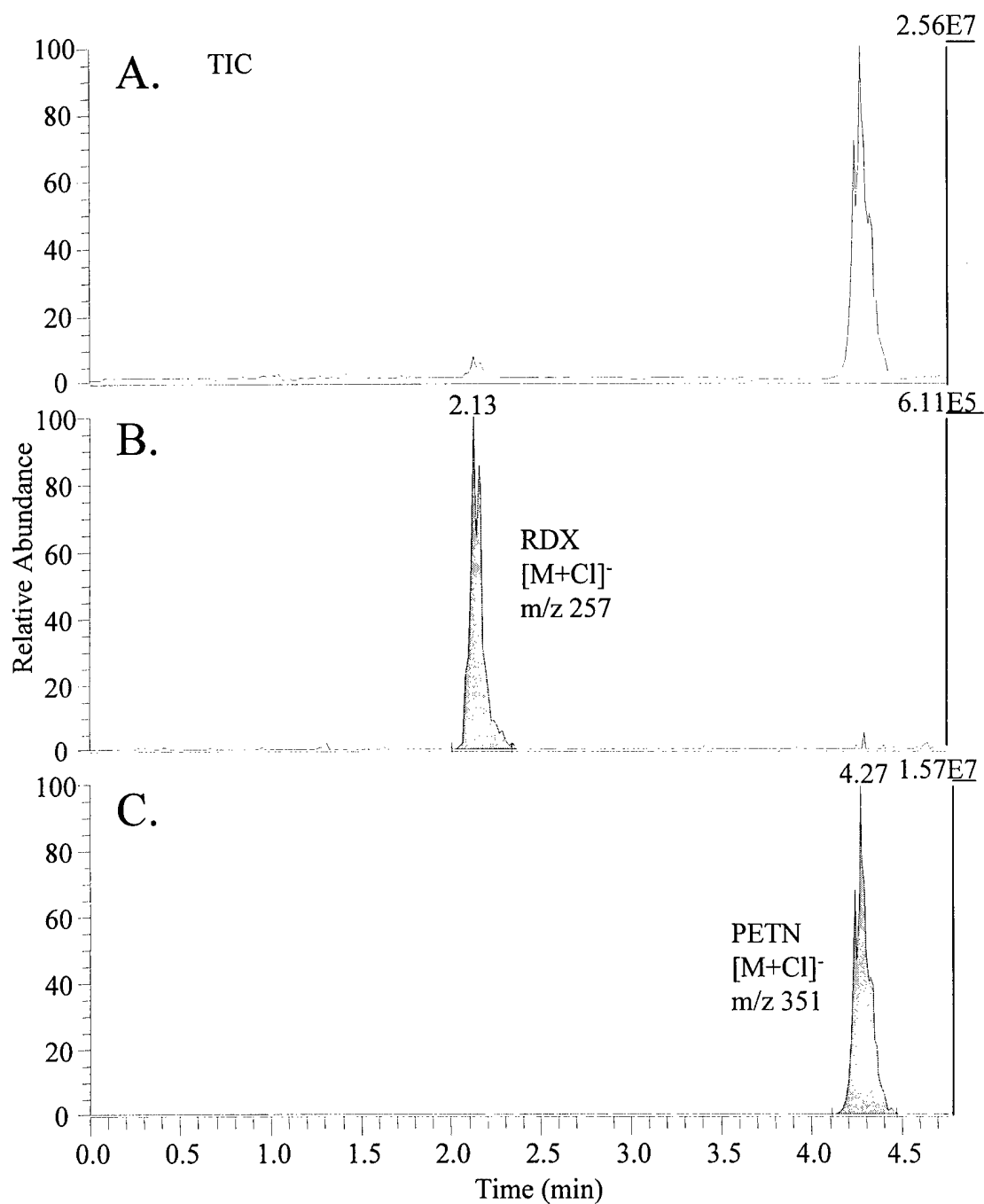


Figure 5-11. LC/APCI-MS chromatograms of SEMTEX: (A) total ion current (TIC) from m/z 120 to 700, (B) m/z 257 ($[M+Cl]^-$ of RDX) eluting at 2.13 min and (C) m/z 351 ($[M+Cl]^-$ of PETN) at 4.27 min.

and negative-ion APCI-MS) is more than adequate. If samples with even lower concentrations were to be analyzed, the added selectivity of MS/MS might be required. Ions from unknown compounds were also detected in the real samples, which could be decomposition products or other contaminants. These unknown ions did not match the characteristics of any explosives or decomposition products identified in Chapter 2.

CHAPTER 6 CONCLUSIONS AND FUTURE WORK

Conclusions

ESI and APCI are two atmospheric pressure ionization methods that are complimentary to each other due to their very different ionization mechanisms. ESI is a condensed-phase ionization method that forms ions in solution before it is converted to the gas phase, whereas APCI is strictly a gas-phase ionization technique. Both have been shown to produce characteristic ions for many different explosives including nitroaromatic compounds, nitrate esters, nitramines, and nitro aliphatic compounds. The majority of these explosives are best ionized in the negative-mode due to the bulky electron-withdrawing nitro groups that facilitate the formation of anions in solution for ESI and which promote charge stability and electron capture for APCI. Very few explosives are more amenable to positive ionization, since these compounds do not possess basic sites that incorporate protonation in solution (ESI) or proton transfer in the gas phase (APCI). Protonation and deprotonation in ESI can be controlled by adding 0.1% of base (e.g. ammonium hydroxide) or acid (e.g. acetic acid), respectively, to the solution.

The most common negative ionization pathway for ESI and APCI is deprotonation in solution and proton abstraction in the gas phase, respectively. This is how nitroaromatic compounds commonly undergo ionization. However, most other explosives are not amenable to these ionization pathways, and form adduct ions instead. Nitroaromatics do not readily form adduct ions due to the high electron density in their

rings, but they have been shown to form adduct ions with acetone and acetonitrile. Tetryl was the only nitroaromatic explosive investigated that readily formed adduct ions with anions present in solution, which is probably due to the nitramine functional group on the aromatic ring. Nitramines and nitrate esters, similar to tetryl, form adduct ions, and are particularly susceptible to any impurities in the solvent system. The nitro groups on these compounds have a strong inductive field effect, which is sufficient for the attachment of nucleophilic anions on sites of low electron density. Nitramines, nitrate esters, and tetryl also form dimers due to these low electron density sites.

The ESI-MS and APCI-MS spectra of tetryl, nitrate esters and nitramines are complicated with various adduct ions that can form depending on the different impurities present in the solvent system. It has been shown that additives can enhance the signal intensity and spectral consistency of these explosives. It was also observed in ESI-MS that increasing concentrations of additive results in the formation of salt clusters that suppress the analyte signal. APCI is also capable of forming adduct ions, and with increasing concentrations of additive, dimer and trimer ions of the anion are formed.

Through MS/MS investigations, it was determined that there are three characteristic classes of adduct ions that are defined by the structural information provided by their daughter ions. The majority of additives investigated form adduct ions, whose MS/MS produce structurally informative daughter ions. The daughter ion spectra of chloride and bromide adduct ions have been shown to be very different from those of most other adduct ions, but remain structurally informative. Trifluoroacetate, iodide, and nitrate, however, do not produce structurally informative daughter ions, and these additives should be avoided.

A major difference between ESI and APCI is when energy is added to transfer molecules from the liquid into the gas phase relative to the formation of ions. With ESI, adduct ions are preformed in solution and need to survive vaporization. These adduct ions are formed by weak van der Waals forces that can be easily dissociated by the energy imparted during the vaporization step. With APCI, these adduct ions have a greater chance of surviving since the vaporization step occurs before adduct ion formation. This is the reason why an LC/APCI-MS and LC/APCI-MS/MS method was developed, combined with the fact that APCI produces less chemical noise and is a more efficient ionization method than ESI.

It was shown that chlorinated solvents in APCI produce intense chloride adducts of certain explosives, and the intensities of these chloride adducts are dependent on the concentration and electron attachment rate constants of the chlorinated solvents used. The mass-sensitive nature of APCI was demonstrated by showing how increasing the sample loop volumes can increase the sensitivity for explosives. The use of chloroform has increased the sensitivity for certain explosives that were not detectable without additives because of their ion destabilization or fragility. The LC/APCI-MS and LC/APCI-MS/MS methods developed using 0.1% chloroform were capable of isocratically separating eight explosive compounds under 5.0 minutes with the identification of major parent ions and daughter ions of each explosive. The method proved to be sensitive for each explosive down to 5 ppb with a linear dynamic range that reaches up to 1000 ppb. This method was also effective at detecting and quantifying trace amounts of explosives in complex matrices, including contaminated water, soil, detonation soot, and SEMTEX, a plastic explosive.

Future Work

Chlorinated solvents have proven to be an effective additive for the APCI-MS of explosives; however, the use of such solvents may be as much of an environmental concern as the explosives being detected. Alternative additives should be volatile and effectively form anions in the gas phase. Propionic acid and sodium nitrite have previously been reported [McClellan, 2000] as effective additives for the ESI-MS of explosives. Sodium nitrite should be avoided, because its use would quickly lead to residual contamination of the tube lens and skimmer cone, especially due to the higher flow rates of APCI compared to ESI. However, propionic acid may prove to be an effective additive for APCI, which is also environmentally sound.

The samples analyzed in this thesis were very concentrated with explosives, and the selectivity of the analytical method developed was more than adequate. If samples with even lower concentrations were to be analyzed, a selected reaction monitoring (SRM) method should be developed using the MS/MS properties determined in Chapter 4. SRM experiments are useful in detecting small quantities of a target compound in a complex mixture, and can provide lower detection limits than the LC/APCI-MS method developed in this thesis. By monitoring the production of one or more targeted product ions from a specified parent ion, the possibility of false positives can also be avoided.

LIST OF REFERENCES

- Barcelo, D.; Maris, F.; Geerdink, R.; Frei, R.; De Jong, G.; Brinkman, U. *J. Chromatogr.* **1987**, 394, 65.
- Bernasconi, C. *J. Org. Chem.* **1971**, 36, 12.
- Bier, M.; Louris, J.; Taylor, D.; Schwartz, J.; Uhrich, M. *Proceedings of the 41st ASMS Conference on Mass Spectrometry and Allied Topics*. San Francisco, CA. **1993**, 456.
- Bier, M.; Schwartz, J.; Zhou, J.; Taylor, D.; Syka, J.; James, M.; Fies, W.; Stafford, G. *Proceedings of the 43rd ASMS Conference on Mass Spectrometry and Allied Topics*. Atlanta, GA. **1995**, 1117.
- Bruins, A. In *Electrospray Ionization Mass Spectrometry*. Cole, R., Ed.; John Wiley & Sons, Inc.: New York, NY. **1997**.
- Bruins, A. *Mass Spectrom. Rev.* **1991**, 10, 53.
- Casetta, B.; Garofolo, F. *Org. Mass Spectrom.* **1994**, 29, 517.
- Cassada, D.; Monson, S.; Snow, D.; Spalding, R. *J. Chromatogr. A.* **1999**, 844, 87.
- Chapman, J. *Practical Organic Mass Spectrometry*. John Wiley & Sons, Inc.: New York, NY. **1993**.
- Cleven, C.; Cox, K.; Cooks, R.; Bier, M. *Rapid Commun. Mass Spectrom.* **1994**, 8, 451.
- Cole, R., Ed. *Electrospray Ionization Mass Spectrometry*. John Wiley & Sons, Inc.: New York, NY. **1997**.
- Cole, R.; Zhu, J. *Rapid Commun. Mass Spectrom.* **1999**, 13, 607.
- Cragin, J.; Leggett, D.; Foley, B.; Schumacher. *TNT, RDX and HMX Explosives in Soils*. CRREL Report 85-15. **1985**.
- Crellin, K.; Widmer, M.; Beauchamp, J. *Anal. Chem.* **1997**, 69, 1092.
- Crockett, A.; Craig, H.; Jenkins, T.; Sisk, W. *EPA Federal Facilities Forum Issue*. **1996**, EPA/540/R-97/501.

- Dole, M.; Mack, L.; Hines, R.; Mobley, R.; Ferguson, L.; Alice, M. *J. Chem. Phys.* **1968**, 49, 2240.
- Dougherty, R.; Roberts, J.; Biros, F. *Anal. Chem.* **1975**, 47, 54.
- Douse, J. *J. Chromatogr.* **1988**, 445, 244.
- Doyle, R.; Campana, J. *J. Phys. Chem.* **1985**, 89, 5285.
- Fainberg, A. *Science*. **1992**, 255, 1531.
- Faye, T.; Brunot, A.; Tabet, J.; Fujii, T. *Rapid Commun. Mass Spectrom.* **2000**, 14, 1066.
- Fetterolf, D. In *Forensic Application of Mass Spectrometry*. Yinon, J., Ed.; CRC Press: New York, NY. **1995**.
- Gamero-Castaño, M.; de la Mora, J. *Anal. Chim. Acta*. **1999**, 1.
- Gaskell, S. *J. of Mass Spectrom.* **1997**, 32, 677.
- Geerdink, R.; Maris, F.; De Jong, G.; Frei, R.; Brinkman, U. *J. Chromatogr.* **1987**, 394, 51.
- Harrison, A. *Chemical Ionization Mass Spectrometry*. CRC Press: New York, NY. **1983**.
- Iribarne, J.; Thomson, B. *J. Chem. Phys.* **1976**, 64, 2287.
- Kaplan, D.; Kaplan, A. *Appl. Environ. Microbiol.* **1982**, 44, 757.
- Kato, Y.; Numajiri, Y. *J. Chromatogr.* **1991**, 562, 81.
- Kebarle, P.; Peschke, M. *Anal. Chim. Acta*. **1999**, 20070, 1.
- Kishore, M.; Ghosh, P. *Int. J. Mass Spectrom. Ion. Phys.* **1979**, 29, 345.
- Kolla, P. *J. Chromatogr. A*. **1994**, 674, 309.
- Kuksis, A.; Marai, L.; Myher, J. *J. Chromatogr.* **1991**, 588, 73.
- Louris, J.; Cooks, R.; Syka, J.; Kelley, P.; Stafford, G.; Todd, J. *Anal. Chem.* **1987**, 59, 1677.
- Marai, L.; Kuksis, A.; Myher, J.; Itabashi, Y. *Biol. Mass Spectrom.* **1992**, 21, 541.
- March, R.; Todd, T., Eds. *Practical Aspects of Ion Trap Mass Spectrometry*. CRC Press: New York, NY. **1995**.
- Mathieu, E. *J. Math. Pure Appl.* **1868**, 13, 137.

- McAvoy, Y.; Dost, K.; Jones, D.; Cole, M.; George, M.; Davidson, G. *For. Sci. Int.* **1999**, 99, 123.
- McClellan, J. *Fundamentals and Applications of Electrospray Ionization-Quadrupole Ion Trap Mass Spectrometry for the Analysis of Explosives*. Ph.D. Dissertation, University of Florida. **2000**.
- McClellan, J.; Holden, M.; Yinon, J.; Yost, R. *Proceedings of the 47th ASMS Conference on Mass Spectrometry and Allied Topics*. Dallas, TX. **1999**, 2444.
- McClellan, J.; Mulholland, J.; Murphy III, J.; Yost, R. *Proceedings of the 47th ASMS Conference on Mass Spectrometry and Allied Topics*. Dallas, TX. **1999**, 2848.
- McLuckey, S.; Van Berkel, G.; Goeringer, D.; Glish, G. *Anal. Chem.* **1994**, 66, 13.
- Miller, M.; Leibowitz, J.; Martz, R. *Proceedings of the 44th ASMS Conference on Mass Spectrometry and Allied Topics*. Portland, OR. **1996**, 1389.
- Miller, J.; Miller, J. *Statistics for Analytical Chemistry*. John Wiley & Sons: New York, NY. **1984**.
- Miller, M.; Mothershead, R.; Leibowitz, J.; Mount, K.; Martz, R. *Proceedings of the 45th ASMS Conference on Mass Spectrometry and Allied Topics*. Palm Springs, CA. **1997**, 52.
- Oehrle, S. *J. Chromatogr. A*. **1996**, 745, 233.
- Oehrle, S. *J. Energetic Mater.* **1977**, 15/1, 21.
- Parker, C.; Yamaguchi, K.; Harvan, D.; Smith, R.; Hass, J. *J. Chromatogr.* **1985**, 319, 273.
- Reich, R. *Proceedings of the American Defense Preparedness Association Insensitive Munitions and Energetics Technology Symposium*. San Diego, CA. **1997**.
- Reich, R.; McClellan, J.; Yost, R. *Proceedings of the 48th ASMS Conference on Mass Spectrometry and Allied Topics*. Long Beach, CA. **2000**, MPA 018.
- Reutter, D.; Buechele, R.; Rudolph, T. *Anal. Chem.* **1983**, 55, 1468A.
- Schilling, A. *Proceedings of the 44th ASMS Conference on Mass Spectrometry and Allied Topics*. Portland, OR. **1996**, 154.
- Schreiber, A.; Efer, J.; Engewald, W. *J. Chromatogr. A*. **2000**, 869, 411.
- Schwartz, J.; Quarmby, S.; Schoen, A. *Proceedings of the 46th ASMS Conference on Mass Spectrometry and Allied Topics*. Orlando, FL. **1998**, 484.

- Stafford, G.; Kelley, P.; Stephens, D., U.S. Patent 4,540,884, **1982**.
- Stafford, G.; Taylor, D.; Bradshaw, S.; Syka, J. *Proceedings of the 35th ASMS Conference on Mass Spectrometry and Allied Topics*. Denver, CO. **1987**, 775.
- Straub, R.; Voyksner, R. *J. Am. Soc. Mass Spectrom.* **1993**, 4, 578.
- Tamiri, T.; Zitrin, S. *J. Energetic Mater.* **1986**, 4, 215.
- Tannenbaum, H.; Roberts, J.; Dougherty, R. *Anal. Chem.* **1975**, 47, 49.
- Van Berkel, G. In *Electrospray Ionization Mass Spectrometry*. Cole, R., Ed.; John Wiley & Sons, Inc.: New York, NY. **1997**, 65.
- Voyksner, R.; Yinon, J. *J. Chromatogr.* **1986**, 354, 393.
- Watson, J. *Introduction to Mass Spectrometry*. Lippincott-Raven Publishers: Philadelphia, PA. **1997**.
- Wu, L.; Almirall, J.; Furton, K. *J. High Resol. Chromatogr.* **1999**, 22, 279.
- Yeager, K. *Explosive Firing Site and Laboratory Safety Course*. Energetic Materials Research and Testing Center. New Mexico Tech, Socorro, NM. **1996**.
- Yinon, J. *Forensic and Environmental Detection of Explosives*. John Wiley & Sons, Inc.: New York, NY. **1999**.
- Yinon, J. *J. Chromatogr. A.* **1996**, 742, 205.
- Yinon, J. *Toxicity and Metabolism of Explosives*. CRC Press: New York, NY. **1990**.
- Yinon, J.; Hwang, D. *J. Chromatogr.* **1983**, 268, 45.
- Yinon, J.; McClellan, J.; Yost, R. *Rapid Comm. Mass Spectrom.* **1997**, 11, 1961.
- Yinon, J.; Zitrin, S. *The Analysis of Explosives*. Pergamon Press: New York, NY. **1981**, vol. 4.
- Yinon, J.; Zitrin, S. *Modern Methods and Applications in Analysis of Explosives*. John Wiley & Sons: New York, NY. **1999**.
- Yinon, J.; Zitrin, S.; Tamiri, T. *Rapid Commun. Mass Spectrom.* **1993**, 7, 1051.

BIOGRAPHICAL SKETCH

Richard Fred Reich, Jr., was born in Escondido, California, in 1972. He lived in southern California attending public schools in Glendale and Bakersfield until he moved to Arizona in 1984, where he attended schools in Flagstaff, Prescott, and Prescott Valley. In 1991 he graduated from Bradshaw Mountain High School as valedictorian and earned a scholarship to attend the University of Arizona.

At the University of Arizona, he began his research experience working at the Department of Anesthesiology at the Arizona Health Sciences Center. There he worked as a laboratory assistant under the supervision of Dr. A. Jay Gandolfi in the investigation of an immune-mediated mechanism for halothane-induced idiosyncratic hepatotoxicity. He also worked as a laboratory assistant at the Department of Surgical Research under the direction of Dr. Stuart Williams, where he assisted in the investigation of endothelial cell transplantation onto polymeric arteriovenous grafts.

Richard graduated cum laude from the University of Arizona in the Fall of 1995 with a B.S. in chemistry and a B.A. in German. He was commissioned in the United States Air Force and served his first assignment as a chemical research officer at the Energetic Materials Branch, Eglin AFB, Florida, from July, 1996, to July, 1999. At the Energetic Materials Branch, also known as the High Explosive Research and Development (HERD) Facility, he first gained an interest in explosives research. There he served as principal investigator of high energy melt-cast explosives developing a new

1,3,3-trinitroazetidine (TNAZ) based explosive formulation. His work resulted in the publication of eight military technical papers, four presentations at Department of Defense and industry symposia, and an Air Force invention, which was later patented.

In 1999, Richard was competitively selected for the Air Force Institute of Technology (AFIT) to pursue his master's degree in chemistry at the civilian school of his choice. In the fall of 1999, he began his eighteen-month academic program at the University of Florida under the direction of Dr. Richard Yost. There he was able to continue his interests in energetic materials by developing analytical methods for the trace detection of explosives using mass spectrometry. After completing his master's degree in analytical chemistry, he will be assigned to the Propulsion Directorate, Wright-Patterson AFB, in Ohio. Richard plans to later pursue his Ph.D. in analytical chemistry, teach at the Air Force Academy, and complete a tour in Germany through the Engineer and Scientist Exchange Program (ESEP).

